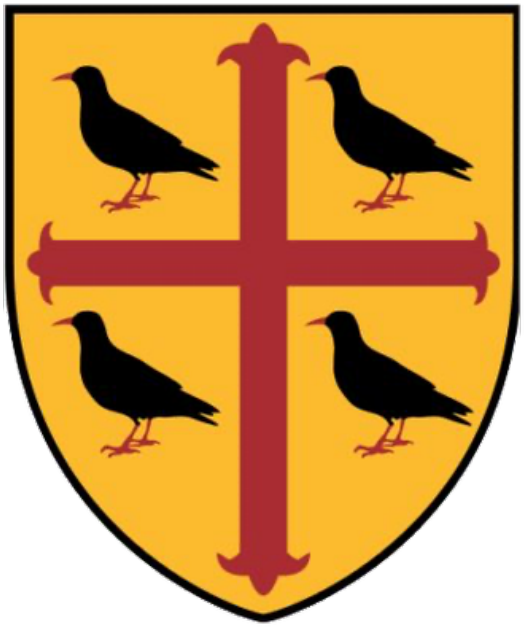
Synthesis and Reactivity of Complexes Containing a Group 13–Group 11 Bond





Caitilín Brigid McManus

St. Edmund Hall

Thesis submitted for the Degree of Doctor of Philosophy

July 2022

Acknowledgments

Above all, I would like to thank my supervisor, Simon Aldridge. Thank you for endless enthusiasm and great ideas, I feel very lucky to have had a supervisor with so much genuine interest in the work we do. Thank you also to Jose Goicoechea for valuable input and great pub conversations.

I owe many thanks to all of the support staff in the CRL including everyone in facilities and the CRL workshop – especially Jude for resurrecting many vacuum pumps from near death. The opportunity to learn X-ray crystallography has been an exciting privilege, and I thank Kirsten, Amber and Keith for their help. Also many thanks to the NMR service staff.

To the many post docs who have taught me so much – chemistry and otherwise: Jamie for his patience and unwavering optimism, giving me the best possible start to my PhD, Petra for rightly putting the fear of God into me, Alexa for Love Island and chemistry discussion in equal measure, MattRoy and Roy's boys for all the laughs, Mathias, whose wonderful use of the English language deserves its own textbook, Andrey, for the best stories and more chemistry knowledge than I will ever retain, Joe for so gladly joining our chaotic gang, and to Malte and Marcel for putting up with us all. Thank you to my colleagues for making the lab a fun place to be, especially the members of LadyLab + Lewis - it perhaps can't be said that we stopped each other from losing our sanity during the nightmare lockdown shifts, but at least we went into madness together. Special thanks go to Aisling - the best #womeninSTEM partner and founder of the Aldridge Running Club, Lewis - for every amazing and terrible playlist, Libby – everything I could ask for in a student, Liam – for great shirts and better fun facts, Aggy, for doing every lab job possible with only a tiny bit of complaining, Steven

Lau, the complicated legend, Xueer (Shirls) - for so many great chats, and Anna for the absolute worst jokes. And everyone else in the Aldridge group who made my PhD enjoyable: Megan, Rob, Xiongfei, Simon T, Huan, Ying Kai, Lu Ying, Andreas, Ily, Artemis and all the part II students. The crosswords, coffee breaks and ABBA Fridays really kept me going.

Outside the lab, I must thank my housemate Ryan for being a great friend and an often-needed reminder of home. Thank you to my parents for supporting me the whole time and doing their very best to understand what exactly it is I do all day. I promise I will get a real job soon. And Tim, it's impossible to thank you enough for being there for me (literally) always, and being the best thing I found in Oxford.

Abstract

This thesis describes the synthesis of heterobimetallic complexes which contain an unsupported bond between a group 13 and a group 11 metal (Cu, Ag, Au). While the primary focus is on bonds to aluminium, which are lesser known, the analogous gallium-coinage metal compounds are also investigated as a point of comparison. The methodology used in this work makes use of the first of a new class of nucleophilic aluminium 'aluminyl' anions, **$K_2[(NON)Al]_2$** (NON = 4,5-bis(2,6-diisopropylanilido)-2,7-di-*tert*-butyl-9,9-dimethylxanthene), which is reacted with group 11 electrophiles of the form R_3PMI (R = Ph, ^{t}Bu, Cy) in a salt metathesis reaction. This approach gives access to rich structural variety, producing bimetallic complexes of the form **(NON)AlMP^{t}Bu$_3$**, a 2:1 di(aluminyl)cuprate system, **$K[Cu\{Al(NON)\}_2]$**, and trimetallic iodide bridged complexes, **$(NON)Al(MPPh_3)_2I$**. These compounds are characterised by X-ray crystallography and multinuclear NMR, with spectroscopic comparisons to the heavier congeners (prepared using the gallyl reagent **$K_2[(NON)Ga]_2$** giving insight into the properties of the aluminyl fragment as a metalloligand.

The reactivity of the linear **(NON)AlMP^{t}Bu$_3$** series towards small molecules is then explored. The compounds in this bimetallic series readily insert carbon based electrophiles (CO_2, carbodiimides) into the Al–M bond to give a complexes containing an $M(CE_2)Al$ bridging unit (E = O, NR), with an unusual μ-κ^1(C):κ^2(E,E′) binding mode. While the carbodiimide insertion products are stable to further reaction, it is observed that the CO_2 bridged species have the potential to react onwards, and that this ability depends on the identity of the group 11 metal. **$(NON)Al(O_2C)AuP^tBu_3$** is inert to further reaction, while **$(NON)Al(O_2C)AgP^tBu_3$** reacts slowly with a second equivalent of CO_2 to give a bridging carbonate complex and CO. Copper compound

(NON)AlCuP^{t}Bu$_3$ reacts rapidly even at very low temperatures, proceeding straight to the carbonate complex. The mechanism of this CO_2 to CO transformation can be investigated and is found to be consistent with rate determining extrusion of CO to form a bridging Al–O–M oxide, followed by uptake of a second molecule of CO_2.

The behaviour of the Al–M bond towards alkynes is then investigated. Internal alkynes insert into the Al–Cu bond of **(NON)AlCuP^{t}Bu$_3$**, giving (aluminylalkenyl)copper compounds with M–C bonds of differing natures. The insertion gives access to both *syn* and *anti* dimetallated alkenes, depending on the reaction conditions. It is also regioselective, producing only one regioisomer when unsymmetrically substituted alkynes are used. The mechanism of the insertion, and a subsequent isomerisation step, are investigated through kinetics studies. The differential reactivity of the (aluminylalkenyl)copper compounds is exploited by selective functionalisation with CO, which inserts only into the Cu–C bond. This results in formation of the first structurally characterised example of a copper acyl complex, a feat made possible by cooperative action of copper and the proximal aluminium centre.

In all, this thesis aims to demonstrate the utility of the potassium aluminyl reagent **K$_2$[(NON)Al]$_2$** as a means to forming direct Al–M bonds, and investigate the reactivity of such heterobimetallic compounds towards challenging small molecules.

Abbreviations

2.2.2 cryptand	4,7,13,16,21,24-hexaoxa-1,1-diazabicyclo[8.8.8]hexacosane
Ac	Acetate
Ar	Aryl
^{Ar}NacNac	$[HC\{C(Me)(N^{Ar})\}_2]^-$
atm	Atmosphere
BCF	Tris(pentafluorophenyl)borane
CAAC	Cyclic (alkyl)(amino) carbenes
Cp	Cyclopentadiene
Cp*	Pentamethylcyclopentadiene
CVD	Chemical vapour deposition
Cy	Cyclohexyl
Cys	Cysteine
DAB	Diazabutadiene
DDP	2-((2,6-diisopropylphenyl)amino)-4-((2,6-diisopropylphenyl)imino)-2-pentene
DFT	Density Functional Theory
Dipp	Di*iso*propylphenyl
DME	Dimethyl ether
Et	Ethyl
Et_2O	Diethyl ether
FLP	Frustrated Lewis Pair
Fp	$FeCp(CO)_2$
Hal	Halide
^{i}Bu	*Iso*-butyl
IDipp	1,3-bis(Dipp)-imidazol-2-ylidene
^{i}Pr	*Iso*-propyl
J	Coupling constant
Me	Methyl
Mes	Mesityl
NHC	N-heterocyclic carbene
NMR	Nuclear Magnetic Resonance
NON	4,5-bis(2,6-diisopropylanilido)-2,7-di-*tert*-butyl-9,9-dimethylxanthene
Ph	Phenyl
SiN^{Dipp}	$[CH_2SiMe_2NDipp]_2$
^{t}Bu	*Tert*-butyl
Tf	Triflate
tmeda	tetramethylethylenediamine
TMP	2,2,6,6-tetramethylpiperidine
TMS	trimethylsilane

Table of Contents

Chapter 1 : Introduction 1

1.1 Bimetallic chemistry 1

1.1.1 Types of bimetallic complexes 2

1.1.2 Metal–metal bonds 3

1.1.3 Reactivity and catalysis 3

1.1.4 Single source precursors and solid state systems 4

1.1.5 Cooperative Lewis pairs 5

1.2 Group 13 chemistry 6

1.2.1 Properties of Group 13 elements 7

1.2.2 Uses of aluminium 8

1.2.3 Low valent aluminium 9

1.2.4 Potential as metalloligands 10

1.3 Coinage metal chemistry 11

1.3.1 Properties of the Group 11 metals 12

1.3.2 Gold – a special case 12

1.3.3 Bimetallic Group 11 complexes 13

1.4 Aluminium-transition metal bonds 14

1.4.1 Alanes 15

1.4.2 Donor-acceptor complexes 16

1.4.3 Covalent Al–M bonds 18

1.5 Anionic group 13 nucleophiles 19

1.5.1 Gallyl anion 20

1.5.2 Boryl anion 21

1.5.3 Nucleophilic aluminium: an aluminyl anion 23

1.6 Project aims and outline 26

1.7 References **28**

Chapter 2 : Experimental Methods ***32***

2.1 Manipulation of air sensitive compounds **32**

2.2 Spectroscopy and analytical techniques **33**

2.2.1 NMR spectroscopy 33

2.2.2 IR spectroscopy 33

2.2.3 Mass spectrometry 33

2.2.4 Elemental analysis 34

2.2.5 DFT calculations 34

2.2.6 X-ray crystallography 35

2.3 Preparation of starting materials **42**

2.3.1 Purification of solvents 42

2.3.2 Starting materials 42

2.4 References **44**

Chapter 3 : Synthesis of group 13–group 11 complexes ***45***

3.1 Introduction **45**

3.1.1 Examples of aluminium–coinage metal complexes 45

3.1.2 Synthesis of unsupported Al–Au bonds using a potassium aluminyl complex 46

3.2 Aims **47**

3.3 Results and discussion **48**

3.3.1 Notes on multinuclear NMR characterisation and stoichiometry 48

3.3.2 Synthesis of a bisaluminocuprate 49

3.3.3 Trimetallic complexes with an $E(MPPh_3)_2I$ core (E = Al, Ga, M = Au, Cu) 53

3.3.4 Synthesis of linear bimetallic complexes 58

3.3.5 The aluminyl fragment as a metalloligand 62

3.3.6 Discussion of Al–M bonding 65

3.4 Conclusions and future work 67

3.5 Synthetic procedures and spectroscopic data for new compounds 71

3.6 References 78

Chapter 4 : Reactivity of silver and copper aluminyl complexes with heteroallenes 80

4.1 : Introduction 80

4.1.1 Chemistry of carbon dioxide 80

4.1.2 Main group CO_2 activation 81

4.1.3 CO_2 activation by heterobimetallic complexes 82

4.2 Aims 84

4.3 Results and discussion 85

4.3.1 Reaction of a silver aluminyl complex with CO_2 85

4.3.2 Reaction of a silver aluminyl complex with a carbodiimide 86

4.3.3 Onward reactivity with CO_2 89

4.3.4 Reaction of a copper aluminyl complex with a carbodiimide 92

4.3.5 Reaction of a copper aluminyl complex with CO_2 95

4.3.6 Experimental investigation of mechanism 97

4.3.7 ^{13}C Labelling experiments 100

4.3.8 Synthesis of an oxide intermediate 101

4.3.9 Quantum chemical studies of mechanism 103

4.3.10 Comparison to similar work 106

4.4 Conclusions and future work 111

4.5 Synthetic procedures and spectroscopic data for new compounds 113

4.6 References 120

Chapter 5 : Reactivity of bimetallic aluminyl complexes towards alkynes 123

5.1 Introduction 123

5.1.1 Chemistry of alkynes 123
5.1.2 Alkynes and coinage metals 123
5.1.3 Alkynes and aluminium 124
5.1.4 Alkyne insertion into M–E bonds (E = B, Si) 125

5.2 Aims 127

5.3 Results and discussion 127

5.3.1 Reactions with a terminal alkynes 127
5.3.2 Reactions of internal alkynes 130
5.3.3 Regioselectivity 136
5.3.4 Migration of R group 141
5.3.5 Mechanistic considerations 143
5.3.6 Kinetic studies using diphenylacetylene 144
5.3.7 Functionalisation 150

5.4 Conclusions and future work 155

5.5 Synthetic procedures and spectroscopic data for new compounds 159

5.6 Kinetic studies 168

5.7 References 169

Chapter 6 : Conclusions 171

Chapter 1 : Introduction

1.1 Bimetallic chemistry

Humans have been studying coinage metal-main group bimetallics since the discovery of bronze, an alloy of copper and tin, in the fourth millennium BC. Yet further back in time, nature crafted metalloenzymes such as nitrogenases which contain multimetallic active sites and can carry out chemical reactions with incredible selectivity and efficiency. The role of each metal has fascinated chemists, who have diligently studied them and sought to understand their activity through structural mimics (**Figure 1.1**).[1,2] The incredible catalytic reactivity of such enzymes to perform diverse transformations such as methane oxidation, nitrogen fixation and water splitting has also inspired organometallic chemists to design synthetic catalysts containing two metals.[3]



Figure 1.1. *Left: The active site of [NiFe] hydrogenase; Right: A structural and functional mimic capable of proton reduction*

Combinations of metals are known to show reactivity patterns that are distinct from their constituent monometallic systems, with an ability to access modes of reactivity that are not possible for a single metal. The concept of cooperativity has been applied to such binuclear systems, whereby two components of a system (eg. two metals) work together to activate a substrate or carry out a reaction, for example through enhanced substrate binding. A plethora of metal–metal bonds from across the Periodic

Table have been synthesised and found to carry out almost as many reactions, including hydrogenations, cross coupling reactions and cycloadditions.[4–8]

1.1.1 Types of bimetallic complexes

Of particular interest are *heterobimetallic* systems, in which the two metals are different. This introduces a further synergistic aspect, where two metals may have very different properties, and their complementary reactivity can achieve transformations not possible for either metal in isolation.[4,9,10] The term bimetallic is used to refer both to compounds in which two metal centres are in close proximity, or where there is a bond between them. Such bonds may be unsupported or may feature bridging ligands or similar scaffolds to fix their position relative to one another. While supported ligand structures are useful in systems where it is important to maintain the integrity of the metal–metal bond, direct unsupported bonds offer a unique opportunity to study the nature of the M–M bond in isolation. In such directly bonded systems, one metal may be considered to be acting as a ligand to the other, and vice versa. It is a fundamental principle of organometallic chemistry that the electronic properties of a metal may be altered by coordination of a ligand, which in turn influences the selectivity of reactions. Therefore, directly bonded bimetallic systems introduce powerful metalloligands that can be further tuned and drastically alter the reactivity at the metal centre(s). The fact that the Periodic Table offers a host of metals of different electronegativities provides ample scope to tune the polarity of an M–M bond, allowing for the activation of a range of strong bonds.[11]

1.1.2 Metal–metal bonds

From a fundamental point of view, bimetallic systems containing a direct bond between two metals are of profound interest because they challenge and inform our understanding of chemical bonding. For example, Power's remarkable 2005 report of a quintuple bonded chromium dimer, **[Ar'CrCrAr']** (Ar' = ^{Dipp}Terphenyl) (**Figure 1.2**) inspired a flurry of theoretical studies and a discussion of bonding concepts.[12,13] The bonding motif, involving five pairs of electrons, consists of one σ bond, two π, and one δ, supported by a further 'side on δ' bond. Main group bimetallic compounds, such as Group 14 dimetallynes, have also required us to rethink traditional ideas of multiple bonds, as prior to the isolation of doubly-bonded tetrylenes it was thought that elements with principal quantum number ≥ 3 should not be capable of forming multiple bonds.[14]

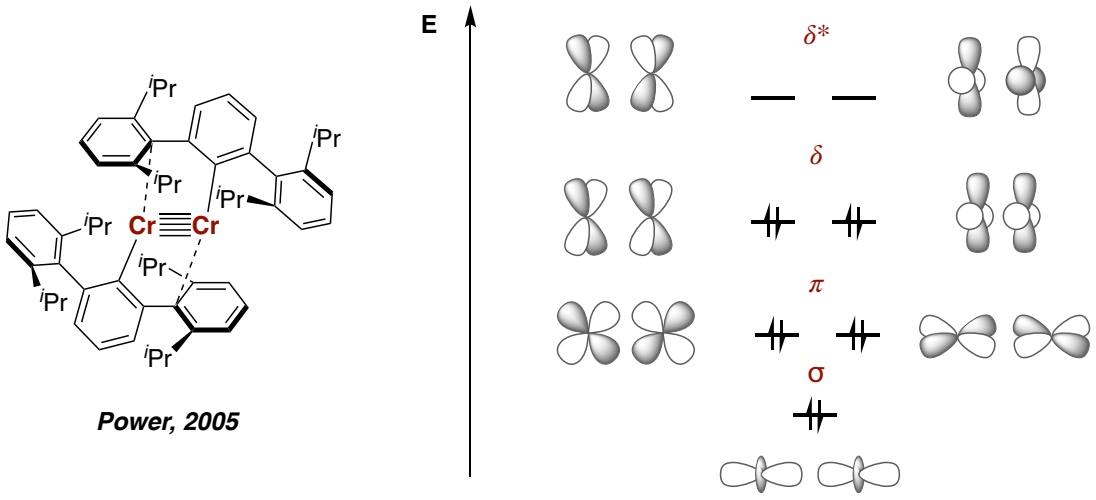
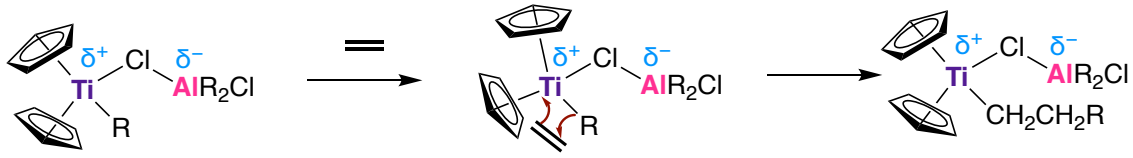


***Figure 1.2**. Left: Quintuple chromium–chromium **[Ar'CrCrAr']** dimer supported by bulky terphenyl ligands; Right: MO diagram showing the components of the quintuple bond*

1.1.3 Reactivity and catalysis

Bimetallic species have found great use in both the stoichiometric and catalytic activation of strong bonds. *Post hoc* analysis of many organic reaction mechanisms

has revealed that two metals are involved in the key steps of bond breaking and formation, leading to enhanced interest in synthesising pre-formed bimetallic species, either as models of intermediates or as catalysts in their own right.[15,16] An area of chemistry which has exploited cooperativity between metals far apart in the Periodic Table to great effect is olefin polymerisation catalysis.[17] A primary example of this is Ziegler Natta catalysis, in which a group 4 metallocene catalyst is activated by an aluminium alkoxide such as methylaluminoxane (MAO) or an aluminium alkyl halide (**Scheme 1.1**).[18]



Scheme 1.1. *Bimetallic titanium/aluminium intermediates in olefin polymerisation*

In recent years, a number of groups have taken a renewed look at alkali metals and the synergistic effects that they can bring about in organic synthesis.[19–21] As very small electropositive metals, they can bring about extreme polarisation. A prime example is the development of Na/Li reagents for the directed metalation of arenes, which complements traditional ortho- directed metalation.[22] These examples from the Main Group show the synthetic power of combining two metals to effect new reactivity.

1.1.4 Single source precursors and solid state systems

The benefit of dual component systems is also acknowledged in heterogeneous catalysis, where bimetallic alloys are growing in popularity, and nanoparticles made of two metals have been used as electrocatalysts for applications such as the oxygen evolution reaction.[23–25] While most synthetic methods for the formation of bimetallic

materials involve separate metal salts, heterobimetallic compounds have attracted great interest as single source precursors for the chemical vapour deposition (CVD) of thin films for electronics.[26–29] For this application, the goal is to exploit a pre-formed ratio of two metals held in a molecular complex by organic ligands which can then be vaporised, leaving the desired bimetallic film. It has been noted that for some metal combinations, direct alloys cannot be formed, but it is possible to synthesise bimetallic molecules or clusters of the metals. Group 13 bimetallics are of particular interest here, due to the ubiquity of materials such as GaAs and aluminium based alloys. Accordingly, much early interest in group 13–d-block metal bonds was prompted by a desire to create bespoke bimetallic films. Coinage metals are useful in electronics due to their high conductivity, and bimetallic molecular precursors have been investigated for this purpose.[30]

1.1.5 Cooperative Lewis pairs

An interesting demonstration of cooperativity and multi-site reactivity that has sprung from Group 13 is the development of Frustrated Lewis Pair (FLP) chemistry.[31] An FLP is a system containing both a Lewis acid (LA) and Lewis base (LB), which cannot form an adduct due to steric hindrance or geometric constraints (or an equilibrium exists between adduct and separated LA/LB) (**Figure 1.3**). This unquenched reactivity can lead to the activation of substrates across the two sites. Although the term was coined in 2007 and has received much attention since, this cooperative reactivity has long been known, and indeed the idea of ‘FLP like’ reactivity was previously identified in enzyme active sites where protein scaffolds maintain the appropriate separation and orientation of donor and acceptor orbitals.[32] It has been recognised then that the concept of FLP reactivity is a subset of general chemical cooperativity, and can be

applied to many forms of Lewis Acid – transition metal chemistry.[33,34] Interesting examples also include 'metal only FLPs' such as those described by the Campos group (**Figure 1.3**), in which an Au(I) Lewis acid and Pt(0) Lewis base were found to cooperatively activate H_2 and acetylene.[35]

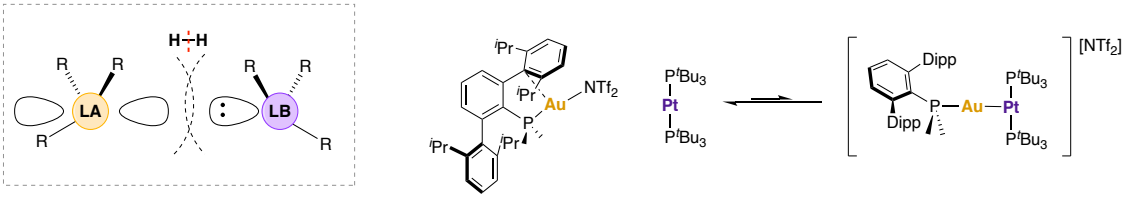


Figure 1.3. *Left: General cooperation of a Lewis acid and base in an FLP; Right: Bimetallic Lewis acid/base cooperation*

These examples are consistent with a growing idea that chemistry need not occur at a single site, and that we can better understand known reactions by studying cooperative effects. While not a new idea by any means, examining aspects of synergy allow us to design systems involving broad concepts such as ligand non-innocence, the importance of second-sphere interactions and the activation of substrates across M–M bonds. It is clear that bimetallic chemistry holds great potential, be that through an internal Lewis acid, or direct reactivity across a heterobimetallic bond. The work reported in this thesis looks at the formation of direct bonds between group 13 elements and the coinage metals of group 11. The primary focus is on aluminium, of which much less is known, although the heavier metal gallium is also used for comparison.

1.2 Group 13 chemistry

Before delving into recent advances in group 13 bimetallics, some key features of the chemistry of this group will be outlined, with a focus on aluminium.

1.2.1 Properties of Group 13 elements

Group 13 consists of the metalloid boron and the metals aluminium, gallium, indium and thallium. A defining feature of group 13 is the preference of the lighter elements for the +3 oxidation state, while descending the group increases the preference for the +1 oxidation state.

Table 1.1. *Standard electrode potentials for a group 13 element M, relative to the standard hydrogen electrode*[36]

	E^0 ($M^{III}_{(aq)}$ + 3e⁻ ⇌ $M_{(s)}$)/ V	E^0 ($M^{I}_{(aq)}$ + e⁻ ⇌ $M_{(s)}$)/ V
B	−0.890	–
Al	−1.662	+0.550
Ga	−0.549	−0.200
In	−0.338	−0.126
Tl	+0.741	−0.336

This is apparent from looking at the electrode potentials for group 13 elements (**Table 1.1**) where it can be seen that $E^0(M/M^{III})$ becomes more positive on going from B to Tl, whereas the opposite is true for $E^0(M/M^{I})$. As such, the chemistry of aluminium is dominated by the +3 oxidation state, with aluminium trihalides AlX_3 being very common, while for thallium, the monohalides are more stable. Such a tendency for the (n−2) valency of the elements to increase with atomic number, and the non-participation of the s-electrons in bonding, is termed the *inert pair effect* and may be explained by a combination of bond dissociation energy and promotion energy (energy required to promote an electron from *n*s to *n*p when forming a trivalent species). While bond energies decrease on descending group 13 (due to poor orbital overlap), the promotion energies actually increase. Therefore the energy 'payback' from bond

formation does not compensate the cost of oxidation.[37] Thus, in any metal–metal bonding, it is the p-orbitals of aluminium which are most relevant.

1.2.2 Uses of aluminium

Metallic aluminium is relatively cheap and is used extensively for its mechanical properties. Chemically, aluminium also has important industrial roles. Possessing an unoccupied p-orbital, electron deficient Al(III) compounds such as $AlCl_3$ are quintessential Lewis acids. This property, in combination with the low cost of aluminium reagents, has made the use of $AlCl_3$ widespread in industrial Lewis acid catalysed reactions such as Friedel Crafts acylation. Aluminium hydrides such as lithium aluminium hydride are highly useful reducing agents in organic synthesis, and a recent report has even detailed a bimetallic mechanism for imine hydrogenation with $LiAlH_4$ (**Figure 1.4**).[38]

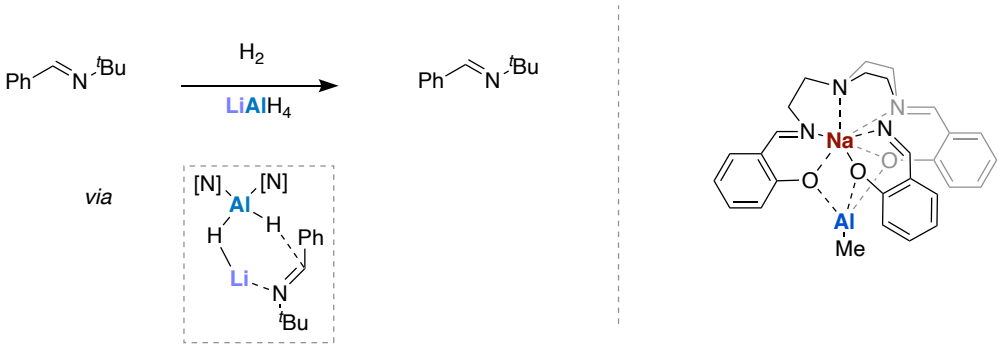


Figure 1.4. *Left: Bimetallic intermediate in imine hydrogenation by $LiAlH_4$; Right: Bimetallic Na/Al complex for ring opening polymerisation catalysis*

In addition to the Ziegler Natta alkene polymerisation described in Section 1.1.3, catalysts derived from aluminium salen complexes (salen = N,N-bis(salicylidene)ethylenediamine) are active for the ring opening polymerisation of epoxides. It is interesting to note that many of the recently developed catalysts for this purpose (such as the Na/Al catalyst reported by Garden shown in **Figure 1.4**) contain

aluminium as well as a second, alkali metal, which is crucial in modulating the catalyst activity.[39–41] This further demonstrates the principles of metal-metal cooperativity, particularly in relation to group 13 compounds.

1.2.3 Low valent aluminium

Despite the strong preference for trivalency, in the last 30 years the field of low valent aluminium chemistry has developed significantly. Similar chemistry had previously been developed for gallium (see Section 1.5.1) but the greater challenge of stabilising Al(I) compared to Ga(I) (as noted above) means that its low valent chemistry has lagged behind that of its heavier congener. Previously, the monohalides AlX were known only in the gas phase, being prone to readily disproportionate to Al(0) and AlX_3. New, highly sterically hindered ligands have proved critical in allowing access to aluminium in the oxidation states 0, +1 or +2. Such large ligands provide kinetic stabilisation at the metal centre, making disproportionation less favourable. Nevertheless, Al(I) compounds are (unsurprisingly) highly reactive. The first example of a stable, isolable Al(I) compound was the neutral tetrameric compound **$(AlCp^*)_4$**, ($Cp^* = C_5Me_5$) reported by Schnöckel and coworkers in 1991 (**Figure 1.5**).[42] This species was prepared from a metastable AlCl solution and $MgCp^*_2$, although a later route involves the potassium reduction of Cp^*AlCl_2.[43] Although a tetramer in the solid state, heating a solution of **$(AlCp^*)_4$** causes **$AlCp^*$** to be generated and react as a monomer. An isolable monomeric Al(I) aluminylene, **^{Dipp}NacNacAl**, was isolated in 2000 by Roesky and coworkers, which was stabilised by a bulky β-diketiminate ligand.[44] This compound, featuring an aluminium based lone pair of electrons, can be thought of as an aluminium analogue of an N-heterocyclic carbene.



Schnöckel, 1991 ***Roesky, 2000***

Figure 1.5. *Neutral Al(I) species*

Together, these neutral species have been used in a plethora of transformations of small molecules, performing CO homologation, cycloadditions and C-H bond activation amongst others.[45,46] Most relevant to the topic of this thesis is the fact that they have both been used in the construction of Al–M bonds, which will be discussed in more detail later in the work.

1.2.4 Potential as metalloligands

The properties of the group 13 elements outlined herein make them prime targets for incorporation into bimetallic systems. Their status as excellent Lewis acids is ideal for synergistic Lewis acid assisted activation of bonds. It is known that the relative electropositivity of the group 13 elements makes them good σ-donors, a point which is further discussed in section 1.5. This property has already been shown to be very important, for example, in transition metal catalysed C–H borylation reactions, in which transition metal boryl species are intermediates. A strong *trans* effect, along with the formally vacant p-orbital centred on boron, are key to both C–H bond breaking and C–B bond forming steps in such chemistry. The same properties have led to diverse uses of the boryl ligand in reactions such as E–H activation and CO_2 reduction (**Figure 1.6**).[47–49] The possibility for very polar linkages between group 13 elements and metals

from elsewhere in the Periodic Table means that complexes featuring such units are well primed for the activation of strong, kinetically inert bonds.

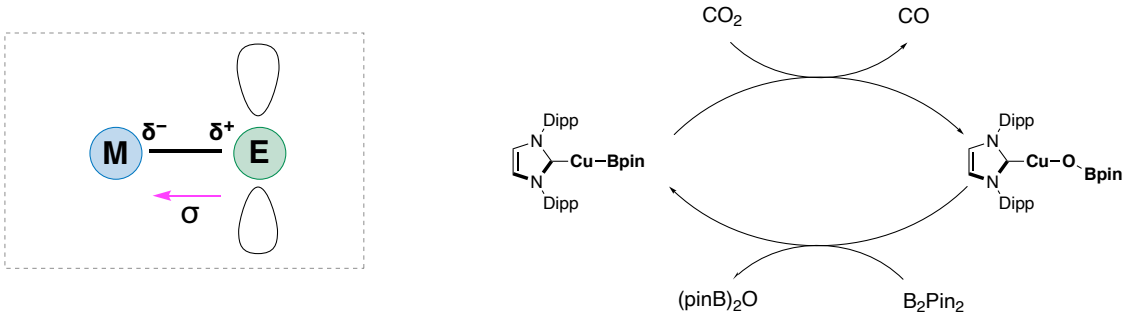


Figure 1.6. *Left: Use of group 13 elements as ligands; Right: CO_2 reduction by a copper boryl complex*

As previously stated, a fundamental concept in organometallic chemistry is the ability of ligands to alter the electronics of metal centres and effect the selectivity of reactions. Group 13 metalloligands expand this concept to a new class of tunable ligands with different properties to traditional carbon or heteroatom based ligands, potentially opening up new reaction modes.

1.3 Coinage metal chemistry

In this work, the bimetallics of interest are complexes which feature a direct, unsupported bond between aluminium and a coinage metal. The coinage metals of group 11, copper, silver and gold, are so called for their historic use as currency. Their relative inertness and lack of susceptibility to oxidation makes them suited to this purpose but their compounds are also active in many areas of chemistry. Interestingly, despite their relative inertness, both Ag and Au form highly active heterogeneous catalysts, where their conducting properties are also valuable.[50] Cationic M(I) complexes are known for their ability to form π-complexes with alkenes and alkynes, a property which will be further explored in Chapter 5.

1.3.1 Properties of the Group 11 metals

The three metals of group 11 are in fact quite different from each other, particularly with respect to their redox chemistry. For first-row copper, the +2 state is most stable and disproportionation of Cu(I) to Cu(0) and Cu(II) is common. Both CuX and CuX_2 (X = halide) species are known, while for silver, which exists primarily as Ag(I), only the photosensitive monohalides are common. Cu(III) is also accessible, with this range of oxidation states making copper suitable for catalytic reactions such as the Chan-Lam and Ullmann C–N coupling reactions.[51] Gold may be found in the +1 or +3 oxidation states, and compounds such as $AuCl_3$ are useful weak acids, but redox chemistry is rare. All three metals in the M(I) state are often found in a two-coordinate, linear geometry, especially when sterically hindered ligands such as NHCs are used.

1.3.2 Gold – a special case

Gold is an outlier in group 11, exhibiting many unusual properties. For example, the ionic radius of gold is in fact marginally smaller than that of silver, a result of the lanthanide contraction.[52,53] Gold also has a much higher electronegativity than either copper or silver (Cu: 1.90, Ag: 1.93, Au: 2.54 on the Pauling scale).[54] This high electronegatively makes it better able to accommodate electron density, and as such, auride anions (Au^-) are chemically feasible (albeit rare).[55] These observations are mostly rationalised on the basis of relativistic effects, resulting from gold's high atomic mass.[56,57] This causes the s-electrons to be more tightly bound and more shielding, while the d-orbitals are more diffuse. Indeed, even the colour of gold arises from relativistic effects. The yellow colour seen is due to transitions between the raised 5d energy levels and lowered 6s orbital based valence band.[58]

1.3.3 Bimetallic Group 11 complexes

Aurophilic interactions are a lesser understood phenomenon whereby Au(I) complexes have a tendency to aggregate, in a similar manner to hydrogen bonding.[59,60] This accounts for the frequent observation of Au–Au distances that are shorter than the sum of the van der Waals radii in both inter and intramolecular systems. Similar concepts of cuprophilicity and argentophilicity have been proposed to explain d^{10}–d^{10} interactions, although they are much less pronounced due to the lesser impact of relativistic effects in these lighter elements. Although binuclear copper compounds are numerous, the assignment of Cu–Cu bonds has been controversial, and the nature of such bonds has attracted much theoretical study. Close silver–silver interactions are known, but no verified covalent bonds. Covalent bonds between gold atoms on the other hand, are more easily prepared but generally limited to Au(II)–Au(II) compounds. A more recent example of an unsupported gold–gold bond in which both gold atoms are in the formal Au(0) state was reported by Bertrand and coworkers in 2013 (**Figure 1.7**).[61] Regarding heterobimetallic complexes, several recent reports describe systems in which gold is bonded to a late transition metal, often with the aid of bridging ligands in clusters.[4] Conversely, silver rarely forms direct covalent bonds to other metals, but may form donor-acceptor complexes with late transition metals such as platinum.[62–65] Many small inter group 11 metal clusters containing d^{10}–d^{10} interactions are known, and used for photophysical applications, but relatively few unsupported M–M bonds exist.[66] A notable example of cooperative reactivity involving copper is the heterolytic B–H bond cleavage across the polar Cu–Fe bond of the bimetallic **[(IDipp)CuFe(Cp)(CO)$_2$]** reported for C–H borylation by Mankad and coworkers (**Figure 1.7**).[67]

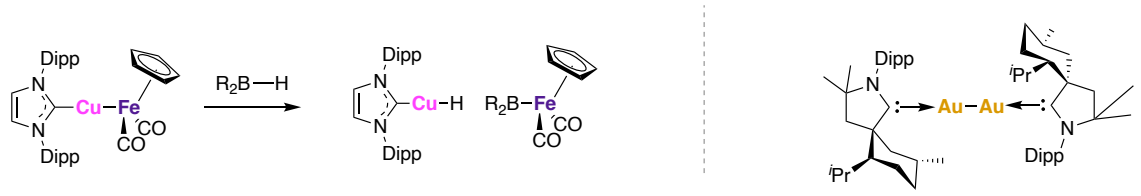


Figure 1.7. *Left: Addition of B–H across a polar Cu–Fe bond; Right: A digold compound supported by CAAC ligands*

The coinage metals have frequently been used as co-catalysts in organic reactions such as the Sonogashira coupling, where they may assist a platinum group metal in C–C bond formation.[15] Likewise, binuclear mechanisms have been elucidated for gold catalysed aminoarylation reactions.[68] The widespread use of the coinage metals, as stoichiometric reagents as well as in catalysis makes them interesting targets for combining with a group 13 metalloligand. Compounds containing such bonds are expected to be polarised in the sense $E^{\delta+}$–$M^{\delta-}$ and as such, have potential for the activation of inert bonds.

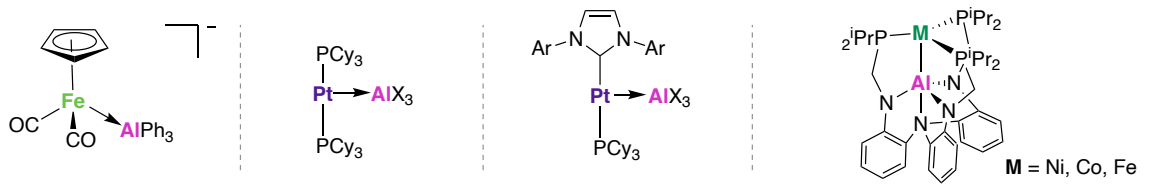
1.4 Aluminium-transition metal bonds

Of the group 13 elements, the least is known about aluminium- transition metal bonds, and so they form the focus of this section. Much of the chemistry outlined in this section has also been widely studied for gallium, and is more developed in that respect. Interest in the area of group 13 – transition metal bonds grew in the 1990s, stemming from interest in both the unusual properties of group 13 metalloligands, and their potential as CVD precursors. There are a number of different strategies for the construction of Al–M bonds, leading to different classes of compounds. Although classification of bonding in Al–M compounds is difficult, we may broadly group the existing examples according to how the Al fragment behaves as a metalloligand: Z-

type (accepts 2 electrons from a metal), L-type (donates 2 electrons to the metal) or X-type (covalent electron sharing bond).[69]

1.4.1 Alanes

As a Lewis acid, aluminium can form adducts with low valent, electron rich metals, such as the early Fe→Al complex **$[Et_4N][(Ph)_3Al–FeCp(CO)_2]$** and the Pt→Al complex **$(Cy_3P)_2Pt–AlCl_3$**.(**Figure 1.8**)[70,71] In such compounds, the aluminium fragment can be considered a Z-type ligand, in which the vacant p-orbital accepts 2 e^- from the transition metal to form with a dative bond. Much work has been done in particular by the Lu group in the use of alane and gallane species as metalloligands. A series of metalloalumatranes based on the tripodal $N(o\text{-}(NHCH_2P(^iPr)_2)C_6H_4)_3$ ligand has been extensively studied, in which an Al(III) centre is ligated by a chelating N-donor scaffold with tethered phosphines bound to the transition metal (**Figure 1.8**). These systems are easily adapted to a range of first row transition metals, and display catalytic activity towards H_2, alkenes and CO_2. However, due to the confinement of the group 13 site within the chelating ligand scaffold, most reactivity occurs at the transition metal site rather than across the M→Al bond. In such a system, the group 13 metal serves to modulate the reactivity of the d-block metal without being directly implicated in bond activation processes.



Burlitch, Hughes, 1979 *Braunschweig, 2007; 2010* *Lu, 2011*

***Figure 1.8**. Examples of M→Al complexes in which Al acts as an electron acceptor*

1.4.2 Donor-acceptor complexes

The aluminium fragment **Cp*Al**, introduced in Section 1.2.3, has found use as an 'exotic' ligand, forming coordination complexes with metals in the s, p, d and f-blocks of the Periodic Table. Upon dissociation of its tetrameric form, **Cp*Al** bears a lone pair of electrons in an Al based σ-orbital (HOMO), allowing it to interact with transition metal d-orbitals and form donor complexes. In such complexes, **Cp*Al** acts as an L-type ligand and is isolobal with PR_3, CO or singlet carbenes (**Figure 1.9**). π-back donation from the metal to Al p-orbitals appears to be limited, particularly in cases where CO ligands are also present, and there is some population of these orbitals by the electrons of the Cp* substituent.[72]

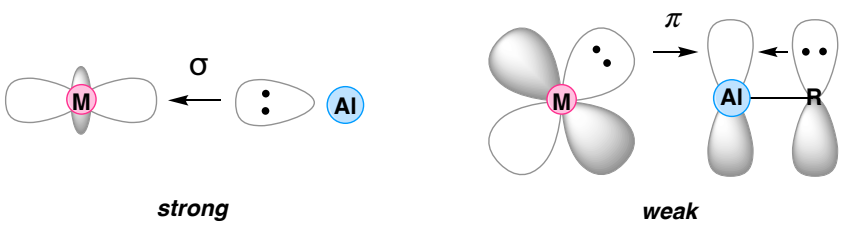
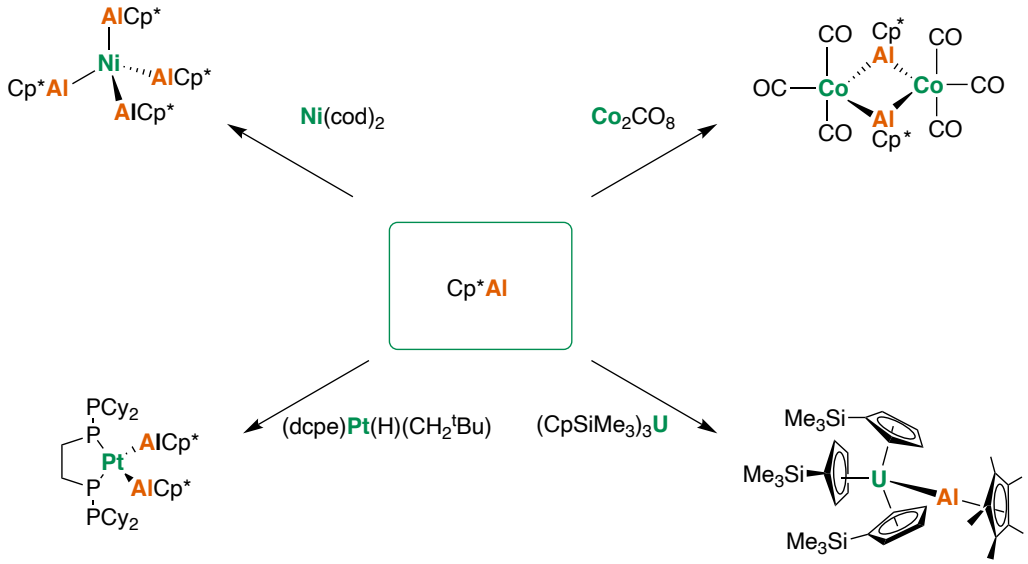


Figure 1.9. *Depiction of the bonding in aluminium diyl complexes consisting of strong donation of the Al lone pair, and weak back donation into a vacant p-orbital*

The groups of Schnöckel, Fischer and Arnold have been prolific in their use of this metalloligand to successfully synthesise a vast number of aluminium donor-acceptor complexes, examples of which are shown in **Scheme 1.2**.[73,74] The first iron-aluminium complex **[(CO)$_4$Fe–AlCp*]** reported in 1997 by Fischer and coworkers was prepared from Al(III) source $[Cp^*AlCl_2]_2$ and the iron nucleophile $K_2[Fe(CO)]_4$, with loss of KCl.[75] It features an unsupported Al–Fe bond of length 2.231(3) Å, shorter than that reported in adduct complexes such as **[Et$_4$N][(Ph)$_3$Al–FeCp(CO)$_2$]** (cf. 2.510(2) Å). The metal-metalloligand interaction in **[(CO)$_4$Fe–AlCp*]** was studied using Charge

Decomposition Analysis, concluding that the Al–Fe bond is best described as donor-acceptor.



Scheme 1.2. *Selected examples of d and f block metal complexes featuring* ***Cp*Al*** *as a ligand*

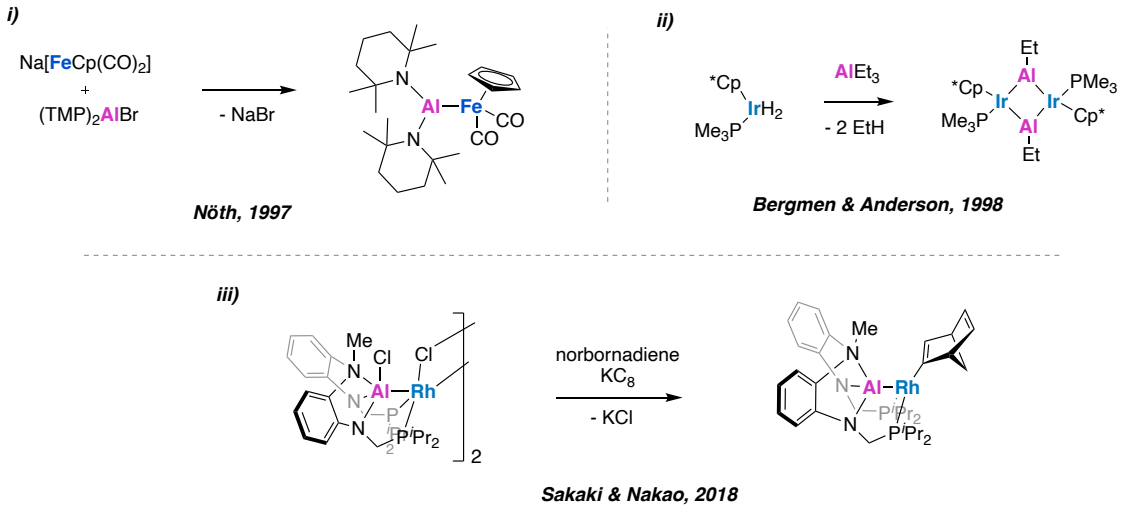
Many routes involve the displacement of a labile CO or olefin ligand as exemplified by the formation of **Ni(Cp*Al)$_4$** from **Cp*Al** and Ni(cod)$_2$. **Ni(AlCp*)$_4$** is unusual in that it does not contain additional supporting ligands apart from Cp*Al, a feature which was initially believed to render it kinetically inert. However, preparation of this homoleptic compound in benzene (rather than the original reaction solvent of hexane), led to C-H activation of benzene, forming a bridging nickel-aluminium hydride complex.[76] Remarkably, using **Cp*Al** it has even been possible to synthesise the first example of an aluminium-actinide bond, as in the U(III) complex reported by Arnold and coworkers.[77]

Use of the **Cp*Al** ligand has led to a myriad of fascinating Al–M bonded species, and their primary application has so far been as molecular precursors for CVD of intermetallic thin films.[78] In this regard, they are highly useful as well defined bimetallic

complexes which have a fixed ratio of aluminium to the chosen transition metal. In such applications, the relatively weak donor-acceptor bond may be advantageous, allowing decomposition at relatively low temperatures. However, this feature also renders onward chemistry challenging and accordingly, little reactivity involving the Al–M bond of such complexes has been reported.

1.4.3 Covalent Al–M bonds

Salt metathesis of a nucleophilic, electron rich metal source and an electropositive metal compound (such as a metal halide) is a simple and common approach used to form polar covalent M–M' bonds.[11,79] In such complexes, the aluminyl fragment is an X-type ligand, which is far less common for aluminium. A notable example synthesised by the metathesis approach, is **[Cp(CO)$_2$Fe−Al(TMP$_2$)]** (**Scheme 1.3**), in which the Al centre is three-coordinate and the Al–Fe bond length (2.450(1) Å) is shorter than the four-coordinate species.[80]



Scheme 1.3. *Synthesis of covalent Al–M bonds by i) nucleophilic attack of an electron rich transition metal on Al(III); ii) alkane elimination; iii) reduction of a supported M→Al bond*

Such three-coordinate aluminyl ligated species are rare; examples include the bridging compound **[Cp*Ir(PMe$_3$)AlEt]$_2$** formed by alkane elimination from an iridium hydride and AlEt$_3$,[81] and a very recent report of a tethered Ir–Al bond formed by iridium insertion into the Al–H bond of an aluminium hydride pincer complex.[82] Further examples of X-type aluminyl metalloligands have very recently emerged, such as an Al–Rh system based on a similar multidentate tethered N,P ligand to that used by the Lu group, which was formed by 2-electron reduction of a preformed dative Al–Rh bond (**Scheme 1.3**).[83,84] In this complex, it is notable that the norbornadiene ligand is projected upwards from the Al–Rh bond, which the authors ascribe to the strong *trans* influence of the aluminyl ligand.

No general procedure for the synthesis of Al–M covalent bonds exists. The metathesis approach has produced several interesting compounds, but it poses a number of limitations. This method necessitates extremely electron rich transition metal partners bearing π-acceptor CO ligands, in order to stabilise the sub-valent metal centre. Therefore the range of compounds that can be made from these precursors is limited. Consideration of this process in reverse i.e. a nucleophilic aluminium source and an electropositive transition metal may be a more productive avenue.

1.5 Anionic group 13 nucleophiles

A fruitful approach to the synthesis of compounds containing a covalent group 13 – metal bond is the use of anionic, low valent group 13 species as precursors. A large number of such anionic group 13 containing N-heterocycles have been developed in the last 20 years, which draw analogies with N-heterocyclic carbenes (NHCs). N-heterocyclic carbene ligands are seemingly ubiquitous in Main Group chemistry for two main reasons: the lone pair of electrons on carbon makes them excellent σ-

donors, capable of stabilising electron deficient species. Furthermore, they are inherently sterically bulky, providing kinetic stabilisation to species prone to oligomerization, and may easily be modified to increase their steric profile.[85,86] Therefore, it is natural that chemists have looked to NHCs as inspiration for new ligands with similar properties. Anionic group 13 heterocycles possess a lone pair of electrons at the group 13 centre, and a formally vacant p-orbital (**Figure 1.10**). This, when combined with a negative charge, allows them to act as nucleophiles towards electropositive metal precursors, thereby constructing covalent E–M bonds (E = Group 13 element) in which the group 13 fragment can be considered as an X-type ligand.

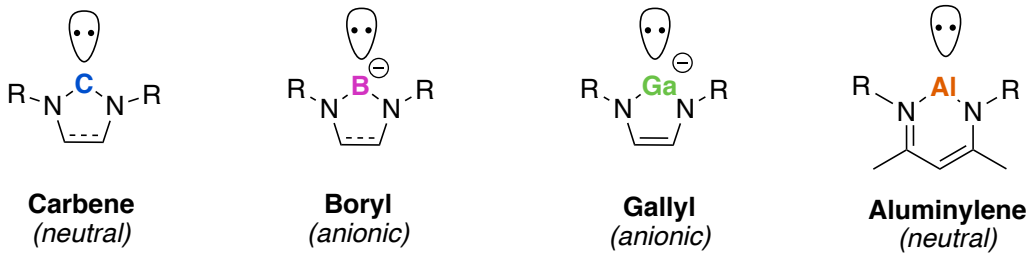
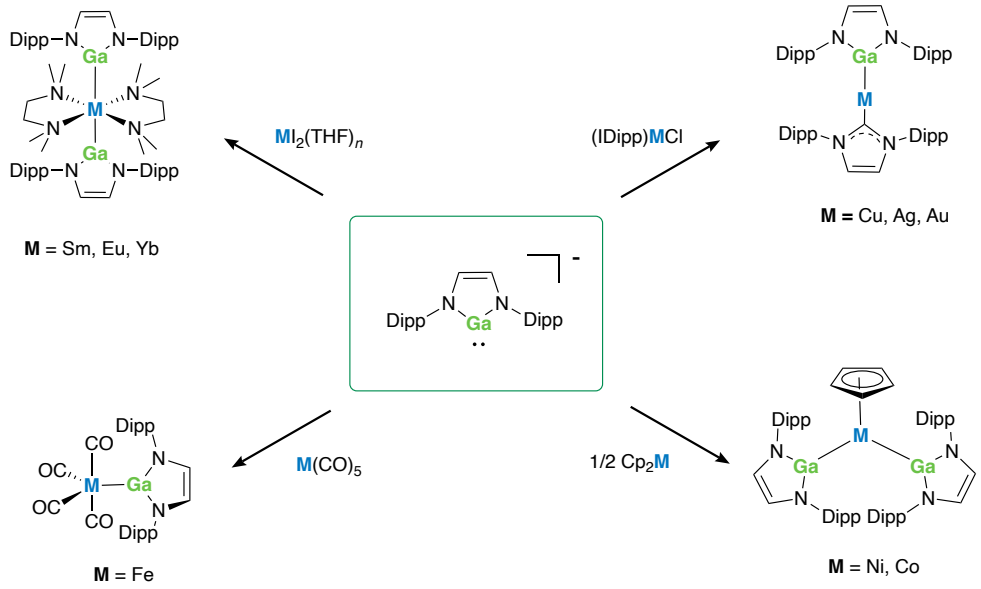


Figure 1.10. *Group 13 analogues of N-heterocyclic carbenes*

1.5.1 Gallyl anion

First reported by Schmidbaur in 1999 and greatly advanced by Jones, a number of Ga(I) N-donor heterocycles have been developed based on 4, 5 or 6-membered rings.[87,88] The most prolific of these in relation to the synthesis of Ga–M bonds is the 5-membered anionic gallyl complex **[Ga(Ar-DAB)]**$^-$ (Ar-DAB = N,N-di*iso*propylaniline diazabutadiene), formed by the potassium reduction of the Ga(III) compound [GaI_2(Ar-DAB$^\bullet$)] in the presence of a chelating ligand such as tmeda or 18-crown-6.[89] The **[Ga(Ar-DAB)]**$^-$ anion has been used extensively to form Ga–M bonds with metals from across all blocks of the Periodic Table, a small selection of which is shown in **Scheme 1.4**.[90–93] Many of these compounds constituted the first examples of such

Ga–M bonds. The reactivity of this Ga(I) heterocycle is diverse, and a range of synthetic methods have been used to prepare the bimetallic species, including salt elimination of KX (X = halide, Cp^-, hydride), displacement of a neutral ligand such as CO and oxidative insertion into a Ga–Ga bond.



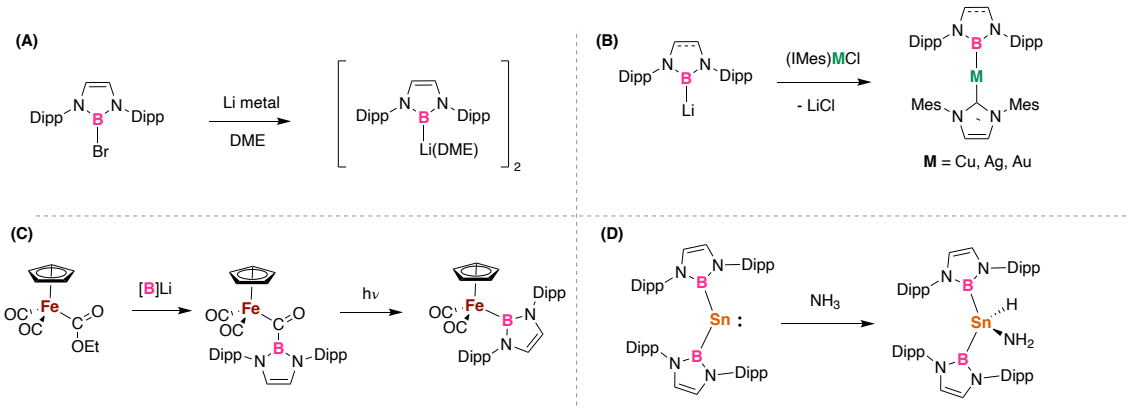
Scheme 1.4. *Complexes featuring a Ga–M bond, formed from the Ga(I) heterocycle [Ga(Ar-DAB)]*

As with the boryl lithium heterocycle **[(Ar-DAB)BLi]** the steric bulk of the Ar-DAB ligand is credited with its ability to stabilise the +1 oxidation state. Studies of the reactivity of Ga–M bonds are few, and it has not achieved the status as a powerful ligand that its lighter boryl cousin enjoys.

1.5.2 Boryl anion

The isolation of 1,3,2-diazaborolyllithium by Yamashita and Nozaki in 2006 was a major breakthrough in low-valent group 13 chemistry. This boryl lithium species is stabilised by sterically bulky Dipp groups, and is a dimer in the solid state, with two boryl lithium fragments bridged by DME molecules (**Scheme 1.5**, **(A)**). **[(Ar-DAB)BLi]** quickly found widespread use as a boryl transfer reagent, and a large number of M–B

species have been formed from it.[94] One such example uses a salt metathesis approach, taking advantage of the nucleophilic boron centre to deliver M–B bonds (M = Cu, Ag, Au) **(B)**.[95] As is expected of a group 13 compound in the formal oxidation state +1, **[(Ar-DAB)BLi]** is highly reducing, and many reactions with metal halides produced elemental metal. In the case of certain d-block compounds, this redox activity could be circumvented by first forming a boryl acyl compound, which could be decarbonylated to form the desired M–B bonded species **(C)**.[96]



Scheme 1.5. *(A) Isolation of a boryl lithium,* ***[(Ar-DAB)BLi]****; (B) Formation of B–M bonds by salt elimination; (C) Formation of B–M bonds by ester decarbonylation; (D) Activation of ammonia by a bisborylstannylene*

The boryl ligand has been used to isolate metals in unusual oxidation states and confer atypical properties onto the metals it is coordinated to. For example, the *bis*borylstannylene compound prepared by Protchenko *et al.* can perform oxidative addition of E-H bonds such as the N–H bond of ammonia **(D)**.[47,97] Such reactivity warrants the pursuit of metal complexes bearing an analogous 'aluminyl' ligand, which would be expected to have equally interesting properties as a metalloligand. Much of the unique reactivity of the boryl ligand has been attributed to its abilities as a σ-donor, which have been shown in experimental and theoretical studies to be greater than that of N-heterocyclic carbenes.[98–101] This donation gives rise to a large observable *trans*

influence. By comparison, spectroscopic studies reveal the gallyl fragment to be a more moderate σ-donor, with a *trans* influence on a par with tertiary phosphines.[102,103] Given these observations, and considering the greater electropositivity of aluminium compared to boron or gallium, it is of great interest to synthesise transition metal complexes bearing an aluminyl fragment, which may be expected to be an even stronger σ-donating ligand.

1.5.3 Nucleophilic aluminium: an aluminyl anion

A roadblock to the development of Al–M bonded complexes has been the paucity of analogous Al(I) anions. The use of Al(III) reagents with nucleophilic transition metal sources relies upon very electron rich transition metal sources stabilised by π-accepting ligands such as CO, curbing the usefulness of such an approach. Although the seminal Al(I) **Cp*Al** complex gave rise to a number of interesting compounds, the labile donor-acceptor bond inhibits further chemistry. Therefore, with a lack of available reagents, the study of Al–M bond reactivity has been limited. Attempts to synthesise an aluminyl anion using similar diazabutadiene ligands as used for boryl and gallyl reagents led only to aluminium metal and protioligand. In 2018, the groups of Aldridge and Goicoechea reported the first example of an Al(I) aluminyl anion, **K_2[Al(NON)]$_2$** (NON = 4,5-bis(2,6-diisopropylanilido)-2,7-di-tert-butyl-9,9-dimethylxanthene) (**Figure 1.11**, **i**)[104]. **K_2[Al(NON)]$_2$** is supported by a diamido xanthene based ligand, featuring a weakly coordinating O atom on the backbone. It is dimeric in both the solid and solution states, with K^+ counterions held in place by π-interactions with the flanking aryl substituents of the ligand. Formed by a 2-electron reduction of the parent Al(III) iodide (NON)AlI using KC_8, this landmark compound bears both a negative charge and a lone pair of electrons centred on aluminium. As

such, and in a reversal of established aluminium reactivity, **K_2[Al(NON)]$_2$** was found to behave as a nucleophilic source of aluminium. Experiments found the potassium aluminyl complex to be capable of oxidatively adding H_2 and C–H activation of benzene, as well as reacting with MeI or MeOTf to form (NON)AlMe, showing that it is indeed an aluminium centred nucleophile. Promisingly, **K_2[Al(NON)]$_2$** could also be combined with the Mg(II) electrophile (^{Mes}NacNac)MgI(OEt)$_2$ to form a complex featuring an unsupported Al–Mg bond (**Figure 1.12**).

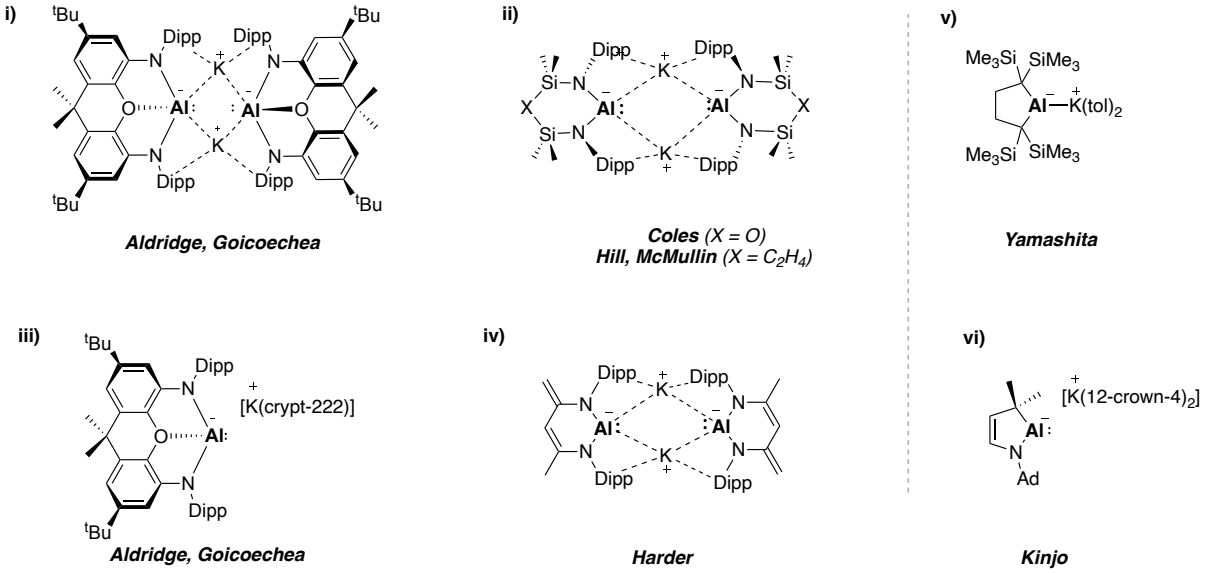


Figure 1.11. *Examples of anionic Al(I) aluminyl complexes. Left: Species based on chelating diamido ligands; Right: monomeric alkyl aluminyl species*

After the isolation of this anionic Al(I) species, a number of other reports quickly followed, many of which were also based on diamido ligands and feature potassium counterions.[105] The group of Coles reported an aluminyl based on a 6-membered ring system in 2019 (**ii**)[106], and a similar 7-membered system was reported by Hill and McMullin in 2020,[107] also prepared by 2 electron reduction of an Al(III) precursor. An interesting example emerged from the Harder group, where an aluminyl anion was generated serendipitously by deprotonation of the ligand backbone of ^{Dipp}NacNacAl

(**iv**). Recent work has expanded the supporting ligand set to include a dialkyl aluminyl species (Yamashita, **v**)[108], and an alkyl-amido aluminyl (Kinjo, **vi**)[109] which is analogous to a cyclic alkyl amido carbene (CAAC).

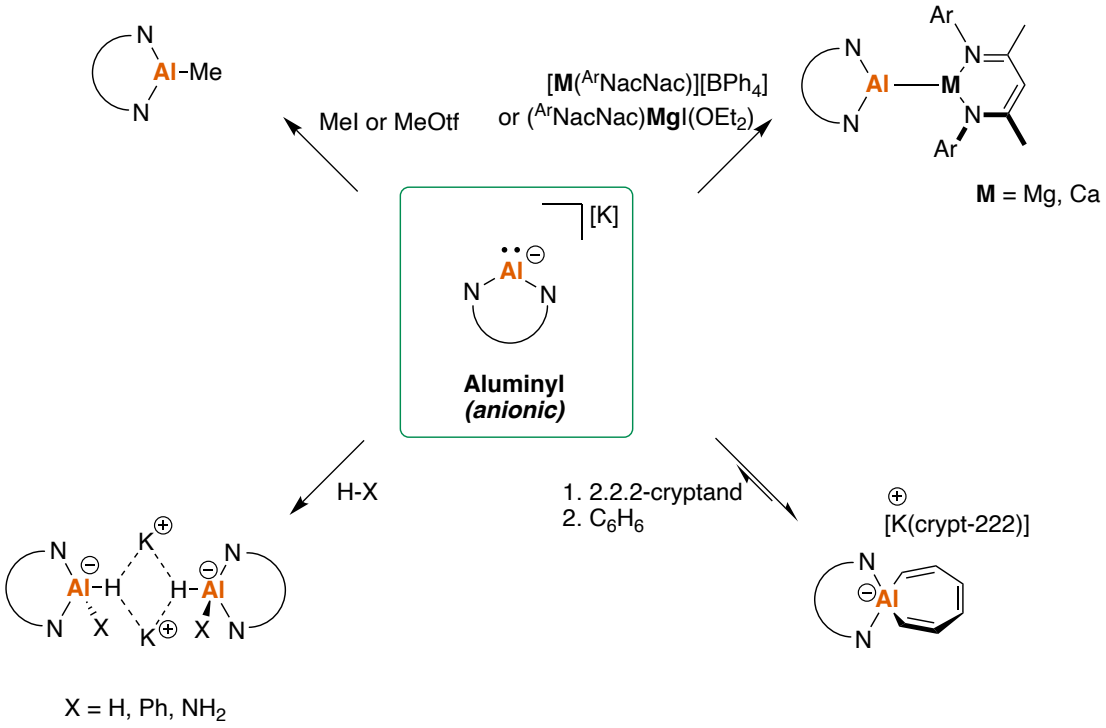


Figure 1.12. *Reactivity of potassium aluminyl species towards electrophiles, E-H bonds and C–C bonds*

It is interesting to note that these compounds are themselves bimetallic, featuring interactions between the Al centre and the alkali metal. Indeed, the role of the second metal has been found to be critical, with a number of papers reporting on variation in structure and reactivity on replacement of the alkali metal with Na, Li, Mg, Ca, Cs or Rb.[107,110–112] Furthermore, sequestration of the potassium from **K_2[Al(NON)]$_2$** by 2.2.2-cryptand produced the charge-separated species (**iii**). This 'naked aluminyl' was found to behave radically differently to its dimeric counterpart, performing cleavage of the C–C bond of benzene instead of C–H activation and suggesting that metal-metal cooperativity may be at play (**Figure 1.12**).[113]

1.6 Project aims and outline

The motivation to study direct bonds between aluminium and group 11 metals is clear, both from the perspective of metal–metal bonding, and the chemistry that arises from it. The aluminyl ligand is likely to be a strong σ-donor, and there is exciting potential for the activation of small molecules across the Al–M bond. Recent advances in low-valent aluminium chemistry have opened up new synthetic avenues to form such complexes, namely the discovery of a nucleophilic Al(I) aluminyl anion. This allows for a salt metathesis process in which aluminium is the nucleophilic partner and the second metal may be a common electrophile such as a metal halide (the reverse of the method described in Section 1.4.3). This work aims to synthesise such aluminyl complexes of the coinage metals, and to investigate the small molecule reactivity that arises from the polarised metal–metal bond. Chapter 3 describes the synthesis of compounds containing direct Al–M (M = Cu, Ag, Au) bonds, using the nucleophilic aluminyl anion **K_2[NON)Al]$_2$**, as the aluminium source and simple coinage metal halide precursors. It will detail the characterisation of these complexes and the differences arising from choice of group 11 metal and supporting ligand. By preparing the gallium analogues of the Al–M bonded species, this work also aims to compare the properties of the aluminyl and gallyl fragments as metalloligands. Moving onto the reactivity of the novel Al–M bonds, Chapter 4 seeks to investigate the behaviour of the metal aluminyl species towards CO_2, a kinetically inert molecule of great environmental interest. Again, the differences in reactivity between the group 11 aluminyl species are studied and rationalised. Chapter 5 expands on the insertion chemistry of Chapter 4, looking at the reactivity of coinage metal aluminyl complexes with alkynes, which are fundamental organic building blocks. The stereo and regioselectivity of the system are studied, and functionalisation reactions which exploit the differing natures of group 11

and group 13 metal centres are investigated. As well as effecting challenging transformations, these reactivity studies aim to probe the nature of the Al–M bond and develop understanding of how small molecules may be activated across a polar heterobimetallic bond.

1.7 References

1 L. Wang, M. Gennari, A. Barrozo, J. Fize, C. Philouze, S. Demeshko, F. Meyer, M. Orio, V. Artero and C. Duboc, *ACS Catal.*, 2020, **10**, 177–186.
2 D. Brazzolotto, M. Gennari, N. Queyriaux, T. R. Simmons, J. Pécaut, S. Demeshko, F. Meyer, M. Orio, V. Artero and C. Duboc, *Nat. Chem.*, 2016, **8**, 1054–1060.
3 L. Que Jr and W. B. Tolman, *Nature*, 2008, **455**, 333–340.
4 P. Buchwalter, J. Rosé and P. Braunstein, *Chem. Rev.*, 2015, 115, 28–126.
5 N. Wheatley and P. Kalck, *Chem. Rev.*, 2002, **99**, 3379–3420.
6 S. Sinhababu, Y. Lakliang and N. P. Mankad, Dalton Trans. 2022, **51**, 6129-6147
7 N. P. Mankad, *Chem. - A Eur. J.*, 2016, **22**, 5822–5829.
8 S. T. Liddle, *Molecular Metal-Metal bonds*, Wiley-VCH Verlag, Weinheim, 2015.
9 R. J. Somerville and J. Campos, *Eur. J. Inorg. Chem.*, 2021, 3488–3498.
10 J. Campos, *Nat. Rev. Chem.*, 2020, **4**, 696–702.
11 L. H. Gade, *Angew. Chemie - Int. Ed.*, 2000, **39**, 2658–2678.
12 T. Nguyen, A. D. Sutton, B. Marcin, J. C. Fettinger, G. L. Long and P. P. Power, *Science*, 2005, **310**, 844–847.
13 U. Radius and F. Breher, *Angew. Chemie - Int. Ed.*, 2006, **45**, 3006–3010.
14 F. Hanusch, L. Groll and S. Inoue, *Chem. Sci.*, 2021, **12**, 2001–2015.
15 D. R. Pye and N. P. Mankad, *Chem. Sci.*, 2017, **8**, 1705–1718.
16 L. Jin, D. R. Tolentino, M. Melaimi and G. Bertrand, *Sci. Adv.*, 2015, 1, **5**, e1500404
17 M. Delferro and T. J. Marks, *Chem. Rev.*, 2011, **111**, 2450–2485.
18 R. A. Collins, A. F. Russell and P. Mountford, *Appl. Petrochemical Res.*, 2015, **5**, 153–171.
19 S. D. Robertson, M. Uzelac and R. E. Mulvey, *Chem. Rev.*, 2019, **119**, 8332–8405.
20 V. A. Pollard, S. A. Orr, R. Mclellan, A. R. Kennedy, E. Hevia and R. E. Mulvey, *Chem. Commun*, 2018, **54**, 1233.
21 V. A. Pollard, M. Á. Fuentes, A. R. Kennedy, R. McLellan and R. E. Mulvey, *Angew. Chemie Int. Ed.*, 2018, **57**, 10651–10655.
22 A. J. Martínez-Martínez, A. R. Kennedy, R. E. Mulvey and C. T. O'Hara, *Science* , 2014, **346**, 834–837.
23 Y. Jia, F. Li, K. Fan and L. Sun, *Adv. Powder Mater.*, 2022, **1**, 100012.
24 I. Mustieles Marin, J. M. Asensio and B. Chaudret, *ACS Nano*, 2021, 15, 3550–3556.
25 S. J. Freakley, Q. He, J. H. Harrhy, L. Lu, D. A. Crole, D. J. Morgan, E. N. Ntainjua, J. K. Edwards, A. F. Carley, A. Y. Borisevich, C. J. Kiely and G. J. Hutchings, *Science.*, 2016, **351**, 965–968.
26 P. Braunsteln, R. Bender and J. Kervennal, *Transit. Met. Clust.*, 1982, **77**, 1065.
27 N. T. Lucas, J. P. Blitz, S. Petrie, R. Stranger, M. G. Humphrey, G. A. Heath and V. Otieno-Alego, *J. Am. Chem. Soc.*, 2002, **124**, 5139–5153.
28 C. L. Daniels, D. L. Mendivelso-Perez, B. A. Rosales, D. You, S. Sahu, J. S. Jones, E. A. Smith, F. P. Gabbaï and J. Vela, *ACS Omega*, 2019, **4**, 5197–5203.
29 R. Ferrando, J. Jellinek and R. L. Johnston, *Chem. Rev.*, 2008, **108**, 845–910.
30 J. P. Coyle, G. Dey, E. R. Sirianni, M. L. Kemell, G. P. A. Yap, M. Ritala, M. Leskelä, S. D. Elliott and S. T. Barry, *Chem. Mater.*, 2013, **25**, 1132–1138.
31 D. W. Stephan, *Acc. Chem. Res.*, 2015, **48**, 306–316.

32 F. G. Fontaine and D. W. Stephan, *Phil. Trans. R. Soc. A.*, 2017, **375**: 20170004
33 S. R. Flynn and D. F. Wass, *ACS Catal.*, 2013, **3**, 2574–2581.
34 S. J. K. Forrest, J. Clifton, N. Fey, P. G. Pringle, H. A. Sparkes and D. F. Wass, *Angew. Chemie - Int. Ed.*, 2015, **54**, 2223–2227.
35 J. Campos, *J. Am. Chem. Soc.*, 2017, **139**, 2944–2947.
36 S. Aldridge and A. J. Downs, *The Group 13 Metals Aluminium, Gallium, Indium and Thallium: Chemical Patterns and Peculiarities*, Wiley, Chichester, 2011.
37 A. G. Massey, *Main Group Chemistry*, John Wiley & Sons, Ltd, Chichester, UK, 2nd edn., 2000.
38 H. Elsen, C. Färber, G. Ballmann and S. Harder, *Angew. Chemie - Int. Ed.*, 2018, **57**, 7156–7160.
39 W. T. Diment, G. L. Gregory, R. W. F. Kerr, A. Phanopoulos, A. Buchard and C. K. Williams, *ACS Catal.*, 2021, **11**, 12532–12542.
40 A. C. Deacy, A. F. R. Kilpatrick, A. Regoutz and C. K. Williams, *Nat. Chem.*, 2020, **12**, 372–380.
41 Y. Zhou, G. S. Nichol and J. A. Garden, *Eur. J. Inorg. Chem.*, 2022, **16**, e202200134..
42 C. Dohmeier, C. Robl, M. Tacke and H. Schnöckel, *Angew. Chemie Int. Ed. English*, 1991, **30**, 564–565.
43 S. Schulz, H. W. Roesky, H. J. Koch, G. M. Sheldrick, D. Stalke and A. Kuhn, *Angew. Chem. Int. Ed*, 1993, **32**, 1729–1731.
44 C. Cui, H. W. Roesky, H. G. Schmidt, M. Noltemeyer, H. Hao and F. Cimpoesu, *Angew. Chemie - Int. Ed.*, 2000, **39**, 4274–4276.
45 M. Zhong, S. Sinhababu and H. W. Roesky, *Dalt. Trans.*, 2020, **49**, 1351–1364.
46 R. Y. Kong and M. R. Crimmin, *J. Am. Chem. Soc.*, 2020, **142**, 11967–11971.
47 A. V. Protchenko, J. I. Bates, L. M. A. Saleh, M. P. Blake, A. D. Schwarz, E. L. Kolychev, A. L. Thompson, C. Jones, P. Mountford and S. Aldridge, *J. Am. Chem. Soc.*, 2016, **138**, 4555–4564.
48 David S. Laitar, and Peter Müller and J. P. Sadighi, *J. Am. Chem. Soc.*, 2005, **127**, 17196–17197.
49 D. S. Laitar, E. Y. Tsui and J. P. Sadighi, *J. Am. Chem. Soc.*, 2006, **128**, 11036–11037.
50 C. W. Corti, R. J. Holliday and D. T. Thompson, *Top. Catal.*, 2007, **44**, 331–343.
51 J. C. Vantourout, H. N. Miras, A. Isidro-Llobet, S. Sproules and A. J. B. Watson, *J. Am. Chem. Soc.*, 2017, **139**, 4769–4779.
52 U. M. Tripathi, A. Bauer and H. Schmidbaur, *J. Chem. Soc. - Dalt. Trans.*, 1997, 2865–2868.
53 A. Bayler, A. Schier, G. A. Bowmaker and H. Schmidbaur, *J. Am. Chem. Soc*, 1996, **118**, 7006–7007.
54 T. Andersen, H. K. Haugen and H. Hotop, *J. Phys. Chem. Ref. Data*, 1999, **28**, 1511–1533.
55 M. Jansen, *Chem. Soc. Rev.*, 2008, **37**, 1826–1835.
56 P. Pyykkö, *Annu. Rev. Phys. Chem.*, 2012, **63**, 45–64.
57 P. Schwerdtfeger, *Heteroat. Chem.*, 2002, **13**, 578–584.
58 N. Bartlett, *Gold Bull.*, 1998, **31**, 22–25.
59 H. Schmidbaur and A. Schier, *Chem. Soc. Rev.*, 2012, **41**, 370–412.
60 H. Schmidbaur, *Gold Bull.*, 2000, **33**, 3–10.
61 D. S. Weinberger, M. Melaimi, C. E. Moore, A. L. Rheingold, G. Frenking, P. Jerabek and G. Bertrand, *Angew. Chemie - Int. Ed.*, 2013, **52**, 8964–8967.
62 T. G. Gray and J. P. Sadighi, in *Molecular Metal-Metal bonds*, ed. S. T. Liddle,

Wiley-VCH Verlag, Weinheim, 2015, p. 397.
63 P. Buchwalter, J. Rosé and P. Braunstein, *Chem. Rev.*, 2014, **115**, 28–126.
64 R. Usón and J. Forniés, *Inorganica Chim. Acta*, 1992, **198**–**200**, 165–177.
65 A. Erxleben and B. Lippert, *J. Chem. Soc. - Dalt. Trans.*, 1996, 2329–2333.
66 S. Sculfort and P. Braunstein, *Chem. Soc. Rev.*, 2011, **40**, 2741–2760.
67 T. J. Mazzacano and N. P. Mankad, *J. Am. Chem. Soc.*, 2013, **135**, 17258–17261.
68 W. E. Brenzovich, D. Benitez, A. D. Lackner, H. P. Shunatona, E. Tkatchouk, W. A. Goddard and F. D. Toste, *Angew. Chemie - Int. Ed.*, 2010, **49**, 5519–5522.
69 M. L. H. Green, *J. Organomet. Chem.*, 1995, **500**, 127–148.
70 H. Braunschweig, P. Brenner, A. Müller, K. Radacki, D. Rais and K. Uttinger, *Chem. - A Eur. J.*, 2007, **13**, 7171–7176.
71 J. M. Burlitch, M. E. Leonowicz, R. B. Petersen and R. E. Hughes, *Inorg. Chem*, 1979, **18**, 1097–1105.
72 J. Uddin and G. Frenking, *J. Am. Chem. Soc.*, 2001, **123**, 1683–1693.
73 C. Üffing, A. Ecker, R. Köppe and H. Schnöckel, *Organometallics*, 1998, **17**, 2373–2375.
74 D. Weiss, T. Steinke, M. Winter, R. A. Fischer, N. Fröhlich, J. Uddin and G. Frenking, *Organometallics*, 2000, **19**, 4583–4588.
75 J. Weiss, D. Stetzkamp, B. Nuber, A. Fischer, Roland, C. Boehme and G. Frenking, *Angew. Chem. Int. Ed.*, 1997, **36**, 70–72.
76 T. Steinke, C. Gemel, M. Cokoja, M. Winter and R. A. Fischer, *Angew. Chem. Int. Ed. Engl.*, 2004, **43**, 43.
77 S. G. Minasian, L. Krinsky, Jamin, V. A. Williams and J. Arnold, *J. Am. Chem. Soc.*, 2008, **130**, 10086–10087.
78 S. González-Gallardo, T. Bollermann, R. A. Fischer and R. Murugavel, *Chem. Rev.*, 2012, **112**, 3136–3170.
79 U. Jayarathne, T. J. Mazzacano, S. Bagherzadeh and N. P. Mankad, *Organometallics*, 2013, **32**, 3986–3992.
80 B. N. Anand, I. Krossing and H. Nöth, *Inorg. Chem.*, 1997, **36**, 1979–1981.
81 J. T. Golden, T. H. Peterson, P. L. Holland, R. G. Bergman and R. A. Andersen, *J. Am. Chem. Soc.*, 1998, **120**, 223–224.
82 S. Morisako, S. Watanabe, S. Ikemoto, S. Muratsugu, M. Tada and M. Yamashita, *Angew. Chemie Int. Ed.*, 2019, **58**, 15031–15035.
83 N. Hara, T. Saito, K. Semba, N. Kuriakose, H. Zheng, S. Sakaki and Y. Nakao, *J. Am. Chem. Soc.*, 2018, **140**, 7070–7073.
84 I. Fujii, K. Semba, Q.-Z. Li, S. Sakaki and Y. Nakao, *J. Am. Chem. Soc*, 2020, **142**, 11647–11652.
85 V. Nesterov, D. Reiter, P. Bag, P. Frisch, R. Holzner, A. Porzelt and S. Inoue, *Chem. Rev.*, 2018, **118**, 9678–9842.
86 M. N. Hopkinson, C. Richter, M. Schedler and F. Glorius, *Nature*, 2014, **510**, 485–496.
87 M. Asay, C. Jones and M. Driess, *Chem. Rev.*, 2011, **111**, 354–396.
88 R. J. Baker and C. Jones, *Coord. Chem. Rev.*, 2005, **249**, 1857–1869.
89 R. J. Baker, R. D. Farley, C. Jones, M. Kloth and D. M. Murphy, *J. Chem. Soc. Dalt. Trans.*, 2002, 3844–3850.
90 C. Jones, D. P. Mills, R. P. Rose, A. Stasch and W. D. Woodul, *J. Organomet. Chem.*, 2010, **695**, 2410–2417.
91 S. T. Liddle, J. McMaster, D. P. Mills, A. J. Blake, C. Jones and W. D. Woodul, *Angew. Chemie Int. Ed.*, 2009, **48**, 1077–1080.

92 C. Jones, A. Stasch and W. D. Woodul, *Chem. Commun.*, 2009, 113–115.
93 R. J. Baker, C. Jones and D. M. Murphy, *Chem. Commun.*, 2005, 1339–1341.
94 L. Weber, *Eur. J. Inorg. Chem.*, 2017, 3461–3488.
95 Y. Segawa, M. Yamashita and K. Nozaki, *Angew. Chemie Int. Ed.*, 2007, **46**, 6710–6713.
96 R. Frank, J. Howell, R. Tirfoin, D. Dange, C. Jones, D. M. P. Mingos and S. Aldridge, *J. Am. Chem. Soc.*, 2014, **136**, 15730–15741.
97 A. V. Protchenko, K. H. Birjkumar, D. Dange, A. D. Schwarz, D. Vidovic, C. Jones, N. Kaltsoyannis, P. Mountford and S. Aldridge, *J. Am. Chem. Soc.*, 2012, **134**, 6500–6503.
98 W. H. Lam, K. C. Lam, Z. Lin, S. Shimada, R. N. Perutz and T. B. Marder, *J. Chem. Soc. Dalt. Trans.*, 2004, **4**, 1556–1562.
99 J. Zhu, Z. Lin and T. B. Marder, *Inorg. Chem.*, 2005, **44**, 9384–9390.
100 G. Sivignon, P. Fleurat-Lessard, J. M. Onno and F. Volatron, *Inorg. Chem.*, 2002, **41**, 6656–6661.
101 H. Niu, R. J. Mangan, A. V Protchenko, N. Phillips, W. Unkrig, C. Friedmann, E. L. Kolychev, R. Tirfoin, J. Hicks and S. Aldridge, *Dalt. Trans.*, 2018, **47**, 7445–7455.
102 S. P. Green, C. Jones, D. P. Mills and A. Stasch, *Organometallics*, 2007, **26**, 3424–3430.
103 A. Stasch, R. P. Rose, D. P. Mills and C. Jones, *J. Chem. Soc. Dalt. Trans*, 2008, 4372–4386.
104 J. Hicks, P. Vasko, J. M. Goicoechea and S. Aldridge, *Nature*, 2018, **557**, 92–95.
105 J. Hicks, P. Vasko, J. M. Goicoechea and S. Aldridge, *Angew. Chemie Int. Ed.*, 2021, **60**, 1702–1713.
106 R. J. Schwamm, M. D. Anker, M. Lein and M. P. Coles, *Angew. Chemie Int. Ed.*, 2019, **58**, 1489–1493.
107 R. J. Schwamm, M. P. Coles, M. S. Hill, M. F. Mahon, C. L. McMullin, N. A. Rajabi and A. S. S. Wilson, *Angew. Chemie Int. Ed.*, 2020, **59**, 3928–3932.
108 S. Kurumada, S. Takamori and M. Yamashita, *Nat. Chem. 2019 121*, 2019, **12**, 36–39.
109 K. Koshino and R. Kinjo, *J. Am. Chem. Soc.*, 2020, jacs.0c03179.
110 M. Roy, J. Hicks, A. Heilmann, A. M. Baston, P. Vasko, J. Goicoechea and S. Aldridge, *Angew. Chemie Int. Ed.*, 2021, anie.202109416.
111 M. J. Evans, M. D. Anker, C. L. McMullin, S. E. Neale and M. P. Coles, *Angew. Chemie - Int. Ed.*, 2021, **60**, 22289–22292.
112 T. X. Gentner, M. J. Evans, A. R. Kennedy, S. E. Neale, C. L. McMullin, M. P. Coles and R. E. Mulvey, *Chem. Commun.*, 2022, **58**, 1390–1393.
113 J. Hicks, P. Vasko, J. M. Goicoechea and S. Aldridge, *J. Am. Chem. Soc.*, 2019, **141**, 11000–11003.

Chapter 2 : Experimental Methods

2.1 Manipulation of air sensitive compounds

Most of the compounds in this thesis are highly air and moisture sensitive. Manipulation of these compounds was enabled by use of a Schlenk line or inert atmosphere glovebox. A Schlenk line is a dual vacuum-inert gas manifold consisting of two manifolds connected by double oblique glass stopcocks. One manifold is connected to the inert gas supply (argon in this case) at one end and vented through a mercury bubbler at the other. The second manifold is connected to a high vacuum pump, *via* a liquid nitrogen-cooled trap, and monitored using a pressure gauge, showing that pressure was maintained at *ca*. $2x10^{-2}$ mbar. This set up allows vessels attached *via* tubing to be easily placed under vacuum or argon. All glassware used was dried overnight in a 200 °C oven, or flame dried using a Bunsen burner. Glassware was kept oxygen free by connecting to the Schlenk line and undertaking at least three cycles of vacuum pumping to *ca.* $4x10^{-2}$ mbar and refilling with argon. Liquid transfer was by cannula or syringe.

A glovebox, maintained under a nitrogen atmosphere, was used for the storage and manipulation of air and moisture sensitive solids. The atmosphere was purified with an activated copper catalyst and 4 Å molecular sieves.

2.2 Spectroscopy and analytical techniques

2.2.1 NMR spectroscopy

NMR spectra were measured on a 400MHz Bruker Avance III HD nanobay NMR spectrometer equipped with a 9.4 T magnet, a 500MHz Bruker Avance III NMR spectrometer equipped with a 11.75 T magnet or a 600 MHz Bruker NEO 600 NMR spectrometer with broadband helium cryoprobe. NMR spectra were measured at ambient temperature and referenced internally to residual protio-solvent (^{1}H) or solvent (^{13}C) resonances and are reported relative to tetramethylsilane (δ = 0 ppm). ^{31}P resonances are referenced externally to H_3PO_4 (85 %). Assignments were confirmed using two-dimensional ^{1}H-^{1}H and ^{13}C-^{1}H NMR correlation experiments. Chemical shifts are quoted in δ (ppm) and coupling constants in Hz. Dry deuterated solvents were obtained by stirring over CaH_2 before distillation under reduced pressure and degassing with three freeze-pump-thaw cycles. Air and moisture sensitive samples were prepared under inert atmosphere in 5 mm Wilmad 507-PP tubes fitted with J. Youngs valves.

2.2.2 IR spectroscopy

IR spectra were measured on a Shimadzu FT-IR Spirit spectrometer equipped with an attenuated total reflectance (ATR) surface, contained in a dinitrogen glovebox, with assistance from Dr. Bradley Cowley of the Williams group.

2.2.3 Mass spectrometry

ESI-MS measurements were run on an Agilent 6120 bench-top single quadrupole instrument. Samples were prepared as dilute solutions in acetonitrile.

2.2.4 Elemental analysis

Elemental analyses were either carried out by London Metropolitan University or Elemental Microanalysis, Devon, UK. Air and moisture sensitive samples were packed in a sealed glass capillary under argon or in a vial within a vial, sealed with Parafilm, under nitrogen. Considerable difficulty was encountered in obtaining elemental analysis results for the phosphorus containing compounds in this thesis, particularly those run at Elemental Microanalysis, Devon. Results returned systematically low in carbon, a phenomenon which is known for phosphorus containing samples.[1,2]

2.2.5 DFT calculations

The quantum chemical studies were carried out by Xianlu Cui and Professor Lili Zhao of the Nanjing Technical University, alongside Professor Gernot Frenking of Philipps-Universität Marburg. Geometry optimizations were carried out using the Gaussian 16 program[3] with the BP86[4,5] functional and the def2-SVP basis set.[6–8] The energetics were further improved by using the larger basis set def2-TZVPP, and dispersion corrections by Grimme with Becke-Johnson damping D3(BJ).[9–11] Solvation effects were taken into account using the SMDmodel,[8] model using the experimentally used solvent benzene, denoted as the BP86+D3(BJ)/def2-TZVPP (SMD, solvent = benzene) //BP86/def2-SVP level.[4,12] Intrinsic reaction coordinate (IRC)[13] calculations were conducted to verify the critical reaction steps. Electronic energies without ZPE corrections are also given for reference in the related schemes. The structures were illustrated using CYLview.

2.2.6 X-ray crystallography

Single-crystal X-ray diffraction data were collected using an Oxford Diffraction Supernova dual-source diffractometer equipped with a 135 mm Atlas CCD area detector. Crystals were selected under Paratone-N oil, mounted on Micromount loops and quench-cooled using an Oxford Cryosystems open flow N_2 cooling device.[14] Data were collected at 150 K using mirror monochromated Cu (λ = 1.5418 Å) or Mo (λ = 0.71073 Å) K_α radiation. All crystallographic data were processed using the CrysAlisPro package,[15] including unit cell parameter refinement and inter-frame scaling (which was carried out using SCALE3 ABSPACK within CrysAlisPro). Equivalent reflections were merged and diffraction patterns processed with the CrysAlisPro suite. Structures were subsequently solved using ShelXT 2018 and refined on F^2 using the ShelXL 2018 package and XSeed.[16,17]

***Table 2.1**. Crystallographic and refinement parameters*

	2	**2'-Au**	**3'**
Formula	$C_{97}H_{131}Al_2CuKN_4O_2$	$C_{91}H_{112}Au2GaIN_2O_3P_2$	$C_{73}H_{105}AgGaN_2OP$
M_r	1541.65	1934.31	1235.14
Cell setting	Triclinic	Monoclinic	Triclinic
Space group	*P-1*	$P2_1/n$	*P*-1
a/Å	12.8390(3)	20.1770(3)	12.8040(6)
b/Å	18.1142(3)	16.9968(3)	14.3764(5)
c/Å	22.4774(5)	25.6615(4)	20.7258(7)
α/°	97.788(2)	90	82.027(3)
β/°	101.490(2)	107.076(2)	72.271(3)
γ/°	107.207(2)	90	70.022(4)
V/Å^3	4786.76(18)	8412.5(2)	3412.7(3)
Z	2	4	2
Indep. reflections	19763	21215	17762
R_{int}	0.037	0.0471	0.0248
Parameters	1147	939	715
R_1 (all data/$I > 2s(I)$)	0.0686/0.0556	0.0644/0/0407	0.0586/0.0407
wR_2 (all data/$I > 2s(I)$)	0.1750/0.1600	0.0838/0/0644	0.1005/0.0904
GooF	1.033	1.032	1.023
Residual max/min	1.40/–0.46	1.34/–1.68	0.90/–0.65
T/K	150(2)	150(2)	150(2)
CCDC Deposition No.	2085387	–	2085388

	$(Ph_3P)_4Cu_4I_2$	**3'-Au**	**5-Ag**
Formula	$C_{74}H_{65}P_4Cu_4I_2O_{0.5}$	C65H95AuGaN2OP	$C_{71}H_{115}AgAlN_4OP$
M_r	1594.1	1218.08	1206.48
Cell setting	Monoclinic	Monoclinic	Orthorhombic
Space group	*C2/c*	*P21/n*	$P2_12_12_1$
a/Å	13.5914(3)	12.1873(2)	17.30440(10)
b/Å	19.1763(3)	31.9227(7)	18.14880(10)
c/Å	27.3025(5)	33.2494(6)	22.24090(10)
α/°	90	90	90
β/°	102.636(2)	97.741(2)	90
γ/°	90	90	90
V/Å^3	6943.6(2)	12817.8(4)	6984.86(6)
Z	4	8	4
Indep. reflections	7154	26463	14559
R_{int}	0.0231	0.0959	0.0373
Parameters	418	1305	791
R_1 (all data/$I > 2s(I)$)	0.0367/0.0317	0.1267/0.0890	0.0322/0.0308
wR_2 (all data/$I > 2s(I)$)	0.0894/0.0856	0.2408/0.2153	0.0813/0.0800
GooF	1.047	1.082	1.043
Residual max/min	1.27/–0.39	8.65/–1.93	0.322/–0.40
T/K	150(2)	150(2)	150(2)
CCDC Deposition No.	2085394	–	2085389

	5-Cu	**6-Ag**	**6-Cu**
Formula	$C_{78}H_{117}AlCuN_4OP$	$C_{75}H_{104}AgAlN_2O_4P$	$C_{150}H_{202}Al_2Cu_2N_4O_8P_2$
M_r	1248.24	1263.42	2432.12
Cell setting	Monoclinic	Triclinic	Triclinic
Space group	$P2_1/n$	$P\bar{1}$	$P\bar{1}$
a/Å	12.6572(4)	13.0018(4)	13.0313(4)
b/Å	19.3809(6)	15.7611(7)	15.8057(7)
c/Å	30.2695(12)	19.2597(10)	18.8852(9)
α/°	90	113.433(4)	112.876(4)
β/°	98.787(4)	99.104(3)	98.229(3)
γ/°	90	91.609(3)	92.821(3)
V/Å^3	7338.2(4)	3557.5(3)	3522.6(3)
Z	4	2	1
Indep. reflections	15157	14719	14058
R_{int}	0.0779	0.1058	Twin model
Parameters	949	813	847
R_1 (all data/$I > 2s(I)$)	0.1236/0.0790	0.1077/0.0615	0.1523/0.0976
wR_2 (all data/$I > 2s(I)$)	0.2153/0.1856	0.1768/0.1427	0.3033/0.2468
GooF	1.031	1.061	1.002
Residual max/min	0.80/–0.42	1.07/–1.17	1.33/–0.48
T/K	150(2)	150(2)	150(2)
CCDC Deposition No.	2085390	2085391	2085392

	7-Ag	**9**	**10-Et**
Formula	$C_{66}H_{103}AgAlN_4O_2P$	$C_{79}H_{109}AgAlN_2O_2P$	$C_{79}H_{115}AlCuN_2OP$
M_r	1150.34	1284.5	1230.21
Cell setting	Monoclinic	Monoclinic	Triclinic
Space group	$P2_1/c$	$P2_1/n$	*P-1*
a/Å	14.3910(8)	17.0250(3)	12.6157(4)
b/Å	19.5868(6)	20.9243(3)	15.1843(5)
c/Å	26.9617(9)	20.0861(4)	20.1243(7)
α/°	90	90	75.776(3)
β/°	102.038(5)	90.876(2)	78.631(3)
γ/°	90	90	84.115(3)
V/Å^3	7432.7(5)	7154.6(2)	3657.6(2)
Z	4	*4*	2
Indep. reflections	15310	14897	15110
R_{int}	0.051	0.0444	0.0477
Parameters	705	797	795
R_1 (all data/$I > 2s(I)$)	0.1053/0.0920	0.0860/0.0785	0.0800/0.0630
wR_2 (all data/$I > 2s(I)$)	0.2760/0.2628	0.2342/0.2266	0.1889/0.1713
GooF	1.028	1.060	1.046
Residual max/min	0.87/–0.243	1.95/–1.19	1.81/–0.64
T/K	150(2)	150(2)	150(2)
CCDC Deposition No.	2085393	–	2157971

	11-Pr,Ph	**11-Ph**	**12-Et**
Formula	$C_{76}H_{115}AlCuN_2OP$	$C_{80}H_{104}AlCuN_2OP$	$C_{69}H_{106}AlCuN_2O_2P$
M_r	1194.18	1231.14	1117.04
Cell setting	Triclinic	Monoclinic	Monoclinic
Space group	*P-1*	$P2_1/n$	$P2_1/n$
a/Å	13.2005(7)	13.51320(10)	13.8505(2)
b/Å	13.5410(10)	25.3595(2)	23.4691(4)
c/Å	22.7180(11)	21.04280(10)	20.3996(3)
α/°	97.054(5)	90	90
β/°	94.267(4)	92.0510(10)	92.351(2)
γ/°	115.698(6)	90	90
V/Å^3	3594.3(4)	7206.50(9)	6625.49(18)
Z	2	4	4
Indep. reflections	14807	14989	13709
R_{int}	0.0477	0.0397	0.0314
Parameters	822	831	773
R_1 (all data/$I > 2s(I)$)	0.1628/0.1253	0.0610/0.0535	0.0539/0.0426
wR_2 (all data/$I > 2s(I)$)	0.3547/0.3156	0.1529/0.1451	0.1211/0.1115
GooF	1.217	1.03	1.031
Residual max/min	3.17/–0.78	1.27/–0.93	0.65/–0.54
T/K	150(2)	150(2)	150(2)
CCDC Deposition No.	2157972	–	2157973

	12-Pr,Ph	**(NON)Al-Et**	**10-Et-CO_2**
Formula	$C_{71}H_{101}AlCuN_2O_2P$	$C_{52}H_{74}AlN_2O$	$C_{66}H_{98}AlCuN_2O_3P$
M_r	1864.66	770.11	1069.88
Cell setting	Triclinic	Triclinic	Orthorhombic
Space group	*P-1*	*P-1*	*Pbca*
a/Å	12.1884(2)	13.0581(5)	22.7343(12)
b/Å	17.4389(4)	13.3038(7)	24.6009(11)
c/Å	19.4541(5)	14.3490(5)	25.2041(9)
α/°	71.108(2)	99.705(4)	90
β/°	79.692(2)	104.191(3)	90
γ/°	80.746(2)	98.075(4)	90
V/Å^3	3825.54(16)	2338.58(18)	14096.3(11)
Z	2	2	8
Indep. reflections	15832	9701	14333
R_{int}	0.0262	0.0303	0.2342
Parameters	791	554	675
R_1 (all data/$I > 2s(I)$)	0.0475/0.0409	0.0558/0.0430	0.3828/0.2612
wR_2 (all data/$I > 2s(I)$)	0.1148/0.1084	0.1187/0.1091	0.6378/0.5478
GooF	1.043	1.028	1.377
Residual max/min	0.52/-0.46	0.38/–0.32	1.24/−1.21
T/K	150(2)	150(2)	150(2)
CCDC Deposition No.	2157974	2157976	–

2.3 Preparation of starting materials

2.3.1 Purification of solvents

Dry solvents were obtained by passing through a column of the appropriate drying agent using a commercially available MBRAUN Solvent Purification System (SPS) and were degassed by sparging with argon. Solvents were stored in J. Young's tap glass ampoules over a potassium mirror, sodium mirror or 4 Å molecular sieves.

2.3.2 Starting materials

Starting materials were purchased from the commercial suppliers listed and used as received unless otherwise stated below.

Table 2.2. *Supplier and purification methods for reagents used*

Reagent	Source	Purification
CuI	Sigma Aldrich	Used as received
AgI	Alfa Aesar	Used as received
P^tBu_3	Sigma Aldrich	Used as received
PPh_3	Sigma Aldrich	Used as received
PCy_3	Sigma Aldrich	Used as received
$^{13}CO_2$	Sigma Aldrich	Used as received
CO	BOC	Transferred from a cylinder and stored in an ampoule over P_2O_5
CO_2	BOC	Used as received
cyclohexylcarbodiimide	Sigma Aldrich	Used as received
1-phenyl-1-pentyne	Alfa Aesar	Stored over 4 Å molecular sieves
1-phenyl-1-butyne	Alfa Aesar	Stored over 4 Å molecular sieves
diphenylacetylene	Sigma Aldrich	Used as recieved
3-hexyne	Alfa Aesar	Stored over 4 Å molecular sieves
di*iso*propylcarbodiimide	Sigma Aldrich	Distilled over CaH_2 and stored over 4 Å molecular sieves

The potassium aluminyl, **K_2[(NON)Al_2]** (**I**) was prepared according to the literature procedure of Hicks *et al*.[18] A modified version of the procedure reported in the same paper for the synthesis of potassium gallyl **K_2[(NON)Ga_2]** (**II**) was used, as adapted by Megan Edwards of the Aldridge group:

To a stirred solution of (NON)GaI in THF (500 mg, 0.57 mmol) at −78°C was added potassium naphthalenide (195 mg, 1.10 mol) in THF (10 mL), portionwise. The reaction was allowed to warm to room temperature and stirred for 1 h, after which time a pale yellow solution with a white precipitate formed. The reaction mixture was filtered and the volatiles removed *in vacuo.* The solid was washed with pentane, giving **II** as a pale yellow solid (400 mg, 89 %).

Potassium naphthaledide was prepared according to literature procedure.[19]

The coinage metal phosphine halides Ph_3PAgI, Ph_3PCuI, $^tBu_3PAgI$, $^tBu_3PCuI$ and Cy_3PAgI were prepared by the same general method based on the procedure of Goel and Beauchamp.[20,21]

R_3PMI (M = Ag, Cu; R = P^tBu_3, PPh_3, PCy_3)

To a solution of MI (1 eq) in an aqueous KI solution was added a solution of PR_3 (1 eq) in diethyl ether. The resulting biphasic mixture was stirred at room temperature for 1 h, during which time a white precipitate formed. The product was collected by vacuum filtration and washed sequentially with cold aqueous KI and diethyl ether before drying under vacuum.

NB: AgI is light sensitive and was handled in glassware wrapped in aluminium foil.

$^tBu_3PAuI$ and Ph_3PAuI were prepared by Dr Jamie Hicks according to the procedure of Schmidbaur and coworkers.[22]

2.4 References

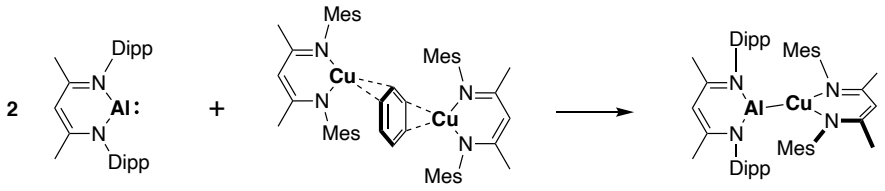
1 M. M. D. Roy, A. Heilmann, M. A. Ellwanger and S. Aldridge, *Angew. Chemie - Int. Ed.*, 2021, **60**, 26550–26554.
2 P. Beck, in *Organic Phosphorus Compounds*, eds. G. M. Kosalapoff and L. Maier, Wiley, New York, 2nd edn., 1972, p. 207.
3 M. J. T. Frisch, S. H. B., G. E. Scuseria, M. A. Robb, J. R. Cheeseman, G. Scalmani, V. Barone, B. Mennucci, G. A. Petersson, H. Nakatsuji, M. Caricato, X. Li, H. P. Hratchian, A. F. Izmaylov, J. Bloino, G. Zheng and J. Sonnenberg, 2009.
4 S. Grimme, S. Ehrlich and L. Goerigk, *J. Comput. Chem.*, 2011, **32**, 1456–1465.
5 A. D. Becke, *Phys. Rev. A*, 1988, **38**, 3098–3100.
6 J. P. Perdew, *Phys. Rev. B*, 1986, **33**, 8822–8824.
7 Y. Zhao and D. G. Truhlar, *Theor. Chem. Acc.*, 2008, **120**, 215–241.
8 A. V Marenich, C. J. Cramer and D. G. Truhlar, *J. Phys. Chem. B*, 2009, **113**, 6378–6396.
9 F. Weigend, *Phys. Chem. Chem. Phys.*, 2006, **8**, 1057–1065.
10 F. Weigend, M. Häser, H. Patzelt and R. Ahlrichs, *Chem. Phys. Lett.*, 1998, **294**, 143–152.
11 F. Weigend and R. Ahlrichs, *Phys. Chem. Chem. Phys.*, 2005, **7**, 3297–3305.
12 S. Grimme, J. Antony and S. Ehrlich, *J. Chem. Phys*, 2010, **132**, 154104.
13 K. Fukui, *Acc. Chem. Res.*, 1981, **14**, 363–368.
14 B. J. Cosier and A. M. Glazer, *J. Appl. Crystallogr.*, 1986, **19**, 105–107.
15 2011.
16 G. M. Sheldrick, *Acta Crystallogr. Sect. A Found. Crystallogr.*, 2008, **64**, 112–122.
17 L. J. Barbour, *J. Supramol. Chem.*, 2001, **1**, 189–191.
18 J. Hicks, P. Vasko, J. M. Goicoechea and S. Aldridge, *Nature*, 2018, **557**, 92–95.
19 B. A. Merrill, in *Encyclopedia of Reagents for Organic Synthesis*, John Wiley & Sons, Ltd, 2001.
20 R. G. Goel and A. L. Beauchamp, *Inorg. Chem.*, 1983, **22**, 395–400.
21 R. G. Goel and P. Pilon, *Inorg. Chem.*, 1978, **17**, 2876–2879.
22 D. Schneider, A. Schier and H. Schmidbaur, *Dalt. Trans.*, 2004, 1995–2005.

Chapter 3 : Synthesis of group 13–group 11 complexes

3.1 Introduction

3.1.1 Examples of aluminium–coinage metal complexes

To date, very few examples of molecular species containing bonds between aluminium and the group 11 metals copper, silver and gold have been described. Many early examples take the form of clusters, such as the intermetallic Al/Cu clusters reported by Fischer.[1] A **[(Cp*Al–Cu)$_6$H$_4$]** cluster was prepared by heating **(Cp*Al)$_4$** with **[(Ph$_3$PCuH)$_6$]** and consists of a Cu_6 core contained within an Al_6 octahedral shell. Similar Cp*Al based gold systems have also been reported.[2] In 2020, the Power group reported the synthesis of a dispersion enhanced Al–Cu complex supported by β-diketimate ligands on both the aluminium and copper components (**Scheme 3.1**).[3] In this complex, it was calculated that 50% of the interaction enthalpies arise from London Dispersion Forces between the mesityl and Dipp groups of the opposing ligands and the orbital component consists mainly of σ-donation of an Al based lone pair to Cu. The bond can therefore be described as a Al:→Cu dative interaction.



Power, 2020

Scheme 3.1. *Synthesis of a dative Al–C bond from a neutral aluminylene*

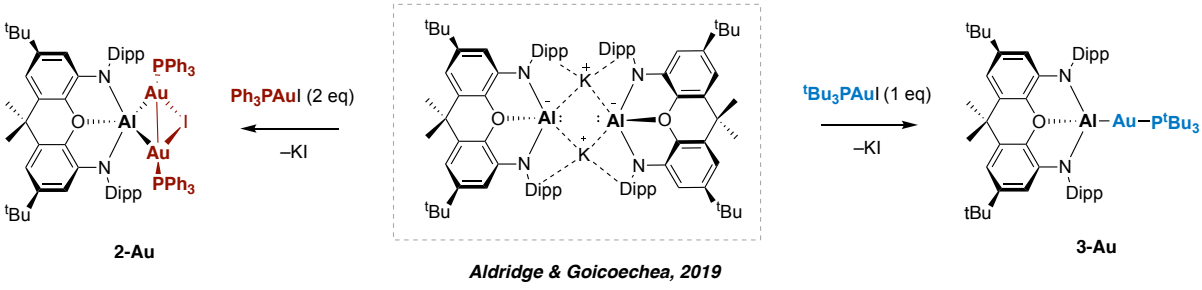
A similar group of compounds were reported by the Crimmin group, using the same neutral aluminylene and Cu(I) arene complexes.[4] This work also emphasises the importance of dispersion forces in stabilising aluminylene transition metal systems,

and highlights the strong σ-donating ability of Al based metalloligands. Examples of group 11 compounds bearing an X-type aluminium ligand prove more elusive, and no prior silver–aluminium species have been described at all.

3.1.2 Synthesis of unsupported Al–Au bonds using a potassium aluminyl complex

The 2018 publication of the xanthene supported potassium aluminyl, **K_2[(NON)Al_2], I** allowed for consideration of salt metathesis as a means to form Al–M bonds, in which anionic Al(I) acts as a nucleophile towards an electropositive metal source. Such an approach has been successfully used for both Ga–M and B–M bond formation, spanning metals from across the Periodic Table (Section 1.5)

Reaction of **I** with 2 equivalents of the Au(I) source Ph_3PAuI has been reported to lead to the loss of KI and formation of **(NON)Al(AuPPh$_3$)$_2$I**, **2-Au** (**Scheme 3.2**).[5] This complex contains a trimetallic metallocycle consisting of one aluminium and two gold atoms, with the Au–Au bonded unit bridged by an iodide ligand. Furthermore, **I** was reacted with ^{t}Bu$_3$PAuI, with the larger phosphine ligand causing a different geometry and product stoichiometry. The product in this case is the two-coordinate gold complex **(NON)AlAuP^{t}Bu$_3$** (**3-Au**), which has a linear Al–Au–P core and a short Al–Au bond of 2.402(3) Å.[2]



Scheme 3.2. *Synthesis of the trimetallic and bimetallic gold complexes **2-Au** and **3-Au***

Given the relative electronegativities of Al and Au, this reaction can be considered a two-electron reduction of Au(I) by Al(I), returning Al to the +3 oxidation state. This bonding description was studied computationally using the Quantum Theory of Atoms in Molecules method (QTAIM), with the calculated charges on Al and Au in **3-Au** found to be +2.21 and −0.82 respectively. The covalent Al–Au bond is therefore highly polarised in the sense $Al^{\delta+}$–$Au^{\delta-}$. The aluminyl fragment functions as an X-type metalloligand and the system is well poised for small molecule activation. Indeed, insertion chemistry with CO_2 is observed, with the regiochemistry reflecting this bond polarity (**Section 4.1**)

3.2 Aims

The synthesis of the gold aluminyl complex **(NON)AlAuP^{t}Bu$_3$** from potassium aluminyl **I** serves as a springboard for the study of aluminium – transition metal covalent bonds. This chapter aims to build on the early work with gold and expand it to the lighter group 11 metals silver and copper, by investigating metathesis reactions of **I** with silver and copper halides, supported by phosphine ligands. Gold is an outlier among the coinage metals, with relativistic effects causing a number of differing properties, such as its high electronegativity and tendency for aurophilic interactions.[6,7] Therefore it may be expected that significant differences will be encountered in the geometric and electronic structures of Al–Cu or Al–Ag species as compared to those reported for gold. Interesting variation in structure and geometry was found when different phosphine ligands were used as co-ligands on the gold centre, as discussed in Section 3.1.2. This potential for structural diversity will also be explored, with different M(I) phosphine precursors in different stoichiometries trialled. An advantage of this method

is the simplicity of the group 11 starting materials, which can easily be prepared from the M(I) halide and the phosphine ligand and are therefore highly tunable.

In addition to the synthesis of Al–M bonds, this chapter will also make use of the Ga(I) nucleophile **K_2[(NON)Ga_2]**, (**II**) a potassium gallyl reagent supported by the same ligand architecture as **I**.[8] **II** will be used in the same way to construct an array of covalent, unsupported Ga–M bonds. Although such bonds are known in the literature for other Ga(I) heterocycles, it has so far not been possible to directly compare Ga–M and Al–M bonds with the same ligand systems. The gallyl complexes will provide insight into how an aluminyl metalloligand behaves compared to the heavier group 13 congener.

Thus, the aim of this chapter is to describe the synthesis and characterisation of a library of complexes featuring unsupported, covalent group 13 – group 11 bonds.

3.3 Results and discussion

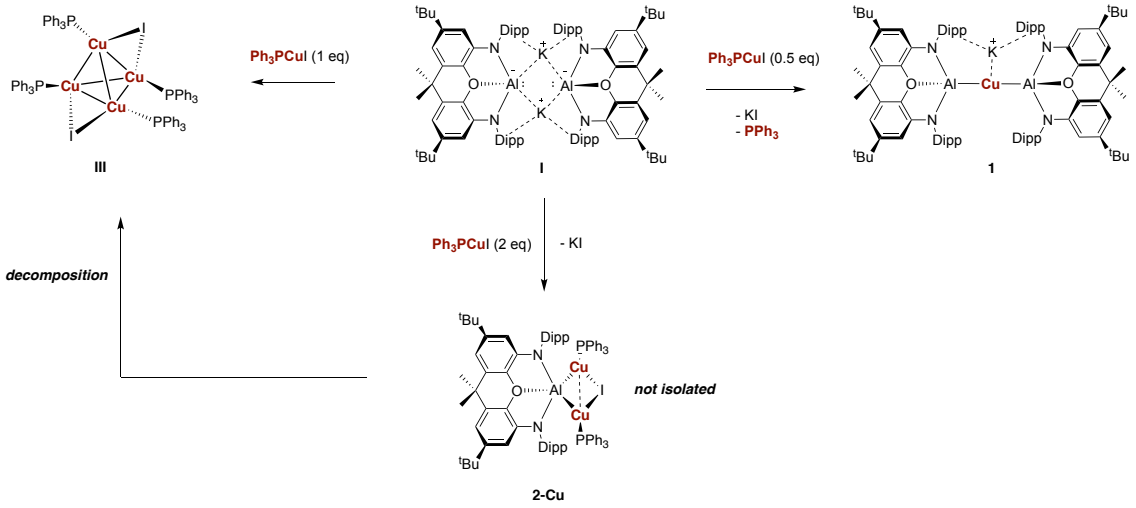
3.3.1 Notes on multinuclear NMR characterisation and stoichiometry

Throughout this thesis, key characteristic regions in the ^{1}H NMR spectra are referred to for the purpose of reaction monitoring. The methine protons of the di*iso*propylaniline (Dipp) substituents on the **NON** ligand appear as a septet in the region 2.5-5.0 ppm. These protons are sensitive to changes at the aluminium centre and as a result, are a good NMR handle with which to monitor the formation of new species. Additionally, the number of Dipp signals is diagnostic of the symmetry of the molecule. It is possible to see up to four resonances from the four ^{i}Pr groups, although in the parent **K_2[(NON)Al]$_2$**, only one is seen due to high symmetry of the ligand environment. ^{31}P NMR is also a highly valuable spectroscopic tool, most simply for determining the presence or absence of a phosphine ligand and secondly for probing the environment

around the group 11 metal it is bound to. Potassium aluminyl compound **I** exists as a dimer, both in the solid state and in solution. However, throughout this work, in considerations of reaction stoichiometry it will be treated as a monomer such that one equivalent of **I** refers to one aluminium metal centre.

3.3.2 Synthesis of a bisaluminocuprate

Addition of 0.5 equivalents of Ph_3PCuI to a benzene solution of **I** leads to precipitation of KI and formation of a bright yellow solution. Dissociation of the phosphine ligand is evidenced by the appearance of a resonance at −6.0 ppm in the ^{31}P NMR spectrum of the reaction mixture, and the fact that isolated samples of **1** display no ^{31}P NMR resonance. This phosphine loss finds precedent in the formation of a Ga–Au–Ga linear unit from the reaction of Ph_3PAuCl and Ga(I) compound Ga(DDP), (DDP = 2-((2,6-diisopropylphenyl)amino-4-((2,6-diiso-propylphenyl)imino)-2-pentene), as reported by Fischer.[9] The product of the reaction can be shown to be the *bis*aluminyl copper complex, **K[Cu{Al(NON)}$_2$]**, **1** (**Scheme 3.3**).



Scheme 3.3. *Reaction of potassium aluminyl* ***I*** *with varying equivalents of* PPh_3CuI

Crystals suitable for X-ray crystallography were grown from a hexane solution, allowing the solid-state structure to be determined (**Figure 3.1**). The structure shows two aluminyl fragments bound to a central copper atom in a near linear geometry [∠(Al(1)–Cu(1)–Al(2)) = 174.88(2)°], as is common for Cu(I) species bearing bulky ligands.[10] The Cu–Al bond lengths (2.4076(5) and 2.4075(5) Å) are shorter than the sum of the covalent radii for copper and aluminium (2.53 Å). Although there are few known Cu–Al bonds for comparison, those in **1** can be placed on the shorter end of the spectrum of those known in solid state Cu/Al clusters, such as Cu_9Al_4, (2.4027(14) to 2.7189(14) Å).[11] They are similar in length to the Cu–Al bond in **(SiN^{Dipp})AlCu^{iPr}NHC** and **(SiN^{Dipp})AlCu^{Me2}CAAC** (SiN^{Dipp} = {CH_2SiMe_2NDipp}$_2$)) (2.3449(4) and 2.4028(7) Å respectively) (see Section 3.3.6), but longer than those in the NacNac-supported complex **HC(MeCMesN)$_2$}CuAl{(NDippCMe)$_2$CH** reported by Power (2.3010(6) Å).[3] The longer bond reflects the strong σ-donating nature of the aluminyl ligands, which are mutually *trans* to each other. **1** also features a potassium counter ion, which is held in place between the two Dipp groups of the opposing **(NON)Al** units, similar to the structure of **I** itself and other reported dimeric potassium aluminyl species.[8] The K···C distances (3.089(3)-3.296(3) Å) are in fact shorter than those in **I** (3.226(3)–3.474(3) Å) which suggests this interaction is stronger in **1**. It is also possible that, the K^+ counterion, which sits between the arene rings, may lead to longer Cu–Al bonds, by preventing close approach of the Al units towards the Cu centre.

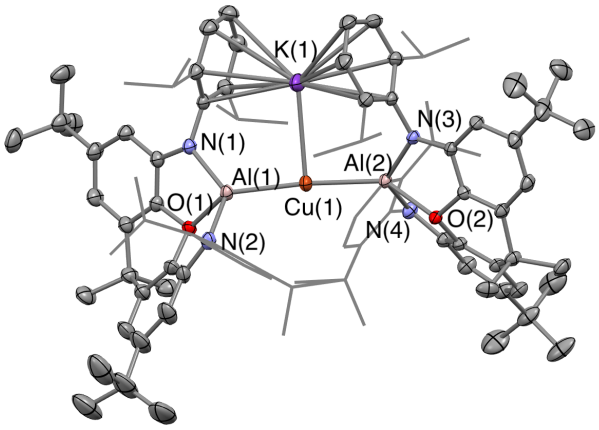


Figure 3.1. *Molecular structure of **1** in the solid state as determined by X-ray crystallography. Thermal ellipsoids set at the 50% probability level. Hydrogen atoms omitted and ^{i}Pr groups shown in wireframe for clarity. Key bond lengths (Å) and angles (°): Al(1)–O(1) 2.0428(15), Cu···K 3.0669(6), Cu(1)–Al(1) 2.4076(5), Cu(2)–Al(1) 2.4075(5), Al(1)–Cu(1)–Al(2) 174.88(2).*

This potassium arene interaction is retained in solution, as is apparent from the ^{1}H NMR spectrum of an isolated sample of **1**, which features broad resonances at room temperature. While the parent potassium aluminyl compound features only one resonance for the Dipp methine protons, **1** gives rise to four such signals, indicating that the molecular symmetry in solution is lower. This can be explained by retention of the potassium arene interaction seen in the solid-state structure of **1**, into the solution phase. Variable temperature NMR confirms this assertion (**Figure 3.2**). While the room temperature spectrum is extremely broad, a spectrum measured at 373 K is much sharper and features only one Dipp ^{i}Pr resonance, indicating free rotation on the NMR timescale and a weakening of the K^{+}-π system interaction. Conversely, a spectrum measured at 203 K shows greatly reduced symmetry, with four distinct Dipp ^{i}Pr resonances and also two doublets corresponding to the xanthene backbone *o*-C*H* protons (while the high temperature spectrum displays only one signal).

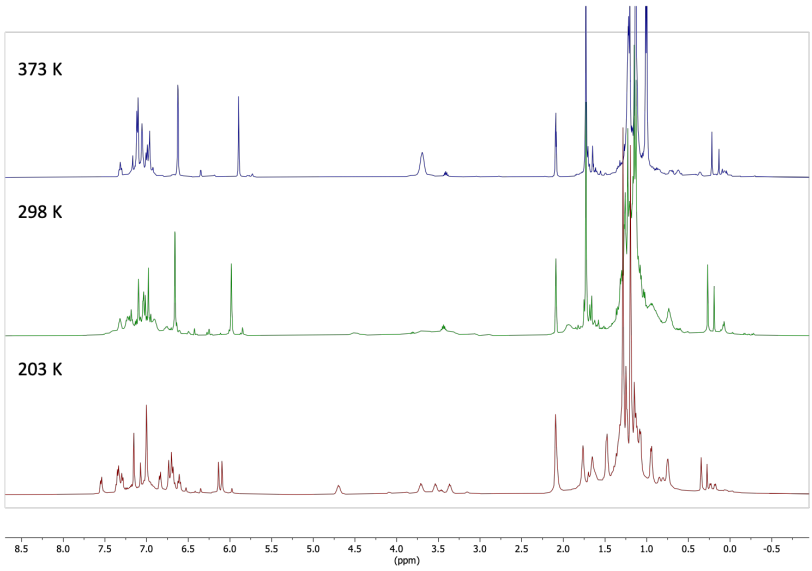


Figure 3.2. *Variable temperature ^{1}H NMR of **1** at 373 K, 298 K and 203K, measured in d_8-toluene*

The stoichiometry of the reaction between **I** and group 11 halide electrophiles is critical to the product formed. Thus, the reaction of **I** with 1 equivalent of Ph_3PCuI does not yield a complex containing a Cu–Al bond. Rather, the mixed valence Cu(I)/Cu(0) cluster **$(Ph_3P)_4Cu_4I_2$** is formed (**Scheme 3.3**). Crystals grown from diethyl ether solution reveal that this compound is a copper-based tetrametallic species, **III**, in the solid state, with iodine atoms bridging alternate copper centres (**Figure 3.3**).

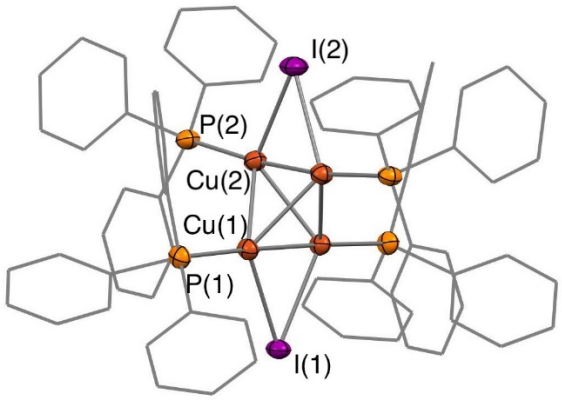


Figure 3.3. *Molecular structure of $(Ph_3P)_4Cu_4I_2$ (**III**) in the solid state as determined by X-ray crystallography. Hydrogen atoms omitted and phenyl rings shown in wireframe format for clarity; thermal ellipsoids drawn at the 50% probability level.*

3.3.3 Trimetallic complexes with an E(MPPh$_3$)$_2$I core (E = Al, Ga, M = Au, Cu)

The formation of **(Ph$_3$P)$_4$Cu$_4$I$_2$** contrasts to the product formed in the reaction of **I** with one equivalent of Ph$_3$PAuI, which gives the trimetallic gold-phosphine aluminyl complex **(NON)Al(AuPPh$_3$)$_2$I, 2-Au** (**Scheme 3.2**) and unreacted aluminyl **I**. Targeting the analogous copper complex, **I** was reacted with 2 equivalents of Ph$_3$PCuI in benzene (**Scheme 3.3**). The similarities of spectroscopic features of the product with those of **2-Au** lead to the postulate of an analogous trimetallic complex **(NON)Al(CuPPh$_3$)$_2$I**, **2-Cu**, in particular: i) the ^{1}H NMR spectrum shows reduced symmetry compared to that of **I**, as indicated by an increase in the number of septets corresponding to the Dipp methine protons from one to two (as in **2-Au**), ii) the appearance of a resonance at 7.85 ppm corresponding to a ligated PPh$_3$ unit (again, present in the ^{1}H spectrum of **2-Au**) and iii) the fact that the ^{31}P spectrum shows two doublets at 3.2 and 10.1 ppm ($^3J_{PP}$ = 39 Hz) (**Figure 3.4**). These doublets are diagnostic of the planar **Al(MPPh$_3$)$_2$I** fragment. In the reported solid-state structure of **2-Au**, the iodide ligand bridges the two gold centres in a slightly unsymmetrical fashion, likely due to steric clash between the **NON** and PPh$_3$ ligands. This causes the phosphorus nuclei to be inequivalent due to how the **NON** ligand sits, and couple to one another, producing the two doublets seen in the ^{31}P NMR spectrum. The fact that this pattern is replicated in the spectrum of **2-Cu** suggests that it is structurally similar to **2-Au**.

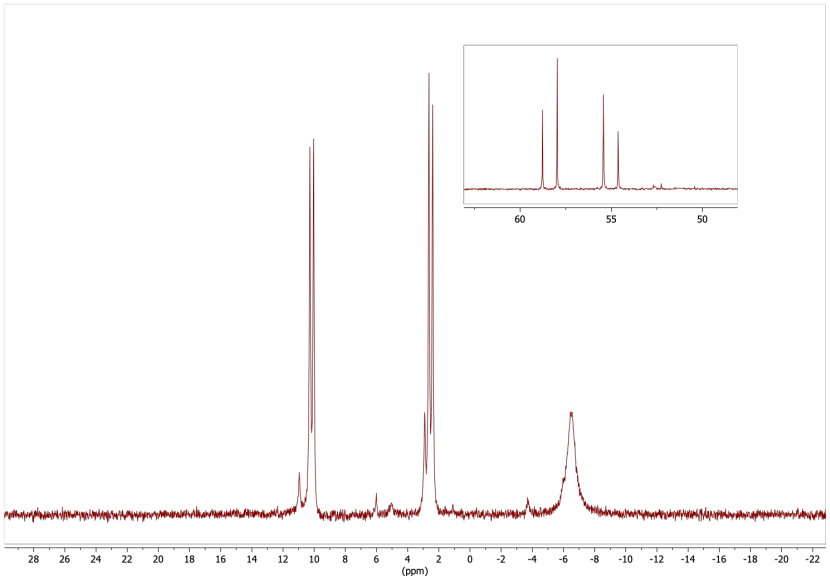


***Figure 3.4**. ^{31}P NMR spectrum of the reaction of **I** and PPh_3CuI (2 eq) to give **2-Cu** and **III** (broad resonance). Inset: ^{31}P NMR spectrum of **2-Au** showing similar doublets*

Despite repeated attempts, **2-Cu** could not be isolated cleanly as a solid, nor could crystals suitable for X-ray diffraction be obtained, even at low temperature. Over the course of 24 hours, **2-Cu** decomposes to give the Cu cluster **III** and a mixture of aluminium containing products. This can be seen in the ^{31}P NMR spectrum by the appearance of a broad resonance at −6.5 ppm, and also verified crystallographically. The formation of this cluster can be viewed as the formal loss of the **$(CuPPh_3)_2I$** unit from **2-Cu**. The instability of **2-Cu** compared to **2-Au** presumably reflects the weaker bonding between the copper centres compared to the Au centres in **2-Au**, and the reduced ability of copper to support a formal oxidation state of zero due to its greater electropositivity.

As well as altering the group 11 metal, variation of the group 13 partner is also possible, for example by using potassium gallyl reagent **II** instead of aluminyl **I**. The gallium analogue of **2-Au**, **$(NON)Ga(AuPPh_3)_2I$, 2'-Au** was synthesised by the reaction of **II** with 2 equivalents of Ph_3PAuI (**Scheme 3.4**). Again, the ^{31}P NMR spectrum of the reaction mixture shows two characteristic doublets at 50.8 and 55.6

ppm ($^3J_{PP}$ = 112 Hz). In this case, crystals suitable for X-ray diffraction could be grown from diethyl ether, allowing for solid state structural characterisation (**Figure 3.5**).

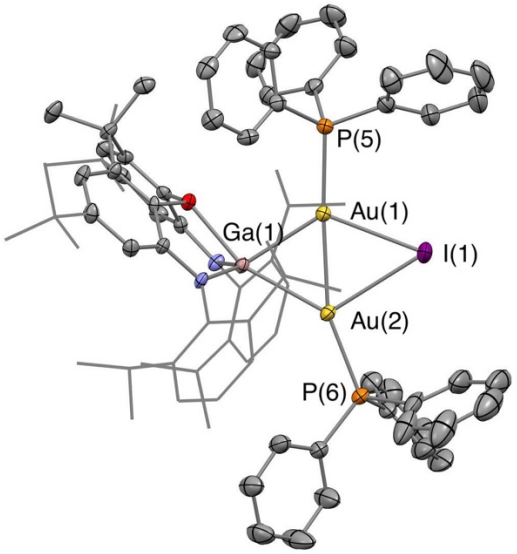
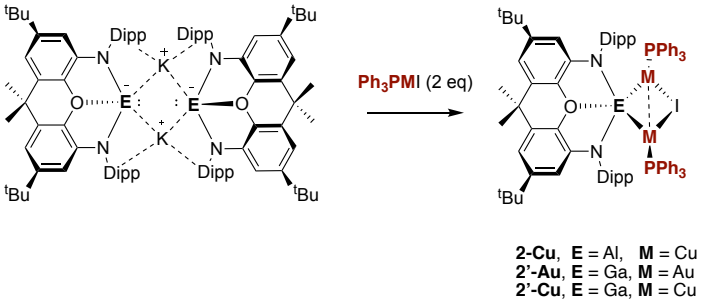


Figure 3.5. *Molecular structure of **2'-Au** as determined by X-ray crystallography. Thermal ellipsoids set at the 50% probability level. Hydrogen atoms omitted and ^{i}Pr groups shown in wireframe for clarity. Key bond lengths (Å) and angles (°): Au(2)–Au(1) = 2.6095(2), Au(2)–I(1) = 2.8308(3), Au(1)–I(1) = 2.9901(4), Au(2)–Ga(1) = 2.5383(5), Au(1)–Ga(1) = 2.5639(4), Au(2) –Ga(1) –Au(1) = 61.517(11), Au(2) –I(1) –Au(1) = 53.183(7).*

This reveals that **2'-Au** is essentially isostructural with the $AlAu_2I$ compound **2-Au**. The $GaAu_2$ metallocycle forms a planar core, with an iodine bridging the Au–Au unit on one side, and Ga on the other. The Au–Au bond length of 2.6095(2) Å is very similar to that of **2-Au** (2.5897(6) Å) and in line with other complexes featuring a single covalent Au–Au bond, such as the **[Au(CAAC)]$_2$** system reported by Bertrand (2.5520(6) Å).[12,13] The two Ga–Au bond lengths (*d*(Au(2)–Ga(1) = 2.5383(5) Å), *d*(Au(1)–Ga(1) = 2.5639(4) Å)) are in the range of previously reported Ga–Au bonds[9,14,15] and are shorter than the Al–Au distances in **2-Au** (*d(*Au(1)–Al(1) = 2.6045(19) Å), *d(*Au(2)–Al1 = 2.5096(19) Å)) (which also show a more significant difference between themselves).

As in **2-Au**, the Au–I bond lengths are unequal (*d*(Au(2)–I(1)) = 2.8308(3) Å, *d*(Au(1)–I(1)) = 2.9901(4) Å). The Au(1)–P(5) bond is projected directly out from the $GaAu_2I$ core, such that the angle Au(2)–Au(1)–P(5) is near linear, (175.17(3)°), while the Au(2)–P(6) bond points towards the iodine atom, resulting in an Au(1)–Au(2)–P(6) angle of 161.02(3)°. These structural differences account for the two different phosphorus environments observed in the ^{31}P NMR spectrum, which produces the characteristic sets of doublets that define this series of complexes.



Scheme 3.4 *Formation of the series of trimetallic complexes* ***2'-Au, 2'-Cu*** *and* ***2-Cu***

Like its aluminium counterpart, **2'-Au** is stable in solution, and no decomposition to products similar to **III** were observed. However, the related copper/gallium complex, **(NON)Ga(CuPPh$_3$)$_2$I** (**2'-Cu**) suffers from the same instability issues as **2-Cu**. **2'-Cu** can be formed *in situ*, by reaction of the potassium gallyl dimer **II** with two equivalents of Ph_3PCuI. *In situ* ^{31}P NMR monitoring indicated the formation of a species featuring a **Ga(CuPPh$_3$)$_2$I** fragment, displaying mutually coupled doublets at 5.5 and 13.5 ppm, ($^3J_{PP}$ = 28 Hz). Attempts at isolation of this compound again produced mixtures of products, including **(Ph$_3$P)$_4$Cu$_4$I$_2$**.

The four complexes bearing the **E(MPPh$_3$)$_2$I** motif can be thought of as arising from initial formation of a two coordinate metal species of the form **(NON)E–M–PPh$_3$**, followed by incorporation of an additional equivalent of Ph_3PMI. This may occur due

to insufficient steric hindrance from the PPh_3 ligand, allowing the second Ph_3PMI equivalent to approach. Even when a stoichiometry of only one group 11 metal centre per group 13 atom is used, a linear bimetallic species is not the main product. This highlights the importance of the steric properties of the supporting phosphine ligand in constructing heterobimetallic species of a given geometry.

Table 3.1 *Comparison of ^{31}P NMR data for compounds* ***2 and 2'***

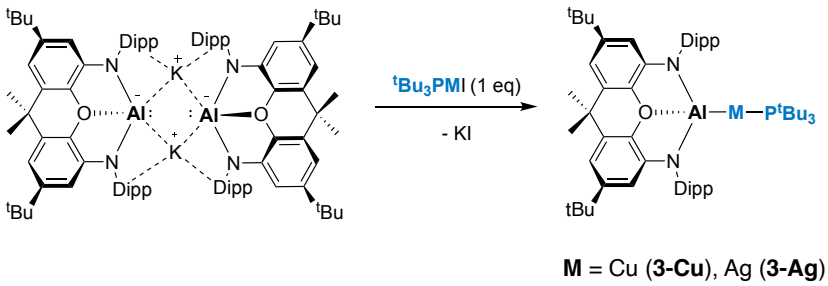
	E	M	δ_P (ppm)	$^3J_{PP}$ (Hz)
2-Au	Al	Au	55.0, 58.4	131
2'-Au	Ga	Au	50.8, 55.6	112
2-Cu	Al	Cu	3.2, 10.1	39
2'Cu	Ga	Cu	5.5, 13.5	28

This series of trimetallic complexes formed of group 11 and group 13 metals offer insight into the influence of each metal. **Table 3.1** shows a comparison of the ^{31}P chemical shifts of each species, and the $^3J_{PP}$ values, which in turn provide information about the nature of the bonding between the metals. Both chemical shift and $^3J_{PP}$ are strongly affected by the identity of the coinage metal. The ^{31}P signals of **2-Au** and **2'-Au** both occur at a much higher chemical shifts than those of **2-Cu** and **2'-Cu**, which are similar in value to each other. Additionally, there is much stronger coupling between the phosphorus centres in the gold-based systems than the copper congeners. This is likely due to the strength of the Au–Au single bond in **2-Au** and **2'-Au**, whereas in the corresponding copper complexes, a covalent Cu–Cu bond is less likely.[16] The group 13 element has a small effect on $^3J_{PP}$, which is slightly higher for the Al containing complexes **2-Au** and **2-Cu** than the Ga equivalents **2'-Au** and **2'-Cu**.

Reactions of the potassium aluminyl compound **I** with Ph_3PAgI in varying stoichiometries were also conducted. However, in all cases ^{31}P NMR monitoring showed only the liberation of free PPh_3 (as evidenced by a resonance at −6.0 ppm), and the reaction mixtures turned black, indicating the formation of metallic silver. This reflects the more positive potential for the Ag(I) to Ag(0) reduction than for Cu.[17] It is clear that the PPh_3 ligand is not suitable for supporting bimetallic silver – aluminyl complexes, and to this end our focus shifted to other phosphine ligands.

3.3.4 Synthesis of linear bimetallic complexes

We next sought to form bimetallic complexes which retain the supporting phosphine ligand. Mindful of the clear importance of both reaction stoichiometry and the steric and electronic properties of the phosphine ligand, the stronger σ-donating and more sterically encumbered P^tBu_3 was targeted. Reaction of **I** with one equivalent of $^tBu_3PMI$ (M = Cu, Ag) led to the formation of the two-coordinate, bimetallic silver and copper aluminyl complexes **(NON)AlAgP^{t}Bu$_3$** (**3-Ag**) and **(NON)AlCuP^{t}Bu$_3$** (**3-Cu**) (**Scheme 3.5**).

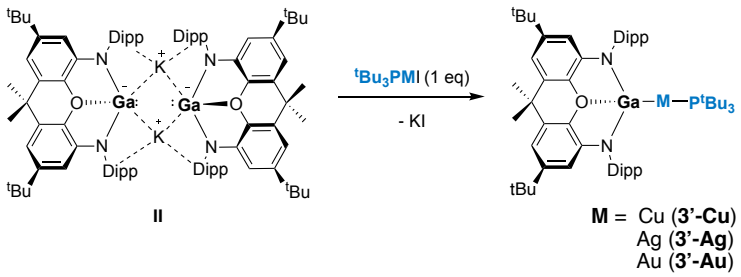


***Scheme 3.5**. Synthesis of two-coordinate silver and copper aluminyl species*

The ^1H NMR spectra of isolated samples of both **3-Ag** and **3-Cu** bear a strong resemblance to that of the structurally characterised compound **(NON)AlAuP^{t}Bu$_3$** (**3-**

Au). Each complex shows an **NON** ligand environment of higher symmetry than the trimetallic complexes described in Section 3.3.3, with one septet resonance corresponding to the Dipp methine protons. The spectra also confirm a ratio of one P^{t}Bu$_3$ ligand per **NON** unit and by extension, one Al per group 11 metal. The ^{31}P NMR resonances indicate a single phosphorus environment and their chemical shift values (38.3, 58.9 and 75.0 ppm for **3-Cu**, **3-Ag** and **3-Au**, respectively) reflect the trend in other ^{t}Bu$_3$PMX type systems such as ^{t}Bu$_3$PMCl.[18–20]

Complexes **3-Ag** and **3-Cu** could be isolated as colourless microcrystalline solids. However, these crystals proved too small for X-ray diffraction studies, even using synchrotron radiation. Fortunately, the gallium analogue **(NON)GaAgP^{t}Bu$_3$** (**3'-Ag**), prepared from potassium gallyl complex **II** and ^{t}Bu$_3$PAgI, proved more amenable and could be crystallised from toluene solution, allowing the structure to be determined by X-ray crystallography (**Scheme 3.6**, **Figure 3.6**). This shows the expected two-coordinate, Ga–Ag–P unit (∠(Al(1)–Cu(1)–Al(2)) = 175.00(2)°), somewhat closer to linearity than the Al–Au–P unit of **3-Au** (167.47(10)°). The Ga–Ag bond length of 2.4548(3) Å is of similar magnitude to the that reported by Jones for the silver gallyl complex **[(Ar-DAB)GaAg(NHC)]** (Ar-DAB = [{N(Dipp)C(H)}$_2$]$^{2-}$) (2.4161(5) Å). Taking this structure, along with the NMR evidence into account, it can be inferred that **3-Ag** and **3-Cu** are isostructural, also featuring a direct Al–M bond.



Scheme 3.6. *Synthesis of Ga–M complexes **3'-Cu**, **3'-Ag**, and **3'-Au** from potassium gallyl **II***

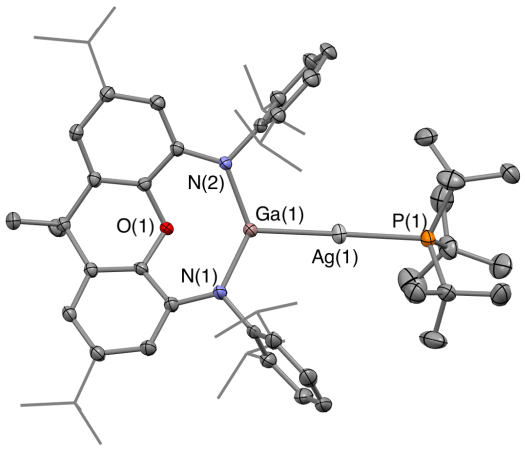


Figure 3.6. *Molecular structure of **3'-Ag** in the solid state as determined by X-ray crystallography. Thermal ellipsoids set at the 50% probability level. Hydrogen atoms omitted and ^{i}Pr groups shown in wireframe for clarity. Key bond lengths (Å) and angles (°): Ga(1)–O(1) 2.3834(14), Ga(1)–Ag(1) 2.4548(3), Ag(1)–P(1) 2.4355(6), Ga(1)–Ag(1)–P(1) 175.00(2).*

The copper gallyl and gold gallyl complexes **(NON)GaCuP^{t}Bu$_3$** (**3'-Cu**), and **(NON)GaAuP^{t}Bu$_3$** (**3'-Au**), could be synthesised in the same fashion from **II** and P^{t}Bu$_3$MI (M = Cu, Au) (**Scheme 3.6**) and give rise to ^{31}P NMR resonances at 46.5 ppm and 97.9 ppm, respectively. The ^{31}P NMR shifts for the gallyl complexes **3'-Cu**, **3'-Ag** and **3'-Au** follow the same trend as those of their aluminium counterparts, with similar values in each case (**Table 3.2**). The series **3-Cu, Ag, Au** and **3'-Cu, Ag, Au** are the first examples of bimetallic aluminyl and gallyl systems bearing the same ligand scaffold, allowing them to be compared systematically.

Table 3.2 *Comparison of ^{31}P NMR chemical shifts for compound series **3** and **3'***

δ_P (ppm)	**Al**	**Ga**
Cu	38.3	46.5
Ag	58.9	65.4
Au	107.3	97.9

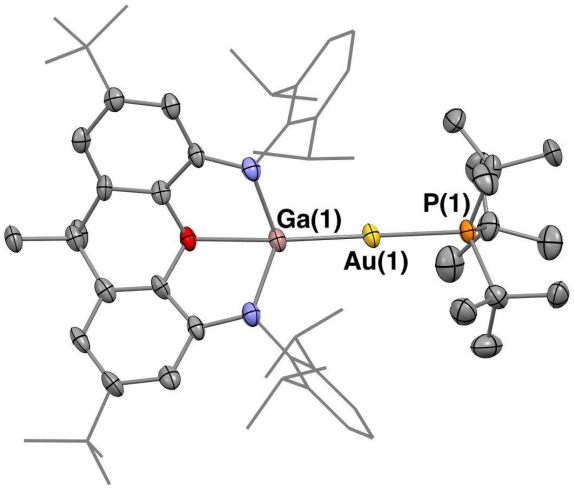


***Figure 3.7**. Molecular structure of **3'-Au** in the solid state as determined by X-ray crystallography. Thermal ellipsoids set at the 50% probability level. Two molecules of **3'-Au** are present in the ASU, only one is shown. All structural information is derived from this molecule. Hydrogen atoms omitted and ^{i}Pr groups shown in wireframe for clarity. Key bond lengths (Å) and angles (°): Ga(1)–Au(1) = 2.4011(12), Au(1)–P(1) = 2.353(2), Ga(1)–O(1) = 2.235(7), Ga(1)–Au(1)–P(1) = 168.71(7).*

Further to this, crystals of gold gallyl complex **3'-Au** could be grown from a benzene solution, allowing the structure to be determined by X-ray crystallography (**Figure 3.7**). This allows direct comparison of the structural parameters of complexes containing a Ga–M bond and an Al–M bond. **3'-Au** crystallises in an almost identical unit cell to its aluminium counterpart **3-Au**, with the asymmetric unit containing two molecules of the gold complex in each. The Ga–Au bond length of 2.4011(12) Å is also comparable to the Al–Au bond length of 2.402(3) Å and the Ga–Au–P and Al–Au–P angles are again close in magnitude (168.71(7) and 167.47(10) respectively). The Ga–O bond length in **3'-Au** is considerably longer than the Al–O bond of **3-Au** (2.235(7) vs 2.046(8) Å). This mirrors the difference in the same bond lengths in the parent potassium aluminyl complex **I** and potassium gallyl complex **II** and suggests that the dative O→E interaction is more important in stabilising the aluminium system than the gallium.[8] Another notable point of difference in the otherwise very similar structures is the Au–P bond distance, which is slightly shorter in **3'-Au** than in **3-Au** (2.353(2) vs 2.395(3)

Å). This suggests that the aluminyl fragment is more strongly donating than the gallyl fragment, with the greater *trans* effect of the aluminyl causing the Au–P bond to lengthen in comparison to the equivalent bond in **3'-Au**. This donor ability can be further analysed by comparing the silver species **3-Ag** and **3'-Ag**.

3.3.5 The aluminyl fragment as a metalloligand

The ^{31}P NMR spectra of **3-Ag** and **3'-Ag** allow for a direct comparison of the properties of the aluminyl and gallyl fragments as metalloligands (**Figure 3.8**). Silver exists as two spin active isotopes, ^{109}Ag and ^{107}Ag with relative natural abundance of 48.1 and 51.8% respectively, which can both couple to a proximal ^{31}P nucleus. Unlike in the starting $^{t}Bu_3$PAgI, coupling to both isotopes is not seen in the ^{31}P NMR spectrum of **3-Ag**, and a broad doublet is observed at 58.9 ppm instead (mean $^{1}J_{PAg}$ = 152 Hz). This is likely due to the broadening effect of the directly bound quadrupolar ^{27}Al nucleus (I = 5/2). In contrast, the ^{31}P NMR spectrum of silver gallyl compound **3'-Ag** shows a resonance at 65.4 ppm with clearly resolved coupling to both silver isotopes ($^{1}J_{PAg}$ = 278, 322 Hz). The magnitude of this coupling is much greater than that measured for **3-Ag**, reflective of the much reduced *trans* influence of the less strongly σ-donating gallyl ligand compared to the aluminyl, which in turn is a consequence of the greater electronegativity of gallium. Indeed, the mean $^{1}J_{PAg}$ value of 152 Hz in **3-Ag** is particularly small compared to, for example, Ag(I) complexes bearing mutually *trans* phosphine and NHC ligands. In the **[Ag(SIPr)(PCy$_3$)][PF$_6$]** compound reported by Cisnetti,[21] values of $^{1}J_{PAg}$ = 463.6, 536.0 Hz were measured, i.e. much larger than in **3-Ag**. This again places the aluminyl ligand very high on the scale of strongly donating ligands.[22]

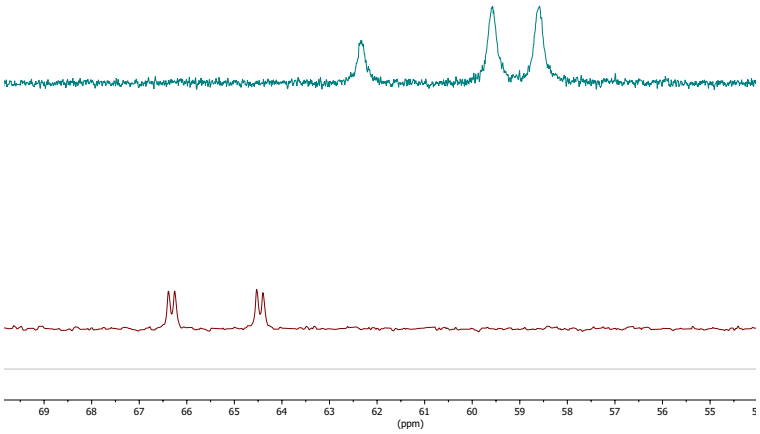


***Figure 3.8**. ^{31}P NMR spectrum of **3-Ag** (above), also showing P^{t}Bu$_3$, and **3'-Ag** (below), measured in C_6D_6*

Further evidence of the strongly electron donating nature of the aluminyl ligand comes from the observation of a P^{t}Bu$_3$ resonance at 62.3 ppm in C_6D_6 solutions of isolated, microcrystalline samples of **3-Ag** (**Figure 3.8**). This is not an impurity, as is made clear by the fact that when **3-Ag** is reacted onward (see Chapter 4), no P^{t}Bu$_3$ signal is observed in *in situ* ^{31}P NMR spectra and conversion is quantitative. Additionally, the ^{1}H NMR spectrum of **3-Ag** shows only one doublet resonance for the P^{t}Bu$_3$ ligand, integrating to the expected 27 protons, and no additional resonance for unligated P^{t}Bu$_3$. This suggests a process which is not visible on the ^{1}H NMR timescale but becomes apparent in the relatively faster timescale of ^{31}P NMR.[23,24] It is hypothesised that the phosphine ligand is labile, and the Ag–P bond is weakened by the *trans* influence of the aluminyl ligand, causing the appearance of P^{t}Bu$_3$ in solution. Poor solubility at low temperatures prevented the study of this behaviour by variable temperature NMR, so the closely related aliphatic phosphine tricyclohexylphosphine, PCy$_3$, was chosen to investigate possible exchange.

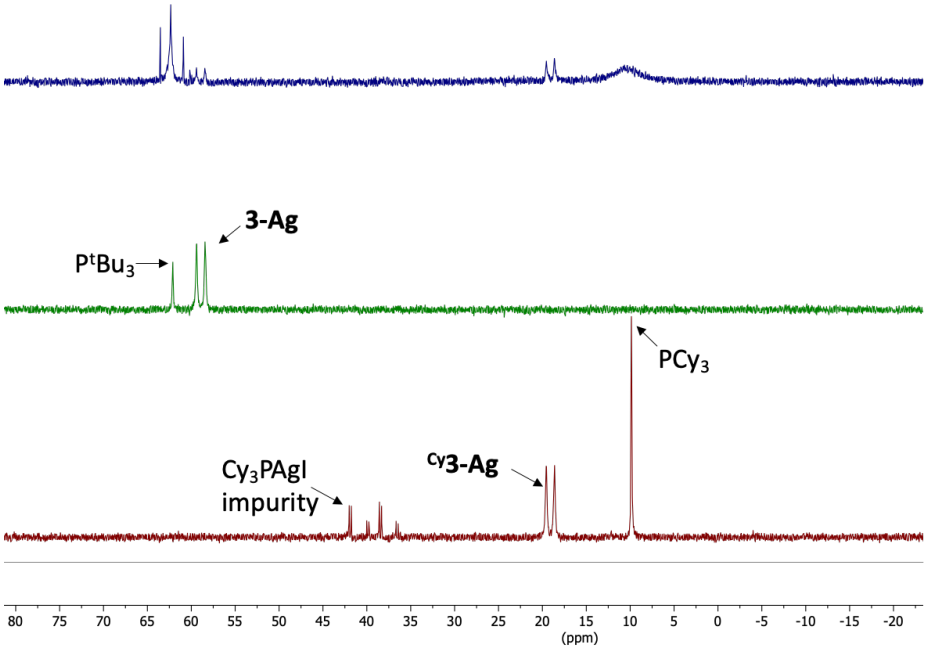
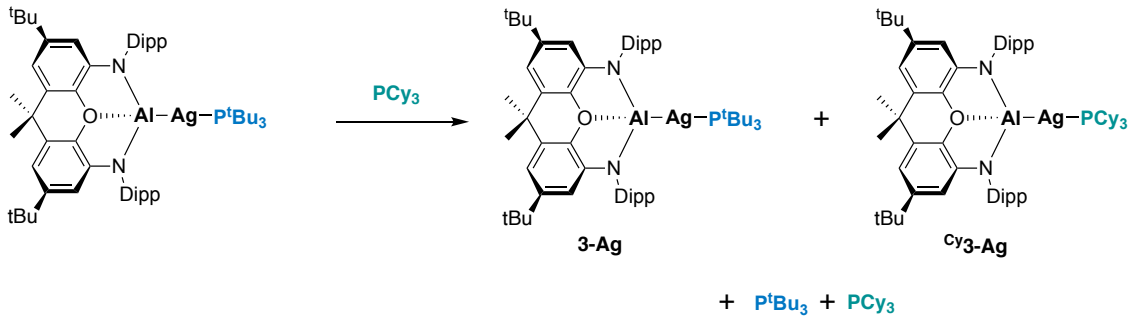


Figure 3.9. *^{31}P NMR spectra measured in C_6D_6 of: ^{Cy}**3-Ag** (bottom), **3-Ag** (centre), resultant mixture of **3-Ag** and ^{Cy}**3-Ag** produced upon addition of PCy_3 to **3-Ag** (top).*

The potassium aluminyl dimer **I** was reacted with one equivalent of Cy_3PAgI, leading to loss of KI and formation of the silver aluminyl complex **(NON)AlAgPCy$_3$**, ^{Cy}**3-Ag**. This is evidenced by the appearance of a broad doublet in the ^{31}P NMR spectrum centred around 19.0 ppm, again with a small $^1J_{PP}$ coupling constant of 154 Hz, indicating that the [$AgPCy_3$] fragment is directly bound to Al. Notably, isolated samples of ^{Cy}**3-Ag**, when dissolved in C_6D_6, also show a resonance corresponding to unligated PCy_3 at 9.8 ppm (**Figure 3.9**)



***Scheme 3.7**. Reaction of **3-Ag** with PCy_3, producing a mixture of **3-Ag**, ^{Cy}**3-Ag**, and the corresponding phosphines P^tBu_3 and PCy_3.*

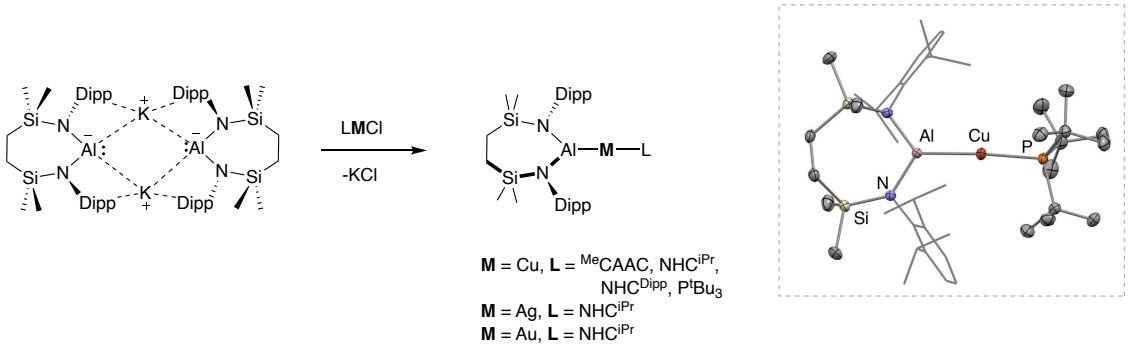
Addition of one equivalent of PCy_3 to a C_6D_6 solution of **3-Ag** leads to a mixture of both **3-Ag** and ^{Cy}**3-Ag**, with P^tBu_3 and PCy_3 also present in the ^{31}P NMR spectrum (**Figure 3.9**, **Scheme 3.7**). This demonstrates the lability of the phosphine ligand towards exchange in solution. This observation is also supported by the fact that **3-Ag** is less stable, both in solution and in the solid state, than the gold and copper complexes **3-Au** and **3-Cu**, and decomposes within a few days. It suggests that in solution, the structure of **3-Ag** may in fact differ from that of the structurally characterised **(NON)AlAuP^{t}Bu$_3$** and **(NON)GaAgP^{t}Bu$_3$**, perhaps also contributing to the difficulty in producing crystals suitable for X-ray diffraction.

The synthesis of the silver aluminyl complex **3-Ag** is a first, with no previous unsupported Al–Ag bonds reported. Copper aluminyl **3-Cu** adds to the very small pool of Al–Cu bonded species which are known, and begins to populate this growing area.

3.3.6 Discussion of Al–M bonding

The advent of nucleophilic Al(I) chemistry has prompted a flurry of available aluminyl reagents.[25] This in turn has opened the door to the synthesis of complexes featuring Al–M bonds *via* a salt metathesis approach, as in the work discussed in this chapter. Particularly relevant to this work are the compounds reported by Hill and McMullin,

synthesised from the reactions of the potassium aluminyl anion **[K{Al(SiN^{Dipp})}]$_2$** and group 11 metal chlorides, supported by CAAC or NHC ligands (**Scheme 3.8**). An initial report in 2021 described two Al–Cu bonded species featuring near linear Al–Cu–C units, with the ^{Me}CAAC (^{Me}CAAC = 1-(2,6-diisopropylphenyl)-3,3,5,5-tetramethylpyrrolidin-2-ylidene) based complex deviating slightly from linearity due to the large steric bulk of the ^{Me}CAAC ligand. The method was very recently extended to the heavier group 11 elements, with a subsequent report describing the synthesis of **(SiN^{Dipp})AlAgNHC^{iPr}** and **(SiN^{Dipp})AlAuNHC^{iPr}**.



Scheme 3.8. *Synthesis of Al–M species from the potassium aluminyl anion* ***[K{Al(SiN^{Dipp})}]$_2$*** *(SiN^{Dipp} ={CH$_2$SiMe$_2$NDipp}$_2$) (left) and molecular structure of* ***(SiN^{Dipp})AlCuP^{t}Bu$_3$*** *reproduced from ref.[26] (right)*

These complexes represent a useful point of comparison to the series **3-Cu**, **3-Ag** and **3-Au**, and indeed the same group intentionally synthesised the phosphine-supported **(SiN^{Dipp})AlCuP^{t}Bu$_3$** for this purpose. They report a ^{31}P NMR resonance for this compound at 43.9 ppm, close to the value of 38.3 ppm for **3-Cu**, and indicating a similar copper environment in both compounds. The structure of **(SiN^{Dipp})AlCuP^{t}Bu$_3$** was also determined by X-ray crystallography, revealing a two-coordinate copper centre bound in a linear fashion to the aluminyl and phosphine fragments (**Scheme 3.8**). This cements the findings of Section 3.3.4, lending further credence to the designated structures of **3-Cu** and **3-Ag.** The Al–Cu bond lengths of the **[(SiN^{Dipp})Al]**

based species bearing phosphine or carbene ligands range from 2.3449(4)–2.4028(7) Å, similar to *bis*aluminocuprate **1** (2.4075(5) Å), but again longer than the Al→Cu dative bond in **[HC(MeCMesN)$_2$}CuAl{(NDippCMe)$_2$CH]**, reported by Power.

A quantum chemical investigation of the Al–M species using QTAIM was conducted by Hill and McMullin, which included copper aluminyl **3-Cu** in its analysis. This found that the Al–Cu bond is covalent, and that the calculated atomic charges on Al (q_{Al} = +1.887) and Cu (q_{Cu} = −0.406) suggest the bond is polarised in the direction Al$^{\delta+}$–Cu$^{\delta-}$. This is in keeping with the QTAIM analysis of Aldridge, Goicoechea and coworkers for the gold aluminyl compound **(NON)AlAuP^{t}Bu$_3$** and indeed, the calculated atomic charges for **(SiN^{Dipp})AlAuNHC^{iPr}** show it to possess the most polarised bond of that series, arising from the high electronegativity of gold. The effect of altering the co-ligand from a carbene to P^{t}Bu$_3$ is such that the central Cu bears a more negative charge. The implications of these findings in relation to the reactivity of the Al–M bonds will be discussed in Chapter 4.

3.4 Conclusions and future work

This chapter has described the synthesis of a family of compounds that feature a direct, unsupported covalent group 13 – group 11 metal–metal bond. The synthetic strategy employed nucleophilic, anionic Al(I) or Ga(I) reagents, reacting them with electropositive M(I) halide partners in salt metathesis reactions to form the desired E–M bond. This approach, while previously known for gallium and boron, had been little used for the formation of Al–M bonds, due to the lack of suitable Al(I) reagents. While the Al–M species are examples of novel bonds between elements, the Ga–M compounds bearing the same ligand skeleton provide an interesting reference point with which to compare these new systems.

A rich variation in structure and geometry of the E–M containing products has been uncovered, depending on reagent stoichiometry and the phosphine co-ligand. Using the copper(I) precursor Ph_3PCuI, three copper containing products could be formed. A ratio of one copper to two aluminium centres led to loss of the phosphine ligand entirely, and formation of the potassium *bis*aluminyl copper complex **K[Cu{Al(NON)}$_2$]**, **1**, which features a linear copper centre coordinated by mutually *trans* aluminyl fragments. This compound contains a rare example of a crystallographically characterised Cu–Al bond. Reacting instead two copper centres per aluminium allows retention of the PPh_3 ligand, forming the trimetallic complex **(NON)Al(CuPPh$_3$)$_2$I**, **2-Cu**, a copper analogue of the previously reported trimetallic system **2-Au**. Unlike its heavier congener, **2-Cu** is unstable in solution and can only be generated *in situ*. It goes on to lose a [$(CuPPh_3)_2$I] unit and produce the tetrameric Cu(I)/Cu(0) cluster **(Ph$_3$P)$_4$Cu$_4$I$_2$**. This compound is also formed in the reaction of one Ph_3PCuI with one aluminyl fragment. The gallium analogues of these compounds, **(NON)Ga(AuPPh$_3$)$_2$I** (**2'-Au**) and **(NON)Ga(CuPPh$_3$)$_2$I** (**2'-Cu**) were synthesised for comparison, and X-ray crystallography revealed that the two gold complexes **2-Au** and **2'-Au** were isostructural. Like its aluminium counterpart, **2'-Cu** was unstable to loss of the copper fragment and could only be generated in situ.

Variation of the phosphine ligand allowed for the synthesis of complexes featuring a 1:1 ratio of aluminium to group 11 metal, and also gave access to a system containing an Al–Ag bond. No prior examples of Al–Ag complexes had been reported.

Reaction of **I** with $^tBu_3PMI$ (M = Ag, Cu) gave the silver and copper aluminyl complexes **(NON)AlAgP^{t}Bu$_3$** (**3-Ag**) and **(NON)AlCuP^{t}Bu$_3$** (**3-Cu**). Although these compounds could not be characterised by X-ray crystallography, spectroscopic evidence strongly suggests that they are isostructural with the previously reported gold aluminyl complex

3-Au, featuring a linear Al–M–P unit. This was further corroborated by the structural characterisation of the silver gallyl complex, **3'-Ag** which contains an unsupported Ga–Ag bond, with the P^{t}Bu$_3$ ligand completing a linear Al–M–P unit. Copper and gold gallyl complexes **3'-Cu** and **3'-Au** could also be isolated, showing the generality of the method.

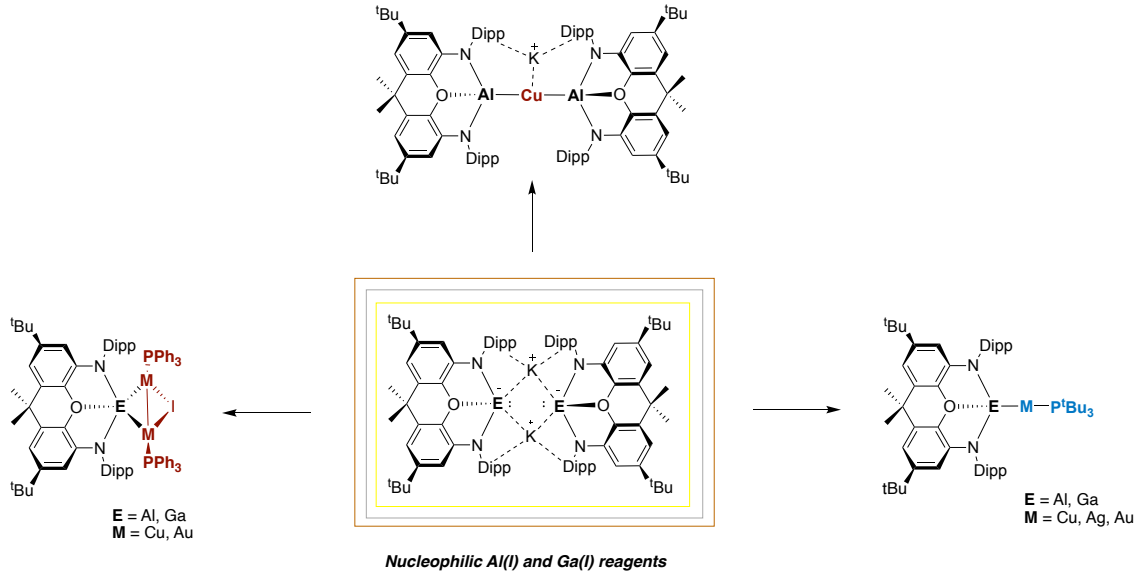


***Figure 3.10**. Summary of complexes containing a direct group 13 – group 11 bond*

The properties of the aluminyl fragment as a metalloligand could be probed by comparison of the ^{31}P NMR spectra of **3-Ag** and **3'-Ag**, which gave insight into the strengths of the Ag–P bond in each complex, and thus the *trans* effect of the opposing ligand. This revealed that the aluminyl moiety is a strong σ-donor, stronger than the gallyl donor formed from the same supporting ligand system. This strong electron donating ability means that complexes **3-Cu** and **3-Ag** contain extremely electron rich group 11 metal sites, a property which will be exploited in the reactivity studies of Chapters 4 and 5.

This work is clearly just the beginning for Al–M covalent bonds, and the rest of the Periodic Table is an open book, waiting to meet an aluminyl ligand. With each metal of interest, there are a wealth of new bonding motifs and properties to be investigated. It may be possible to replicate the extensive body of work that has been carried out using the Ga(I) heterocycle, **[:Ga(Ar-DAB)]-** and lithium boryl reagents (boryl = B{N(Dipp)CH}$_2$ or B{N(Dipp)C(^{t}Bu)NNPh}), supporting metals in unusual oxidation states.[27] However, other metals also bring challenges to this methodology which may make it difficult to form unsupported Al–M bonds using Al(I) sources. Al(I) is inherently highly reducing, more so than Ga(I).[28] This presents a problem for the synthesis of Al–M bonds, as many redox active metals may simply be reduced, rather than forming the desired metal–metal bond. Judicious choice of supporting ligands, as well as the ever-growing selection of nucleophilic Al(I) compounds, may help to overcome this challenge. For example, it has recently been shown that magnesium and zinc aluminyl complexes are less reducing than the potassium derivatives.[29,30]

With this library of directly bonded E–M complexes in hand, we have begun to explore the chemistry of this unique class of bond through reactions with kinetically challenging small molecules. This work is detailed in the forthcoming chapters.

3.5 Synthetic procedures and spectroscopic data for new compounds

Synthesis of K[{(NON)Al}$_2$Cu, 1

A suspension of Ph_3PCuI (0.060g, 0.066 mmol) and **I** (0.200g, 0.136 mmol) in benzene (10 mL) was stirred at room temperature for 16 h. The resulting mixture was filtered, and volatiles removed under vacuum. The residue was dissolved in hexane (10 mL), filtered, concentrated to 5 mL and heated to 50°C. Slow cooling to room temperature yielded yellow crystals of **2**. Yield: 60 mg, 53 %.

^{1}H NMR (400 MHz, C_6D_6, 273 K): δ_H = 1.00 (d, $^3J_{HH}$ = 6.9 Hz, 12H, CH(CH_3)$_2$), 1.27 (s, 18H, C(CH_3)$_3$), 1.42 (d, $^3J_{HH}$ = 6.8 Hz, 12H, CH(CH_3)$_2$), 1.65 (s, 6H, C(CH_3)$_2$), 3.77 (sept, $^3J_{HH}$ = 6.8 Hz, 4H, C*H*(CH$_3$)$_2$), 6.36 (d, $^4J_{HH}$ = 1.9 Hz, 2H, XA-*o*-C*H*), 6.76 (d, $^4J_{HH}$ = 1.9 Hz , 2H, XA-*p*-C*H*), 7.24-26 (m, 6H, Ar*H*).

^{13}C{^{1}H} NMR (126 MHz, C_7D_8, 373 K): δ_C = 25.4, 26.2 (CH(*C*H$_3$)2), 29.9 (*C*H(CH$_3$)$_2$), 31.9 (xan-C(*C*H$_3$)$_2$), 32.1 (C(*C*H$_3$)$_3$), 35.4 (*C*(CH$_3$)$_3$), 38.0 (xan-*C*(CH$_3$)$_2$), 106.5, 109.1, 124.4, 124.5, 128.5, 134.4, 134.7, 143.4, 143.9, 148.6, 150.3 (Ar-C).

The ^{1}H and ^{13}C NMR spectra of **1** are relatively broad at room temperature and suffer from reduced compound solubility as the temperature is lowered. Spectra are therefore reported at 373 K, at which temperature the signals are relatively sharp, and are consistent with rapid exchange.

Elemental microanalysis: calc. for $C_{94}H_{124}Al_2CuKN_4O_2$: C 75.34 %, H 8.34 %, N 3.74 %, meas.: C 74.81 %, H 8.72 %, N 3.30 %

***In situ* synthesis of (NON)Al(CuPPh$_3$)$_2$I (2-Cu)**

To a solution of **I** (0.020 g, 0.025 mmol) in C_6D_6 (10 mL) was added Ph_3PCuI (0.024 g, 0.026 mmol). Over the course of 1 h, a precipitate formed and formation of **2-Cu** was apparent by multi-nuclear NMR.

^{1}H NMR (400 MHz, C_6D_6, 298 K): δ = 0.68 (s, 3H, C(C*H*$_3$)$_2$), 0.72 (d, $^3J_{HH}$ = 6.9 Hz, 6H, CH(C*H*$_3$)$_2$), 1.07 (d, $^3J_{HH}$ = 6.2 Hz, 6H, CH(C*H*$_3$)$_2$), 1.09 (d, $^3J_{HH}$ = 6.2 Hz, 6H, CH(C*H*$_3$)$_2$), 1.22 (d, $^3J_{HH}$ = 7.3 Hz, 6H, CH(C*H*$_3$)$_2$), 1.28 (s, 18H, C(C*H*$_3$)$_3$), 1.49 (s, 3H, C(C*H*$_3$)$_2$), 3.35 (sept., $^3J_{HH}$ = 6.7 Hz, 2H, C*H*(CH$_3$)$_2$), 4.20 (sept., $^3J_{HH}$ = 6.7 Hz, 2H, C*H*(CH$_3$)$_2$), 6.26 (d, $^4J_{HH}$ = 2.0 Hz, 2H, XA-*o*-C*H*), 6.63 (d, $^4J_{HH}$ = 2.0 Hz, 2H, XA-*p*-C*H*), 6.87-7.80 (m, 36H Ar*H*);

No ^{13}C NMR data could be obtained due to decomposition of **2-Cu** in solution.

^{31}P{^{1}H} NMR (162 MHz, C_6D_6, 298 K): δ_P = 3.2 (d, $^3J_{PP}$ = 39 Hz), 10.1 (d, $^3J_{PP}$ = 39 Hz)

***In situ* synthesis of (NON)Ga(CuPPh$_3$)$_2$I (2'-Cu)**

To a solution of **II** (0.200 g, 0.136 mmol) in toluene (10 mL) was added a suspension of Ph_3PCuI (0.240g, 0.264 mmol) in toluene (10 mL) at room temperature over 5 min. The reaction was stirred for 1 h, after which time a precipitate formed and formation of **2-Cu** was apparent by multi-nuclear NMR.

^{1}H NMR (400 MHz, C_6D_6, 298 K): δ = 0.70 (s, 3H, C(C*H*$_3$)$_2$), 1.13 (d, $^3J_{HH}$ = 7.1 Hz, 12H, CH(C*H*$_3$)$_2$), 1.34 (d, $^3J_{HH}$ = 7.3 Hz, 6H, CH(C*H*$_3$)$_2$), 1.21 (s, 9H, C(C*H*$_3$)$_3$), 1.33 (s, 9H, C(C*H*$_3$)$_3$), 1.35 (d, $^3J_{HH}$ = 7.3 Hz, 6H, CH(C*H*$_3$)$_2$), 1.59 (s, 3H, C(C*H*$_3$)$_2$), 3.37 (sept., $^3J_{HH}$ = 6.7 Hz, 1H, C*H*(CH$_3$)$_2$), 3.48 (sept., $^3J_{HH}$ = 6.7 Hz, 1H, C*H*(CH$_3$)$_2$), 4.03 (sept., $^3J_{HH}$ = 6.7 Hz, 1H, C*H*(CH$_3$)$_2$), 3.37 (sept., $^3J_{HH}$ = 6.7 Hz, 1H, C*H*(CH$_3$)$_2$), 4.15

(sept., $^{3}J_{HH}$ = 6.7 Hz, 1H, C*H*(CH_3)$_2$), 6.28 (s, 1H, XA-*o*-C*H*), 6.35 (s, 1H, XA-*p*-C*H*), 6.64 (s, 1H, XA-*o*-C*H*), 6.81 (s, 1H, XA-*p*-C*H*), 7.20-7.63 (m, 36H Ar*H*);

No ^{13}C NMR data could be obtained due to decomposition of **2'-Cu** in solution.

^{31}P{^{1}H} NMR (162 MHz, C_6D_6, 298 K): δ_P = 5.5 (d, $^{3}J_{PP}$ = 39 Hz), 13.5 (d, $^{3}J_{PP}$ = 28 Hz)

Synthesis of (NON)Ga(AuPPh$_3$)$_2$I (2'-Au)

To a solution of **II** (0.200 g, 0.136 mmol) in toluene (10 mL) was added a suspension of Ph_3PCuI (0.240g, 0.264 mmol) in toluene (10 mL) at room temperature over 5 min. The solution was stirred for 1 h, and the volatiles were then removed under vacuum. The residue was taken up in diethyl ether (5 mL) and filtered. The resulting yellow solution was concentrated to 2 mL and stored at −30°C, leading to formation of yellow crystals of **2'-Au**. Yield: 110 mg, 42%)

The ^{1}H NMR spectrum of **2'-Au** is broad at room temperature and difficult to assign. Therefore the spectrum is given at 373 K, at which temperature the signals are still relatively broad, but can be differentiated and assigned. The spectrum is more symmetrical at this temperature than at room temperature. The ^{13}C NMR spectrum of **2'-Au** is very weak at room temperature and could not be assigned.

^{1}H NMR (400 MHz, C_6D_6, 298 K): δ_H = 1.10 (d, $^{3}J_{HH}$ = 7.0 Hz, 12H, CH(C*H*$_3$)$_2$), 1.18 (d, $^{3}J_{HH}$ = 6.8 Hz, 12H, CH(C*H*$_3$)$_2$), 1.23 (s, 18H, C(C*H*$_3$)$_3$), 1.58 (s, 6H, C(C*H*$_3$)$_2$), 3.69 (br, 4H, C*H*(CH_3)$_2$), 6.21 (2H, XA-*o*-C*H*), 6.70 (2H, XA-*p*-C*H*), 7.24-26 (m, 36H Ar*H*).

^{31}P{^{1}H} NMR (162 MHz, C_6D_6, 298 K): δ_P = 50.8 (d, $^{3}J_{PP}$ = 39 Hz), 55.6 (d, $^{3}J_{PP}$ = 112 Hz)

Synthesis of (NON)AlAgP^{t}Bu$_3$ (3-Ag)

A suspension of ^{t}Bu$_3$PAgI (0.110 g, 0.271 mmol) and **I** (0.200 g, 0.136 mmol) in toluene (10 mL) was stirred at room temperature for 16 h. The resulting mixture was filtered to give a pale green solution which was concentrated to 3 mL and slowly cooled to 3 °C. Colourless microcrystals of **3-Ag** were isolated by filtration and washed with pentane. Yield: 0.120 g, 46 %.

^{1}H NMR (400 MHz, C_6D_6, 298 K): δ_H = 0.91 (d, $^3J_{HP}$ = 10.7 Hz, 27H, PC(C*H*$_3$)$_3$), 1.23 (d, $^3J_{HH}$ = 6.9 Hz, 12H, CH(C*H*$_3$)$_2$), 1.27 (s, 18H, C(C*H*$_3$)$_3$), 1.42 (d, $^3J_{HH}$ = 6.8 Hz, 12H, CH(C*H*$_3$)$_2$), 1.65 (s, 6H, C(C*H*$_3$)$_2$), 3.77 (sept, $^3J_{HH}$ = 6.8 Hz, 4H, C*H*(CH$_3$)$_2$), 6.36 (d, $^4J_{HH}$ = 1.9 Hz, 2H, XA-*o*-C*H*), 6.76 (d, $^4J_{HH}$ = 1.9 Hz , 2H, XA-*p*-C*H*), 7.24-26 (m, 6H Ar*H*).

^{13}C{^{1}H} NMR (126 MHz, C_6D_6, 298 K): δ_C = 25.5, 25.7 (CH(*C*H$_3$)$_2$) 27.8 (*C*(CH$_3$)$_2$), 29.3 (*C*H(CH$_3$)$_2$), 31.8 (C(*C*H$_3$)$_3$), 32.1 (d, $^2J_{CP}$ = 6.0 Hz, P{C(*C*H$_3$)$_3$}$_3$), 35.1 (*C*(CH$_3$)$_3$), 36.7 (dd, $^2J_{CAg}$ = 4.0, 6.8 Hz, P{*C*(CH$_3$)$_3$}$_3$), 37.2(*C*(CH$_3$)$_2$), 105.8, 110.5, 123.9, 125.6, 128.3, 132.6, 142.2, 142.8, 143.3, 148.0, 148.3 (Ar*C*). **^{31}P{^{1}H} NMR** (162 MHz, C_6D_6, 298 K): δ_P = 58.9 (d, $^1J_{PAg}$ = 160.6 Hz) 62.1 (s) (P^{t}Bu$_3$)

Elemental microanalysis: calc. for $C_{59}H_{89}AgAlN_2OP$: C 70.29 %, H 8.90 %, N 2.78 %, meas.: C 67.38 %, H 8.52 %, N 2.81 %

Synthesis of (NON)GaAgP^{t}Bu$_3$ (3'-Ag)

A solution of **II** (200 mg, 0.128 mmol) and ^{t}Bu$_3$PAgI (108 mg, 0.256 mmol) in toluene (10 mL) was stirred at room temperature for 4 h. The resulting mixture was filtered to give a yellow solution which was concentrated to ca. 5 mL. Crystals of **3'-Ag** suitable for X-ray crystallography were obtained by slow cooling to 3 °C. Yield: 210 mg, 78 %.

^{1}H NMR (400 MHz, C_6D_6, 298 K): δ_H = 0.84 (d, $^{3}J_{HP}$ = 12.1 Hz, 27H, PC(C*H*$_3$)$_3$), 1.25 (d, $^{3}J_{HH}$ = 6.7 Hz, 12H, CH(C*H*$_3$)$_2$), 1.33 (s, 18H, C(C*H*$_3$)$_3$), 1.35 (d, $^{3}J_{HH}$ = 7.1 Hz, 12H, CH(C*H*$_3$)$_2$), 1.74 (s, 6H, C(C*H*$_3$)$_2$), 3.80 (sept, $^{3}J_{HH}$ = 6.8 Hz, 4H, C*H*(CH$_3$)$_2$), 6.39 (d, $^{4}J_{HH}$ = 2.0 Hz, 2H, XA-*o*-C*H*), 6.81 (d, $^{4}J_{HH}$ = 2.0 Hz , 2H, XA-*p*-C*H*), 7.20-7.27 (m, 6H Ar*H*).

^{13}C{^{1}H} NMR (126 MHz, C_6D_6, 298 K): δ_C = 25.3, 25.9 (CH(*C*H$_3$)$_2$) 27.7 (*C*(CH$_3$)$_2$), 29.3 (*C*H(CH$_3$)$_2$), 31.9 (C(*C*H$_3$)$_3$), 32.1 (d, $^{2}J_{CP}$ = 6.0 Hz, P{C(*C*H$_3$)$_3$}$_3$), 35.1 (*C*(CH$_3$)$_3$), 36.8 (*C*(CH$_3$)$_2$), 37.3 (P{*C*(CH$_3$)$_3$}$_3$), 105.7, 110.6, 124.0, 125.7, 133.7, 142.6, 143.2, 143.8, 147.8, 148.1 (Ar*C*).

^{31}P{^{1}H} NMR (162 MHz, C_6D_6, 298 K): δ_P = 65.4 (dd, $^{1}J_{P\text{-}107Ag}$ = 278, $^{1}J_{P\text{-}109Ag}$ = 322 Hz). Elemental microanalysis: calc. for $C_{59}H_{89}AgGaN_2OP$: C 67.43 %, H 8.54 %, N 2.67 %; meas.: C 66.81 %, H 8.14 %, N 2.64 %.

Synthesis of (NON)CuAgP^{t}Bu$_3$ (3-Cu)

A suspension of ^{t}Bu$_3$PCuI (0.107 g, 0.271 mmol) and **I** (0.200 g 0.136 mmol) in toluene (10 mL) was stirred at room temperature for 16 h. The resulting mixture was filtered to give a pale green solution which was concentrated to 3 mL and slowly cooled to 3 °C. Colourless microcrystals of **3-Cu** were isolated by filtration and washed with pentane. Yield: 110 mg, 42 %.

^{1}H NMR (400 MHz, C_6D_6, 298 K): δ_H = 0.90 (d, $^{3}J_{HP}$ = 12.2 Hz, 27H, PC(C*H*$_3$)$_3$), 1.21 (d, $^{3}J_{HH}$ = 6.9 Hz, 12H, CH(C*H*$_3$)$_2$), 1.28 (s, 18H, C(C*H*$_3$)$_3$), 1.45 (d, $^{3}J_{HH}$ = 7.0 Hz, 12H, CH(C*H*$_3$)$_2$), 1.67 (s, 6H, C(C*H*$_3$)$_2$), 3.79 (sept, $^{3}J_{HH}$ = 7.0 Hz, 4H, C*H*(CH$_3$)$_2$), 6.31 (d, $^{4}J_{HH}$ = 1.9 Hz, 2H, XA-*o*-C*H*), 6.76 (d, $^{4}J_{HH}$ = 1.9 Hz , 2H, XA-*p*-C*H*), 7.19-27 (m, 6H Ar*H*).

$^{13}C\{^1H\}$ NMR (126 MHz, C_6D_6, 298 K): δ = 25.3, 25.9 ($CH(CH_3)_2$) 27.7 ($C(CH_3)_2$), 29.3 ($CH(CH_3)_2$), 31.9 ($C(CH_3)_3$), 32.1 (d, $^2J_{CP}$ = 6.0 Hz, $P\{C(CH_3)_3\}_3$), 35.1 ($C(CH_3)_3$), 36.8 ($C(CH_3)_2$), 37.3 ($P\{C(CH_3)_3\}_3$), 105.7, 110.6, 124.0, 125.7, 133.7, 142.6, 143.2, 143.79, 147.8, 148.1 (Ar-*C*).

$^{31}P\{^1H\}$ NMR (162 MHz, C_6D_6, 298 K): δ_P = 38.3. Elemental microanalysis: calc. for $C_{59}H_{89}CuAlN_2OP$: C 73.52 %, H 9.31 %, N 2.91 %, found: C 72.72 %, H 8.75 %, N 3.05 %

Synthesis of (NON)GaCuP^{t}Bu$_3$ (3'-Cu)

A solution of **II** (0.200 g, 0.128 mmol) and ^{t}Bu$_3$PCuI (112 mg, 0.256 mmol) in toluene (10 mL) was stirred at room temperature for 4 h. The resulting mixture was filtered to give a yellow solution which was concentrated to ca. 5 mL. **3'-Cu** was obtained from this solution as a microcrystalline solid which was washed with pentane. Yield: 170 mg, 70%

^1H NMR (400 MHz, C_6D_6, 298 K): δ_H = 0.82 (d, $^3J_{HP}$ = 12.4 Hz, 27H, $PC(CH_3)_3$), 1.23 (d, $^3J_{HH}$ = 6.7 Hz, 12H, $CH(CH_3)_2$), 1.32 (s, 18H, $C(CH_3)_3$), 1.36 (d, $^3J_{HH}$ = 7.1 Hz, 12H, $CH(CH_3)_2$), 1.75 (s, 6H, $C(CH_3)_2$), 3.80 (sept, $^3J_{HH}$ = 6.8 Hz, 4H, $CH(CH_3)_2$), 6.31 (d, $^4J_{HH}$ = 2.0 Hz, 2H, XA-*o*-C*H*), 6.79 (d, $^4J_{HH}$ = 2.0 Hz , 2H, XA-*p*-C*H*), 7.12-7.29 (m, 6H Ar*H*).

$^{13}C\{^1H\}$ NMR (126 MHz, C_6D_6, 298 K):): δ = 25.3, 26.2 ($CH(CH_3)_2$) 27.5 ($C(CH_3)_2$), 28.8 ($CH(CH_3)_2$), 32.0 (d, $^2J_{CP}$ = 6.0 Hz, $P\{C(CH_3)_3\}_3$), 32.1 ($C(CH_3)_3$), 35.0 ($C(CH_3)_3$), 36.9 ($C(CH_3)_2$), 37.9 ($P\{C(CH_3)_3\}_3$), 106.2, 110.5, 123.9, 125.4, 128.3, 135.0, 143.4, 143.5, 144.7, 146.7, 148.5 (Ar-*C*).

$^{31}P\{^1H\}$ NMR (162 MHz, C_6D_6, 298 K): δ_P = 46.5

Synthesis of (NON)GaAuP^{t}Bu$_3$ (3'-Au)

A mixture of **II** (22 mg, 0.0201 mmol) and ^{t}Bu$_3$PAuI (10 mg, 0.019 mmol) in benzene (1.0 mL) was stirred at room temperature for 4 h, after which time a white precipitate formed. The reaction mixture was filtered to give a colourless solution. Microcrystalline **3'-Au** was obtained by slow evaporation of this solution (18 mg, 83 %)

^{1}H NMR (400 MHz, C_6D_6, 298 K): δ_H = 0.90 (d, $^{3}J_{HP}$ = 13.0 Hz, 27H, PC(C*H*$_3$)$_3$), 1.23 (d, $^{3}J_{HH}$ = 7.1 Hz, 12H, CH(C*H*$_3$)$_2$), 1.30 (s, 18H, C(C*H*$_3$)$_3$), 1.36 (d, $^{3}J_{HH}$ = 7.1 Hz, 12H, CH(C*H*$_3$)$_2$), 1.73 (s, 6H, C(C*H*$_3$)$_2$), 3.79 (sept, $^{3}J_{HH}$ = 6.8 Hz, 4H, C*H*(CH$_3$)$_2$), 6.37 (d, $^{4}J_{HH}$ = 2.0 Hz, 2H, XA-*o*-C*H*), 6.81 (d, $^{4}J_{HH}$ = 2.0 Hz , 2H, XA-*p*-C*H*), 7.12-7.29 (m, 6H Ar*H*).

^{13}C{^{1}H} NMR (126 MHz, C_6D_6, 298 K): δ = 25.2, 26.1 (CH(*C*H$_3$)$_2$) 27.8 (*C*(CH$_3$)$_2$), 29.3 (*C*H(CH$_3$)$_2$), 31.9 (C(*C*H$_3$)$_3$), 32.4 (d, $^{2}J_{CP}$ = 6.0 Hz, P{C(*C*H$_3$)$_3$}$_3$), 35.4 (*C*(CH$_3$)$_3$), 37.1 (*C*(CH$_3$)$_2$), 38.1 (P{*C*(CH$_3$)$_3$}$_3$), 105.3, 110.6, 124.1, 126.0, 133.7, 142.2, 143.2, 143.6, 147.8, 148.2 (Ar-*C*).

^{31}P{^{1}H} NMR (162 MHz, C_6D_6, 298 K): δ_P = 97.9

3.6 References

1 C. Ganesamoorthy, J. Weßing, C. Kroll, R. W. Seidel, C. Gemel and R. A. Fischer, *Angew. Chemie - Int. Ed.*, 2014, **53**, 7943–7947.
2 A. Puls, P. Jerabek, W. Kurashige, M. Förster, M. Molon, T. Bollermann, M. Winter, C. Gemel, Y. Negishi, G. Frenking and R. A. Fischer, *Angew. Chemie - Int. Ed.*, 2014, **53**, 4327–4331.
3 K. L. Mears, C. R. Stennett, E. K. Taskinen, C. E. Knapp, C. J. Carmalt, H. M. Tuononen and P. P. Power, *J. Am. Chem. Soc.*, 2020, **142**, 19874–19878.
4 R. Y. Kong and M. R. Crimmin, *Dalt. Trans.*, 2021, **50**, 7810–7817.
5 J. Hicks, A. Mansikkamäki, P. Vasko, J. M. Goicoechea and S. Aldridge, *Nat. Chem.*, 2019, **11**, 237–241.
6 N. Kaltsoyannis, *J. Chem. Soc. - Dalt. Trans.*, 1997, 1–11.
7 N. Bartlett, *Gold Bull.*, 1998, **31**, 22–25.
8 J. Hicks, P. Vasko, J. M. Goicoechea and S. Aldridge, *Nature*, 2018, **557**, 92–95.
9 A. Kempter, C. Gemel and R. A. Fischer, *Inorg. Chem.*, 2005, **44**, 163–165.
10 P. P. Power, K. Ruhlandt-Senge and S. C. Shoner, *Inorg. Chem*, 1991, **30**, 5013–5015.
11 M. Ler, A. Lars and S. Westman, *Acta Crystallogr. Sect. A*, 1977, **51**, 399–404.
12 F. P. Gabbaï, A. Schier, J. Riede and H. Schmidbaur, *Inorg. Chem.*, 1995, **34**, 3855–3856.
13 D. S. Weinberger, M. Melaimi, C. E. Moore, A. L. Rheingold, G. Frenking, P. Jerabek and G. Bertrand, *Angew. Chemie - Int. Ed.*, 2013, **52**, 8964–8967.
14 S. P. Green, C. Jones, D. P. Mills and A. Stasch, *Organometallics*, 2007, **26**, 3424–3430.
15 U. Anandhi and P. R. Sharp, *Angew. Chemie - Int. Ed.*, 2004, **43**, 6128–6131.
16 H. Schmidbaur and A. Schier, *Chem. Soc. Rev.*, 2012, **41**, 370–412.
17 P. Atkins and J. de Paulo, *Atkins' Physical Chemistry*, Oxford University Press, Oxford, 9th edn., 2009.
18 R. G. Goel and P. Pilon, *Inorg. Chem.*, 1978, **17**, 2876–2879.
19 R. G. Goel and A. L. Beauchamp, *Inorg. Chem.*, 1983, **22**, 395–400.
20 D. Schneider, A. Schier and H. Schmidbaur, *Dalt. Trans.*, 2004, 1995–2005.
21 C. Gibard, K. Fauché, R. Guillot, L. Jouffret, M. Traïkia, A. Gautier and F. Cisnetti, *J. Organomet. Chem.*, 2017, **840**, 70–74.
22 Y. Segawa, M. Yamashita and K. Nozaki, *Angew. Chemie - Int. Ed.*, 2007, **46**, 6710–6713.
23 R. G. Bryant, *J. Chem. Educ.*, 1983, **60**, 933–935.
24 P. A. W. Dean, J. J. Vittal and R. S. Srivastava, *Can. J. Chem.*, 1987, **65**, 2628–2633.
25 J. Hicks, P. Vasko, J. M. Goicoechea and S. Aldridge, *Angew. Chemie Int. Ed.*, 2021, **60**, 1702–1713.
26 H.-Y. Liu, S. E. Neale, M. S. Hill, M. F. Mahon and C. L. McMullin, *Dalt. Trans.*, 2022, **51**, 3913–3924.
27 M. Asay, C. Jones and M. Driess, *Chem. Rev.*, 2011, **111**, 354–396.
28 A. J. Downs, *Chemistry of aluminium, gallium, indium and thallium*, Blackie Academic and Professional, London, 1993.
29 M. Roy, J. Hicks, A. Heilmann, A. M. Baston, P. Vasko, J. Goicoechea and S.

Aldridge, *Angew. Chemie Int. Ed.*, 2021, **60**, 41, 22301-22306.
30 M. J. Evans, M. D. Anker, C. L. McMullin, S. E. Neale and M. P. Coles, *Angew. Chemie*, 2021, **133**, 22463–22466.

Chapter 4 : Reactivity of silver and copper aluminyl complexes with heteroallenes

4.1 : Introduction

4.1.1 Chemistry of carbon dioxide

Second only to water, carbon dioxide (CO_2) is perhaps the chemical best known to the general public. It plays an important role in photosynthesis and has allowed life on earth to flourish through its ability to absorb infrared radiation from the sun. However, rising levels of atmospheric CO_2 produced by burning fossil fuels are the leading cause of climate change, which will have an enormous negative impact on our environment, ranging from flooding to food insecurity.[1] While cessation of anthropogenic CO_2 production is necessary to prevent further damage, it is imperative that carbon is also removed from the atmosphere.[2] Carbon capture and storage technology will lead to high availability of CO_2 as a chemical feedstock, and this waste CO_2 may be used as a reagent to form value-added products.[3] Despite being a kinetically inert weak electrophile, CO_2 serves as an organic building block, finding use in industrial processes such as urea production and aspirin synthesis.[4] Also of increasing interest is CO_2 reduction chemistry, which forms part of a range of strategies to replicate photosynthesis for energy generation. Many of the transformations of CO_2 into commodity chemicals are made possible by organometallic reagents and catalysts which control the product selectivity. [5,6]

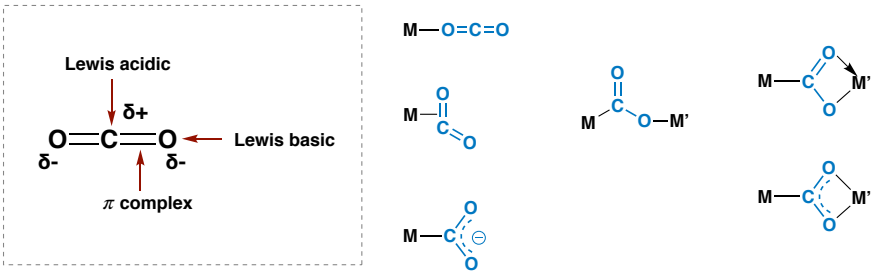


***Figure 4.1**. Identification of reactive sites on the CO_2 molecule (left) and binding modes of CO_2 to mono- and binuclear metals (right).*

A key challenge in carbon dioxide valorisation is selectivity.[7] Multiple products are possible from CO_2 reduction reactions involving metal catalysts, including CO, CH_3OH and $HCOOH/HCOO^-$, as well as coupled products such as oxalate or ethanol. Typically, the coordination of CO_2 to a metal determines the product(s) of this reaction.[8,9] Several binding modes are possible for CO_2 (**Figure 4.1**). Being a polar molecule, CO_2 can bind through its Lewis basic oxygen atoms or the electropositive carbon. It is also possible to form π complexes *via* the C=O double bonds. Bimetallic activation of CO_2 can result in bridging complexes, with O binding in mono- or bidentate fashion. A detailed understanding of metal – CO_2 interactions is key to the development of systems for the selective fixation of this inert molecule.

4.1.2 Main group CO_2 activation

Although much of the work on CO_2 fixation has focussed on transition metals, main group chemistry has a long history in this area. Most famously, Grignard reagents can nucleophilically add to CO_2, forming C–C bonds.[10] The insertion of CO_2 into metal hydride bonds is well known for main group systems, leading to formate products, finding use in hydroformylation reactions.[11] Also gaining traction is the activation of CO_2 by Frustrated Lewis Pairs (FLPs), which show great promise for this purpose.[12] In 2009, Ashley and O'Hare showed that the FLP system based on TMP/BCF (TMP

= 2,2,6,6-tetramethylpiperidine, BCF = $B(C_6F_5)_3$) could bring about the stoichiometric hydrogenation of CO_2 to CH_3OH, albeit at 160°C over a period of 6 days (**Figure 4.2**, i).[13] The groups of Stephan, Hu and Wu have built on this, designing FLP systems to catalytically transform CO_2 to formate, CH_3I, CH_4 or Me_3SiOCH_3.[14,15] In these systems, the Lewis acidic and Lewis basic sites present in the FLP work cooperatively to bind to the different CO_2 reactive centres.[16,17]

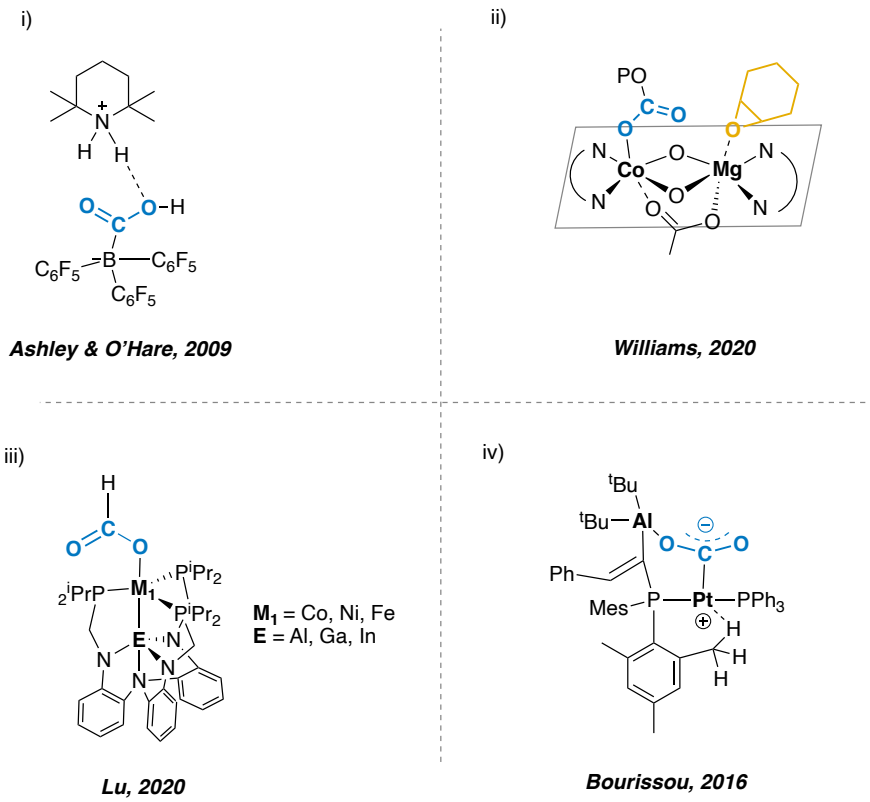


***Figure 4.2**. Cooperative activation of CO_2: i) FLP mediated CO_2 activation; ii) Binding of CO_2 and an epoxide to the two metal sites of MgCo polymerisation catalyst; iii) Transition metal complexes supported by a group 13 metalloligand, capable of CO_2 hydrogenation; iv) Al assisted activation of CO_2 at a Pt site*

4.1.3 CO_2 activation by heterobimetallic complexes

As an extension of this dual reactivity, bimetallic complexes have attracted interest for CO_2 activation due to the potential for cooperative reactivity that the two metals can provide.[18–21] Indeed, in the carbon monoxide dehydrogenase (CODH) enzyme active

site, CO_2 is activated by an Ni/Fe core, with one metal functioning as a Lewis acid and the other as a Lewis base.[22] A number of examples are shown in **Figure 4.2**. In the copolymerisation of CO_2 and epoxides, the heterodinuclear catalyst **LMgCo(OAc)** (L = di-^{t}Bu-tetramethyl-tetraaza-dibenzenacyclohexadecaphane-bis(olate)) binds CO_2 at cobalt and the epoxide at magnesium, lowering the transition state energy for chain growth *via* ring opening (ii). The Lu group have reported extensively on a series of first row transition metal complexes supported by group 13 metalloligands, **M_1–E–L** where **L** is the tripodal tris(phosphinoamido)amine ligand [N(*o*-($NCH_2P^iPr_2$)-C_6H_4)$_3$]$^{3-}$) (iii). In these complexes, which catalyse a CO_2 to formate transformation, the group 13 element was shown to be critical, as **$NiLH_3$** itself is not reactive towards CO_2 hydrogenation. Again demonstrating the partnership of group 13 and d-block metals, a Pt→Al compound has been shown by Bourissou and coworkers to activate CO_2 in an FLP-like manner (iv).[23]

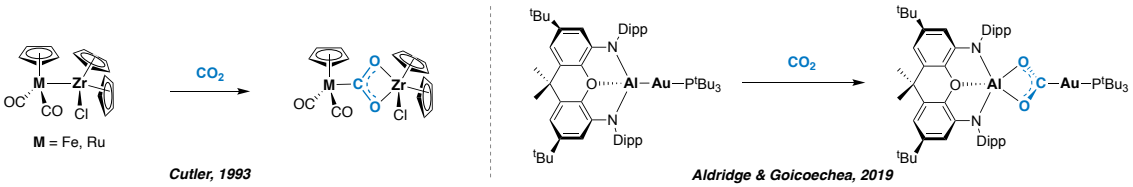


***Figure 4.3**. Examples of direct CO_2 insertion into M–M' bonds: CO_2 insertion into an M–Zr (M = Fe, Ru) complex (left), CO_2 insertion into the gold aluminyl, forming an Au–μ-CO_2-Al unit (right)*

Less well investigated is the direct insertion of CO_2 into metal–metal bonds, of which very few examples are known. The first report of such a reaction was the insertion of CO_2 into an M–Zr bond of the complexes **$Cp(CO)_2M–Zr(Cl)Cp_2$** (M = Fe, Ru) in 1994, although no crystallographic evidence of this coordination mode was obtained (**Figure 4.3**). A landmark result came with the synthesis of the gold aluminyl complex **(NON)AlAuP^{t}Bu$_3$** (**3-Au**) described in Section 3.1.2, which was published in 2019 by

Aldridge and Goicoechea.[24] The reaction of **3-Au** with CO_2 at room temperature resulted in insertion of CO_2 into the Al–Au bond (**Figure 4.3**). The μ-κ^1(C):κ^2(O,O') binding mode in the product was confirmed crystallographically, making it the first such example of CO_2 insertion into an M–M' bond. The regiochemistry of the insertion is such that the gold centre within **3-Au** formally undertakes nucleophilic attack on the central carbon of CO_2. This reactivity was previously unprecedented for gold, which is widely used as an electropositive metal in the +1 oxidation state in catalysis.[25] Complex **3-Au** showed similar reactivity towards the carbodiimide ^{i}PrNCN^{i}Pr, which also inserts into the Al–Au bond, further demonstrating a reversal of the traditional reactivity of gold.

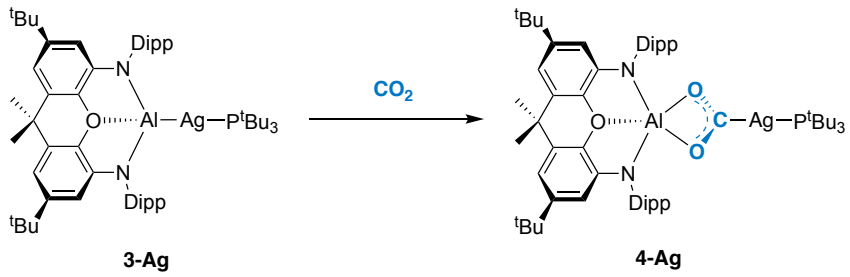
4.2 Aims

The report of gold aluminyl **3-Au** opened the door to new bimetallic reactivity, showing that the gold atom can act as a nucleophile towards CO_2 and ^{i}PrNCN^{i}Pr. With the silver and copper complexes of Chapter 3 in hand, it might be possible to expand this unprecedented chemistry to the lighter group 11 metals. The aim of the work presented in this chapter is to investigate the reactivity of the coinage metal–aluminyl complexes described in Chapter 3 towards CO_2 and other heteroallenes. In doing so, insight into the nature of the metal–metal bonding in mixed coinage metal/group 13 systems will be gained. It is anticipated that the variation in properties of the group 11 metals (such as electronegativity) will lead to differences in their reactivity towards carbon based electrophiles such as CO_2. These differences will inform the understanding of bimetallic complexes featuring a direct aluminium–group 11 covalent bond.

4.3 Results and discussion

4.3.1 Reaction of a silver aluminyl complex with CO_2

A suspension of silver aluminyl **(NON)Al–AgP^{t}Bu$_3$**, **3-Ag**, in benzene was exposed to an atmosphere of CO_2 at room temperature, resulting in immediate dissolution to form a colourless solution (**Scheme 4.1**). An *in situ* ^{31}P spectrum shows disappearance of the broad doublet at 59.0 ppm associated with **3-Ag**, and clean conversion to a single new product which gives rise to a signal at 76.0 ppm, showing coupling to both ^{107}Ag and ^{109}Ag nuclei ($^1J_{PAg}$ = 406, 465 Hz). This enhanced resolution compared to **3-Ag** indicates that the silver is no longer directly bound to the quadrupolar Al centre. The magnitudes of the coupling constants are similar to values previously reported for silver complexes bearing both a phosphine and an NHC ligand.[26–28] This suggests that silver is now ligated to a carbenic carbon centre. To further probe the system, **3-Ag** was reacted with $^{13}CO_2$. The ^{31}P NMR spectrum (**Figure 4.4**) now shows additional coupling to the ^{13}C nucleus ($^2J_{CP}$ = 81 Hz), which is indicative of a linear P–Ag–C unit, such as the phosphine-silver-NHC complexes described by Braunstein and Danopoulos (cf. $^2J_{CP}$ = 62 Hz).[27] The ^{13}C NMR spectrum of the isolated product is particularly enlightening, showing a downfield shifted 8-line signal at 237.7 ppm (**Figure 4.5**). This multiplet arises from coupling to both silver and ^{31}P isotopes ($^1J_{107AgC}$ = 229 Hz, $^1J_{109AgC}$ = 266 Hz, $^2J_{CP}$ = 81 Hz). The chemical shift of the resonance is characteristic of a carbenic carbon,[29] and indeed is very close to that of the gold dioxocarbene formed by the reaction of **3-Au** with CO_2.[24] Similar shifts have been reported for an iron-bound carboxylate and, more recently, a stanna-carboxylate (239.5 and 220.6 ppm respectively).[30,31]



Scheme 4.1 *Reaction of* ***3-Ag*** *with CO_2 (1 atm, room temperature, toluene).*

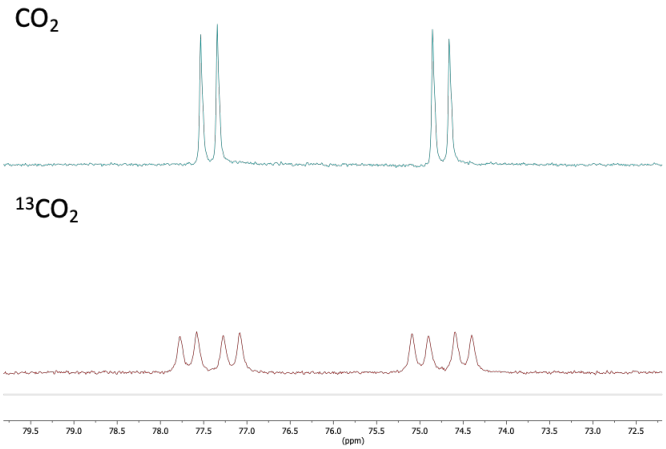


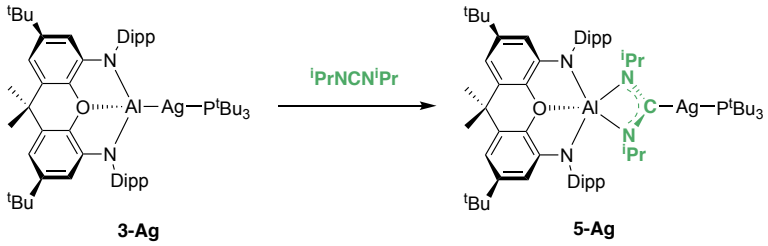
Figure 4.4. *^{31}P NMR spectrum of* ***4-Ag*** *prepared from* ***3-Ag*** *with CO_2 (above) and $^{13}CO_2$ (below), showing additional coupling to ^{13}C.*

This combined multinuclear NMR evidence strongly suggests that the CO_2 has inserted into the Ag−Al bond, forming a dioxocarbene analogous to that formed by the reaction of gold aluminyl **3-Au** with CO_2. Although **3-Ag** can be cleanly isolated as a white solid, it was not possible to obtain crystals suitable for X-ray diffraction. Therefore, we turned to the alternative heteroallene di*iso*propylcarbodiimide to provide a structural mimic for carbon dioxide.

4.3.2 Reaction of a silver aluminyl complex with a carbodiimide

Addition of 1 equivalent of di*iso*propylcarbodiimide to a benzene suspension of **3-Ag** causes immediate dissolution to produce a colourless solution (**Scheme 4.2**). As with the formation of **4-Ag**, ^{31}P NMR shows conversion to a single product, as evidenced

by the appearance a signal with two silver satellites at 73.4 ppm with similar coupling constants to that of **4-Ag** ($^{1}J_{PAg}$ = 352, 408 Hz). The ^{1}H spectrum implies a decrease in symmetry of the product as compared to the starting material **3-Ag**, manifested by an increase in the number of Dipp methine protons. Accordingly, two resonances relating to the carbodiimide isopropyl groups can be seen, as compared to one in the free di*iso*propylcarbodiimide. In addition, the ^{13}C NMR spectrum exhibits an 8-line multiplet at 220.2 ppm, closely resembling the same region in the spectrum of **4-Ag** (**Figure 4.5**). Single crystals of compound **5-Ag** could be obtained from a hexane solution, allowing the solid-state structure to be determined (**Figure 4.6**).



Scheme 4.2. *Insertion of ^{i}PrNCN^{i}Pr into the Al–Ag bond of* ***3-Ag***

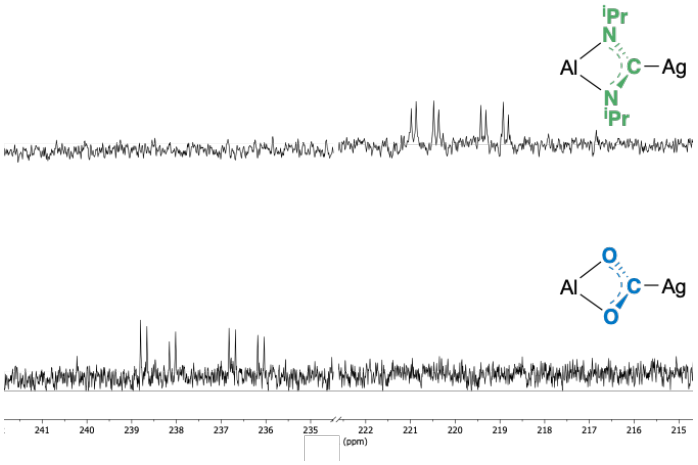


Figure 4.5. *Excerpt from the ^{13}C NMR spectrum of* ***4-Ag*** *and* ***5-Ag*** *showing the 8-line splitting pattern corresponding to the silver-bound carbenic carbon.*

The structure shows that **5-Ag** is the product of carbodiimide insertion into the Al−Ag bond, with the two nitrogen atoms coordinated to the aluminium centre and the carbon bonded to silver (**Scheme 4.2**). The two-coordinate silver forms part of a linear C−Ag−P unit (∠C(48)–Ag(1)–P(1) = 176.76(8)°), such that the carbodiimide fragment can be described as a diaminocarbene, supported by an aluminate backbone, donating to the silver atom. The C−N bond lengths of 1.346(3) and 1.345(3) Å are between the typical lengths for C−N single and double bonds (C–N ≈ 1.45 Å, C=N ≈ 1.30 Å),[32] consistent with a two-electron reduction of the carbodiimide unit. The regiochemistry of this insertion requires the silver atom to formally behave as a nucleophile, attacking the electrophilic carbon of the carbodiimide. This chemistry further demonstrates the unique ability of the strongly σ-donating aluminyl fragment to confer nucleophilicity onto a group 11 metal.

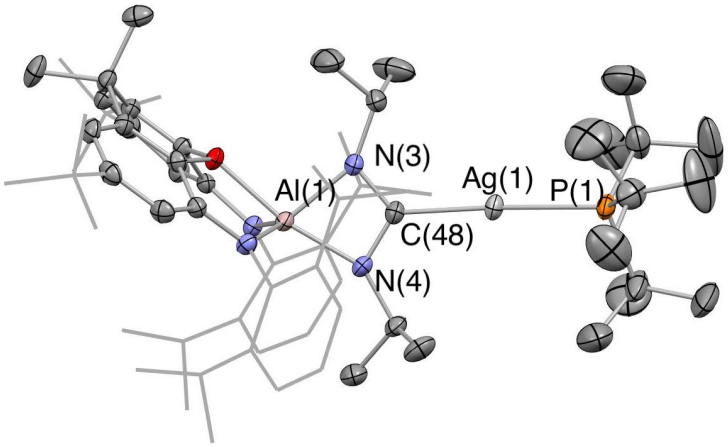


Figure 4.6. *Molecular structure of* ***5-Ag*** *in the solid state as determined by X-ray crystallography. Thermal ellipsoids set at the 50% probability level. Hydrogen atoms omitted and ^{i}Pr/^{t}Bu shown in wireframe for clarity. Key bond lengths (Å) and angles (°): Ag(1)–C(48): 2.118(2), Ag(1)–P(1): 2.3851(6), N(3)–C(48): 1.346(3), N(4)–C(48): 1.345(3).*

Literature examples of complexes with an NHC–Ag–P moiety are few in number, and indeed no examples of a dioxocarbene–Ag–phosphine species have been reported. However, the distinctive ^{13}C coupling pattern of **5-Ag** finds precedent in the complexes

reported by Braunstein,[27] of the form **$[Ag_2(L^{tBu})_2][BF_4]_2$** ($L^{tBu}$ = 3-butyl-1-(3-((di-*tert*-butyl-phosphino)methyl)phenyl)-imidazol-2-ylidene): $^1J_{107AgC}$ = 190 Hz, $^1J_{109AgC}$ = 219 Hz, $^2J_{CP}$ = 62 Hz *cf.* $^1J_{107AgC}$ = 182 Hz, $^1J_{109AgC}$ = 210 Hz, $^2J_{CP}$ = 63 Hz in **5-Ag**).

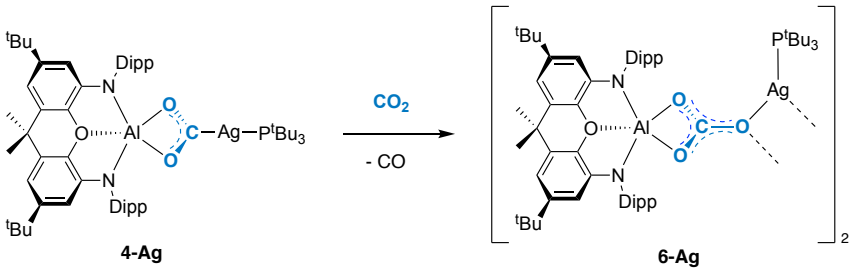
From the similarity of the spectroscopic data, it can be inferred that the product of the reaction of **3-Ag** with CO_2 is the dioxocarbene **4-Ag**, which binds through carbon to silver, with each oxygen atom bonded to aluminium in a μ-κ^1(C):κ^2(O,O') fashion (**Scheme 4.1**). The description of these complexes as dioxo- or diamino- carbenes can be used to explain the observed ^{13}C NMR shifts. Complex **4-Ag** has a higher chemical shift for the silver-bound carbon than **5-Ag** (237.7 vs 220.2 ppm), which is consistent with general trends in carbenes whereby increased π-donation from nitrogen (compared to oxygen) causes a lower δ_C value.[33] The same trend is apparent for the equivalent gold complexes **4-Au** (242.3 ppm) and Al–Au carbodiimide insertion product **5-Au** (219.9ppm).

The μ-κ^1(C):κ^2(E,E') (E = O, N) binding mode observed in this series of compounds is rare. Previous examples of bridging metallacarboxylates have been prepared via reactions of pre-formed carboxylate species with a separate metal based electrophile.[30,34] A discussion of recently reported compounds which also display this unusual binding mode is given in Section 4.3.10.

4.3.3 Onward reactivity with CO_2

Compound **4-Ag** is stable in the solid state and can be heated in benzene solution under argon atmosphere for periods of over a week without showing signs of degradation. However, heating a C_6D_6 solution of **4-Ag** to 80°C under an atmosphere of CO_2 for 24 h results in conversion to the carbonate complex, **6-Ag** (**Scheme 4.3**). Alternatively, the same compound may be formed by heating a solution of **3-Ag** at

80°C under CO_2 atmosphere for 48 h. Formation of **6-Ag** is very slow at room temperature, with negligible conversion observed by ^{1}H NMR after one week.



Scheme 4.3. *Incorporation of a second equivalent of carbon dioxide on heating to form the bridging carbonate* ***6-Ag****, with loss of CO.*

The ^{13}C NMR spectrum of **6-Ag** is diagnostic, showing a broad resonance at 167.2 ppm corresponding to the carbonate carbon. This chemical shift is similar to the previously reported aluminium carbonate formed from potassium aluminyl **I** and CO_2, which is found at 164.5 ppm, and to the bridging Ge and Sn carbonate species described by Caise *et al.* (163.5 and 168.2 ppm).[31,35] Interestingly, the ^{31}P spectrum of **6-Ag** in d_8-toluene at room temperature does not show the two silver satellites common to **4-Ag** and **5-Ag**, but rather a broad resonance centred around 76.6 ppm (**Figure 4.7**). Upon cooling to 213K, this sharpens into a doublet with $^1J_{PAg}$ = 486 Hz. This suggests the phosphine ligand may be labile at higher temperatures, as was postulated for **3-Ag** itself. This is also apparent in the ^{1}H NMR spectrum, in which the P^{t}Bu$_3$ resonance is broad and shows no $^3J_{HP}$ coupling but becomes a sharp doublet with $^3J_{HP}$ = 12.0 Hz at 213K.

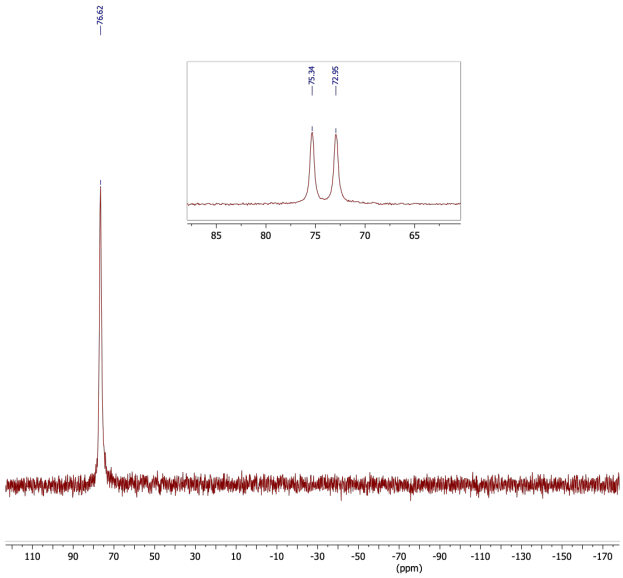


***Figure 4.7**. ^{31}P NMR spectrum of **6-Ag** measured in d_8-toluene at 298K (main) and 213K (inset).*

Crystals of **6-Ag** suitable for X-ray diffraction were grown from a warm benzene solution, allowing the molecular structure to be determined (**Figure 4.8**). This reveals that **6-Ag** is a centrosymmetric dimer in the solid state, with a diamond-shaped core formed by two silver and two oxygen atoms. The $[CO_3]^{2-}$ unit bridges the silver and aluminium atoms, with one oxygen bound to silver, and two bound to aluminium. From the C–O bond lengths, it is apparent that the C–O bond projecting towards silver has more double bond character, as it is shorter than those projecting towards aluminium (*d*(O(1)-C(61)) = 1.266(6) Å, *cf.* *d*(O(3)-C(61)) = 1.307(6) and *d*(O(2)-C(61)) = 1.297(5) Å). This is in line with there being more negative charge localization on the oxygen atoms bonded to the harder Al centre than those bonded to Ag.

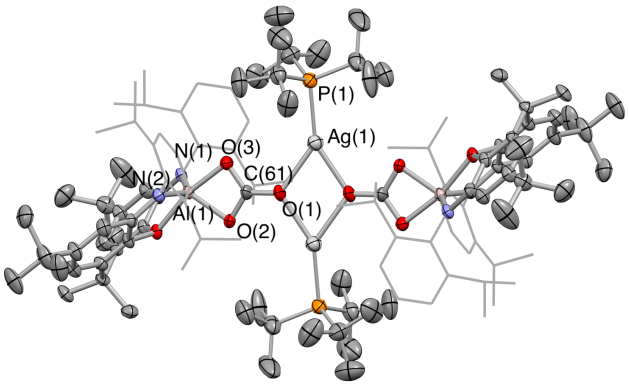


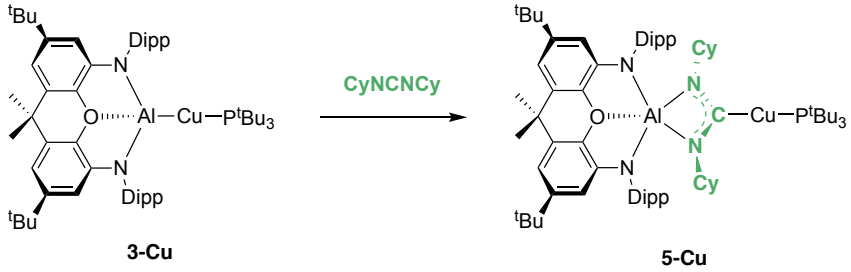
Figure 4.8. *Molecular structure of* ***6-Ag*** *in the solid state as determined by X-ray crystallography. Thermal ellipsoids shown at 50%. Hydrogen atoms and solvent molecules omitted and Dipp groups shown in wireframe for clarity. Key bond lengths (Å) and angles (°): Ag(1)–O(1): 2.249(4), O(3)–C(61): 1.307(6), O(2)–C(61): 1.297(5), O(1)–C(61): 1.266(6).*

Silver has been little used in CO_2 activation chemistry until recently, and most examples come from the solid-state literature.[36,37] Molecular silver compounds largely find use in cycloaddition reactions with CO_2 and alkynes, and in carboxylates the metal typically binds to an oxygen atom.[38,39] The results reported in this section show how combining silver with the strongly σ-donating aluminyl fragment in a bimetallic complex can allow the silver atom to bind to CO_2 in a previously unknown fashion. The reactivity of copper complexes with CO_2 is more widely studied.[40] Seeking to see how the aluminyl ligand can alter standard Cu chemistry, **3-Cu** was also reacted with heteroallenes.

4.3.4 Reaction of a copper aluminyl complex with a carbodiimide

The copper aluminyl **(NON)Al–CuP^{t}Bu$_3$** (**3-Cu**) was also subjected to reactions with CO_2 and carbodiimides (**Scheme 4.4**). For the copper congener, the carbodiimide CyNCNCy was used instead of ^{i}PrNCN^{i}Pr due to higher crystallinity of the products, leading to better opportunities to characterise the products in the solid state by X-ray diffraction. Addition of 1 equivalent of CyNCNCy to a suspension of **3-Cu** led to

immediate dissolution, indicating that a reaction had occurred. A ^{31}P NMR spectrum of the reaction mixture shows the disappearance of the singlet associated with **3-Cu** and appearance of a single resonance at 59.6 ppm. As in the ^{1}H NMR spectrum of carbodiimide insertion product **5-Ag**, there is an increase in the number of resonances relating to both the N–Cy protons and ligand ^{i}Pr protons, indicating that they are no longer in a symmetric environment. The ^{13}C NMR spectrum provides key insight into the structure of the product, carbodiimide insertion product **5-Cu**. A lowfield doublet at 215.5 ppm ($^{2}J_{CP}$ = 57.5 Hz) is present, indicating a carbenic carbon atom directly bound to the CuP^{t}Bu$_3$ unit. This chemical shift is in the same region as for the diamino carbenes **5-Au** and **5-Ag** (219.9 and 220.2 respectively), formed by insertion of ^{i}PrNCN^{i}Pr into the Al–M bonds of **3-Au** and **3-Ag**. The lower chemical shift compared to dioxocarbene **4-Ag** is likely a consequence of increased π donation from nitrogen compared to oxygen, as has been documented for other heteroatom based carbenes.[33]



Scheme 4.4. *Insertion of dicyclohexylcarbodiimide into the Al–Cu bond of copper aluminyl* ***3-Cu***

Furthermore, single crystals grown from benzene allowed solid state characterisation by X-ray diffraction, confirming that, as with the silver and gold analogues, the carbodiimide has inserted into the Al–Cu bond (**Figure 4.9**). As in **5-Ag**, the Cu atom is two-coordinate, with coordination in a linear manner to the phosphine ligand and the 4-membered aluminate-NHC moiety (∠(C(48)–Cu(1)–P(1)) = 179.04(13)°). Again, the

elongated C–N bond lengths demonstrate reduction of the CyNCNCy unit (*d*(N(3)–C(48)) = 1.333(5) Å, *d*(N(4)–C(48)) = 1.341(5) Å).

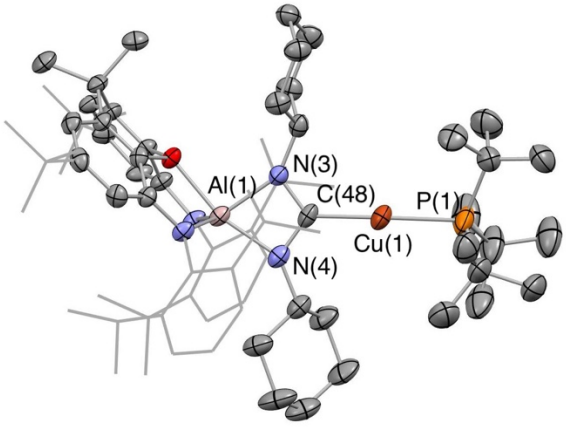


Figure 4.9. *Molecular structure of* ***5-Cu*** *in the solid state as determined by X-ray crystallography. Thermal ellipsoids set at the 50% probability level. Hydrogen atoms omitted and Dipp groups shown in wireframe for clarity. Key bond lengths (Å) and angles (°): Cu(1)–C(48): 1.952(4), Al(1)–N(4): 1.908(3), Al(1)–N(3): 1.921(3), C(48) –Cu(1) –P(1) = 179.04(13).*

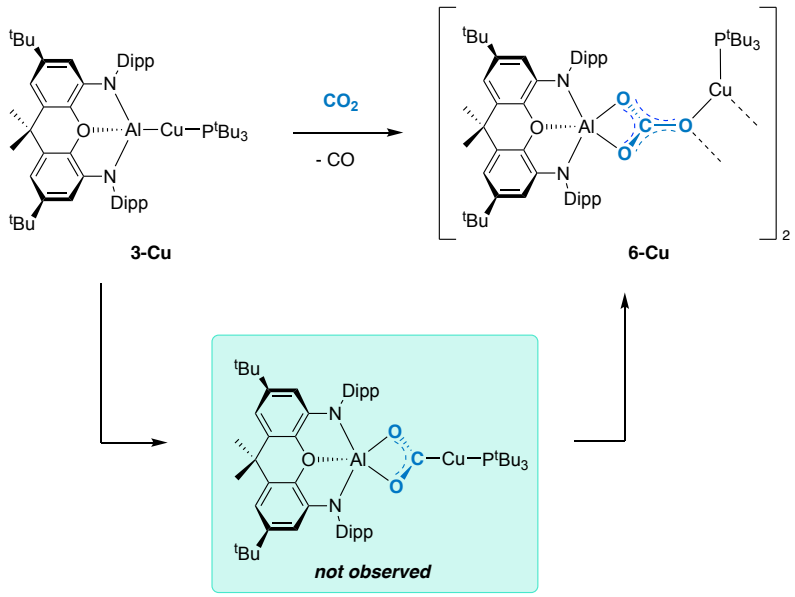
Comparisons can be drawn across the series of carbodiimide insertion products **5-Au**, **5-Ag** and **5-Cu**, which show variation depending on the group 11 metal, and support the description of these compounds as M(I) species coordinated to mutually *trans* phosphine and diamino carbene ligands.[26,41] The near linear metal geometries, along with the M–P distances and ^{13}C NMR chemical shifts (**Table 4.1**), all bear resemblance to previously reported group 11 carbene-phosphine complexes of the form **[(R$_3$P)M(IDipp)]$^+$** (M = Cu, Ag, Au; R = Cy/^{t}Bu; IDipp = 1,3-(di*iso*propylphenyl)-imidazol-ylidene).[26,41] The angles at the carbenic carbon, defined by the two α-N substituents, are rather wide compared to other 4-membered heterocyclic carbenes,[42] which is reflected in the similarity of the spectroscopic data to those of imidazolylidene based systems. This demonstrates the effect of the large size of the aluminium atom in the heterocycle backbone, as well as the more polar nature of the Al–N bonds as compared to NHCs.

Table 4.1. *Selected structural and spectroscopic properties of carbodiimide insertion products* ***5-Cu****,* ***5-Ag*** *and* ***5-Au***

M	*d*(M–C) (Å)	*d*(M–P) (Å)	∠(C–M–P) (°)	δ_C (ppm)	δ_P (ppm)
Cu	1.952(4)	2.2163(13)	179.04(13)	215.5	59.6
Ag	2.118(2)	2.3851(6)	176.76(8)	220.2	73.4
Au	2.158(10)	2.316(3)	175.7(3)	219.9	90.6

4.3.5 Reaction of a copper aluminyl complex with CO_2

The reaction of copper aluminyl **3-Cu** with CO_2 proceeds rapidly at room temperature in benzene, which is again apparent by complete dissolution of the starting suspension to give a colourless solution. The ^{31}P NMR spectrum of the reaction mixture shows a sole new resonance at 62.5 ppm, as well as the disappearance of the signal at 38.3 ppm associated with the starting material. However, unlike that of **5-Cu**, the ^{13}C NMR spectrum of this compound does not feature a lowfield doublet, as would be expected for a carbene-like carbon. Instead, a resonance at 170 ppm indicates that the reaction has proceeded through to give a carbonate, even at room temperature (**Scheme 4.5**).



Scheme 4.5. *Formation of carbonate complex* ***6-Cu*** *by reaction of copper aluminyl* ***3-Cu*** *with CO_2, proposed to proceed via an unobserved CO_2 insertion.*

This inference was confirmed by structural characterisation by X-ray diffraction of crystals of carbonate complex **6-Cu** grown from a benzene solution. This shows the product to be a centrosymmetric dimer, isostructural with silver carbonate **6-Ag** (**Figure 4.10**). The Cu–O bond lengths in **6-Cu** are marginally shorter than those of **6-Ag** (*d*(Cu(1)–O(4)) = 2.062(3) Å vs *d*(Ag(1)–O(1)) = 2.249(4) Å), reflective of the smaller covalent radius of copper compared to silver (1.13 vs 1.33 Å).[43]

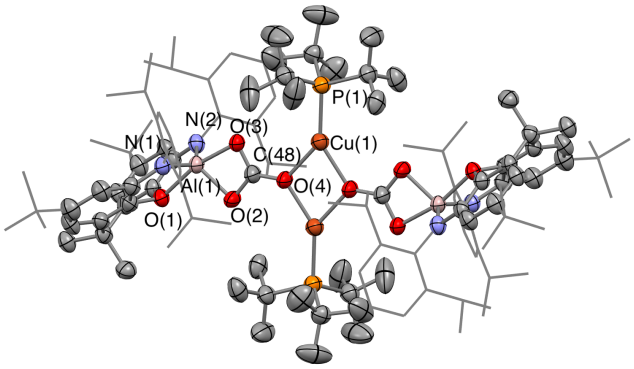


Figure 4.10. *Molecular structure of* ***6-Cu*** *in the solid state as determined by X-ray crystallography. Thermal ellipsoids set at the 50% probability level. Hydrogen atoms omitted and Dipp groups shown in wireframe format for clarity. Key bond lengths (Å) and angles (°): Cu(1)–O(4): 2.062(3), C(48)–O(3): 1.874(3), C(48)–O(4): 1.268(6), C(48)–O(2): 1.296(6).*

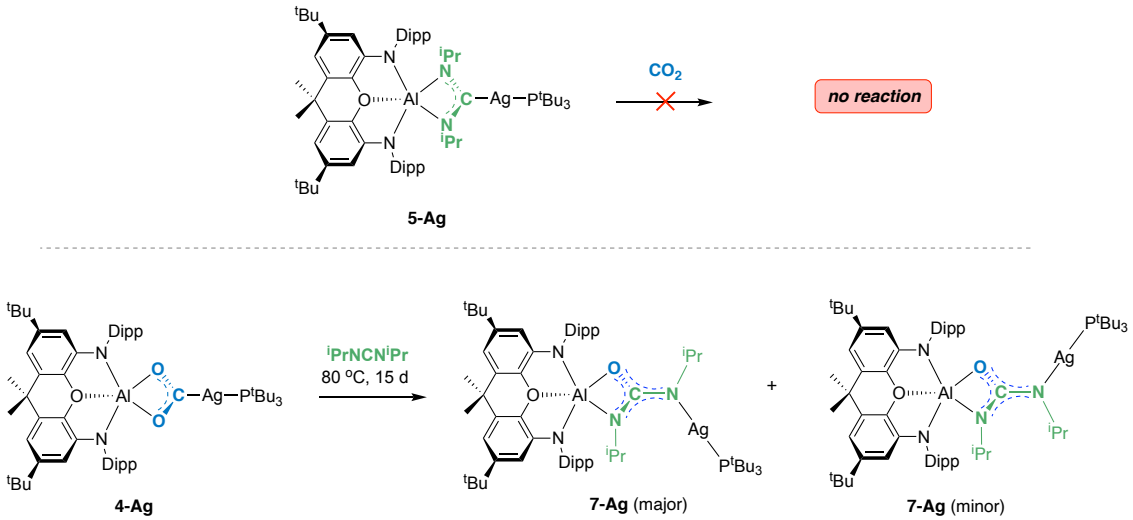
It may be hypothesised that **6-Cu** is formed *via* the insertion of CO_2 into the Al–Cu bond to form a dioxocarbene, analogously to the reaction of **3-Ag** with CO_2. The reaction was studied *in situ* by low temperature ^{31}P and ^{1}H NMR spectroscopy, in an attempt to observe this potential intermediate. However, at −80°C, complete conversion to the carbonate was apparent, and no intermediate could be detected, even at this low temperature.

Tying together the observed reactivity of the copper, silver and gold complexes, it can be shown by X-ray crystallography that all three complexes readily insert carbodiimides, implying nucleophilic character at the group 11 metal site. These complexes are thermally stable, with no further reactivity seen with excess

carbodiimide. This contrasts with the reactivity towards CO_2, where the same initial insertion is seen, but onward reactivity is possible to an extent that depends on the identity of the group 11 metal. In the case of gold, no onward reaction is seen, and dioxocarbene 4-Au is stable under forcing conditions. For silver, the CO_2 insertion product can be isolated and characterised, but at elevated temperatures this can react with a second CO_2 equivalent to form a carbonate. With copper, complete conversion to the corresponding carbonate is rapid and occurs at such low temperatures that no initial insertion product can be observed even at −80°C. This trend in the group 11 metals can be rationalised on the basis of the known oxo- and carbophilicities of the group 11 metals, whereby M–O bond strengths decrease on moving from copper to gold, and the M–C bond increases in strength.[44,45] Having observed this intriguing trend in reactivity, we sought to further understand the *mechanism* of the carbonate formation process through experimental methods.

4.3.6 Experimental investigation of mechanism

Given the unique accessibility of all the relevant species (dioxocarbene and carbonate), we chose to focus on the silver compounds **4-Ag** and **6-Ag** to study the mechanism of the uptake and conversion of CO_2. Knowing that formation of the carbonate requires uptake of two equivalents of CO_2, it was decided to study 'crossover' reactions involving both CO_2 and a carbodiimide, to separately probe these two steps. Carbodiimide insertion product **5-Ag** proved unreactive towards CO_2, with no reaction observed even under forcing conditions. Conversely, the CO_2 insertion product **4-Ag** reacted very slowly with ^{i}PrNCN^{i}Pr, with consumption of the starting material complete after 15 days at 80 °C (**Scheme 4.6**).



Scheme 4.6. *Crossover experiments between diaminocarbene **5-Ag** and CO_2 (above); and between dioxocarbene **4-Ag** and ^{i}PrNCN^{i}Pr to form the bridging ureate **7-Ag** (below).*

After this time, the ^{31}P NMR spectrum shows two sets of signals in a 2:1 ratio at 78.8 and 80.1 ppm (both with $^{1}J_{107AgP}$ = 540, $^{1}J_{109AgP}$ = 623 Hz) (**Figure 4.11**). The ^{13}C NMR spectrum shows two resonances in a similar ratio at 167.8 and 167.2 ppm, a chemical shift which is similar to that of the carbonate complex **6-Ag** (167.2 ppm). A resonance at 184.5 ppm, corresponding to free CO, is also visible. The ^{1}H NMR spectrum of the reaction mixture also shows two **NON**-containing species, each with integrations consistent with one set of P^{t}Bu$_3$ signals per **NON** ligand.

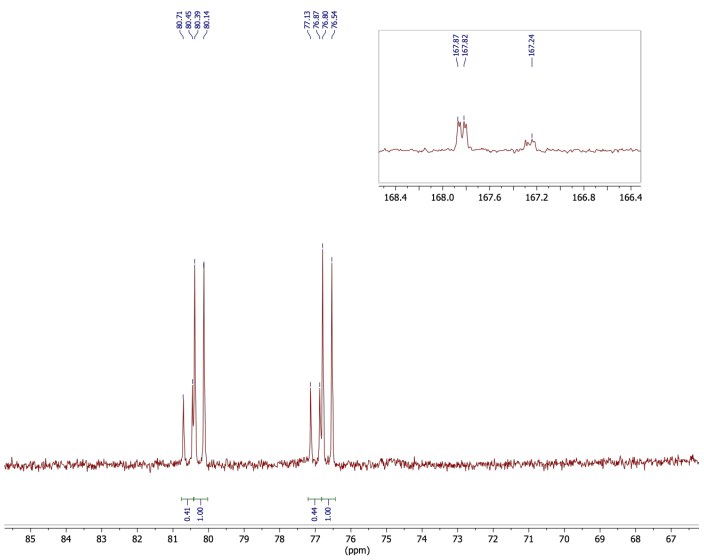


Figure 4.11. *^{31}P NMR spectrum in C_6D_6 of the reaction of **4-Ag** with ^{i}PrNCN^{i}Pr showing the two isomers of ureate compound **7-Ag**, inset: an excerpt from the ^{13}C NMR spectrum of the same reaction.*

Crystals could be obtained by cooling a pentane solution to −30°C. X-ray diffraction reveals that the solid-state structure of the product, **7-Ag**, is a ureate (**Figure 4.12**). This compound is formed by the overall loss of CO (as evidenced in the ^{13}C NMR spectrum) and incorporation of one equivalent of ^{i}PrNCN^{i}Pr. In the molecular structure, silver remains two-coordinate, bound to the phosphine ligand and one nitrogen of the ^{i}PrNCN^{i}Pr unit in a linear manner. The aluminium centre is coordinated by one of the N atoms and to one O, forming a 4 membered metallocycle. The planar core of the molecule features a short central C–N bond (*d(*N(1)–C(51): 1.304(6)), with the O and Ag atoms *trans* to each other. It is likely that restricted rotation around this C–N bond is responsible for the mixture of products seen by NMR, with the alternate *cis* isomer constituting the minor product. Isolated crystalline samples of **7-Ag** redissolved in C_6D_6 display the same ratio of products and the two cannot be separated. This experiment shows that an important step may be loss of CO from **4-Ag** and that the equivalent step (loss of ^{i}PrNC) is not possible from **5-Ag**.

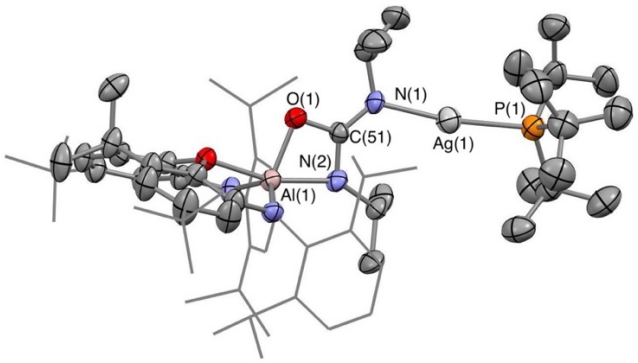


Figure 4.12. *Molecular structure of* ***7-Ag*** *as determined by X-ray crystallography. Thermal ellipsoids set at the 50% probability level. Hydrogen atoms omitted and Dipp groups shown in wireframe format for clarity. Key bond lengths (Å) and angles (°): Ag(1)–P(1): 2.3572(14), Ag(1)–N(1): 2.130(4), N(1)–C(51): 1.304(6), N(2)–C(51): 1.339(6), Al(1)–O(1): 1.842(3), O(1)–C(51): 1.344(5).*

4.3.7 ^{13}C Labelling experiments

With the knowledge that a molecule of CO can be extruded from the dioxocarbene **4-Ag**, and that the resulting species can incorporate a second heteroallene, a crossover reaction involving isotopically labelled $^{13}CO_2$ was designed. It was previously observed in the *in situ* ^{13}C NMR spectrum of the reaction of **3-Ag** with CO_2 to form carbonate species **6-Ag**, that free CO is released during the process.

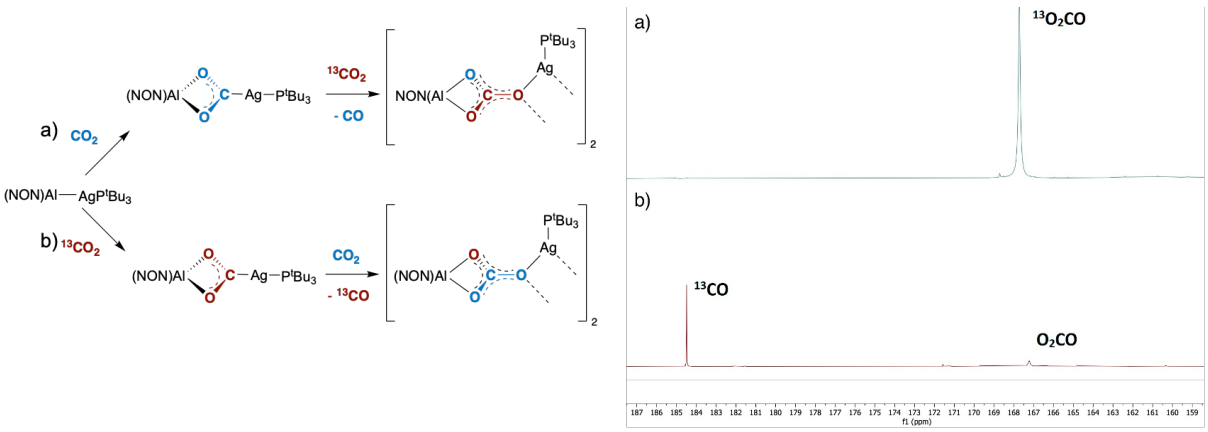


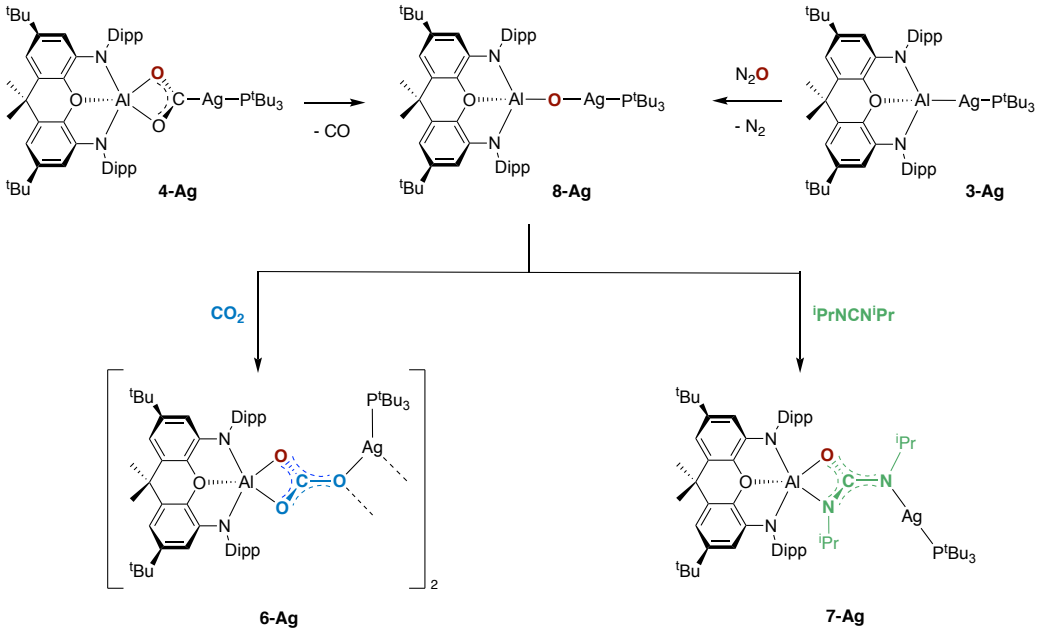
Figure 4.13*. Crossover experiment using $^{13}CO_2$. a) addition of $^{13}CO_2$ to* ***4-Ag****, giving* ***^{13}C-6-Ag*** *and CO, b) addition of CO_2 to* ***^{13}C-4-Ag****, giving* ***6-Ag*** *and ^{13}CO.*

Two experiments were carried out: a) A sample of **4-Ag** in C_6D_6, prepared from unlabelled CO_2, was exposed to $^{13}CO_2$ and heated to 80°C until the reaction was complete (as determined by ^1H and ^{31}P NMR). b) A sample of (**NON)Al(O$_2$^{13}C)AgP^{t}Bu$_3$** (**^{13}C-4-Ag**) was prepared using $^{13}CO_2$ and then subsequently exposed to unlabelled CO_2 and heated in the same fashion. Analysis of the *in situ* ^{13}C NMR spectra of these reactions (**Figure 4.13**) shows that the CO is extruded from the first equivalent of CO_2, and the carbonate product is formed from the second CO_2 molecule. This is consistent with the results of the carbodiimide crossover experiment, which also saw loss of CO followed by incorporation of a second heteroallene.

4.3.8 Synthesis of an oxide intermediate

The extrusion of CO from dioxocarbene **4-Ag** led us to propose an intermediate in the conversion of **3-Ag** to **6-Ag**: an oxide, bridging the Ag and Al atoms. Such oxodimetallic species have been proposed (and crystallographically characterised) as intermediates in a number of bimetallic CO_2 to CO reductions involving digermynes, distannynes and cobalt(I).[19,31,46] Seeking to isolate this proposed intermediate, silver aluminyl **3-Ag** was exposed to the oxygen atom transfer agent N_2O, at −78°C (**Scheme 4.7**). The *in situ* ^1H NMR spectrum shows formation of a new **NON** containing product, with corresponding P^{t}Bu$_3$ signals in a 1:1 ratio. The ^{31}P spectrum features a resonance at 82.0 ppm displaying silver satellites ($^1J_{107AgP}$ = 551, $^1J_{109AgP}$ = 640 Hz). The large increase in the coupling constants compared to the starting **3-Ag** ($^1J_{Pag}$ = 152 Hz) indicates that silver is no longer bound to the strongly σ-donating aluminyl ligand, but is now bound to a much weaker σ-donor. The putative bridging oxide **(NON)Al-O-Ag(P^{t}Bu$_3$)** (**8-Ag**), proved to be highly reactive and attempts to

isolate it cleanly or grow single crystals suitable for X-ray diffraction proved unsuccessful. Therefore, for reactivity studies, **8-Ag** was generated *in situ* at low temperature and the solution was subsequently degassed to remove excess N_2O.



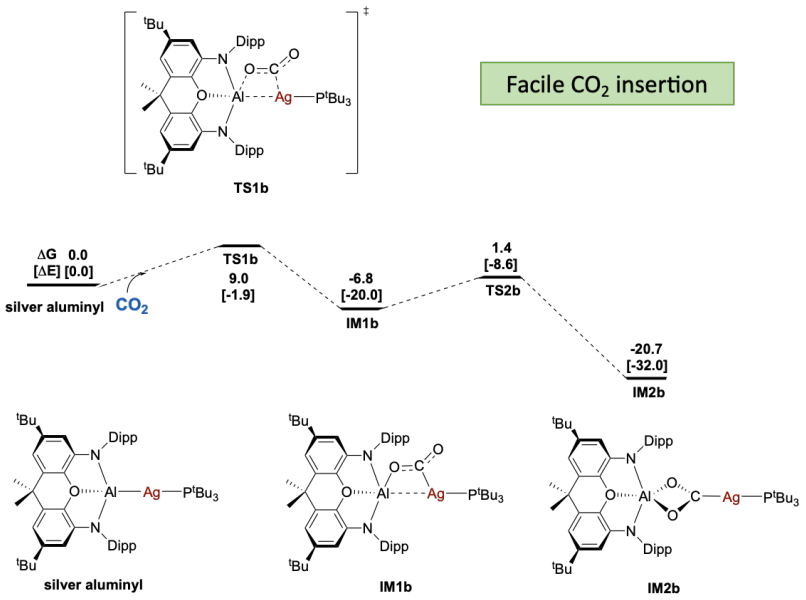
Scheme 4.7. *Synthesis of bridging oxide **8-Ag** by reaction of silver aluminyl **3-Ag** with N_2O. Reacting this oxide with CO_2 or ^{i}PrNCN^{i}Pr rapidly forms carbonate **6-Ag** or ureate **7-Ag**.*

Having generated **8-Ag**, the solution was exposed to CO_2 (1 atm). Reaction was rapid, with complete conversion to a single product apparent by ^{1}H and ^{31}P NMR after 10 min. NMR spectroscopy, as well as X-ray crystallography, confirmed that the product is the carbonate, **6-Ag**. In a similar manner, addition of 1 equivalent of ^{i}PrNCN^{i}Pr to **8-Ag** at room temperature rapidly produces the ureate complex **7-Ag**, with the same isomer composition as previously seen in the reaction of **4-Ag** with ^{i}PrNCN^{i}Pr (**Scheme 4.7**). The timescale and conditions required for this reaction stand in stark contrast with formation of **7-Ag** directly from silver aluminyl **4-Ag** (cf. 80°C, 15 d), suggesting that formation of the oxide itself may be rate limiting. With this experimental

evidence in hand, we turned to quantum chemical investigations to examine potential reaction pathways for the copper, silver and gold aluminyl systems towards CO_2.

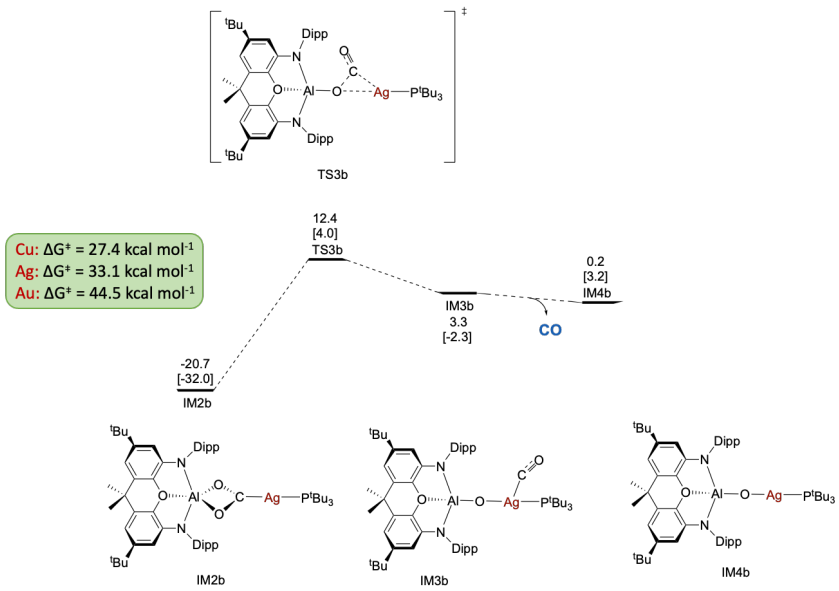
4.3.9 Quantum chemical studies of mechanism

The quantum chemical studies were carried out by Xianlu Cui and Lili Zhao of Nanjing Technical University, alongside Gernot Frenking of Philipps-Universität Marburg. The reaction course was calculated using Density Functional Theory (DFT) at the BP86+D3(BJ)/def2-TZVPP level using BP86/def2-SVP optimized geometries. The calculations were carried out on Cu, Au and Ag systems, however for clarity, only the silver system is shown in **Scheme 4.8**, **Scheme 4.9** and **Scheme 4.10**. The reaction course can be examined as two additions of CO_2 to the system: first to give a dioxocarbene, and secondly to form a carbonate. The first process is facile for Cu, Ag and Au, with low activation barriers for the addition of CO_2 to all three metal aluminyl complexes (**Scheme 4.8**). The initial approach of CO_2 is side on, with a [2+2] addition occurring between the Al–M and one of the C=O bonds. The orientation of the C=O bond reflects the polarity of the Al–M ie. $Al^{\delta+}$–$M^{\delta-}$, which has been well established for other Al–M systems.[24,47–49] The 'side-on' CO_2 bound intermediate **IM1b** readily rearranges to **IM2b** (**4-Ag**).

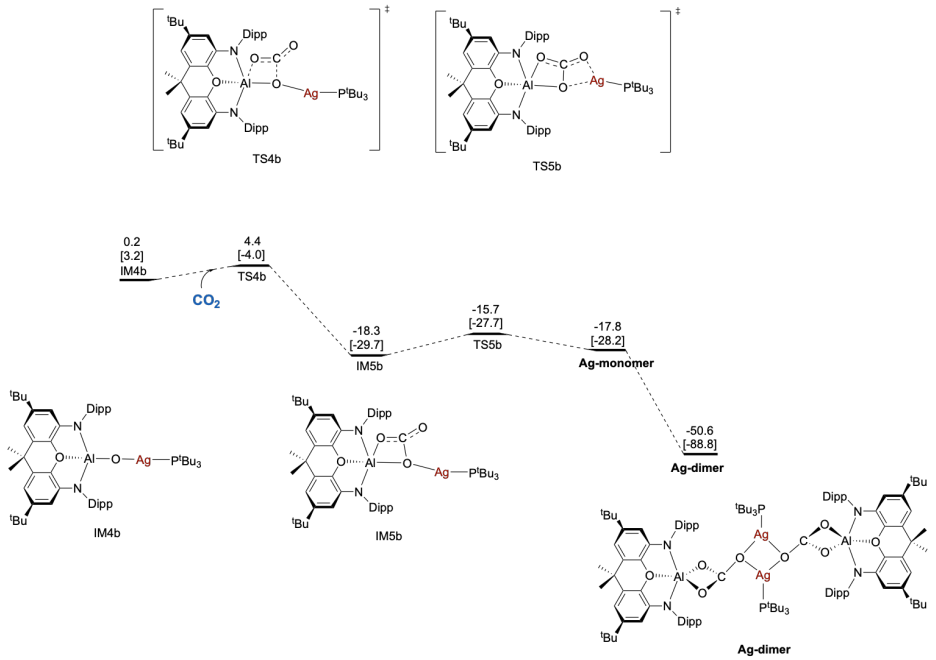


***Scheme 4.8**. Computed Gibbs energy profiles (in kcal mol^{-1}) for **3-Ag** through to **4-Ag** at the BP86+D3(BJ)/def2-TZVPP (SMD, solvent = benzene)//BP86/def2-SVP level, and the electronic energies are given in bracket for reference.*

The second stage of the process proceeds via extrusion of CO from **IM2b**, to the bridging Al–O–Ag species **IM4b**, preceded by the silver carbonyl intermediate **IM3b** (**Scheme 4.9**). A second molecule of CO_2 then adds across the Al–O bond and isomerization to the monomer Ag-monomer occurs. This is followed by dimerization to give the final dimeric carbonate (**Scheme 4.10**).



Scheme 4.9. *Computed Gibbs energy profiles (in kcal mol^{-1}) for* ***4-Ag*** *through to* ***8-Ag*** *at the BP86+D3(BJ)/def2-TZVPP (SMD, solvent = benzene)//BP86/def2-SVP level, and the electronic energies are given in bracket for reference.*



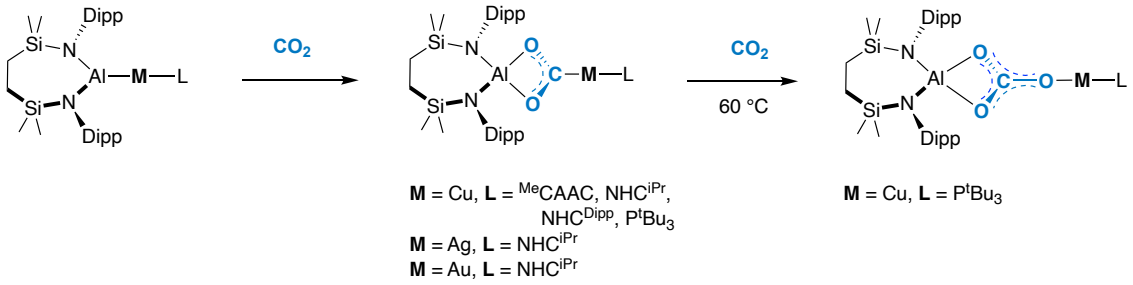
Scheme 4.10. *Computed Gibbs energy profiles (in kcal mol^{-1}) for* ***8-Ag*** *through to* ***6-Ag*** *at the BP86+D3(BJ)/def2-TZVPP (SMD, solvent = benzene)//BP86/def2-SVP level, and the electronic energies are given in bracket for reference.*

The highest activation barrier in the overall process is for the extrusion of CO from **IM2b**, which has a value of $\Delta G^{\ddagger}$ = 33.1 kcal mol^{-1}. The trend in values for the equivalent barriers calculated for the Cu (27.4 kcal mol^{-1}) and Au (44.5 kcal mol^{-1}) analogues reflect the trend in reactivity observed experimentally. The barrier to CO extrusion (and thus onward reaction to the carbonate) is lowest for the copper-based system, which proceeds through to give a carbonate at low temperatures. The intermediate activation barrier calculated for silver fits with the experimental reactivity profile, in which carbonate formation requires heating to 80°C for 2 d under CO_2. Likewise, the barrier of 44.5 kcal mol^{-1} calculated for the extrusion of CO from **4-Au** is consistent with the fact that **4-Au** can be readily isolated and does not form a carbonate species even when heated for prolonged periods of time. An almost identical mechanism for the overall CO_2 to carbonate transformation was calculated by Hill and McMullin in a recent study of Al – group 11 bonds, beginning with nucleophilic attack by the group 11 metal, and featuring CO extrusion as the rate determining step.[50] A 2021 computational work by Sorbelli *et al.* sought to further examine the insertion of CO_2 into the Al–Au bond of **3-Au**, as detailed by Hicks *et al*. They arrived at a very similar potential energy profile to that outlined above, but also highlighted the possibility for diradical character in the Al–Au bond.[51] This description of the Al–Au bond as diradical in nature has been refuted in a recent theoretical study by Sheong, Lin and coworkers, who use CASSCF to determine that the nucleophilic reactivity of the coinage metal (Au or Cu) arises from closed shell interactions.[52]

4.3.10 Comparison to similar work

There has been a recent surge in the field of CO_2 activation by Al–M heterobimetallic systems, with a number of papers being published in the wake of the gold aluminyl

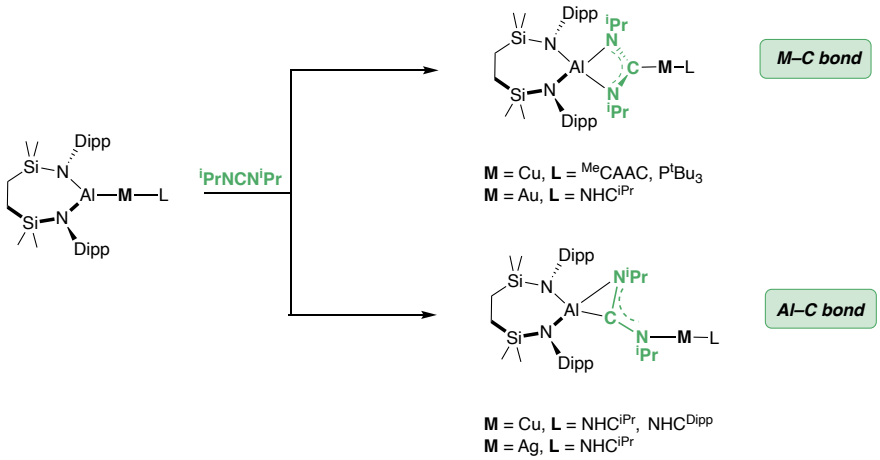
work by Hicks *et al*. In parallel to the research presented in this chapter, Al–M (M = Cu, Ag, Au) systems have been studied by the groups of Hill and McMullin, derived from the potassium aluminyl anion **[K{Al(SiN^{Dipp})}]$_2$** (SiN^{Dipp} ={CH$_2$SiMe$_2$NDipp}$_2$)[48,50] (**Section 3.3.6**). The reactivity of these species towards heteroallenes shows many similarities to the series **3-Cu**, **3-Ag**, **3-Au**, but also differs in key aspects. These differences provide insight into the influence of both the aluminium fragment and the group 11 metal co-ligand on small molecule activation.



Scheme 4.11. *Summary of the reactivity of* ***(SiN^{Dipp})*** *based Al–M species towards CO_2.*

It was found that variation of the group 11 metal and its co-ligand had little effect on the initial product formed by reaction with CO_2. The CO_2 insertion products analogous to **4-Ag** and **4-Au** were formed universally, with the same μ-κ^1(C):κ^2(O,O') binding mode observed throughout (**Scheme 4.11**). These compounds all display a ^{13}C NMR resonance in the range δ = 230-240 ppm, consistent with the values for the carbene carbon in **4-Au** and **4-Ag**. The authors theorised that using a P^{t}Bu$_3$ ligand, as in this work, might alter the reactivity of the system. Accordingly, although the complex **(SiN^{Dipp})AlCuP^{t}Bu$_3$** reacts with CO_2 at room temperature to form **(SiN^{Dipp})Al(O$_2$C)CuP^{t}Bu$_3$**, carbonate resonances were observed in the ^{13}C NMR spectrum upon heating to 60°C overnight. Interestingly, silver gallyl compound **3'-Ag** is unreactive towards CO_2 under all conditions trialled. This result has been further

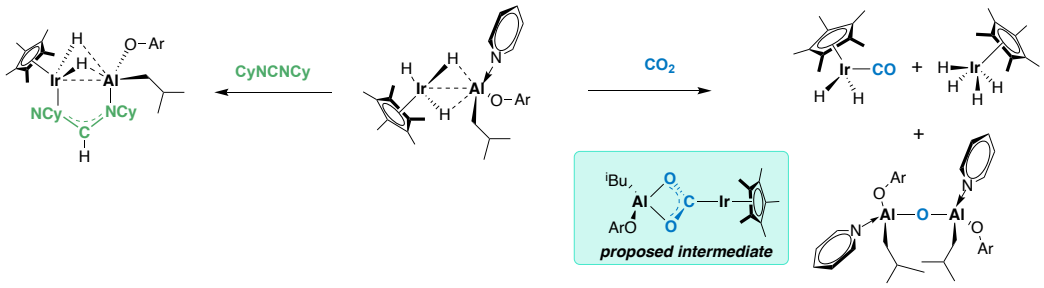
investigated in a computational study by Sorbelli *et al*, again looking only at the gold-based system, which predicts that Al–Au species are unique among group 13 – gold complexes in their ability to activate CO_2.[53]



Scheme 4.12. *Reactivity of* ***(SiN^{Dipp})Al–M–L*** *complexes towards carbodiimides*

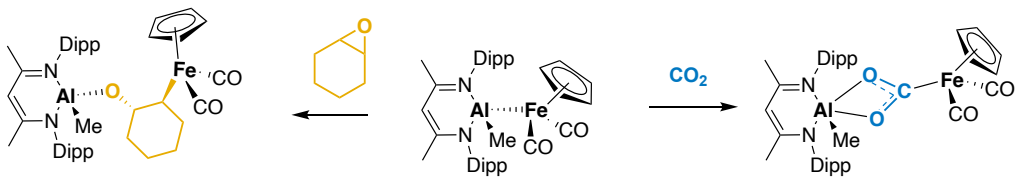
The reactivity of the **(SiN^{Dipp})Al–M–L** complexes towards carbodiimides reveals further subtleties in the nature of the Al–M bond. Two binding modes were observed for the carbodiimide unit: the symmetric manner seen with CO_2 and common to **5-Au**, **5-Ag** and **5-Cu** of this work; and an unsymmetric mode in which M is bound to one N atom, and the Al binds to both the central carbon and second N atom, forming a strained AlCN metallocycle (**Scheme 4.12**). The first of these possibilities results in an M–C bond and can be seen as arising from nucleophilic attack by M on the electrophilic carbon. The unsymmetrical binding mode produces an Al–C bond, suggesting that the polarity of the Al–M bond has been altered. For the Al–Au bond, it is perhaps not surprising that the Au atom behaves as a nucleophile, given the electron affinity value[54] of Al and Au (Au: 2.30 eV). For Cu and Ag (1.23 eV, 1.30 eV) the effect of the aluminyl fragment and co-ligand are greater, with the **NON** based aluminyl

appearing to confer increased nucleophilicity to the coinage metal partner than the **(SiN^{Dipp})Al** fragment.



Scheme 4.13. *Reactions of an iridium aluminyl hydride complex with CO_2 and CyNCNCy*

Another recent example of CO_2 activation by a heterobimetallic aluminium complex is the iridium aluminium hydride species, **[Cp*IrH$_3$Al(^{i}Bu)(OAr)]** reported by Camp, Maron and co-workers.[47] The products of bimetallic activation of CO_2 in this case are an iridium carbonyl and a bridging Al–O–Al oxide (**Scheme 4.13**). The authors propose nucleophilic attack on C by Ir to give a dioxocarbene intermediate, followed by hydride-mediated CO loss. Retention of the carbonyl by Ir reflects the greater binding of CO ligands to d^6 metals than d^{10} metals such as Au, Ag and Cu. Again, the reactivity with CyNCNCy diverges, with hydride migration to the central C atom resulting in a bridging amidinate.



Scheme 4.14. *Reaction of ^{Dipp}NacNacAl(Me)Fp with an epoxide and CO_2*

In a 2022 work by Mankad and co-workers,[55] the NacNac supported Al–Fe complex **^{Dipp}NacNacAl(Me)Fp** (Fp = $FeCp(CO)_2$) was found to react with CO_2 at room temperature, resulting in the bridged CO_2 compound **^{Dipp}NacNacAl(Me)(μ:κ$_2$-O$_2$C)Fp** (**Scheme 4.14**). Interestingly, a concerted CO_2 insertion mechanism, like that described for the earlier examples, was found to be energetically unfeasible under the experimental reaction conditions. Instead, a radical pair mechanism involving CO_2 activation at aluminium(II) species ^{Dipp}NacNac(Me)Al• followed by recombination with Fp• was invoked. This was also supported by the *trans* geometry of epoxide activation observed, ruling out a concerted pathway. This work again highlights the importance of the transition metal partner, with the radical pair mechanism more reminiscent of 3d metal systems.[56]

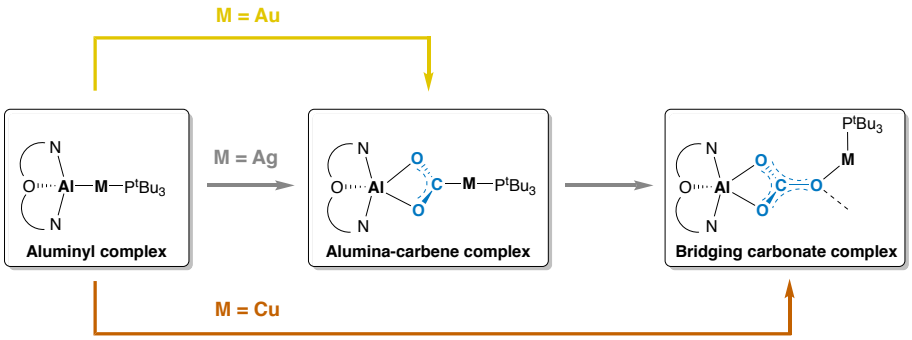
Although examples are still very limited in number, a consequence of the relative scarcity of directly bonded Al–M species, some trends can be drawn from the systems presented in this section. The bridging μ-κ^1(C):κ^2(O,O') motif is common to many Al–M systems, and can form either by concerted insertion of CO_2 into the Al–M bond involving nucleophilic attack on CO_2 by M (as in this work and that of Hill and McMullin) or by the radical pair mechanism described by the Mankad group. Given the rarity of this binding mode in CO_2 activation chemistry, and the importance of CO_2 binding mode to selectivity, it is notable as a possible strategy for control of CO_2 valorisation. It is clear that if one wishes to effect such a CO_2 activation, heterobimetallic aluminium complexes are a promising target. Following insertion, onward reactivity typically begins with carbonyl extrusion, which is dependent on the identity of the transition metal partner, forming either metal carbonyl or carbonate complexes. The products of the reactions of the Al–M species with carbodiimides show more diversity in their metal binding modes. This can perhaps be explained by a greater influence of Al–M bond

polarity on the initial heteroallene approach and the fact that Al oxophilicity can be seen as a large driving force in the CO_2 reaction.

4.4 Conclusions and future work

This chapter has described the reactivity of the silver and copper aluminyl complexes **(NON)AlMP^{t}Bu$_3$** (M = Cu, Ag), **3-Ag** and **3-Cu** towards the heteroallenes CO_2 and RNCNR (R = ^{i}Pr, Cy). It was found that for both silver and copper, carbodiimides could insert into the Al–M bond, with the regiochemistry of the insertion reflecting the polarity of the bond ie. $Al^{\delta+}$–$M^{\delta-}$. This resulted in access to a series of alumina-diaminocarbene complexes of the group 11 metals. The reactivity towards CO_2 was found to differ with variation of the metal. Previously reported **3-Au** inserts CO_2 in the same manner as the carbodiimide, forming a dioxocarbene which is stable to heating. The analogous silver dioxocarbene can also be isolated from the reaction of **3-Ag** with CO_2, but on heating to 80°C overnight, a second molecule of CO_2 is incorporated, forming a carbonate compound. For copper, this onward reaction is much faster, with complete conversion to the carbonate apparent even at −80°C and no carbene intermediate observable experimentally. The mechanism of this insertion and conversion of CO_2 was investigated experimentally in crossover experiments involving either a carbodiimide or $^{13}CO_2$. It was found that a bridging oxide Al–O–M, formed by extrusion of CO from the dioxocarbene, is a likely intermediate in the reaction. Computational studies predict that this CO extrusion is rate limiting, with the calculated barriers of $\Delta G^{\ddagger}$ = 26.6, 33.1, 44.5 kcal mol^{-1} for Cu, Ag and Au respectively, reflecting the trend in observed reactivity. These results add to the active and fast-growing field of CO_2 activation by heterobimetallic complexes involving aluminium and a transition metal.[55] They demonstrate the ability of the aluminyl ligand to act as a strong σ-donor and act

cooperatively with a transition metal partner to activate kinetically inert small molecules.



Scheme 4.15. *Summary of the reactivity of group 11 metal aluminyl complexes towards CO_2*

Future work on this topic could involve onward reaction of the CO_2 activated products, as well as attempts to build reversibility into the systems with the aim of catalytic activity. Further computational studies would be of benefit to examine in depth the nature of the Al–Cu and Al–Ag bond, similar to those that have been performed for **3-Au**. Of course, as more Al(I) reagents are developed, a wider range of Al–M bonds featuring metals from across the Periodic Table may become accessible. CO_2 serves as a useful probe for the reactivity of such complexes, and further new chemistry with respect to CO_2 is to be expected in the future.

Having explored the varied reactivity of the bimetallic group 11 – aluminyl complexes towards heteroallenes, we turned our attention to other small molecules with relevance to organic synthesis. Chapter 5 describes the chemistry of coinage metal – aluminyl complexes with alkynes.

4.5 Synthetic procedures and spectroscopic data for new compounds

Synthesis of (NON)Al(O_2C)AgP^tBu_3 (4-Ag) A suspension of **3-Ag** (100 mg, 0.100 mmol) in benzene was degassed and exposed to CO_2 (ca. 1.0 atm). After 15 min, volatiles were removed under vacuum and the residue washed with pentane to give **4-Ag** as a white solid. Yield: 80 mg, 76 %.

^{1}H NMR (400 MHz, C_6D_6, 298 K): δ_H = 0.81 (d, $^3J_{HP}$ = 12.7 Hz, 27H, PC(CH_3)$_3$), 1.23 (d, $^3J_{HH}$ = 6.9 Hz, 12H, CH(CH_3)$_2$), 1.28 (s, 18H, C(CH_3)$_3$), 1.49 (d, $^3J_{HH}$ = 6.8 Hz, 12H, CH(CH_3)$_2$), 1.60 (s, 6H, C(CH_3)$_2$), 3.90 (sept, $^3J_{HH}$ = 6.8 Hz, 4H, CH(CH$_3$)$_2$), 6.38 (d, $^4J_{HH}$ = 1.9 Hz, 2H, XA-*o*-CH), 6.75 (d, $^4J_{HH}$ = 1.9 Hz, 2H, XA-*p*-CH), 7.21-7.32 (m, 6H ArH).

^{13}C{^{1}H} NMR (126 MHz, C_6D_6, 298 K): δ_C = 25.4, 25.9 (CH(*C*H$_3$)$_2$) 27.8 (*C*(CH$_3$)$_2$), 28.4 (*C*H(CH$_3$)$_2$), 31.9 (C(*C*H$_3$)$_3$), 32.3 (b) (P{C(*C*H$_3$)$_3$}$_3$), 35.2 (*C*(CH$_3$)$_3$), 36.5 (dd, $^2J_{CAg}$ = 2.5, 7.0 Hz , P{*C*(CH$_3$)$_3$}$_3$), 37.1 (*C*(CH$_3$)$_2$), 106.4, 110.7, 124.7, 125.6, 132.4, 140.6, 142.6, 144.7, 147.6, 148.3 (Ar-*C*), 237.8 (ddd, $^1J_{C107Ag}$ = 231 Hz, $^1J_{C109Ag}$ = 267 Hz, $^2J_{CP}$ = 81 Hz, *C*Ag).

^{31}P{^{1}H} NMR (162 MHz, C_6D_6, 298 K): δ_P = 76.0 (dd, $^1J_{P\text{-}107Ag}$ = 403, $^1J_{P\text{-}109Ag}$ = 463 Hz).

Elemental microanalysis: calc. for $C_{60}H_{89}AgAlN_2O_3P$: C 68.49 %, H 8.53 %, N 2.66 %; meas.: C 66.68 %, H 8.69 %, N 2.80 %.

Synthesis of (NON)Al{(N^{i}Pr)$_2$C}AgP^tBu_3 (5-Ag): To a solution of **3-Ag** (80 mg, 0.079 mmol) in benzene (5 mL) was added diisopropylcarbodiimide (0.012 ml, 0.079 mmol) at room temperature. The reaction mixture was stirred for 3 h and volatiles then

removed under vacuum. The resulting solid was dissolved in pentane and the solution concentrated to 1 mL. On cooling to − 30 °C, colourless crystals of **5-Ag** suitable for X-ray crystallography formed over the course of 18 h. Yield: 45 mg, 49%.

^{1}H NMR (400 MHz, C_6D_6, 298 K): δ_H = 0.44 (d, $^{3}J_{HP}$ = 6.6 Hz, 6H, NCH(CH_3)$_2$), 1.02 (d, $^{3}J_{HP}$ = 12.9 Hz, 27H, PC(CH_3)$_3$), 1.19 (d, $^{3}J_{HH}$ = 6.6 Hz, 6H, CH(CH_3)$_2$), 1.32 (s, 18H, C(CH_3)$_3$), 1.39 (d, $^{3}J_{HH}$ = 6.7 Hz, 6H, CH(CH_3)$_2$), 1.40 (d, $^{3}J_{HH}$ = 6.6 Hz, 6H, CH(CH_3)$_2$), 1.51 (d, $^{3}J_{HP}$ = 6.5 Hz, 6H, NCH(CH_3)$_2$), 1.55 (d, $^{3}J_{HH}$ = 6.8 Hz, 6H, CH(CH_3)$_2$), 1.70 (s, 3H, C(CH_3)$_2$), 1.90 (s, 3H, C(CH_3)$_2$), 3.24 (sept, $^{3}J_{HH}$ = 6.6 Hz, 1H, NCH(CH$_3$)$_2$), 3.74 (sept, $^{3}J_{HH}$ = 6.8 Hz, 2H, CH(CH$_3$)$_2$), 3.91 (sept, $^{3}J_{HH}$ = 6.6 Hz, 1H, NCH(CH$_3$)$_2$), 4.24 (sept, $^{3}J_{HH}$ = 6.8 Hz, 2H, CH(CH$_3$)$_2$), 6.22 (d, $^{4}J_{HH}$ = 1.8 Hz, 2H, XA-*o*-CH), 6.76 (d, $^{4}J_{HH}$ = 2.0 Hz , 2H, XA-*p*-CH), 7.28-7.44 (m, 6H ArH).

^{13}C{^{1}H} NMR (126 MHz, C_6D_6, 298 K): δ_C = 23.5 (C(CH$_3$)$_2$), 25.0 (NCH(CH$_3$)$_2$), 25.2, 25.9, 26.3, 26.5 (CH(CH$_3$)$_2$) 26.8, 27.0 (CH(CH$_3$)$_2$), 29.0 (NCH(CH$_3$)$_2$), 32.0 (PC(CH$_3$)$_3$), 32.1 (C(CH$_3$)$_3$), 34.0 (C(CH$_3$)$_2$), 35.2 (C(CH$_3$)$_3$), 36.8 (dd, $^{1}J_{CP}$ = 5.9 Hz, $^{2}J_{CAg}$ = 1.5 Hz, PC(CH$_3$)$_3$), 37.0 (C(CH$_3$)$_2$), 52.2 (d, $^{3}J_{CAg}$ = 4.4 Hz, NCH(CH$_3$)$_2$), 54.1 (d, $^{3}J_{CAg}$ = 4.4 Hz, NCH(CH$_3$)$_2$), 105.5, 110.8, 124.0, 124.5, 125.5, 128.4, 128.3, 131.3, 139.6, 145.3, 145.5, 147.1, 147.3, 148.7 (ArC), 219.9 (ddd, $^{1}J_{C107Ag}$ = 182, $^{1}J_{C109Ag}$ = 210, $^{2}J_{CP}$ = 63 Hz, CAg).

^{31}P{^{1}H} NMR (162 MHz, C_6D_6, 298 K): δ_P = 73.4 (dd, $^{1}J_{P\text{-}107Ag}$ = 352, $^{1}J_{P\text{-}109Ag}$ = 408 Hz).

Elemental microanalysis: calc. for $C_{66}H_{103}AgAlN_4OP$: C 69.88 %, H 9.15 %, N 4.94 %; meas.: C 69.66 %, H 9.40 %, N 4.59 %.

Synthesis of (NON)Al{(NCy)$_2$C}CuP^{t}Bu$_3$ (5-Cu): A solution of **3-Cu** (40 mg, 0.041 mmol) and dicyclohexylcarbodiimide (8 mg, 0.041 mmol) in benzene (5 mL) was

stirred at room temperature for 16 h. The reaction mixture was concentrated to 0.5 mL and filtered. Colourless crystals of **5-Cu** suitable for X-ray crystallography formed on standing at room temperature. Yield: 44 mg, 90 %.

^{1}H NMR (400 MHz, C_6D_6, 298 K): δ_H = 1.10 (d, $^{3}J_{HP}$ = 12.9 Hz, 27H, PC(C*H*$_3$)$_3$), 1.17 (d, $^{3}J_{HH}$ = 6.6 Hz, 6H, CH(C*H*$_3$)$_2$), 1.31 (s, C(C*H*$_3$)$_3$), 1.43 (d, $^{3}J_{HH}$ = 6.6 Hz, 6H, CH(C*H*$_3$)$_2$), 1.51 (d, $^{3}J_{HH}$ = 6.8 Hz, 6H, CH(C*H*$_3$)$_2$), 1.69 (s, 3H, C(C*H*$_3$)$_2$), 1.74 (br, 6H, Cy*H*), 2.00 (s, 3H, C(C*H*$_3$)$_2$), 2.23 (br, Cy*H*), 2.78 (m, 1H, NC*H* Cy), 3.60 (m, 1H, NC*H* Cy), 3.73 (sept, $^{3}J_{HH}$ = 6.8 Hz, 2H, C*H*(CH$_3$)$_2$), 4.21 (sept, $^{3}J_{HH}$ = 6.8 Hz, 2H, C*H*(CH$_3$)$_2$), 6.19 (d, $^{4}J_{HH}$ = 1.8 Hz, 2H, XA-*o*-C*H*), 6.76 (d, $^{4}J_{HH}$ = 2.0 Hz, 2H, XA-*p*-C*H*), 7.23-7.42 (m, 6H Ar*H*).

^{13}C {^{1}H} NMR (126 MHz, C_6D_6, 298 K): δ_C = 25.2, 25.9, (CH(*C*H$_3$)$_2$) 26.1, 26.3 (CH(*C*H$_3$)$_2$), 26.6 (d, $^{1}J_{CC}$ = 2 Hz, *C*H$_2$ Cy), 26.8, (CH(*C*H$_3$)$_2$), 27.0, (*C*H(CH$_3$)$_2$), 29.2 (*C*H$_2$ Cy) 32.0 (C(*C*H$_3$)$_3$, 32.1 (d, $^{1}J_{CP}$ = 6 Hz, *C*H$_2$ Cy), 32.4 (d, $^{1}J_{CP}$ = 6 Hz, *C*H$_2$ Cy), 33.8, (*C*H$_2$ Cy), 35.1, (C(*C*H$_3$)$_3$, 35.6, 36.6, 37.0, (*C*(CH$_3$)$_2$), 37.6 (d, $^{1}J_{CP}$ = 5 Hz, P*C*(CH$_3$)$_3$), 59.6, 62.3 (N*C* Cy), 105.5, 110.9, 123.8, 124.4, 125.4, 128.5, 131.5, 139.8, 145.5, 145.6, 147.0, 147.2, 148.7 (Ar-*C*), 215.5 (d, $^{2}J_{CP}$ = 58 Hz, *C*-Cu).

^{31}P{^{1}H} NMR (162 MHz, C_6D_6, 298 K): δ = 59.6 (s).

Elemental microanalysis: calc. for $C_{72}H_{111}CuAlN_4OP$: C 73.90 %, H 9.56 %, N 4.79 %; meas.: C 70.88 %, H 9.06 %, N 4.84 %.

Synthesis of (NON)Al(O$_2$CO)AgP^{t}Bu$_3$ (6-Ag): A solution of **4-Ag** (100 mg, 0.095 mmol) in benzene (2 mL) was degassed and exposed to CO_2 (ca. 1 atm). The reaction mixture was left at room temperature for 18 h, after which time clean conversion to **6-Ag** was observed by ^{31}P NMR spectroscopy. The reaction mixture was heated to 80°C for 24 h before being cooled to room temperature. Volatiles were removed under

vacuum and the product extracted into hexane. Colourless crystals formed on standing at room temperature. Yield: 58 mg, 57 %. Single crystals suitable for X-ray crystallography were grown from warm benzene. **^{1}H NMR** (400 MHz, C_7D_8, 298 K): δ_H = 1.05 (br d, $^{3}J_{HP}$ = 11.2 Hz, 27H, PC(CH_3)$_3$), 1.25 (d, $^{3}J_{HH}$ = 6.7 Hz, 12H, CH(CH_3)$_2$), 1.29 (s, 18H, C(CH_3)$_3$), 1.49 (d, $^{3}J_{HH}$ = 6.7 Hz, 12H, CH(CH_3)$_2$), 1.61 (s, 6H, C(CH_3)$_2$), 3.93 (sept, $^{3}J_{HH}$ = 6.6 Hz, 4H, CH(CH$_3$)$_2$), 6.31 (d, $^{4}J_{HH}$ = 1.7 Hz, 2H, XA-*o*-CH), 6.73 (d, $^{4}J_{HH}$ = 1.7 Hz , 2H, XA-*p*-CH), 7.20-32 (m, 6H ArH). **^{13}C{^{1}H}** NMR (126 MHz, C_6D_6, 298 K): δ_C = 25.5, 26.0 (CH(*C*H$_3$)$_2$) 28.6 (*C*(CH$_3$)$_2$), 30.7 (*C*H(CH$_3$)$_2$), 31.9 (C(*C*H$_3$)$_3$), 32.2 (d, $^{2}J_{CP}$ = 5.0 Hz, P{C(*C*H$_3$)$_3$}$_3$), 35.2 (*C*(CH$_3$)$_3$), 37.2 (P{*C*(CH$_3$)$_3$}$_3$), 37.1 (*C*(CH$_3$)$_2$), 106.1, 110.5, 123.9, 125.3, 128.3, 132.5, 140.6, 143.7, 143.9, 145.2, 147.8, 148.1 (Ar-*C*); 167.2 (O_2-*C*-O). **^{31}P{^{1}H} NMR** (162 MHz, C_7D_8, 298 K): δ_P = 74.0 (br). ^{31}P{^{1}H} NMR (162 MHz, C_7D_8, 203 K): δ_P = 74.0 (d, $^{1}J_{PAg}$ = 486 Hz). Elemental microanalysis: calc. for **6-Ag**·C_6H_6, $C_{66}H_{95}AgAlN_2O_4P$: C 69.15 %, H 8.35 %, N 2.44 %; meas.: C 68.75 %, H 8.75 %, N 2.82 %.

Synthesis of (NON)Al(O$_2$CO)CuP^{t}Bu$_3$ (6-Cu): A solution of **3-Cu** (100 mg, 0.103 mmol) in benzene (2 mL) in a J. Young's ampoule was degassed and exposed to CO_2 (ca. 1 atm). After 15 min, volatiles were removed under vacuum and the residue extracted into pentane. Colourless crystals formed on standing at room temperature. Yield: 65 mg, 61%. Crystals suitable for X-ray crystallography were grown from warm benzene.

^{1}H NMR (400 MHz, C_6D_6, 298 K): δ_H = 0.86 (d, $^{3}J_{HP}$ = 12.7 Hz, 27H, PC(CH_3)$_3$), 1.23 (d, $^{3}J_{HH}$ = 6.9 Hz, 12H, CH(CH_3)$_2$), 1.27 (s, 18H, C(CH_3)$_3$), 1.45 (d, $^{3}J_{HH}$ = 7.0 Hz, 12H, CH(CH_3)$_2$), 1.60 (s, 6H, C(CH_3)$_2$), 3.87 (sept, $^{3}J_{HH}$ = 6.8 Hz, 4H, CH(CH$_3$)$_2$), 6.40 (d,

$^4J_{HH}$ = 1.9 Hz, 2H, XA-*o*-C*H*), 6.75 (d, $^4J_{HH}$ = 1.9 Hz , 2H, XA-*p*-C*H*), 7.23-7.32 (m, 6H Ar*H*).

^{13}C{^{1}H} NMR (126 MHz, C_6D_6, 298 K): δ_C = 25.2, 25.9 (CH(*C*H$_3$)$_2$) 26.7 (*C*(CH$_3$)$_2$), 28.6 (*C*H(CH$_3$)$_2$), 31.9 (C(*C*H$_3$)$_3$), 35.2 (*C*(CH$_3$)$_3$), 36.5 (d, $^2J_{CP}$ = 6.0 Hz, P{C(*C*H$_3$)$_3$}$_3$), 37.1 (P{*C*(CH$_3$)$_3$}$_3$), 106.7, 110.6, 124.0, 125.5, 132.4, 140.3, 142.8, 144.7, 147.8, 148.4 (Ar*C*), 170.1 (O_2*C*O).

^{31}P{^{1}H} NMR (162 MHz, C_6D_6, 298 K): δ_P = 62.5 (s).

Elemental microanalysis: calc. for **6-Cu**·C_6H_6, $C_{66}H_{95}AlCuN_2O_4P$: C 71.93 %, H 8.64 %, N 2.54 %; meas.: C 71.44 %, H 8.14 %, N 2.88 %.

Synthesis of (NON)Al{O(^{i}PrN)CN^{i}Pr}Ag (7-Ag): To solution of **4-Ag** (60 mg, 0.057 mmol) in benzene was added diisopropylcarbodiimide (8.8 µl, 0.057 mmol). The reaction was heated to 80 °C for 15 d, after which time the solvent was removed under vacuum. Crystals suitable for X-ray diffraction were obtained by slow cooling of a pentane solution to −30 °C.

7-Ag exists as two isomers and isolated samples of **7-Ag** dissolved in C_6D_6 retain the ratio 2:1 of major:minor product apparent in ^{1}H, ^{31}P and ^{13}C NMR. This results in much overlap in the ^{1}H and ^{13}C spectra and so partial assignments made with the aid of 2D NMR are given.

^{1}H NMR (400 MHz, C_6D_6, 298 K): Major: δ_P = 0.33 (d, $^3J_{HH}$ = 7.2 Hz, N-C*H*(CH$_3$)$_2$), 0.91 (d, $^3J_{HP}$ = 13.6 Hz, 27H, PC(C*H*$_3$)$_3$), 0.99 (s, 6H, C(C*H*$_3$)$_2$), 1.27 (s, 18H, C(C*H*$_3$)$_3$), 1.45 (d, $^3J_{HH}$ = 6.27, 6H, C*H*(CH$_3$)$_2$), 3.25 (sept, $^3J_{HH}$ = 5.98, 1H, C*H*(CH$_3$)$_2$), 3.54 (sept, $^3J_{HH}$ = 6.62, 1H, C*H*(CH$_3$)$_2$), 3.73 (sept, $^3J_{HH}$ = 6.62, 1H, C*H*(CH$_3$)$_2$), 4.15 (sept, $^3J_{HH}$ = 6.51, 2H, C*H*(CH$_3$)$_2$), 6.29 (d, $^4J_{HH}$ = 1.6 Hz, 2H, XA-*o*-C*H*), 6.75 (d, $^4J_{HH}$ = 1.9 Hz , 2H, XA-*p*-C*H*)(overlap with minor), 7.10-7.40 (m, 6H, Ar*H*), Minor: 0.02 (d, $^3J_{HH}$ = 7.2

Hz, N-C*H*(CH_3)$_2$), 0.91 (d, $^3J_{HP}$ = 13.6 Hz, 27H, PC(C*H*$_3$)$_3$), 0.94 (s, 6H, C(C*H*$_3$)$_2$), 1.33 (s, 18H, C(C*H*$_3$)$_3$), 2.31 (sept, $^3J_{HH}$ = 6.55, 1H, C*H*(CH_3)$_2$, 0.65 (sept, $^3J_{HH}$ = 6.61, 1H, C*H*(CH_3)$_2$, 3.60, (sept, $^3J_{HH}$ = 6.31, 2H, C*H*(CH_3)$_2$, 4.05 (sept, $^3J_{HH}$ = 6.52, 1H, C*H*(CH_3)$_2$, 6.24 (d, $^4J_{HH}$ = 1.8 Hz, 2H, XA-*o*-C*H*), 6.75 (d, $^4J_{HH}$ = 1.9 Hz , 2H, XA-*p*-C*H*)(overlap with major), 7.10-7.40 (m, 6H, Ar*H*),

^{13}C{^{1}H} NMR (126 MHz, C_6D_6, 298 K): δ_C = 21.6, (*C*H_3), 22.4 (N-*C*H(CH_3)$_2$) 23.3, 24.5, 24.7, 25.2, 26.3, 26.6, 27.6, 28.0, 28.7, 29.0, 29.1, 29.2 (*C*H_3), 32.0 (*C*H(CH_3)$_2$), 32.5 (PC(*C*H_3)$_3$), 35.2 (*C*H(CH_3)$_2$), 37.0 (d, $^2J_{CP}$ = 7.0 Hz, P*C*(CH_3)$_3$), 43.8, 44.0, 47.3, 48.9 (*C*HCH_3), 105.9, 106.8, 110.7, 111.0, 123.6, 123.9, 124.3, 124.5, 125.6, 126.0, 132.3, 140.2, 140.6, 143.5, 144.5, 145.1, 145.3, 147.1, 147.2, 147.8, 148.5, 149.3 (*C*-Ar) 167.2 (dd, $^1J_{AgC}$ = 6.5 Hz, $^2J_{PC}$ = 2.3 Hz, *C*-Ag [minor]), 167.8, (dd, $^1J_{AgC}$ = 6.5 Hz, $^2J_{PC}$ = 2.3 Hz, *C*-Ag [major]).

^{31}P{^{1}H} NMR (162 MHz, C_6D_6): δ_P = 80.1 (dd, $^1J_{P\text{-}107Ag}$ = 540, $^1J_{P\text{-}109Ag}$ = 623 Hz) (major), 78.8 (dd, $^1J_{P\text{-}107Ag}$ = 540, $^1J_{P\text{-}109Ag}$ = 623 Hz) (minor).

***In situ* generation of (NON)AlOAgP^{t}Bu$_3$ (8-Ag):** A solution of **3-Ag** (20 mg, 0.020 mmol) in toluene was degassed and exposed to N_2O (ca. 1 atm) at –78 °C then allowed to reach room temperature. This product was not isolated due to instability on prolonged standing at room temperature.

^{1}H NMR (400 MHz, C_7D_8, 298 K): δ_H = 0.87 (br d, $^3J_{HP}$ = 9.7 Hz, 27H, PC(C*H*$_3$)$_3$), 1.22 (br, 12H, CH(C*H*$_3$)$_2$), 1.24 (s, 18H, C(C*H*$_3$)$_3$), 1.48 (d, $^3J_{HH}$ = 7.2 Hz, 12H, CH(C*H*$_3$)$_2$), 1.59 (s, 6H, C(C*H*$_3$)$_2$), 3.93 (sept, $^3J_{HH}$ = 6.6 Hz, 4H, C*H*(CH_3)$_2$), 6.27 (d, $^4J_{HH}$ = 1.9 Hz, 2H, XA-*o*-C*H*), 6.67 (d, $^4J_{HH}$ = 1.9 Hz , 2H, XA-*p*-C*H*), 7.10-23 (m, 6H Ar*H*).

^{31}P{^{1}H} NMR (162 MHz, C_7D_8, 298 K): δ_P = 82.0 (br dd, $^1J_{P107Ag}$ = 551, $^1J_{P109Ag}$ = 640 Hz). The ^{1}H NMR spectrum also contains traces of (NON)H_2 as a result of

decomposition; no ^{13}C NMR spectrum could be measured due to instability at room temperature.

4.6 References

1 A. Okem, B. Rama, H. O. Pörtner, D. C. Roberts, M. Tignor, E. Poloczanska, K. Mintenbeck, A. Alegría, M. Craig, S. Langsdorf, S. Löschke and V. Möller, *Climate Change 2022: Impacts, Adaptation and Vulnerability, IPCC*, 2022.

2 A. Siemenski, *Technology, readiness and costs of CCS; The Circular Carbon Economy: Keystone to global sustainability series*, 2021.

3 M. Cokoja, C. Bruckmeier, B. Rieger, W. A. Herrmann and F. E. Kühn, *Angew. Chemie - Int. Ed.*, 2011, **50**, 8510–8537.

4 J. A. Rudd, *Nat. Chem.*, **14**, 360.

5 Q. Liu, L. Wu, R. Jackstell and M. Beller, *Nat. Commun.*, 2015, , 5933.

6 K. Huang, C. L. Sun and Z. J. Shi, *Chem. Soc. Rev.*, 2011, **40**, 2435–2452.

7 J. Qiao, Y. Liu, F. Hong and J. Zhang, *Chem. Soc. Rev.*, 2014, **43**, 631–675.

8 J. Mascetti, in *Carbon Dioxide as Chemical Feedstock*, ed. M. Aresta, Wiley-VCH Verlag, Weinheim, 2010, pp. 55–88.

9 H. Arakawa, M. Aresta, J. Armor, M. Barteau, E. Beckman, A. Bell, J. Bercaw, C. Creutz, E. Dinjus, D. A. Dixon, K. Domen, D. Dubois, J. Eckert, E. Fujita, D. Gibson, W. Goddard, W. Goodman, J. Keller, G. J. Kubas, H. H. Kung, J. E. Lyons, L. E. Manzer, T. J. Marks, K. Morokuma, K. M. Nicholas, R. Periana, L. Que, J. Rostrup-Nielson, W. M. H. Sachtler, L. D. Schmidt, A. Sen, G. A. Somorjai, P. C. Stair, B. R. Stults and W. Tumas, *Chem. Rev.*, 2001, **101**, 953–996.

10 D. Seyferth, *Organometallics*, 2009, **28**, 1598–1605.

11 M. M. D. Roy, A. A. Omaña, A. S. S. Wilson, M. S. Hill, S. Aldridge and E. Rivard, *Chem. Rev.*, 2021, 121, 12784–12965.

12 D. W. Stephan, *Acc. Chem. Res.*, 2015, **48**, 306–316.

13 A. E. Ashley, A. L. Thompson and D. O'Hare, *Angew. Chemie - Int. Ed.*, 2009, **48**, 9839–9843.

14 T. Zhao, X. Hu, Y. Wu and Z. Zhang, *Angew. Chemie*, 2019, **131**, 732–736.

15 T. Wang, M. Xu, A. R. Jupp, Z. W. Qu, S. Grimme and D. W. Stephan, *Angew. Chemie - Int. Ed.*, 2021, **60**, 25771–25775.

16 N. Von Wolff, G. Lefèvre, J. C. Berthet, P. Thuéry and T. Cantat, *ACS Catal.*, 2016, **6**, 4526–4535.

17 M. A. Courtemanche, M. A. Légaré, L. Maron and F. G. Fontaine, *J. Am. Chem. Soc.*, 2013, **135**, 9326–9329.

18 J. Campos, *Nat. Rev. Chem.*, 2020, **4**, 696–702.

19 L. Roy, M. H. Al-Afyouni, D. E. Derosha, B. Mondal, I. M. Dimucci, K. M. Lancaster, J. Shearer, E. Bill, W. W. Brennessel, F. Neese, S. Ye and P. L. Holland, *Chem. Sci.*, 2019, **10**, 918–929.

20 J. Li, M. Hermann, G. Frenking and C. Jones, *Angew. Chemie - Int. Ed.*, 2012, **51**, 8611–8614.

21 S. Sinhababu, Y. Lakliang and N. Mankad, *Dalt. Trans.*, 2022, **51**, 6129-6147..

22 J. H. Jeoung and H. Dobbek, *Science*, 2007, **318**, 1461–1464.

23 M. Devillard, R. Declercq, E. Nicolas, A. W. Ehlers, J. Backs, N. Saffon-Merceron, G. Bouhadir, J. C. Slootweg, W. Uhl and D. Bourissou, *J. Am. Chem. Soc.*, 2016, **138**, 4917–4926.

24 J. Hicks, A. Mansikkamäki, P. Vasko, J. M. Goicoechea and S. Aldridge, *Nat. Chem.*, 2019, **11**, 237–241.

25 F. A. Cotton, G. Wilkninson, C. A. Murillo and M. Bochmann, *Advanced Inorganic Chemistry*, Wiley-interscience, Hoboken, New Jersey, 6th edn., 1999.
26 C. Gibard, K. Fauché, R. Guillot, L. Jouffret, M. Traïkia, A. Gautier and F. Cisnetti, *J. Organomet. Chem.*, 2017, **840**, 70–74.
27 T. Simler, P. Braunstein and A. A. Danopoulos, *Dalt. Trans.*, 2016, **45**, 5122–5139.
28 X. Liu and P. Braunstein, *Inorg. Chem.*, 2013, **52**, 7367–7379.
29 J. C. Y. Lin, R. T. W. Huang, C. S. Lee, A. Bhattacharyya, W. S. Hwang and I. J. B. Lin, *Chem. Rev.*, 2009, **109**, 3561–3598.
30 M. Hirano, M. Akita, K. Tani, K. Kumagai, N. C. Kasuga, A. Fukuoka and S. Komiya, *Organometallics*, 1997, **16**, 4206–4213.
31 A. Caise, L. P. Griffin, C. McManus, A. Heilmann and S. Aldridge, *Angew. Chemie Int. Ed.*, **61**, 17, e20217496..
32 B. Cordero, V. Gómez, A. E. Platero-Prats, M. Revés, J. Echeverría, E. Cremades, F. Barragán and S. Alvarez, *Dalt. Trans.*, 2008, 2832–2838.
33 D. Bourissou, O. Guerret, F. P. Gabbaï and G. Bertrand, *Chem. Rev.*, 2000, **100**, 39–91.
34 C. Yoo and Y. Lee, *Chem. Sci.*, 2016, **8**, 600–605.
35 J. Hicks, A. Heilmann, P. Vasko, J. M. Goicoechea and S. Aldridge, *Angew. Chemie - Int. Ed.*, 2019, **58**, 17265–17268.
36 C. Kim, H. S. Jeon, T. Eom, M. S. Jee, H. Kim, C. M. Friend, B. K. Min and Y. J. Hwang, *J. Am. Chem. Soc.*, 2015, **137**, 13844–13850.
37 Y. Ye, H. Yang, J. Qian, H. Su, K. J. Lee, T. Cheng, H. Xiao, J. Yano, W. A. Goddard and E. J. Crumlin, *Nat. Commun.*, 2019, 10, 1875
38 Q. W. Song, W. Q. Chen, R. Ma, A. Yu, Q. Y. Li, Y. Chang and L. N. He, *ChemSusChem*, 2015, **8**, 821–827.
39 L. P. Olson, D. R. Whitcomb, M. Rajeswaran, T. N. Blanton and B. J. Stwertka, *Chem. Mater.*, 2006, **18**, 1667–1674.
40 E. Ruiz-López, J. Gandara-Loe, F. Baena-Moreno, T. R. Reina and J. A. Odriozola, *Renew. Sustain. Energy Rev.*, 2022, **161**, 112329
41 F. Lazreg, A. M. Z. Slawin and C. S. J. Cazin, *Organometallics*, 2012, **31**, 7969–7975.
42 E. Despagnet-Ayoub and R. H. Grubbs, *J. Am. Chem. Soc.*, 2004, **126**, 10198–10199.
43 A. Bayler, A. Schier, G. A. Bowmaker and H. Schmidbaur, *J. Am. Chem. Soc*, 1996, **118**, 7006–7007.
44 C. Boehme and G. Frenking, *Organometallics*, 1998, **17**, 5801–5809.
45 K. A. Moltved and K. P. Kepp, *J. Phys. Chem. C*, 2019, **123**, 18432–18444.
46 J. Li, M. Hermann, G. Frenking and C. Jones, *Angew. Chemie - Int. Ed.*, 2012, **51**, 8611–8614.
47 L. Escomel, N. Soulé, E. Robin, I. Del Rosal, L. Maron, E. Jeanneau, C. Thieuleux and C. Camp, *Inorg. Chem.*, 2022, **61**, 15, 5715-5730..
48 H.-Y. Liu, R. J. Schwamm, M. S. Hill, M. F. Mahon, C. L. McMullin and N. A. Rajabi, *Angew. Chemie Int. Ed.*, 2021, **60**, 14390–14393.
49 A. Suzuki, X. Guo, Z. Lin and M. Yamashita, *Chem. Sci.*, 2021, **12**, 917–928.
50 H.-Y. Liu, S. E. Neale, M. S. Hill, M. F. Mahon and C. L. McMullin, *Dalt. Trans.*, 2022, **51**, 3913–3924.
51 D. Sorbelli, L. Belpassi and P. Belanzoni, *J. Am. Chem. Soc*, 2021, **143**, 14433–14437.
52 X. Guo, T. Yang, Y. Zhang, K. Sheong and Z. Lin, *Inorg. Chem.*, 2022, 61, 26,

10255–10262
.
53 D. Sorbelli, L. Belpassi and P. Belanzoni, *Inorg. Chem.*, 2022, **61**, 1704–1716.
54 T. Andersen, H. K. Haugen and H. Hotop, *J. Phys. Chem. Ref. Data*, 1999, **28**, 1511–1533.
55 S. Sinhababu, M. R. Radzhabov, J. Telser and N. P. Mankad, *J. Am. Chem. Soc.*, 2022, **144**, 3210–3221.
56 R. H. Crabtree, *The Organometallic Chemistry of the Transition Metals*, Wiley, Chichester, 5th edn., 2009.

Chapter 5 : Reactivity of bimetallic aluminyl complexes towards alkynes

5.1 Introduction

5.1.1 Chemistry of alkynes

Alkynes are highly accessible chemicals, making them versatile and fundamental building blocks in organic synthesis.[1] A key facet of their reactivity is their ability to undergo 1,2-additions, forming substituted vinyl species. Regarding organometallic species, both internal and terminal alkynes insert into M–X bonds (X = H, C, Hal), resulting in metalated alkenes which can act either as intermediates in catalytic cycles, or as stoichiometric reagents for further chemistry (**Figure 5.1**).[2] The reactivity of terminal alkynes often differs from that of internal alkynes, due to the presence of an acidic proton (pK_a *ca.* 26).[3]

5.1.2 Alkynes and coinage metals

The coinage metals (copper, silver and gold) have an extensive track record in alkyne chemistry and can mediate numerous important transformations such as cycloadditions, carbon–heteroatom bond formation and cross-coupling reactions.[4–7] The coinage metals are notable for their excellent ability to form π-complexes with the C–C triple bond, which is often exploited in their reactions with alkynes (**Figure 5.1**).[8] σ-bonded alkynide complexes are also known, although without the stabilisation of large ligands, they are frequently explosive.[9] Au(I) in particular has come to the fore as the most effective catalyst for the Lewis Acid activation of alkynes towards nucleophilic attack, making Au(I) catalysis ubiquitous in complex natural product

synthesis.[6,10–12] Silver has more recently been used as a cheaper alternative to gold in catalytic applications. [7,13]

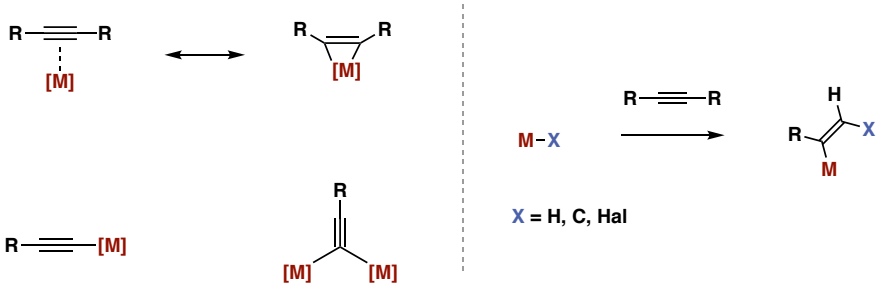


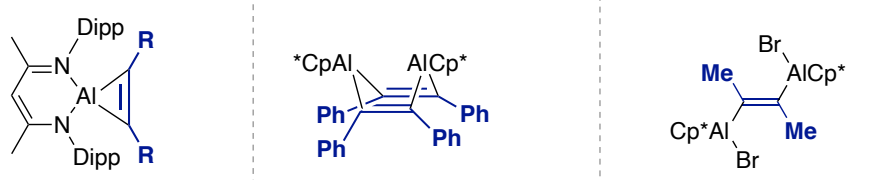
***Figure 5.1**. Left: Modes of alkyne activation by metal species; Right: the syn insertion of alkynes into an M–X bond (X = H, C, Hal).*

Copper also has numerous uses in alkyne chemistry. The copper(I)-catalyzed azide-alkyne cycloaddition reaction is a prime example of 'click chemistry' and has found use in materials synthesis and biochemical labelling. The mechanism has prompted much study, with several intermediates proposed including Cu(I) π-complexes, mononuclear alkynyl species and dicopper μ-alkynyl complexes.[14] The carbocupration of alkynes involves insertion of an alkyne into a Cu–C bond, resulting in a tetra-substituted alkenylcopper compound, which can then undergo further reactions at the copper site.[15] Alkyne functionalisation is not limited to transition metals, with recent years seeing an expansion in reports of the activation of alkynes by main group systems, including aluminium.

5.1.3 Alkynes and aluminium

The hydroalumination of alkynes is well established, using stoichiometric aluminium reagents such as di(*iso*butyl)aluminium hydride (DIBAL-H) or lithium aluminium hydride to afford alkenyl aluminium compounds with good stereoselectivity.[16,17] These aluminated alkenes can then be functionalised by making use of the mild

nucleophilicity of the Al–C bond.[18] Aluminium hydride species have been proven to be excellent catalysts for the hydroboration of terminal alkynes.[19–21] Low valent aluminium species are also known to react with C–C triple bonds, undergoing [2+1] cycloaddition reactions to form strained aluminacyclopropenes such as that reported by Roesky,[22] or the dimeric 1,4-dialuminacyclohexadiene system described by Cowley (**Figure 5.2**).[23] Yet another mode of reactivity was identified in a 2018 report by Braunschweig, in which a cyclopentadienyl-substituted dialane is seen to effect the dialumination of 2-butyne.[24] This one-step difunctionalisation of alkynes produces a homodimetallated alkene. Few examples of heterodimetallated alkenes, which are substituted with two different metals, are known, and all of these examples require a platinum group metal catalyst for their formation.[25]



Roesky, 2006 ***Cowley, 2018*** ***Braunschweig, 2018***

Figure 5.2. *Cycloaddition and insertion products formed by the reaction of low valent Al species with alkynes.*

5.1.4 Alkyne insertion into M–E bonds (E = B, Si)

While a small number of homodimetallated systems have been prepared by the reaction of alkynes with dimeric M–M species,[26,27] the formation of heterodimetallated alkenes by direct insertion into an M–M' bond is unknown, and indeed even for M–E (E = B, Si) bonds only a few systems have been reported. A 2013 report by Bourissou and Amgoune described the reaction of terminal and internal alkynes with a gold silyl species, which proceeds under 'drastic' conditions (3 weeks at 65°C) with activated

alkynes (**Figure 5.3**).[28] This system is notable in that it produces exclusively *cis* disubstituted alkenes, and because it was shown to be regioselective in its reactivity towards unsymmetrically substituted alkynes. A follow-up study attributed this *cis* selectivity to a two-step pathway involving π-coordination of the alkyne to Au, followed by insertion into the Au–Si bond in a *syn* fashion *via* a concerted inner-sphere mechanism.[29] The resulting β-silyl vinylgold complexes could be further functionalised by transmetalation or Pd-catalysed C–C cross coupling, demonstrating the value of metalated alkenes.

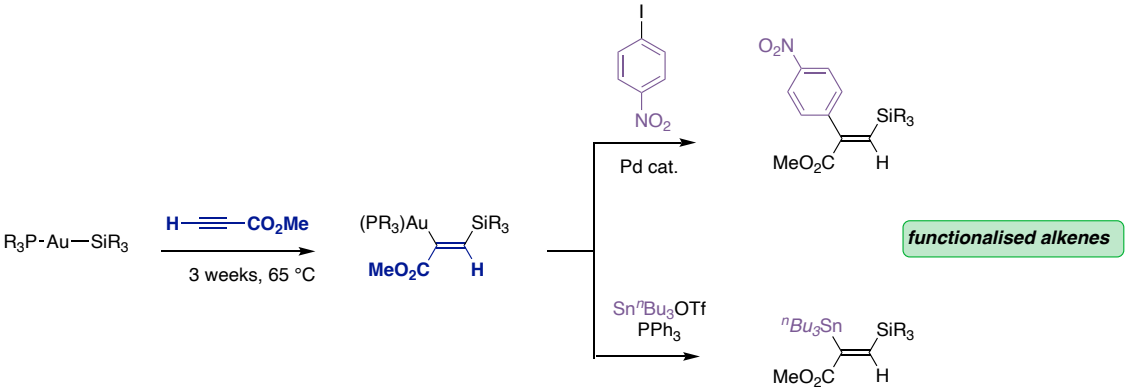


Figure 5.3 *Syn addition of Au–Si across a C–C triple bond and subsequent functionalisation at the Au site, reported by Bourissou and Amgoune.*

More recently, Yamashita and coworkers reported on an interesting isomerisation reaction producing borylalkenyl gold complexes.[30] In this reaction, a terminal alkyne inserts in a *syn* fashion into the Au–B bond of an NHC supported gold boryl species, transiently forming a *cis*-borylalkenyl gold complex. Isomerisation then occurs *via* a retro-1,2-metalate shift, leading to either the *trans* alkene or a migration product in which the R group of the alkyne and the boryl Ar substituent are exchanged (**Figure 5.4**). No regioselectivity was reported for this system.

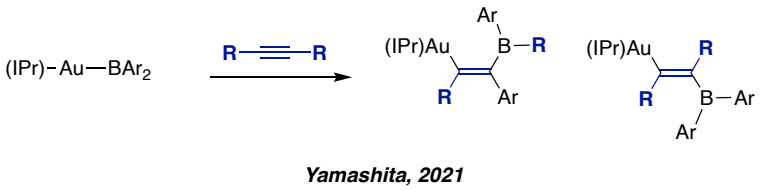


Figure 5.4. *Reaction of a gold boryl to give borylalkenyl gold complexes.*

5.2 Aims

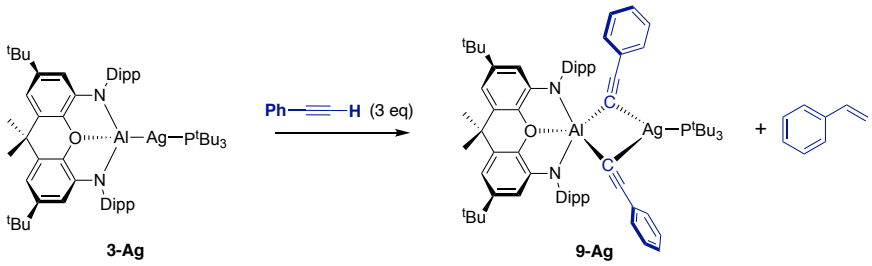
Little is known about the reactivity of heterobimetallic species with alkynes, although reports of (*E*)-selective semi-hydrogenation show they have much promise.[31–33] The metal aluminyl complexes **3-Cu**, **3-Ag** and **3-Au** described in Chapter 3 have great potential for insertion chemistry, as evidenced in Chapter 4 through the ability to insert CO_2 into the Al–M bond. Thus, it may be anticipated that insertion of alkynes into the Al–M bond may be feasible, producing dimetallated alkenes. Both alkenylaluminium and alkenylcopper reagents are useful species for introducing an alkene functionality into a molecule, with the polar M–C bond constituting a mild nucleophile. This chapter aims to explore the reactivity of the group 11 aluminyl complexes towards both terminal and internal alkynes, potentially resulting in insertion of the alkyne into the Al–M bond. Again, differences in reactivity between the different coinage metal aluminyl complexes may be anticipated, as was seen in earlier chapters. The bimetallic nature of the products will be exploited by seeking to further functionalise them in a manner which takes advantage of the different chemical properties of Al and group 11 metals.

5.3 Results and discussion

5.3.1 Reactions with terminal alkynes

The terminal alkyne phenylacetylene was added to a C_6D_6 solution of silver aluminyl complex **(NON)AlAgP^{t}Bu$_3$** (**3-Ag**) (**Scheme 5.1**). Over the course of 18 h, the

formation of a new product was apparent by the appearance of a signal featuring silver satellites in the ^{31}P NMR spectrum at 80.1 ppm ($^{1}J_{PAg}$ = 560, 647 Hz). The large value of the coupling constants compared to that of **3-Ag** (cf. 160 Hz) indicates that Ag is no longer directly bound to the strongly σ-donating aluminyl fragment. The ^{1}H NMR spectrum shows an increase in the number of septets arising from the Dipp methine protons as compared to **3-Ag**, indicating the product has reduced symmetry with respect to the starting material. Interestingly, an *in situ* ^{1}H NMR spectrum also reveals the presence of styrene, as evidenced by a set of doublets at 5.05 and 5.57 ppm.



Scheme 5.1. *Reaction of* ***3-Ag*** *with phenylacetylene, forming a bridged bimetallic acetylide and styrene.*

Colourless crystals were grown from a diethyl ether solution, allowing the solid state structure to be determined by X-ray crystallography (**Figure 5.5**). The structure shows that the product is a bimetallic species in which the silver and aluminium centres are bridged by two phenylacetylide ligands, with the metals each binding to the terminal carbon of the acetylide unit. The planar core of the molecule is unsymmetrical, in that the Ag–C bond lengths differ by 0.1 Å (*d*(Ag(1)–C(57)) = 2.462(4) Å, *d*(Ag(1)–C(49)) = 2.358(3) Å) and the phenyl rings of the acetylide ligands are offset with respect to one another. This bridging μ_2-η^1,η^1 bonding mode is known for group 11 clusters, with acetylide commonly bridging two silver or copper atoms,[34,35] but it is rare for heterobimetallic systems.

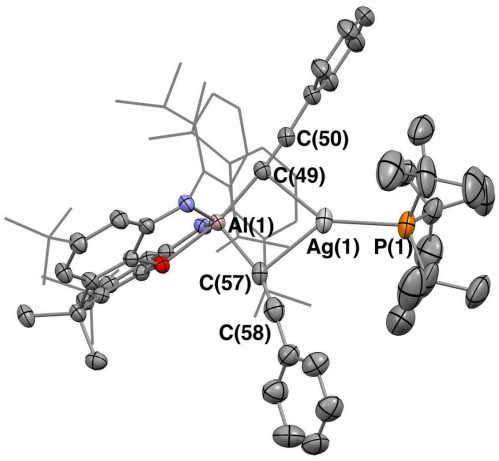


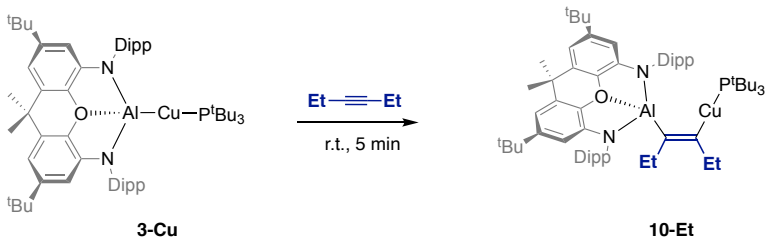
***Figure 5.5**. Molecular structure of **9-Ag** in the solid state as determined by X-ray crystallography. Thermal ellipsoids set at the 50% probability level. Hydrogen atoms omitted and Dipp/^{t}Bu groups shown in wireframe for clarity. Key bond lengths (Å) and angles (°): Ag(1)–C(57) 2.462(4), Ag(1)–C(49) 2.358(3), Ag(1) –P(1) 2.4336(11), Al(1)–C(57) 2.003(4), Al(1)–C(49) 2.016(4), C(49)–Ag(1)–C(57) 79.12(12), C(57)–Al(1)–C(49) 99.62(15)*

9-Ag can be seen as arising from deprotonation of the acidic alkyne proton by the aluminium centre, forming an aluminium hydride and silver acetylide. The aluminium hydride can then react with a second and third equivalent of phenylacetylene, forming the bimetallic complex **9-Ag** and styrene *via* insertion and metathesis steps. Deprotonation of terminal alkynes by aluminium species is well described, and frequently exploited in hydroboration chemistry.[19] Given that demetallation in the desired fashion was not achieved, this process was not investigated in detail. However, it would be possible to do this through experiments using deuterated phenylacetylene, in combination with variable temperature NMR. Although the products of the reactions of **3-Au** and **3-Cu** with phenylacetylene could not be isolated satisfactorily, the similarity of the ^{1}H NMR spectra of each, as well as the observed formation of styrene, implies that they are likely very similar to the structurally characterised bimetallic species **9-Ag**.

With a view to investigating the reactivity of bimetallic Al–M species towards C–C triple bonds in the absence of an acidic proton, our attention was directed towards internal alkynes.

5.3.2 Reactions of internal alkynes

The reaction of a benzene solution of the copper aluminyl complex **(NON)AlCuP^{t}Bu$_3$** (**3-Cu**) with one equivalent of 3-hexyne at room temperature results in the rapid formation of a single species, characterised in the ^{31}P NMR spectrum by a resonance at 55.5 ppm. Crystals of this species, **10-Et**, could be grown from a hexane solution, allowing the structure to be determined by X-ray crystallography (**Figure 5.6**). This reveals that the Al–Cu bond of **3-Cu** has added across the triple bond of EtCCEt in a *syn* fashion, forming the aluminocuprated alkene **10-Et** (**Scheme 5.2**). **10-Et** is the first example of an (aluminylalkenyl)copper complex – an alkene substituted by both a copper and aluminium metal centre. Furthermore, the reaction represents the first structurally characterised example of a 1,2-heterodimetallation reaction occurring *via* direct insertion of an alkyne into an M–M' bond. Previously, such species had only been accessible by Pt-catalysed or stepwise methods, and were uncommon at that.[2] From a crystallographic perspective, the C–C bond length of 1.252(4) Å is on the shorter end of typical C=C double bond lengths. The core of the molecule is planar and the C–Cu–P unit is close to linear (171.11(8)º), as expected for the Cu(I) centre. The Al and Cu atoms are arranged in a *syn* configuration about the double bond.



Scheme 5.2**. Syn insertion of 3-hexyne into the Al–Cu bond of **3-Cu

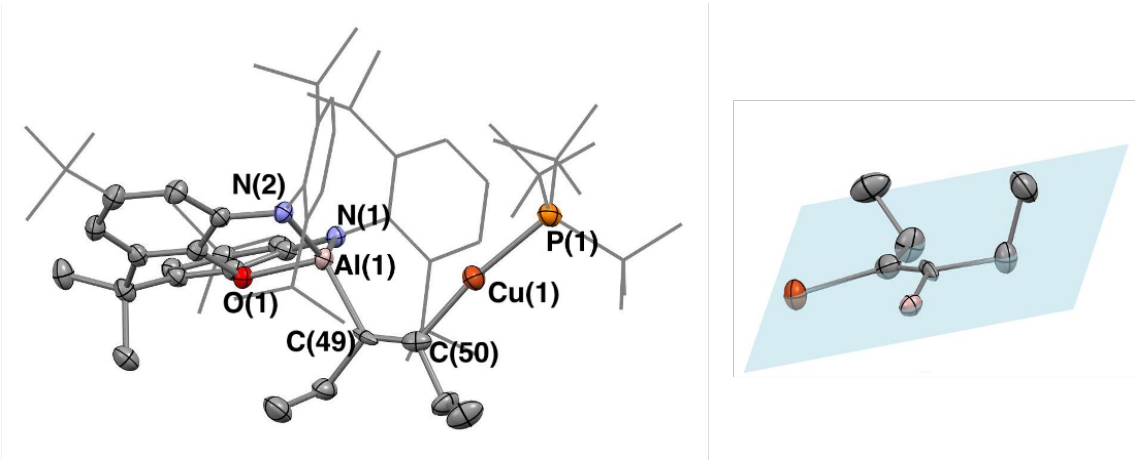


Figure 5.6. *Right: molecular structure of* ***10-Et*** *in the solid state as determined by X-ray crystallography. Thermal ellipsoids set at the 50% probability level. Hydrogen atoms omitted and Dipp/*^{t}*Bu groups shown in wireframe for clarity. Key bond lengths (Å) and angles (°): C(49)–C(50) 1.252(4), Cu(1)-C(50) 1.940(2), Al(1)–C(49) 2.026(3), Cu(1)–P(1) 2.2096(7), C(60)–Cu(1)–P(1) 171.11(8), C(50)–C(49)–Al(1) 126.55(17), C(49)–C(50)–Cu(1) 127.93(19). Left: Section showing the planarity of the atoms around the central C=C double bond*

The ^{1}H NMR spectrum of **10-Et** (**Figure 5.7**) displays two septets corresponding to the Dipp methine protons, indicating a reduction in symmetry compared to **3-Cu**. Two new quartets arising from CH_2 protons of the ethyl groups can be seen at 2.86 and 2.92 ppm. Notably, the signal at 2.86 ppm displays additional coupling to the P^{t}Bu$_3$ ligand ($^4J_{PH}$ = 3 Hz), indicating that it is *geminal* to the [CuP^{t}Bu$_3$] unit.

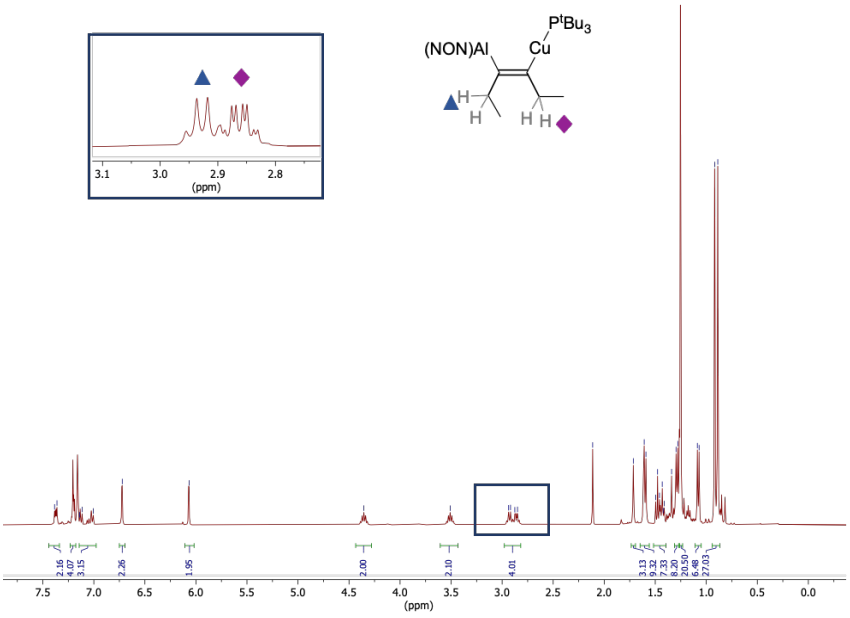


Figure 5.7. *^{1}H NMR spectrum of* ***10-Et****. Inset: Resonances corresponding to the CH_2 protons* geminal *to [(NON)Al] and [CuP^{t}Bu$_3$]*

The effect of the proximal phosphine ligand can also be seen in the ^{13}C NMR spectrum (**Figure 5.8**), in which the two olefinic carbons may be distinguished by the fact that the carbon bound to copper experiences coupling to the *trans* P^tBu_3 ligand and gives rise to a doublet ($^2J_{CP}$ = 73 Hz) at 188.3 ppm. The aluminium-bound carbon experiences no such coupling, and gives rise to a resonance at 151.1 ppm, i.e. slightly higher than previously reported alkenyl aluminium species.[23,30] This pattern of a Cu–*C* doublet and accompanying Al–*C* resonance proves to be diagnostic of an alkene substituted by both Al(NON) and [CuP^tBu_3] fragments.

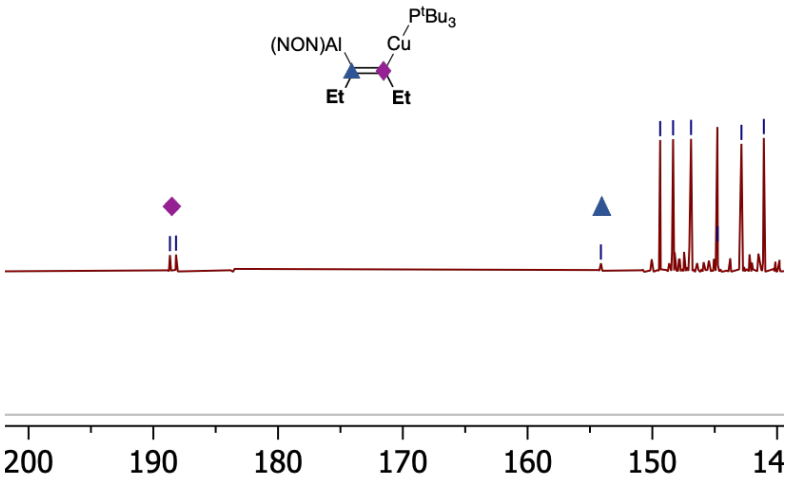


***Figure 5.8**. Excerpt from the ^{13}C NMR spectrum of **10-Et** showing the characteristic pattern of an alkene substituted by an [(NON)Al] and a [CuP^tBu_3] unit*

Although **10-Et** can be isolated cleanly in crystalline form and is stable indefinitely in the solid state, onward reaction is seen at room temperature in toluene solution, even in the absence of excess 3-hexyne. Complete consumption of **10-Et** is apparent after 24 h, and *in situ* ^{31}P NMR shows the formation of a second species defined by a resonance at 58.5 ppm. The ^1H NMR spectrum now features a second set of two quartets, shifted compared to those in **10-Et** but with the same $^4J_{PH}$ coupling pattern.

Likewise, a ^{13}C NMR spectrum measured at t = 8 h features a new doublet at 183.0 ppm ($^{2}J_{PC}$ = 71 Hz) and a resonance at 153.7 ppm, closely resembling the spectrum of **10-Et** (**Figure 5.9**). This spectroscopic evidence leads to the assignment of this new species as **11-Et**, an isomer of **10-Et** in which the Al and Cu fragments are mutually *trans.* Although this *trans* product could not be structurally verified, comparison to the structurally characterised species **11-Pr,Ph** (**Figure 5.12**) offers confidence in this assignment, as it confirms the viability of the *syn* to *anti* isomerisation.

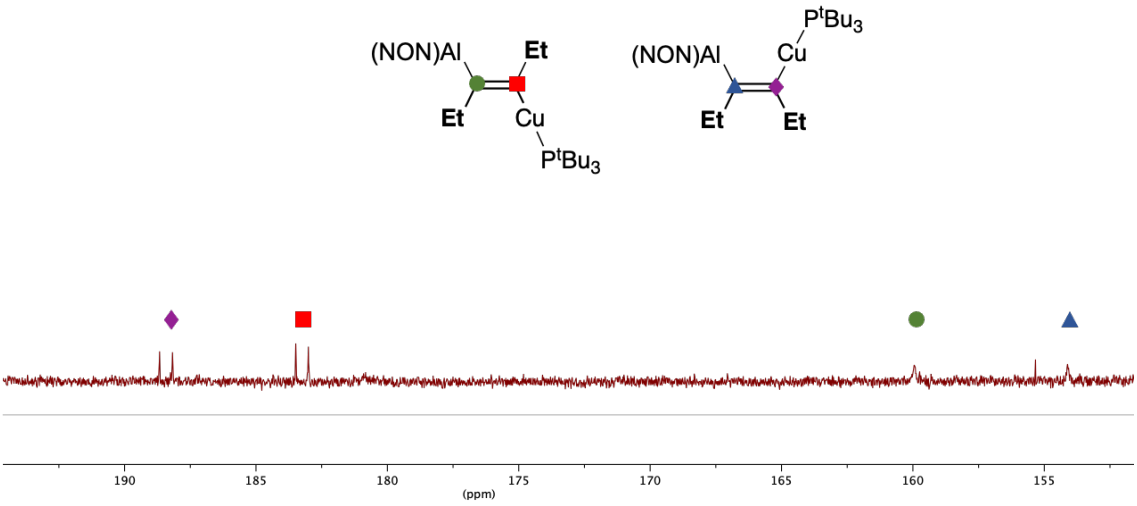
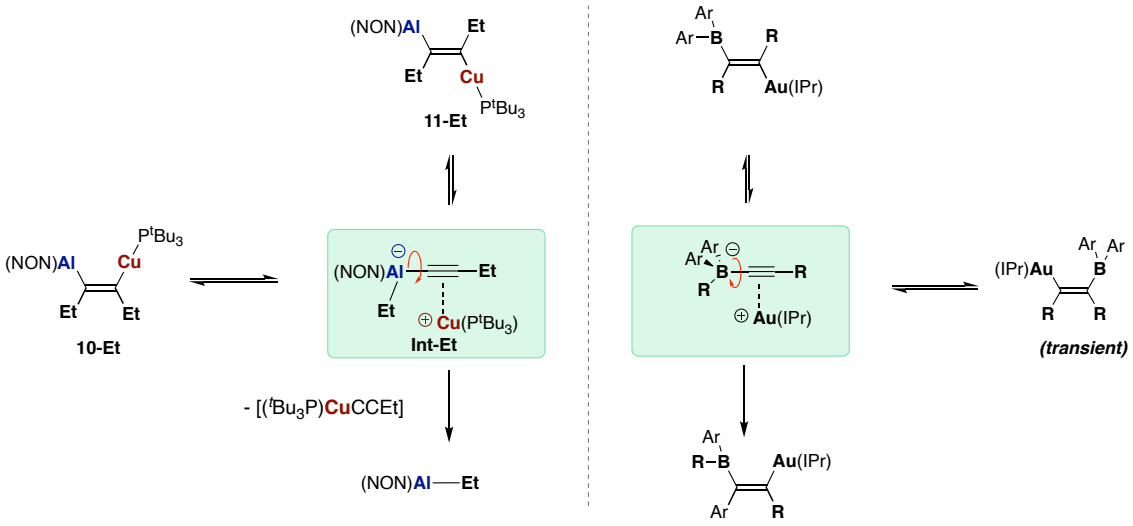


Figure 5.9. *Excerpt from the ^{13}C NMR spectrum of a mixture of **10-Et** and **11-Et**, in which the Al-C resonance and Cu-C doublet for each species can be seen*

A potential mechanism for this isomerisation process can be proposed, based on similarity to the mechanism described by Yamashita and coworkers[30] for the isomerisation of a borylalkenyl gold complex, leading to (depending on the alkyne) either the *trans* disubstituted alkyne, or a product in which the Au and B fragments are *syn* but one of the alkyne substituents has migrated to boron (**Scheme 5.3**). The authors postulate that the intermediate in this reaction is a gold alkynyl-borate, which exists as different rotamers. From this intermediate, either the R group or the *o*-tol substituent at boron may undergo a 1,2-metalate shift, producing the *trans* alkene or

R-migrated product respectively. DFT calculations were used to compare the relative stability of the isomers, and thereby rationalise which product is formed.



Scheme 5.3. *Left: proposed pathway for the isomerisation of* ***10-Et*** *to* ***11-Et*** *via* a copper alkynyl aluminate **Int-Et**; *Right: similar intermediate in the isomerisation of borylalkenyl gold complexes*

The occurrence of a similar mechanism for the conversion of **10-Et** to **11-Et** is supported by the fact that after extended reaction times (48 h), the aluminium ethyl complex **(NON)AlEt** is formed and can be characterised by ^{1}H and ^{13}C NMR spectroscopy, as well as single crystal X-ray diffraction (**Figure 5.10**). This demonstrates the viability of migration of the ethyl group from C to Al, with scission of the C–C bond. While in the gold boryl case the Ar substituent may undergo 1,2-metalate shift to reform a disubstituted alkene, the chelating **NON** ligand does not allow this and so the Al–C bond is broken, resulting in formation of **(NON)AlEt**. This step also implies the formation of a copper acetylide product ^{t}Bu$_3$PCuCCEt. It was not possible to isolate this product, likely due to the lability of group 11 acetylides not supported by sterically hindered ligands, and the only phosphorus containing product observed after 48 h was free P^{t}Bu$_3$. The alternate migration from the proposed copper alkynyl aluminate, **Int-Et**, results in the *trans* alkene **11-Et**. A palladium alkynyl copper

complex has recently been characterised and studied as a structural model of intermediates in the Sonogashira reaction, showing the viability of this class of compound.[36]

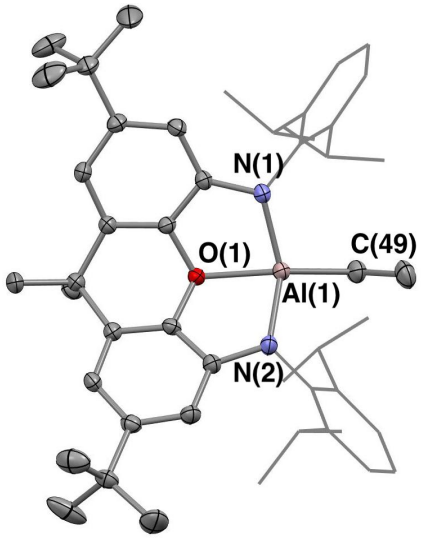


Figure 5.10. *Molecular structure of* ***(NON)AlEt*** *in the solid state as determined by X-ray crystallography. Thermal ellipsoids set at the 50% probability level. Hydrogen atoms omitted and Dipp groups shown in wireframe for clarity. Key bond lengths (Å) and angles (°): Al(1)–C(49) = 1.9637(15), Al(1–)O(1) = 1.9951(10),*

Interestingly, neither gold aluminyl **3-Au** or silver aluminyl **3-Ag** are reactive towards 3-hexyne (or any other terminal alkynes trialled), with no reaction observed by ^{1}H or ^{31}P NMR spectroscopy after ca. 1 week. This is perhaps surprising given the widely documented reactivity of Au(I) complexes towards alkynes, which readily form π-complexes as part of catalytic processes. Likewise, the gold boryl system reported by Yamashita was shown to react readily with terminal alkynes. This suggests that the gold centre in **3-Au** is significantly different from typical gold complexes, and that the aluminyl ligand has altered the electronics of the metal centre to such an extent that this coordination is not possible.

5.3.3 Regioselectivity

Regioselectivity is key to the useful functionalisation of alkyne species. Given the heterobimetallic nature of **3-Cu,** there is the potential for multiple products to be formed and so it was of interest to probe the regiochemistry of the insertion reaction using unsymmetrically substituted alkynes. Initially, as a direct analogue to EtCCEt, 1-phenyl-butyne (PhCCEt) was targeted. However, the products of this reaction proved difficult to crystallise (and therefore structurally characterise) and so the closely related alkyne 1-phenyl-pentyne was studied instead. The reactivity of PhCCR substrates (R = Et, ^{n}Pr) toward copper aluminyl **3-Cu** appear to be near identical in both rate and selectivity. Addition of one equivalent of PhCC^{n}Pr to a benzene solution of **3-Cu** at room temperature results in a rapid reaction to give a major and minor product, as evidenced by two new resonances in the ^{31}P NMR spectrum at 60.2 (major) and 61.5 ppm (minor) in a roughly 3:1 ratio after 15 min. Performing the reaction at 10 °C allows only the major product to be formed exclusively at short reaction times. This species again shows a reduction in symmetry of the **NON** ligand environment compared to **3-Cu**, as evidenced by the appearance of two Dipp methine proton septets in the ^{1}H NMR spectrum. The ^{1}H NMR spectrum also shows characteristic signals relating to the incorporated PhCC^{n}Pr fragment. The resonance corresponding to the CH_2CH$_2$CH$_3$ protons is found as a triplet displaying second order coupling (**Figure 5.11**). This signal is characteristic of an AA'XX' spin system, which is typically described for *n*-propyl groups featuring restricted rotation.[37] Notably, there is no ^{31}P coupling, leading to the assignment of this initially formed product as **10-Pr,Ph**, formed by the *syn* insertion of PhCC^{n}Pr into the Al–Cu bond such that the alkyl group is *geminal* to the [(NON)Al] fragment, and the phenyl group *geminal* to [CuP^{t}Bu$_3$]

(**Scheme 5.4**). Although **10-Pr,Ph** could not be isolated, trapping experiments with CO (**Section 5.3.7**) confirm both the regiochemistry and the *syn* selectivity of this process.

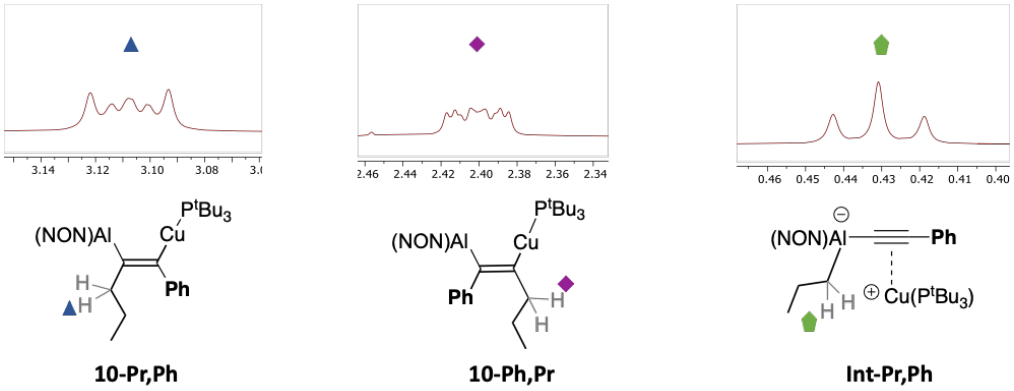


Figure 5.11. *Excerpt from the ^{1}H NMR spectrum of the reaction of **3-Cu** and PhCC^{n}Pr at t = 18 hr, showing the resonances for CH_2 protons geminal to Al, as in **10-Pr,Ph** and **11-Pr,Ph;** geminal to CuP^{t}Bu$_3$, as in **10-Ph,Pr**; and directly bound to Al, as in **Int-Pr,Ph** and **(NON)Al^{n}Pr***

Extended reaction times and mildly elevated temperatures (18 h, 45 °C) lead to formation of a single product, as evidenced by a sole resonance in the ^{31}P NMR spectrum at 57.0 pm. The ^{13}C NMR spectrum of this product displays the now familiar downfield doublet at 187.0 ppm ($^2J_{CP}$ = 63 Hz), indicating that the product is an aluminocuprated alkene. The ^{1}H NMR spectrum bears a strong resemblance to that of the initially formed compound **10-Pr,Ph**, featuring the same resonances but shifted slightly. Diagnostically, the resonance corresponding to the *n*-propyl CH_2 protons has no coupling to ^{31}P, suggesting that the regiochemistry of the product is such that the alkyl group is *geminal* to aluminium. This regiochemistry could be confirmed by X-ray diffraction analysis of crystals grown from a hexane solution (**Figure 5.12**).

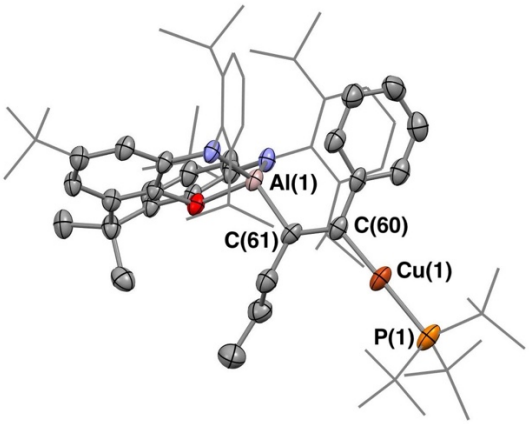
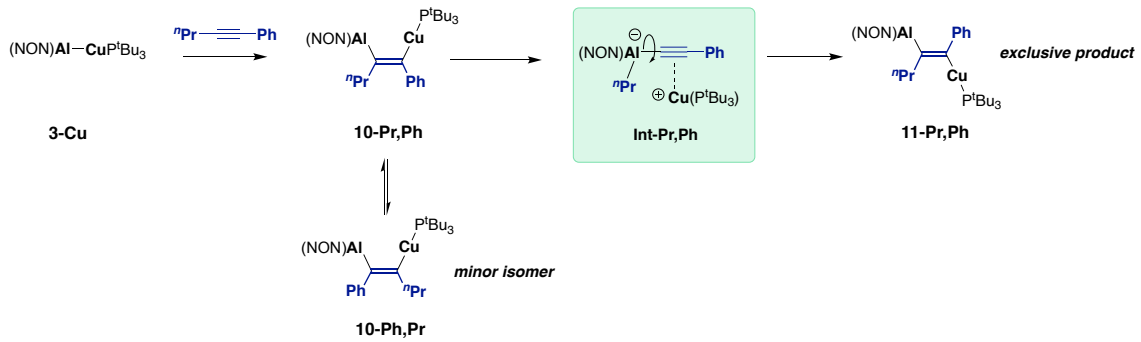


Figure 5.12. *Molecular structure of **11-Pr,Ph** in the solid state as determined by X-ray crystallography. Thermal ellipsoids set at the 50% probability level. Hydrogen atoms omitted and Dipp/^{t}Bu groups shown in wireframe for clarity. Key bond lengths (Å) and angles (°): C(60)–C(61) 1.361(7), Al(1)–C(61) 1.974(4), Cu(1)–C(60) 1.919(4), Cu(1)–P(1) 2.2073(14), C(60)–Cu(1)–P(1) 178.89(17), C(60)–C(61)–Al(1) 119.6(4), C(61)–C(60)–Cu(1) 124.5(4).*

The structure confirms the insertion of PhCC^{n}Pr into the Al–Cu bond. In this case, the aluminium and copper fragments are *trans* to each other, again forming part of a planar core. The C–C bond length of 1.361(7) Å is indicative of a C=C double bond and the C–Cu–P angle is somewhat more linear than that of **10-Et** (178.89(17) vs 171.11(8)°). This can be attributed to the greater steric clash from the Dipp groups of the **NON** ligand when the [CuP^{t}Bu$_3$] and [(NON)Al] fragments are *cis* to each other. The clean formation of **11-Pr,Ph** demonstrates the regioselectivity of the dimetallation reaction.



Scheme 5.4. *Regioselective syn addition of Al–Cu across the alkyne triple bond, followed by isomerisation to the trans alkene **11-Pr,Ph***

Also visible throughout the course of the reaction is a resonance at 58.3 ppm in the ^{31}P NMR spectrum. In the corresponding ^{1}H NMR spectrum, this species displays signals associated with an *n*-propyl group, however in this case the CH_2CH$_2$CH$_3$ is a doublet of triplets, arising from coupling to an adjacent [CuP^{t}Bu$_3$] fragment (**Figure 5.11**). Therefore this species can be hypothesized to be due to the alternate regioisomer **10-Ph,Pr**. This was confirmed by an *in situ* ^{13}C NMR spectrum, which showed a characteristic doublet at 183.5 ($^{2}J_{CP}$ = 67 Hz) which could be seen by 2D NMR to couple to the doublet of triplets. This regioisomer occurs only as a minor component in the reaction, and eventually converts to **11-Pr,Ph**. However, its formation suggests that the alkyne insertion may be reversible, as initially only the *cis* isomer **10-Pr,Ph**, is formed.

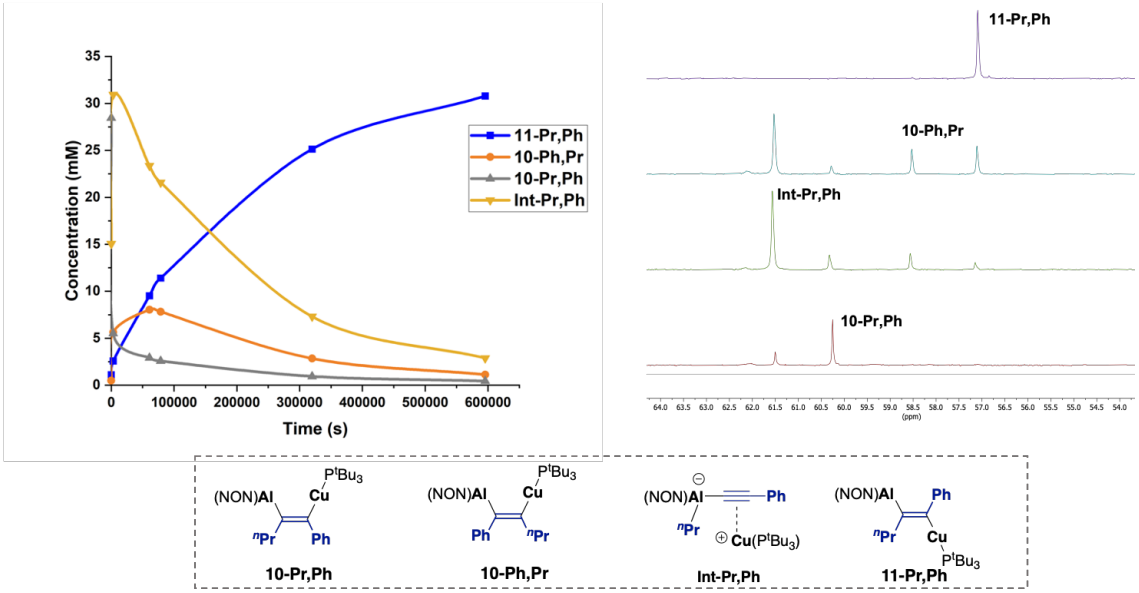


Figure 5.13. *Left: Reaction profile of the reaction of* ***3-Cu*** *with 1 eq PhCC^{n}Pr, measured in C_6D_6 at 298 K. The initial insertion is too fast at room temperature to be shown in this plot. Lines do not indicate mathematical fitting. Right: Representative ^{31}P NMR spectra used to produce the plot.*

Moreover, monitoring the reaction by ^{31}P and ^{1}H NMR, it can be seen that the conversion of *syn* insertion product **10-Pr,Ph** to *trans* alkene **11-Pr,Ph** occurs *via* a persistent intermediate (**Figure 5.13**). Although **10-Pr,Ph** forms initially, it rapidly

reacts onwards to form a new species, characterised by a resonance in the ^{31}P NMR spectrum at 61.5 ppm and reaching a maximum at t = 30 min, as can be seen in the reaction profile. The ^{1}H NMR spectrum measured at this time is illuminating: the resonance corresponding to the CH_2 protons of the *n*-propyl group occurs at a much lower chemical shift (0.31 ppm) than those of the dimetallated alkenes **10-Pr,Ph**, **10-Ph,Pr** and **11-Pr,Ph**. This value is close to that of an aluminium alkyl such as **(NON)AlEt** or **(NON)Al*n*Pr** (cf. 0.53 ppm). Furthermore, the resonance is a simple triplet, with neither the ^{31}P coupling of **10-Ph,Pr** nor the second order coupling diagnostic of the restricted rotation in **10-Pr,Ph** and **11-Pr,Ph** (**Figure 5.11**). Again, this is similar to the spectrum of **(NON)Al*n*Pr**. This spectroscopic evidence suggests that the intermediate features an *n*-propyl group directly bound to aluminium, and therefore is postulated to be the copper alkynyl aluminate, analogous to that proposed in the isomerisation of **10-Et** to **11-Et** (**Scheme 5.4**). While neither of the carbon atoms of the C–C bond could be definitively located in an *in situ* ^{13}C NMR spectrum, 2D NMR shows that the signals corresponding to this alkyl group correlate only with each other and not to any others, as would be expected for an Al-bound *n*-propyl group.

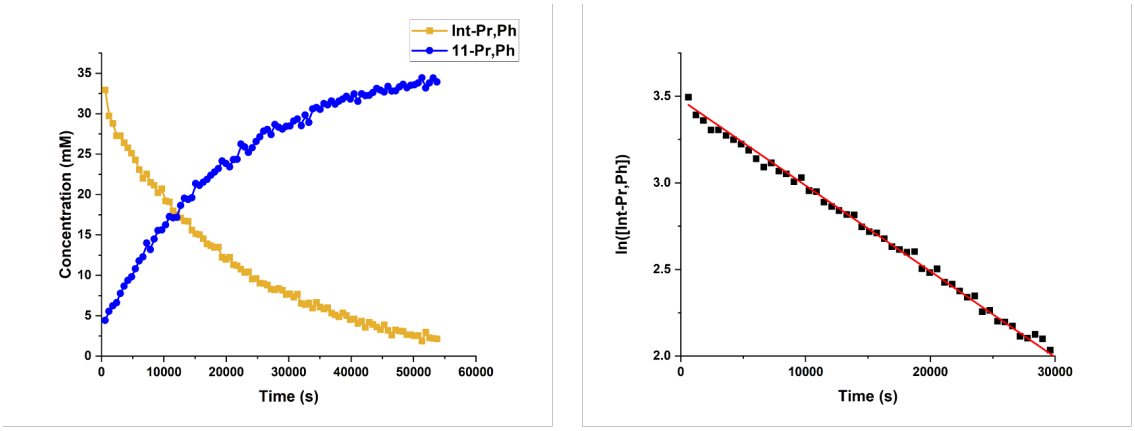


Figure 5.14. *Left: Plot of concentration against time showing the conversion of alkynyl species* ***Int-Pr,Ph*** *to trans alkene* ***11-Pr,Ph.*** *. Measured at 318 K in C_6D_6 for the reaction of* ***3-Cu*** *with 1 eq PhCC^{n}Pr.; Right: Linear plot of ln([**Int-Pr,Ph**]) against time for the same reaction.*

The conversion of this copper alkynyl aluminate into the *trans*-aluminylalkenyl copper complex **11-Pr,Ph** was studied more closely, by monitoring by ^{31}P NMR at 318 K (**Figure 5.14**). A plot of ln([**Int-Pr,Ph**]) against time results in a linear fit, indicating that **Int-Pr,Ph** converts simply to **11-Pr,Ph** in a process which is first-order with respect to [**Int-Pr,Ph**]. This is in keeping with the proposed mechanism in which **11-Pr,Ph** is formed from **Int-Pr,Ph** *via* a 1,2-metallate shift. The observation of this intermediate provides further evidence of the isomerisation/migration mechanism *via* a copper alkynyl aluminate.

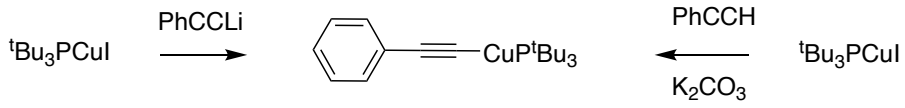
5.3.4 Migration of R group

From copper alkynyl aluminate **Int-Pr,Ph** it is theoretically possible to form either the *trans* alkene **11-Pr,Ph** or the migrated product **(NON)Al*n*Pr**. However, **11-Pr,Ph** is very stable in solution, and the possible migration product, **(NON)Al*n*Pr,** is not observed by ^{1}H NMR even after heating to 80°C for 24 hr. This is in contrast to what is seen with **11-Et**, formed by the insertion of EtCCEt into **3-Cu**, which undergoes migration of the ethyl group to form the aluminium alkyl **(NON)AlEt**. To understand this disparity, a number of alkyne substrates were investigated, with results shown in **Table 5.1**. A general trend is apparent from the substrates trialled, in that alkynes bearing alkyl substituents are more prone to migration than aryl substituents. However, the combination of both alkyne R groups is key: while **(NON)AlEt** can be isolated from the reaction of **3-Cu** with EtCCEt, it is not formed in the reaction with PhCCEt, which produces *trans*-aluminylalkenyl copper complex **11-Et,Ph** as the sole product after heating to 45°C for 18 h.

Table 5.1. *Alkyne substrates which undergo migration to* ***(NON)Al–R****; *Me migrates to give* ***(NON)AlMe****. Conditions: C_6D_6, 18h, 45 °C*

Migration	No migration
EtCCEt	PhCC^{n}Pr
MeCCMe	PhCCEt
^{n}PrCC^{n}Pr	PhCCPh
PhCCMe*	PhCCTMS

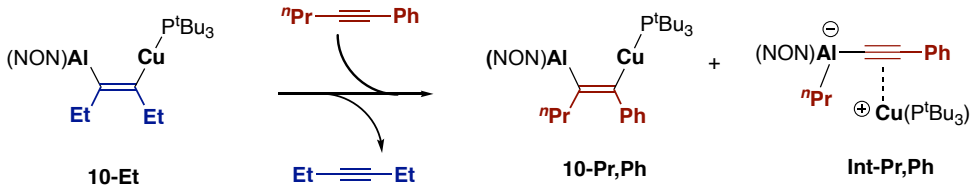
The end product may be rationalised by returning to the mechanism hypothesised in Section 5.3.2 (**Scheme 5.3**), in which both the *trans* dimetallated alkene and an aluminium alkyl can be formed from the same copper alkynyl aluminate intermediate. Computational insight may shed light on the relative energies of the two possible products, and the likelihood of their formation. Attempts were made to independently synthesise the expected copper containing product of the reaction of **3-Cu** with PhCCMe, copper acetylide **PhCCCuP^{t}Bu$_3$**. While most copper acetylides are polymeric and unstable, sterically hindered carbene ligands have been used to isolate a limited number of monomeric species.[38–40] Following two separate routes to **PhCCCuP^{t}Bu$_3$** led to two different products, as determined by ^{31}P NMR spectroscopy. Neither of these products was identified in the reaction mixture of **3-Cu** with PhCCMe. It is likely that the copper containing product is not stable and decomposes to products including P^{t}Bu$_3$.



Scheme 5.5. *Attempted synthesis of* ***PhCCCuP^{t}Bu$_3$*** *from ^{t}Bu$_3$PCuI.*

5.3.5 Mechanistic considerations

The formation of two regioisomers **10-Pr,Ph** and **10-Ph,Pr** which eventually give the *trans* alkene **11-Pr,Ph** suggests the possibility of reversible alkyne insertion as a way to convert between regioisomers. This reversibility could be demonstrated in practice by the addition of one equivalent of PhCC^{n}Pr to a C_6D_6 solution of **10-Et** (**Scheme 5.6**). *In situ* ^{31}P NMR spectroscopy shows the disappearance of the signal at 55.0 ppm associated with **10-Et** and growth of the signals associated with **10-Pr,Ph** (60.2 ppm) and **Int-Pr,Ph** (61.5 ppm), forming in the same ratio after 1 h as seen in the reaction of **3-Cu** itself with PhCC^{n}Pr. Consistent with this exchange, one equivalent of 3-hexyne can be seen in the ^{1}H NMR spectrum, showing that it has been released from **10-Et.**



Scheme 5.6. *Exchange of the inserted alkyne fragment in* ***10-Et***

To investigate the possibility of the copper aluminyl complex **3-Cu** reforming, **10-Et** was reacted with CO_2. It is known from the work in Chapter 4 that **3-Cu** reacts rapidly with CO_2 to give the carbonate complex **6-Cu**. However, exposure of a benzene solution of **10-Et** to CO_2 does not result in formation of the carbonate complex **6-Cu**, but rather, a new product forms, characterised by a broad resonance in the ^{31}P NMR spectrum at 73.7 ppm. The ^{1}H NMR spectrum features two quartets corresponding to ethyl CH_2 protons, and no free 3-hexyne, indicating that the EtCCEt fragment is still retained. Crystals grown from a toluene/hexane solution confirm the connectivity of the product, showing that CO_2 has inserted into the C–Cu bond of **3-Cu** to give a cyclic carbonate, **10-Et-CO$_2$** (**Figure 5.15**). Although the observation of this product does not

rule out the possibility of reformation of the Al–Cu bond, it implies that insertion of CO_2 into the Cu–C bond is much faster.

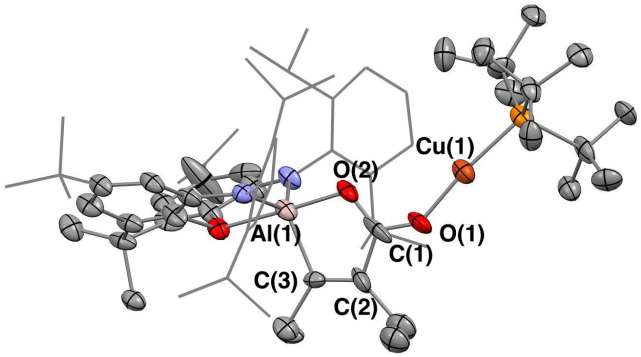


Figure 5.15. *Molecular structure of* ***10-Et-CO₂*** *in the solid state as determined by X-ray crystallography. Thermal ellipsoids set at the 15% probability level. Hydrogen atoms omitted and Dipp/^{t}Bu groups shown in wireframe for clarity. This structure is of very low quality due to the small size of the crystals. Therefore, no structural information aside from connectivity can be meaningfully derived from the data.*

5.3.6 Kinetic studies using diphenylacetylene

In order to study the mechanism of alkyne insertion and the isomerisation process, the alkyne diphenylacetylene was chosen for further studies. As a symmetrically substituted alkyne, only one regioisomer of the expected (aluminylalkenyl) copper product is possible, and it was also anticipated that the phenyl group should not be able to undergo migration, in contrast to what has been seen for EtCCEt. However, this substrate in fact revealed some interesting variation in chemical behaviour to what was seen for either EtCCEt or PhCC^{n}Pr.

The reaction of **3-Cu** with one equivalent of diphenylacetylene proceeds slowly at room temperature, forming a major and minor product characterised by resonances in the ^{31}P NMR spectrum at 62.1 and 58.6 ppm respectively. Upon heating for 18 h at 45°C, conversion to the product associated with the resonance at 58.6 ppm is complete. The ^{13}C NMR spectrum of this product features a doublet relating to an olefinic carbon at 194.0 ppm ($^2J_{CP}$ = 57 Hz), and corresponding Al–C signal at 162.6 ppm. Crystals grown from a hexane solution were analysed by X-ray diffraction and

confirm the identity of the product as **11-Ph**, in which the Al and Cu atoms are mutually *trans* (**Figure 5.16**).

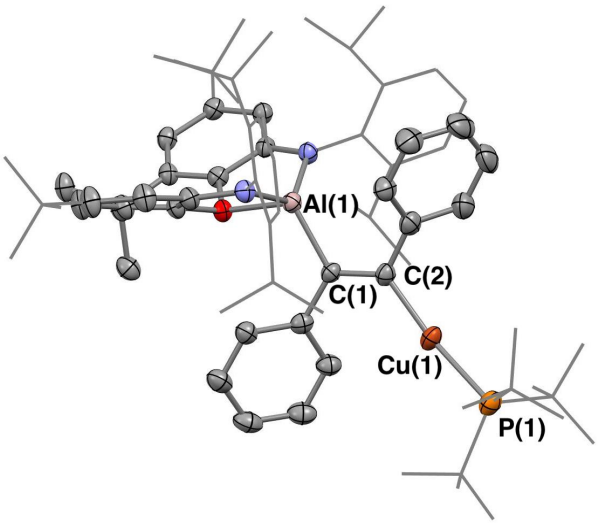


***Figure 5.16**. Molecular structure of **11-Ph** in the solid state as determined by X-ray crystallography. Thermal ellipsoids set at the 50% probability level. Hydrogen atoms omitted and Dipp/^{t}Bu groups shown in wireframe for clarity. Minor rotamer omitted. Key bond lengths (Å) and angles (°): Cu(1)–P(1) = 2.2026(11), C(1)–C(2) = 1.370(3), Cu(1)–C(2) = 1.924(3) Al(1)–C(1) = 1.9609(19), C(2)–Cu(1)–P(1) = 169.51(8), C(2)–C(1)–A(l)1 = 119.35(17), C(1)–C(2)–Cu(1) = 127.48(15).*

11-Ph crystallises as two rotamers (crystallographic occupancy 10:1), in which the Ph–C=C–Ph moieties are orthogonal to each other. Interestingly, this distribution of rotational isomers appears to be retained in solution, as the ^{31}P NMR spectrum for isolated crystals of **11-Ph** in C_6D_6 features two signals (58.6 and 57.5 ppm) which integrate to the same 10:1 ratio as found in the solid-state structure. A ^{13}C NMR spectrum taken at the midway point of the reaction of **3-Cu** and PhCCPh displays an additional set of the resonances characteristic of an aluminocuprated alkene: a doublet at 185.4 ppm ($^2J_{CP}$ = 72 Hz), and an Al–C resonance at 159.7 ppm. These resonances are assigned to the *syn* addition product **10-Ph**, the major initial product of the reaction.

A temporal plot of the reaction (**Figure 5.17**) shows the two processes at work: initial insertion of PhCCPh giving rise to *syn* **10-Ph** and *anti* **11-Ph**, and isomerisation to give

solely **11-Ph**. The *syn* product forms fastest and rises to a maximum before giving way to the trans product. Unlike the reaction of **3-Cu** with PhCC^{n}Pr, no π-bound intermediate species is observed.

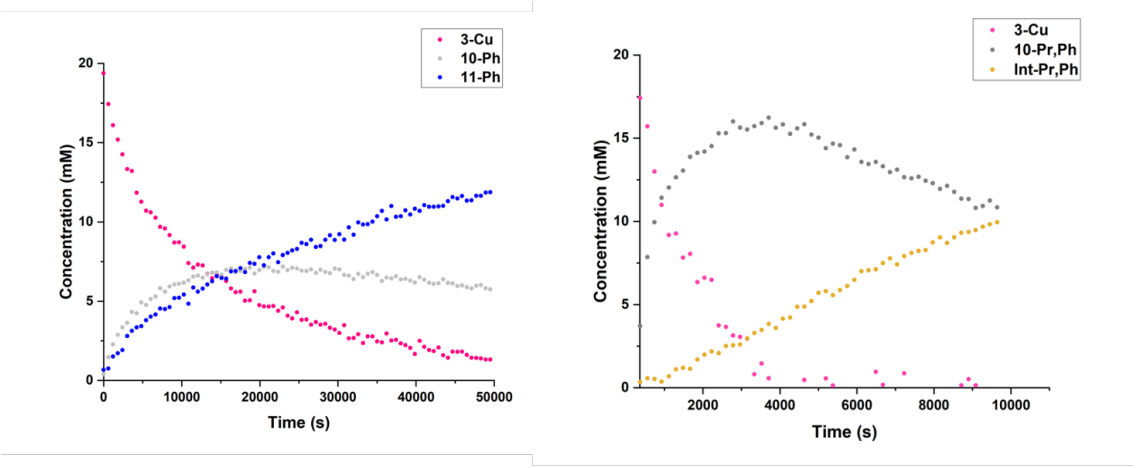


Figure 5.17. *Left: Temporal profile for the reaction of* ***3-Cu*** *with PhCCPh. Conditions: C_6D_6, 45 °C, 1 eq PhCCPh; Right: Temporal profile for the reaction of* ***3-Cu*** *with PhCC^{n}Pr. Conditions: C_6D_6, 10 °C, 1 eq PhCC^{n}Pr.*

There are two possible pathways by which a *trans* alkene geometry may be obtained: A) concerted *syn* addition of Al–Cu across the C–C triple bond followed by isomerisation to the *trans* alkene; B) Stepwise *anti* addition of [Al] and [Cu] across the C–C triple bond (**Figure 5.18**). In the report of alkyne insertion into an Au–B bond by Yamashita and coworkers, little consideration is given to this process, which is purported to occur *via* 1,2-addition to form the *(cis-)*borylalkenyl gold species. For the gold-silyl system reported by Bourissou, which was found to produce exclusively *syn* β-silyl alkenyl gold complexes, the mechanism of the insertion of the alkyne into the Au–Si bond was studied experimentally and computationally. Kinetic studies found that the insertion is first order with respect to both the gold-silyl species and the alkyne. The entropy of activation was determined experimentally and found to be large and negative, in agreement with an associative mechanism. DFT studies found that a 1,2-

addition pathway was unlikely, but rather a two step coordination-insertion mechanism was preferred.

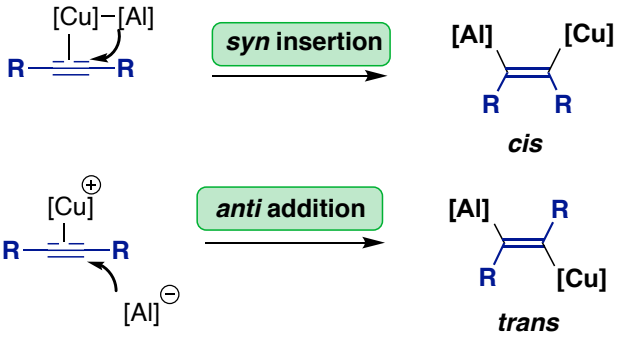


Figure 5.18. *Possible mechanisms for the formation of aluminylalkenyl copper complexes* via *inner sphere and outer sphere mechanisms.*

From the facile isolation of *cis*-alkenylaluminyl copper compound **10-Et** and the observation that *cis* isomer **10-Pr,Ph** initially forms completely from **3-Cu** before any trans isomer is seen (**Figure 5.13**), it is likely that stepwise process (A) is occurring for these substrates. For these alkynes, no *trans* isomer is seen at short reaction times. However, with diphenylacetylene as the substrate, different behaviour is observed, as the temporal plot shows that **10-Ph** and **11-Ph** form *concurrently*, albeit with the rate of formation of **10-Ph** (k_{cis}) being roughly double that of the rate of formation of **11-Ph** (k_{trans}). This allows for the possibility that **11-Ph** is formed directly from **3-Cu** by *anti* addition, rather than going through the *syn* product **10-Ph**. Indeed, if **11-Ph** could only be formed from **10-Ph**, we would expect its rate of formation to be fastest when the concentration of **10-Ph** in solution is highest. Examination of the shape of the curve in **Figure 5.17** shows this is not the case. An interesting point of comparison to illustrate the possibility of direct *anti* addition is the semi-hydrogenation of alkynes by bimetallic species in the presence of H_2, which has attracted interest recently due to a number of reports of catalysts producing good selectivity for (*E*)-alkenes.[32,41,42] The

mechanism for many of these systems is very similar, involving bimetallic activation of H_2 resulting in initial *syn* reduction to the *(Z)*-alkene, followed by a second process whereby the (*Z*)-alkene isomerises to an (*E*)-alkene. The isomerisation proceeds through an sp^3 hybridised carbon, allowing free rotation. This process is a case of tandem catalysis: the *E*-alkene cannot be formed directly, only by proceeding through the *Z*-alkene. This is clear from the temporal profiles reported by Lu and co-workers for their series of rare-earth supported nickel catalysts **NiML$_3$** (L = $[^{i}Pr_2PCH_2NPh]^-$, M = Sc, Y, La, Lu or Ga) (**Figure 5.19**). In plots of concentration against time for the semihydrogenation of PhCCPh by **NiML$_3$**, the rate of formation of *E*-stillbene is at a maximum (steeper slope) when the concentration of *Z*-stillbene is at its highest.

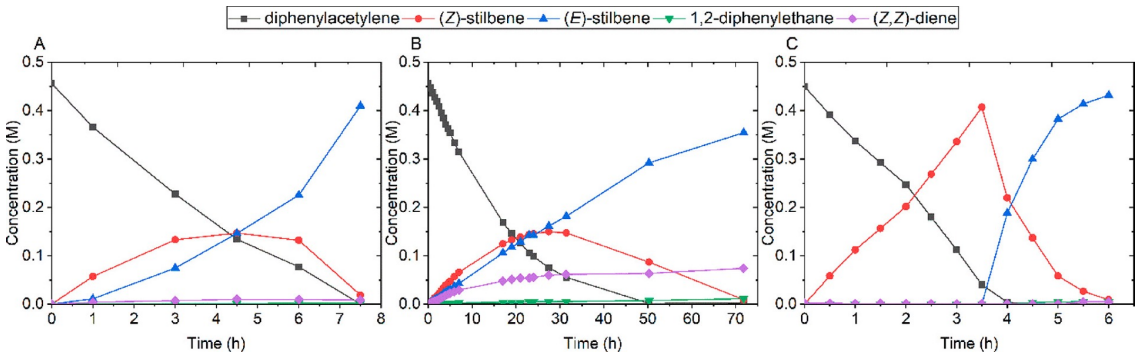


Figure 5.19. *Reaction time course for the semihydrogenation of diphenylacetylene to (E)-stilbene for catalysts: A) Ni–Ga, B) Ni–Sc, and C) Ni–Y, as reported by the Lu group. Reprinted with permission from J. Am. Chem. Soc. 2020, 142, 11, 5396–5407. Copyright 2020 American Chemical Society*

This behaviour contrasts with the plot shown in **Figure 5.17**, in which the formation of *trans* isomer **11-Ph** is faster at shorter reaction times then slows down, implying direct formation from **3-Cu**, as well as the later isomerisation from **10-Ph**. Mechanistically, this requires either the Al–Cu bond of **3-Cu** to dissociate in solution, or for more than one molecule of **3-Cu** to be involved in the *anti* addition. To further investigate the mechanism, kinetic data were obtained using the initial rates method, by varying the concentrations of **3-Cu** and PhCCPh. It was found that the insertion reaction is first

order in [alkyne], as a plot of rate against [PhCCPh] can be fitted linearly through the origin (**Figure 5.20**). Likewise, varying the concentration of starting material **3-Cu** also results in a linear plot, indicating that the reaction is first order in **3-Cu**.

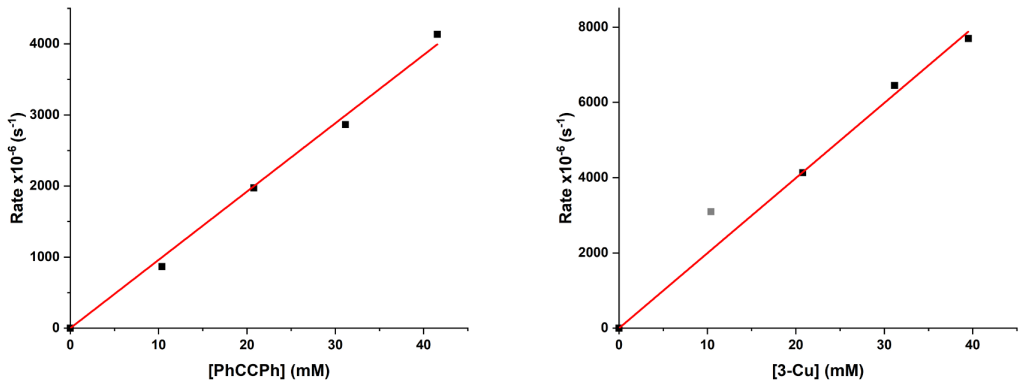


Figure 5.20. *Plot of Rate v [PhCCPh] (left) and Rate v [**3-Cu**] (right) for the reaction of **3-Cu** with PhCCPh. In this plot, the value for 11.4 mM is shown but has been treated as an outlier. This measurement involved weighing out a very small quantity and therefore carries a high uncertainty.*

From this we ascertain that there is one molecule of PhCCPh involved in the rate determining step, and also one molecule of **3-Cu** such that the rate law is:

$$\text{rate} = k[\textbf{3-Cu}][\text{PhCCPh}]$$

This is consistent with either *syn* or *anti* addition. While some information can be gleaned from this kinetic data, it is best used in combination with theoretical studies of the reaction mechanism. This will allow for possible mechanisms to be fitted with the kinetic data and give a full picture of this interesting reactivity. Quantum chemical studies with our collaborators are ongoing. The results may provide insight into why diphenylacetylene behaves so differently to either 3-hexyne or 1-phenyl-pentyne. At this stage, it can be postulated that the phenyl group may be crucial to this differing reactivity. As discussed in Section 5.3.4, alkynes bearing phenyl groups tend not to lead to aluminium products of the form **(NON)Al-R**, due to the reduced affinity of the Ph group to undergo migration. As migration of one R group is a key step in the

proposed mechanism for the *cis/trans* isomerisation *via* alkynyl species **Int-Et** or **Int-Pr,Ph** (**Scheme 5.3**, **Scheme 5.4**), it may be the case that this pathway is not possible for PhCCPh. Instead, isomerisation could occur by loss of PhCCPh from **10-Ph** and *anti* addition to form **11-Ph**. This is supported by the fact that while **Int-Pr,Ph** could be observed by multinuclear NMR, no intermediates can be seen in the conversion of **10-Ph** to **11-Ph**. Again, computational studies of the mechanism will prove very useful in examining this hypothesis.

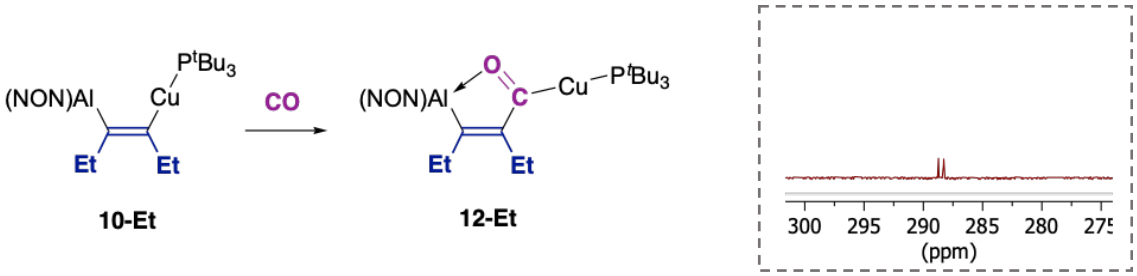
Having studied the formation of a number of alkenylaluminylcopper species from **3-Cu**, their functionalisation was then investigated.

5.3.7 Functionalisation

The presence of two different metals attached to an alkene core presents a unique opportunity for onward functionalisation, with the potential for differential reactivity at the Al–C and Cu–C bonds. These two M–C bonds are quite different in nature (with Al typically 'harder' than Cu) and it may be possible for the molecule to act as bifunctional nucleophile. While functionalisation at the gold site was explored previously for the gold silyl system of Bourissou and Amgoune (**Figure 5.3**), we sought to target reactions which may involve both metal centres in different roles. Carbon monoxide was initially chosen to explore onward reactivity, primarily because of the precedent for the constrasting affinity of CO for Al and Cu. While Cu can weakly coordinate CO, no aluminium carbonyl species are known.[43] Therefore, preferential binding of CO at copper may direct the reactivity.

Exposure of a hexane solution of **10-Et** to CO (1 atm) resulted in a rapid colour change from colourless to bright yellow. An *in situ* ^{31}P NMR spectrum shows formation of a single product, as evidenced by a lone resonance at 60.3 ppm. The ^{1}H NMR spectrum

shows two new quartets corresponding to ethyl CH_2 protons at 2.72 and 2.77 ppm, but now with no coupling to ^{31}P, indicating that the product no longer has an ethyl group *geminal* to the [CuP^tBu_3] moiety.



Scheme 5.7. *Left: Insertion of CO into the C–Cu bond of* ***10-Et****; Right: excerpt from the ^{13}C NMR spectrum of* ***12-Et*** *showing the doublet corresponding to the acyl carbon.*

Crystals suitable for X-ray diffraction could be obtained by concentration of the hexane reaction mixture, allowing the structure to be determined (**Figure 5.21**). The structure confirms the selective insertion of CO into the Cu–C bond, rather than the Al–C bond, forming a 5 membered AlCCCO metallocycle, with a pendant CuP^tBu_3 group. The C=O bond length in **12-Et** (1.279(2) Å) is in the range of typical organic carbonyl groups and the central ring is essentially planar. Examining the acyl functionality spectroscopically, ^{13}C NMR reveals that the [CuP^tBu_3] bound C=O carbon gives rise to a very low-field shifted doublet at 288.9 ppm, ($^2J_{CP}$ = 66 Hz) (**Scheme 5.7**). This is a particularly high chemical shift value amongst metal acyl complexes; for example, iridium acyl species typically give rise to chemical shifts in the range 200-230 ppm.[44,45] This comparatively high chemical shift is presumably caused by coordination of the O atom to the Lewis acidic Al centre, which has a deshielding effect on the carbonyl. This effect is replicated in the FT-IR spectrum of **12-Et**, in which the carbonyl stretching vibration is found at 1539 cm^{-1}, i.e. lower than typical C=O stretches. The frequency of the stretching mode is also lowered by conjugation with the C=C bond. The IR

frequencies were calculated by Agamemnon Crumpton of the Aldridge group and found to be in good agreement with the experimentally obtained spectrum (1556 cm^{-1} for C=O stretching frequency).

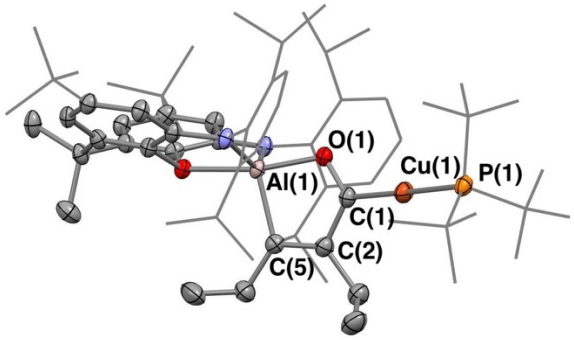


Figure 5.21. *Molecular structure of* ***12-Et*** *in the solid state as determined by X-ray crystallography. Thermal ellipsoids set at the 50% probability level. Hydrogen atoms omitted and Dipp/^{t}Bu groups shown in wireframe for clarity. Key bond lengths (Å) and angles (°): (Cu(1)–C(2) 1.9255(16), Al(1)–O(1) 1.8843(12), Al(1)–C(5) 2.0027(17), O(1)–C(1) 1.279(2), C(5)–C(2) 1.362(2).*

Compound **12-Et** is the first isolable example of a copper acyl species. Group 9 acyl complexes are well known for their role in industrially important hydroformylation reactions.[46,47] For example, the Cativa process (**Figure 5.22**) for the carbonylation of methanol features the insertion of CO into an Ir–CH_3 bond to give an iridium acyl complex. Moreover, acyl ligands can be found in the active site of mononuclear [Fe]-hydrogenase enzymes and structural mimics have sought to replicate and understand the importance of this ligand environment (**Figure 5.22**).

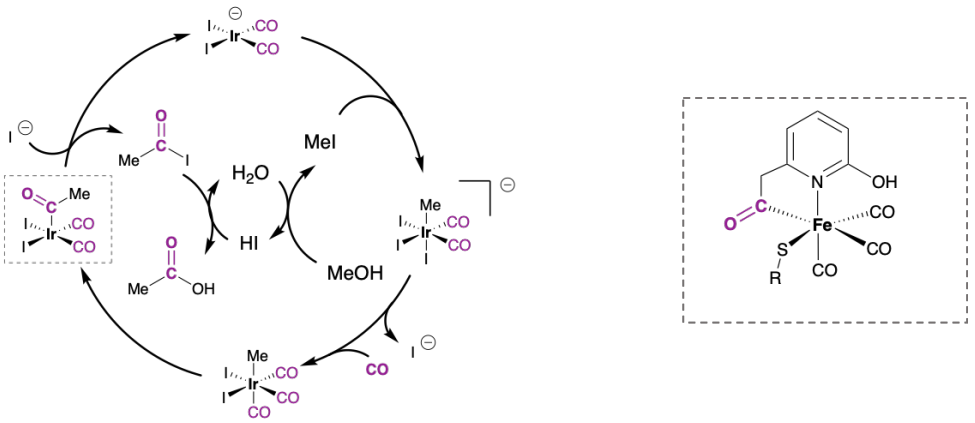
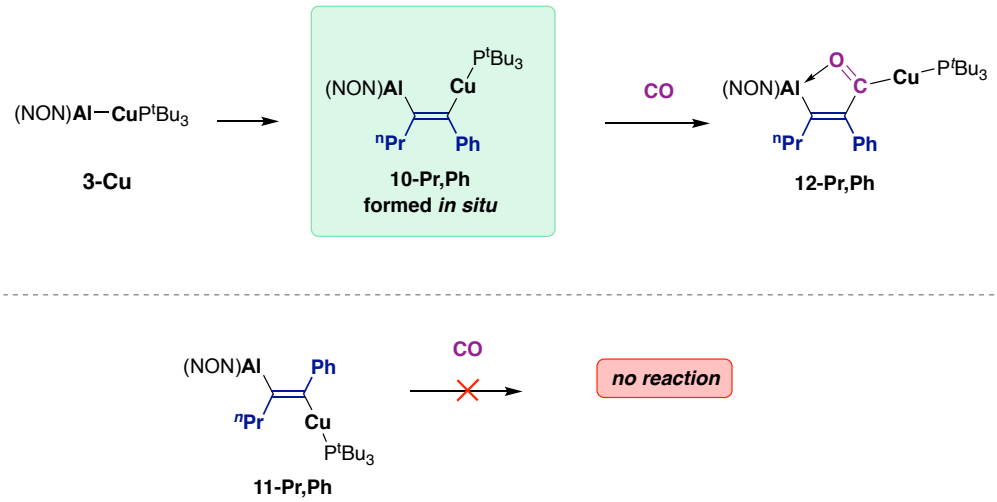


Figure 5.22*. Left: The Cativa process for the carbonylation of methanol, featuring an iridium acyl; Right: A structural mimic of an [Fe]-hydrogenase active site, bearing an acyl ligand (Hu, 2014)*

Although they have also been proposed as intermediates in catalytic reactions such as borocarbonylation and amidation,[48–50] no isolated copper acyl complexes have been reported prior to this work, likely due to their propensity to undergo rearrangement. Although cobalt catalysts have also been developed, industrial hydroformylation relies heavily on rhodium and iridium, which are expensive. Only one example of hydroformylation using a more abundant and inexpensive copper complex has been very recently reported, featuring a copper acyl as part of the proposed catalytic cycle for this reaction.[51] Therefore it is of great value to isolate and characterise these industrially relevant intermediates.



Scheme 5.8. *Trapping of* ***10-Pr,Ph*** *by reaction with CO, a reaction not possible for anti isomer* ***11-Pr,Ph***

The CO reactivity also provides insight into the reaction of **3-Cu** with PhCC^{n}Pr. It can also be used to 'trap' the *syn* isomer **10-Pr,Ph** which was formed rapidly in the reaction of **3-Cu** with PhCC^{n}Pr but could not be isolated cleanly due to onward isomerisation. A solution of **10-Pr,Ph**, prepared *in situ,* was frozen, and CO added to the headspace (**Scheme 5.8**). The reaction was allowed to thaw under a CO atmosphere, producing a yellow solution. The ^{1}H NMR spectrum of the product closely resembles that of both

the structurally characterised *anti* alkene **11-Pr,Ph** and the initially formed formed *syn* species **10-Pr,Ph**, featuring the same *n*-propyl CH_2 resonance with second-order coupling. The ^{13}C NMR spectrum again reveals the presence of an acyl carbon, evidenced by a doublet at 287.4 ppm ($^2J_{CP}$ = 65 Hz). Crystals of this product, **12-Pr,Ph** could be grown from a hexane solution and allowed the solid state structure to be determined by X-ray crystallography (**Figure 5.23**). This shows that CO has again selectively inserted into the Cu–C bond of **10-Pr,Ph** to form an AlCCCO heterocycle. Importantly, the structure confirms the alkyne insertion regiochemistry implied by the NMR evidence i.e. the product initially formed in the reaction of **3-Cu** with PhC^{n}Pr features an *n*-propyl group *geminal* to aluminium.

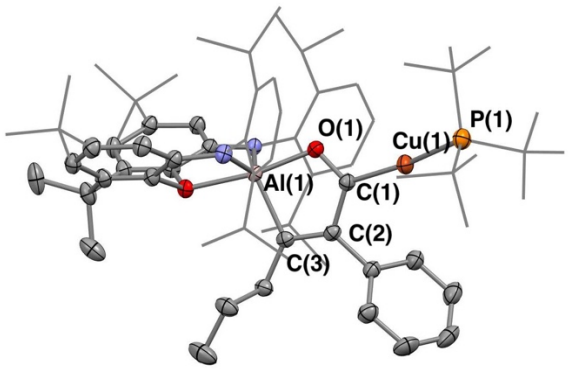


Figure 5.23. *Molecular structure of* ***12-Pr,Ph*** *in the solid state as determined by X-ray crystallography. Thermal ellipsoids set at the 50% probability level. Hydrogen atoms omitted and Dipp/^{t}Bu groups shown in wireframe for clarity. Key bond lengths (Å) and angles (°): C(3)–C(2) 1.3597(19), O(1)–C(1) 1.2763(16), C(1)–C(2) 1.4908(18), Al(1)–O(1) 1.8806(10).*

Aside from the selectivity for Cu–C bonds, a further important aspect of the reactivity of the (aluminylalkenyl)copper complexes towards CO is that the reaction does not proceed when the aluminium and copper are *trans* to each other i.e. no reaction is observed when **11-Pr,Ph** is exposed to CO (**Scheme 5.8**). This indicates that the proximal aluminium is necessary for the insertion to occur and the copper acyl may

only be formed through the co-operative reactivity of both aluminium and copper. Presumably, a short-lived copper carbonyl intermediate would be activated towards migration of the alkenyl fragment by the Lewis acidic O, and this co-operative behaviour is critical to the formation of the copper acyl species. It is also worth noting that copper aluminyl complex **3-Cu** does not itself react with CO, showing the difference in reactivity between directly bonded Al–Cu species and those in which Al and Cu are proximal.

The metallocycle **12-Et** could be simply hydrolysed by addition of water, leading to the clean formation of the aldehyde (*E*)-2-ethylpent-2-enal, which was identified by ^{1}H NMR spectroscopy and mass spectrometry (**Figure 5.24**). This represents the overall hydroformylation of an alkyne, enabled by bimetallic copper aluminyl complex.

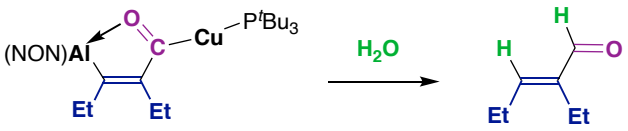


Figure 5.24. *Hydrolysis of cyclic acyl species* ***12-Et*** *to form an aldehyde*

5.4 Conclusions and future work

The reactivity of the coinage metal aluminyl complexes **3-Cu**, **3-Ag** and **3-Au** towards alkynes was found to vary according to the nature of the metal and also the alkyne substrate. All three complexes were reactive towards the terminal alkyne phenylacetylene, and in the case of silver, the bimetallic bridged μ-acetylide complex **9-Ag** could be isolated. This complex arises from deprotonation of the acidic terminal proton of two molecules of PhCCH, and in turn leads to formation of styrene, a product of the reduction of phenylacetylene.

Significant differences between the reactivity of the coinage metal complexes were apparent upon investigating their behaviour towards internal alkynes, which do not have an acidic proton. While **3-Ag** and **3-Au** were unreactive towards internal alkynes, **3-Cu** reacts rapidly with 3-hexyne, adding across the CC triple bond to produce the *cis*-(aluminylalkenyl)copper complex **10-Et**. This is the first example of the direct insertion of an alkyne into an M–M' bond. The *cis* dimetallated alkene subsequently isomerises to the corresponding *trans* isomer **11-Et** in a process proposed to occur *via* an alkynylcopper aluminate intermediate. After a longer reaction time, the aluminium alkyl species **(NON)AlEt** was isolated, which may also be formed by a 1,2-metalate shift from the copper alkynyl aluminate species.

The regioselectivity of the insertion process was investigated using the unsymmetrically substituted alkyne 1-phenyl-butyne (PhCC^{n}Pr), which was found to selectively form a single regioisomer of the *cis*-(aluminylalkenyl)copper complex, **10-Pr,Ph** as the kinetic product. Isomerisation was again observed, this time leading to isolation of *trans*-(aluminylalkenyl)copper **11-Pr,Ph** as the thermodynamic product. In this case, the alkynylcopper aluminate intermediate **Int-Pr,Ph** is stable enough to be observed by NMR, and can be shown to convert to **11-Pr,Ph** by a process which is first-order in [**Int-Pr,Ph**], providing evidence of the proposed isomerisation mechanism. Expanding the alkyne substrate scope to diphenylacetylene revealed an interesting variance in mechanism. For this substrate, it appears likely that both *syn* and *anti* addition can occur, giving *cis* and *trans*-(aluminylalkenyl)copper complexes **10-Ph** and **11-Ph** together. This mechanism was investigated through kinetics studies, which will inform ongoing computational work.

Functionalisation of the (aluminylalkenyl)copper complexes was explored, and it was found that cooperative reactivity between the Al and Cu metal sites could be exploited

for this purpose. Insertion of CO into the Cu–C bond of the *cis* (aluminylalkenyl)copper complexes can be achieved, leading to the first isolated examples of copper acyl species, **12-Et** and **12-Pr,Ph**. Interestingly, no reaction occurs when the Al and the Cu fragments are *anti* to each other, as in **11-Pr,Ph**, demonstrating the importance of cooperation between the proximal metal centres, which is only possible in this geometry. The CO insertion also allowed the regiochemistry of the kinetic *syn* product of the reaction of **3-Cu** and PhCC^{n}Pr to be confirmed as featuring the *n*-propyl group *geminal* to the [(NON)Al] fragment. The cyclic acylcopper species could be cleanly hydrolysed to give an aldehyde, representing overall hydroformylation of the starting alkyne.

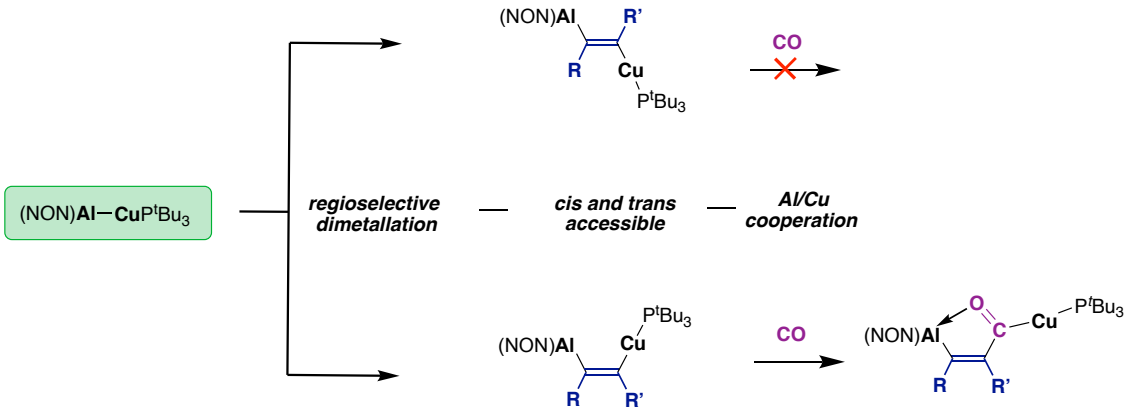


Figure 5.25. *Summary of the reactivity of **3-Cu** towards internal alkynes and onward functionalisation to give the first copper acyl.*

This hydrolysis is a simple proof-of-concept reaction, and the further utility of the species is yet to be fully investigated. While hydrolysis is a rather blunt instrument, milder approaches may allow for preservation of the metal-ligand environment, with the potential for catalysis. If reformation of the Al–Cu bond could be achieved, this would be feasible. The demonstration of the reversibility of the alkyne insertion, whereby 3-hexyne could be substituted for 1-phenylbutyne, also suggests an exciting

possibility for catalytic reactivity, a prospect which certainly warrants further study. While experimental methods gave insight into the mechanism of the reaction and the isomerisation process, there is a clear need for theoretical study to shed light on the complexity of the system. DFT calculations to this end are ongoing.

The extent of the differential reactivity of the dimetallated alkenes is yet to be explored. Reactions with dielectrophiles such as α,β-unsaturated carbonyl compounds may lead to cyclic products, with the Al–C and Cu–C bonds reacting at the C=O and C=C sites respectively. The ability to 'desymmetrize' heterosubstituted alkynes could also be useful for reactions such as selective deuteration. Cross coupling *via* the copper centre and transmetallation at Al are just two further examples of reactions that might exploit the contrasting reactivity of the two metal sites in the (aluminylalkenyl)copper complexes.

As with the work in Chapter 3 on the insertion of CO_2 into Al–M bonds, it is likely that the ancillary ligand bound to M, as well as the aluminyl fragment ligand, may influence the reaction greatly. Certainly, even within the systems studied in this work, there appears to be a close balance of energetics involved in determining whether *trans*-(aluminylalkenyl)copper complexes or alkyl aluminium species are formed. Exploring the reactivity of other Al–M species bearing (for example) carbene ligands may alter both the regio- and stereochemistry of the reaction. More generally, the ability to access both *cis* and *trans* dimetallated alkenes through direct insertion into an M–M' bond sets a precedent as a method to obtain these highly functionalised and synthetically useful molecules. This will surely prompt further research as the field of heterobimetallic chemistry continues to grow.

5.5 Synthetic procedures and spectroscopic data for new compounds

Synthesis of (NON)Al(μ-(CCPh)$_2$AgP^{t}Bu$_3$ (**9-Ag**)

To a suspension of **3-Ag** (70 mg, 0.069 mmol) in toluene (3 mL) was added phenylacetylene (7 mg, 0.347 mmol). The resulting solution was stirred at room temperature for 2 h, after which time the volatiles were removed *in vacuo*. The residue was dissolved in diethyl ether (2 mL) and colourless crystals formed rapidly at room temperature (50 mg, 81%).

^{1}H NMR (400 MHz, C_6D_6, 298 K): δ_H = 0.76 (d, $^3J_{HP}$ = 12.2 Hz, 27H, PC(C*H*$_3$)$_3$), 1.20 (d, $^3J_{HH}$ = 7.6 Hz, 12H, CH(C*H*$_3$)$_2$), 1.37 (s, 18H, C(C*H*$_3$)$_3$), 1.43 (d, $^3J_{HH}$ = 6.8 Hz, 6H, CH(C*H*$_3$)$_2$), 1.75 (d, $^3J_{HH}$ = 7.4 Hz, 6H, CH(C*H*$_3$)$_2$), 1.57 (s, 3H, C(C*H*$_3$)$_2$), 1.68 (s, 3H, C(C*H*$_3$)$_2$), 4.01 (sept, $^3J_{HH}$ = 6.9 Hz, 2H, C*H*(CH$_3$)$_2$), 4.43 (sept, $^3J_{HH}$ = 6.9 Hz, 2H, C*H*(CH$_3$)$_2$), 6.35 (d, $^4J_{HH}$ = 1.9 Hz, 2H, XA-*o*-C*H*), 6.69 (d, $^4J_{HH}$ = 1.9 Hz , 2H, XA-*p*-C*H*), 7.01-38 (m, 16H Ar*H*).

^{13}C{^{1}H} NMR (126 MHz, C_6D_6, 298 K): No ^{13}C NMR data could be obtained due to difficulty in isolating sufficient quantities of clean material.

^{31}P{^{1}H} NMR (162 MHz, C_6D_6, 298 K): 80.1 (dd, $^1J_{P\text{-}107Ag}$ = 560 Hz, $^1J_{P\text{-}109Ag}$ = 647 Hz).

Synthesis of *cis*-3-[(NON)Al]-4-[CuP^{t}Bu$_3$]-hex-3-ene (**10-Et**)

To a stirred suspension of **3-Cu** (100 mg, 0.103 mmol) in toluene (3 mL) was added 3-hexyne (18 µL, 0.154 mmol). The resulting colourless solution was stirred for 30 min and then concentrated to 2 mL. Colourless crystals suitable for X-ray diffraction could be obtained from slow cooling of this solution to 4°C (78 mg, 72%).

^{1}H NMR (400 MHz, C_6D_6, 298 K): δ_H = 0.90 (d, $^3J_{HP}$ = 12.8 Hz, 27H, PC(C*H*$_3$)$_3$), 1.07 (d, $^3J_{HH}$ = 7.6 Hz, 6H, CH(C*H*$_3$)$_2$), 1.25 (s, 18H, C(C*H*$_3$)$_3$), 1.28 (d, $^3J_{HH}$ = 6.8 Hz, 6H,

CH(CH_3)$_2$), 1.43 (t, $^3J_{HH}$ = 7.8 Hz, 3H, CH$_2$CH_3), 1.48 (t, $^3J_{HH}$ = 7.8 Hz, 3H, CH$_2$CH_3), 1.60 (d, $^3J_{HH}$ = 6.5 Hz, 12H, CH(CH_3)$_2$)1.71 (s, 6H, C(CH_3)$_2$), 2.86 (qd, $^3J_{HH}$ = 7.5 Hz, $^3J_{HP}$ = 3.0 Hz, 2H, CH_2CH$_3$), 2.92 (q, $^3J_{HH}$ = 7.6 Hz, 2H, CH_2CH$_3$), 3.51 (sept, $^3J_{HH}$ = 6.9 Hz, 2H, CH(CH$_3$)$_2$), 4.35 (sept, $^3J_{HH}$ = 6.9 Hz, 2H, CH(CH$_3$)$_2$), 6.07 (d, $^4J_{HH}$ = 1.9 Hz, 2H, XA-*o*-CH), 6.72 (d, $^4J_{HH}$ = 1.9 Hz , 2H, XA-*p*-CH), 7.01-38 (m, 6H ArH).

^{13}C{^{1}H} NMR (126 MHz, C_6D_6, 298 K): δ_C = 15.5, 16.8, (CH$_2$*C*H$_3$), 25.9, 26.4 (*CH*(CH3)2), 27.3 (d, $^3J_{CP}$ = 7.0 Hz , *C*H$_2$CH$_3$), 29.1 (*C*H$_2$CH$_3$), 31.8 (C(*C*H3)3), 28.2, 29.2 (CH(*C*H$_3$)$_2$), 32.1 (d, $^2J_{CP}$ = 6.0 Hz, P{C(*C*H$_3$)$_3$}$_3$), 35.1 (*C*(CH$_3$)$_3$), 36.0 (d, $^1J_{CP}$ = 6.0 Hz, P{*C*(CH$_3$)$_3$}$_3$), 37.9 (*C*(CH$_3$)$_2$), 106.6, 111.8, 123.8, 126.2, 133.6, 141.0, 142.8, 144.7, 146.9, 148.3, 149.3 (Ar*C*), 154.1 (C=*C*-Al), 188.3 (d, $^2J_{CP}$ = 73 Hz, C=*C*-Cu).

^{31}P{^{1}H} NMR (162 MHz, C_6D_6, 298 K): δ_P = 55.5.

$C_{65}H_{99}AlCuN_2OP$ requires: C, 74.64%; H, 9.54%; N, 2.68%; found: C, 74.55%; H, 9.38%; N, 2.47%.

Synthesis of (NON)AlEt

A solution of **10-Et** (60 mg, 0.057 mmol) in benzene (2 mL) was stirred at room temperature for 48 h, during which time a metallic precipitate formed. The solution was filtered and the volatiles removed *in vacuo*. The residue was taken up in hexane (1 mL), from which colourless crystals suitable for X-ray diffraction were obtained (35 mg, 84%).

^{1}H NMR (400 MHz, C_6D_6, 298 K): δ = 0.40 (q, $^3J_{HH}$ = 8.4 Hz, 2H, CH_2CH$_3$), 0.87 (t, $^3J_{HH}$ = 7.8 Hz, 3H, CH$_2$CH_3), 1.12 (d, $^3J_{HH}$ = 7.2 Hz, 12H, ArCH(CH_3)$_2$), 1.18 (s, 18H, C(CH_3)$_3$), 1.30 (d, $^3J_{HH}$ = 7.4 Hz, 12H, ArCH(CH_3)$_2$), 1.58 (s, 6H, C(CH_3)$_2$), 3.57 (sept., $^3J_{HH}$ = 6.6 Hz, 4H, ArCH(CH$_3$)$_2$), 6.35 (d, $^4J_{HH}$ = 1.9 Hz, 2H, XA-*o*-CH), 6.75 (d, $^4J_{HH}$ = 1.9 Hz , 2H, XA-*p*-CH), 7.20-27 (m, 6H ArH).

$^{13}C\{^1H\}$ NMR (101 MHz, C_6D_6): δ = -1.27 (CH_2CH_3), 8.80 (CH_2CH_3), 23.0, 25.9 ($CH(CH_3)_2$), 27.1 (XA-$C(CH_3)_2$), 29.1 ($CH(CH_3)_2$), 31.7 ($C(CH_3)_3$), 35.0 ($C(CH_3)_3$), 37.6 (XA-$C(CH_3)_2$), 107.8, 111.5, 124.5, 125.3, 126.7, 134.0, 141.0, 142.0, 143.7, 147.0, 149.3 (Ar-*C*).

***In situ* synthesis of *cis*-4-[(NON)Al]-5-[CuP^{t}Bu$_3$]-5-phenyl-pent-3-ene (10-Pr,Ph)**

To a suspension of **3-Cu** (20 mg, 0.023 mmol) in C_6D_6 was added 1-phenyl-pentyne (3.0 µL, 0.023 mmol). This compound was not isolated due to a facile onward reaction.

^1H NMR (400 MHz, C_6D_6, 298 K): δ_H = 0.82 (d, $^3J_{HP}$ = 12.0 Hz, 27H, $PC(CH_3)_3$), 1.07 (d, $^3J_{HH}$ = 6.9 Hz, 6H, $CH(CH_3)_2$), 1.22 (s, 18H, $C(CH_3)_3$), 1.29 (overlap) (t, $^3J_{HH}$ = 7.0 Hz , 3H, $CH_2CH_2CH_3$), 1.29 (d, $^3J_{HH}$ = 7.0 Hz, 12H, $CH(CH_3)_2$), 1.61 (d, $^3J_{HH}$ = 6.9 Hz, 6H, $CH(CH_3)_2$), 1.67 (s, 3H, $C(CH_3)_2$), 1.74 (s, 3H, $C(CH_3)_2$), 1.95 (m, 2H, $CH_2CH_2CH_3$), 2.74 (m, 2H, $CH_2CH_2CH_3$), 3.55 (sept, $^3J_{HH}$ = 7.2 Hz, 2H, $CH(CH_3)_2$), 4.21 (sept, $^3J_{HH}$ = 7.0 Hz, 2H, $CH(CH_3)_2$), 6.16 (d, $^4J_{HH}$ = 1.9 Hz, 2H, XA-*o*-C*H*), 6.76 (d, $^4J_{HH}$ = 1.9 Hz , 2H, XA-*p*-C*H*), 6.94 (m, 2H ArH), 7.18-7.40 (m, 9H ArH).

$^{31}P\{^1H\}$ NMR (162 MHz, C_6D_6, 298 K): δ_P = 60.2.

Synthesis of *trans*-4-[(NON)Al]-5-[CuP^{t}Bu$_3$]-5-phenyl-pent-3-ene (11-Pr,Ph)

1-phenyl-pentyne (20 µl, 0.123 mmol) was added to a stirred suspension of **3-Cu** (100 mg, 0.103 mmol) in benzene (4 mL). The reaction mixture was stirred at 45°C for 18 h. The resulting solution was lyophilized twice from benzene to give an off-white solid. Colourless crystals were obtained by cooling a hexane solution to -30°C (64 mg, 56%).

^1H NMR (400 MHz, C_6D_6, 298 K): δ_H = 1.03 (d, $^3J_{HH}$ = 6.9 Hz, 6H, $CH(CH_3)_2$), 1.09 (d, $^3J_{HP}$ = 12.2 Hz, 27H, $PC(CH_3)_3$), 1.23 (s, 18H, $C(CH_3)_3$), 1.29 (overlap) (t, $^3J_{HH}$ = 7.0 Hz , 3H, $CH_2CH_2CH_3$), 1.29 (d, $^3J_{HH}$ = 7.0 Hz, 6H, $CH(CH_3)_2$), 1.34 (d, $^3J_{HH}$ = 6.9 Hz,

12H, CH(CH_3)$_2$), 1.66 (s, 3H, C(CH_3)$_2$), 1.68 (d, $^3J_{HH}$ = 6.9 Hz, 12H, CH(CH_3)$_2$), 1.80 (s, 3H, C(CH_3)$_2$), 2.17 (m, 2H, $CH_2CH_2CH_3$), 3.11 (m, 2H, $CH_2CH_2CH_3$), 3.32 (sept, $^3J_{HH}$ = 7.2 Hz, 2H, CH(CH$_3$)$_2$), 3.93 (sept, $^3J_{HH}$ = 7.0 Hz, 2H, CH(CH$_3$)$_2$), 6.18 (d, $^4J_{HH}$ = 1.9 Hz, 2H, XA-*o*-CH), 6.52-6.70 (m, 2H ArH), 6.73 (d, $^4J_{HH}$ = 1.9 Hz , 2H, XA-*p*-CH), 6.85 (d, 8.08 Hz, 2H, *m*-*H*-Ar), 7.18-7.30 (m, 2H ArH), 7.35 (dd, 8.08 Hz, 2H, *o*-*H*-Ar).

^{13}C{^{1}H} NMR (126 MHz, C_6D_6, 298 K): δ = 14.4 ($CH_2CH_2CH_3$), 16.23 ($CH_2CH_2CH_3$), 22.3 (*C*(CH$_3$)$_2$), 23.2, 24.0 (CH(*C*H$_3$)$_2$), 27.4 (*C*H(CH$_3$)$_2$), 29.5 (*C*H(CH$_3$)$_2$), 31.7 (CH(*C*H$_3$)$_2$), 31.8 (C(*C*H$_3$)$_3$), 32.1 (d, $^2J_{CP}$ = 6.0 Hz, P{C(*C*H$_3$)$_3$}$_3$), 32.6 (*C*(CH$_3$)$_2$), 35.4 (*C*(CH$_3$)$_2$), 36.7 (d, $^2J_{CP}$ = 6.0 Hz P{*C*(CH$_3$)$_3$}$_3$), 48.7 (*C*H$_2$CH$_2$CH$_3$) 106.5, 112.1, 122.6, 123.6, 125.1, 125.9, 128.3, 129.8, 133.7, 141.6, 142.5, 144.6, 146.9, 148.1, 148.3, 160.7, 163.9 (C-Ar), 163.9 (C=*C*-Al) 187.0 (d, $^2J_{CP}$ = 63.0 Hz, C=*C*-Cu).

^{31}P{^{1}H} NMR (162 MHz, C_6D_6, 298 K): δ_P = 57.0.

$C_{70}H_{101}AlCuN_2OP$ requires: C, 75.88%; H, 9.19%; N, 2.53%; found: C, 76.02%; H, 9.31%; N, 2.40%.

Synthesis of (NON)Al{$C_6H_{10}O_2$}CuP^tBu_3 (10-Et-CO_2)

A solution of **10-Et** (100 mg, 0.095 mmol) in toluene (2 mL) in a J. Young's tap ampoule was degassed *via* freeze-pump-thaw. The headspace was backfilled with CO_2 (1 bar). The solution was layered with hexane and cooled to –30°C. Colourless crystals formed after 3 d (45 mg, 43%).

^{1}H NMR (400 MHz, C_6D_6, 298 K): δ_H = 0.88 (br, 27H, PC(CH_3)$_3$), 1.16 (d, $^3J_{HH}$ = 9.0 Hz, 6H, CH(CH_3)$_2$), 1.26 (s, 18H, C(CH_3)$_3$), 1.36 (t, $^3J_{HH}$ = 7.8 Hz, 3H, CH_2CH_3), 1.39 (d, $^3J_{HH}$ = 6.5 Hz, 6H, CH(CH_3)$_2$), 1.46 (t, $^3J_{HH}$ = 7.8 Hz, 3H, CH_2CH_3), 1.84 (s, 3H, C(CH_3)$_2$), 1.87 (s, 3H, C(CH_3)$_2$), 2.54 (q, $^3J_{HH}$ = 7.5 Hz, 2H, CH_2CH$_3$), 2.84 (q, $^3J_{HH}$ = 7.6 Hz, 2H, CH_2CH$_3$), 3.73 (sept, $^3J_{HH}$ = 6.9 Hz, 2H, CH(CH$_3$)$_2$), 3.81 (sept, $^3J_{HH}$ = 6.9

Hz, 2H, C*H*(CH_3)$_2$), 6.14 (d, $^4J_{HH}$ = 1.9 Hz, 2H, XA-*o*-C*H*), 6.75 (d, $^4J_{HH}$ = 1.9 Hz , 2H, XA-*p*-C*H*), 7.15-34 (m, 6H Ar*H*).

^{13}C{^{1}H} NMR (126 MHz, C_6D_6, 298 K): δ_C = 14.3, 15.8 (CH_2CH_3), 23.0, (*C*H(CH_3)$_2$), 25.3, 25.7 (*C*$H_2$$CH_3$), 26.0, 26.1, 26.4 (C(*C*H_3)$_3$), 28.0, 28.4 (*C*(CH_3)$_2$), 31.9, 32.0 (CH(*C*H_3)$_2$), 32.1 (d, $^2J_{CP}$ = 6.0 Hz, P{C(*C*H_3)$_3$}$_3$), 31.9 (*C*(CH_3)$_3$), 37.4 (P{*C*(CH_3)$_3$}$_3$), 105.3, 110.8, 123.2, 132.8 (Ar-*C*), 140.1 (O*C*O-Cu), 141.4, 144.9, 145.8, 147.5, 148.1, (Ar-*C*), 181.9 (*C*-Cu), 189.4 (*C*-Al).

^{31}P{^{1}H} NMR (162 MHz, C_6D_6, 298 K): δ_P = 73.7.

Synthesis of *trans*-(NON)Al-PhCCPh-CuP^{t}Bu$_3$ (11-Ph)

Diphenylacetylene (27 mg, 0.154 mmol) was added to a stirred suspension of **3-Cu** (100 mg, 0.103 mmol) in benzene (3 mL). The reaction mixture was stirred at 45°C for 18 h. The resulting solution was lyophilized twice from benzene to give an off-white solid. Colourless crystals were obtained by cooling a hexane solution of this solid to -30°C. (85 mg, 72%).

Compound **11-Ph** crystallises with a rotamer of the same molecule, orthogonal to the major component. This is retained in solution and the two can be differentiated by NMR spectroscopy. The ^{31}P NMR spectrum shows this minor rotamer present in the same ratio (10:1) as in the solid state.

^{1}H NMR (400 MHz, C_6D_6, 298 K): δ_H = 1.01 (d, $^3J_{HP}$ = 12.6 Hz, 27H, PC(C*H*$_3$)$_3$), 1.21 (s, 18H, C(C*H*$_3$)$_3$), 1.28 (d, $^3J_{HH}$ = 6.9 Hz, 12H, CH(C*H*$_3$)$_2$), 1.59 (d, $^3J_{HH}$ = 7.6 Hz, 12H, CH(C*H*$_3$)$_2$), 1.63 (s, 3H, C(C*H*$_3$)$_2$), 1.66 (s, 3H, C(C*H*$_3$)$_2$), 3.21 (sept, $^3J_{HH}$ = 7.0 Hz, 2H, C*H*(CH_3)$_2$), 4.01 (sept, $^3J_{HH}$ = 6.9 Hz, 2H, C*H*(CH_3)$_2$), 6.16 (d, $^4J_{HH}$ = 1.9 Hz, 2H, XA-*o*-C*H*), 6.72 (d, $^4J_{HH}$ = 1.9 Hz , 2H, XA-*p*-C*H*), 6.92 (d, $^3J_{HH}$ = 6.3 Hz, 2H, *H*-Ar) 7.01-38 (m, 6H Ar*H*), 8.09 (d, $^3J_{HH}$ = 6.9 Hz, 2H, *H*-Ar).

$^{13}C\{^1H\}$ NMR (126 MHz, C_6D_6, 298 K): δ_C = 24.5, 25.1 ($CH(CH_3)_2$), 26.19 (d, $^2J_{CP}$ = 11 Hz, $P\{C(CH_3)_3\}_3$), 27.4, 29.3 ($C(CH_3)_2$), 31.8 ($C(CH_3)_3$), 32.0 (d, $^1J_{CP}$ = 5.8 Hz, $P\{C(CH_3)_3\}_3$), 36.4, 36.6 ($C(CH_3)_2$), 37.5 ($C(CH_3)_2$), 90.1 (Ph*C*C*C*Ph), 106.7, 112.1, 122.7, 123.8, 123.9, 125.1, 126.1, 128.4, 128.6, 129.8, 133.5, 140.9, 142.6, 144.3, 147.0, 148.3 (d, $^3J_{CP}$ = 8.2 Hz), 152.9, 160.1 (ipso Ar-*C*), 162.7 (C=*C*-Al), 194.0 (d, $^2J_{CP}$ = 57 Hz, C=*C*-Cu).

$^{31}P\{^1H\}$ NMR (162 MHz, C_6D_6, 298 K): δ_P = 58.6 (major), 57.5 (minor).

***In situ* synthesis of *cis*-(NON)Al-PhCCPh-CuP^{t}Bu$_3$ (10-Ph)**

10-Ph was characterised *in situ* from a mixture of **10-Ph** and **11-Ph**, formed by addition of PhCCPh (5.4 mg, 0.030 mmol) to a suspension of **3-Cu** (20 mg, 0.020 mmol) in C_6D_6 (0.5 mL). The solution was heated to 45°C for 4 h, at which time a 1:1 mixture of **10-Ph** and **11-Ph** was apparent by ^{31}P and ^1H NMR.

^1H NMR (400 MHz, C_6D_6, 298 K): δ_H = 1.12 (d, $^3J_{HP}$ = 11.7 Hz, 27H, $PC(CH_3)_3$), 1.20 (s, 18H, $C(CH_3)_3$), 1.32 (d, $^3J_{HH}$ = 7.1 Hz, 12H, $CH(CH_3)_2$), 1.80 (d, $^3J_{HH}$ = 6.6 Hz, 12H, $CH(CH_3)_2$), 1.73 (s, 3H, $C(CH_3)_2$), 1.79 (s, 3H, $C(CH_3)_2$), 3.29 (sept, $^3J_{HH}$ = 6.7 Hz, 2H, $CH(CH_3)_2$), 4.21 (sept, $^3J_{HH}$ = 6.7 Hz, 2H, $CH(CH_3)_2$), 5.94 (d, $^3J_{HH}$ = 8.8 Hz, 2H, *H*-Ar), 6.31 (d, $^4J_{HH}$ = 1.9 Hz, 2H, XA-*o*-C*H*), 6.75 (d, $^4J_{HH}$ = 1.9 Hz , 2H, XA-*p*-C*H*), 7.01-40 (m, 6H Ar*H*), 7.46 (d, $^3J_{HH}$ = 8.8 Hz, 2H, *H*-Ar) 7.50 (m, 10H, PhCCPh).

$^{13}C\{^1H\}$ NMR (126 MHz, C_6D_6, 298 K): 152.9, 160.1 (*ipso-C-Ar*), 159.7 (C=*C*-Al), 185.4 (d, $^2J_{CP}$ = 72 Hz, C=*C*-Cu).

The ^{13}C NMR resonances for the NON and P^{t}Bu$_3$ ligands of **10-Ph** and **11-Ph** are overlapping and difficult to distinguish. However, the lowfield resonances associated with the inserted alkyne can be clearly assigned.

$^{31}P\{^1H\}$ NMR (162 MHz, C_6D_6, 298 K): δ_P = 62.1.

Synthesis of (NON)Al{$C_6H_{10}O$}CuP^tBu_3 (12-Et)

A solution of **10-Et** (100 mg, 0.095 mmol) in benzene (2 mL) in a J. Young's tap ampoule was degassed *via* freeze-pump-thaw. The headspace was backfilled with CO (1 bar) and the solution turned from colourless to yellow. Volatiles were removed *in vacuo* and the residue was dissolved in hexane (~1 mL). Yellow crystals formed upon standing at room temperature (45 mg, 44%).

^{1}H NMR (400 MHz, C_6D_6, 298 K): δ_H = 0.90 (d, $^3J_{HP}$ = 11.9 Hz, 27H, PC(CH_3)$_3$), 1.18 (d, $^3J_{HH}$ = 7.3 Hz, 6H, CH(CH_3)$_2$), 1.22 (d, $^3J_{HH}$ = 6.4 Hz, 12H, CH(CH_3)$_2$), 1.27 (s, 18H, C(CH_3)$_3$), 1.48 (d, $^3J_{HH}$ = 7.0 Hz, 6H, CH(CH_3)$_2$), 1.56 (t, $^3J_{HH}$ = 7.0 Hz, 3H, CH_2CH_3), 1.78 (s, 3H, C(CH_3)$_2$), 1.83 (s, 3H, C(CH_3)$_2$), 2.72 (q, $^3J_{HH}$ = 7.5 Hz, 2H, C$H_2$$CH_3$), 2.76 (q, $^3J_{HH}$ = 7.7 Hz, 2H, C$H_2$$CH_3$), 3.52 (sept, $^3J_{HH}$ = 7.4 Hz, 2H, CH(CH_3)$_2$), 4.05 (sept, $^3J_{HH}$ = 6.4 Hz, 2H, CH(CH_3)$_2$), 6.21 (d, $^4J_{HH}$ = 1.9 Hz, 2H, XA-*o*-CH), 6.72 (d, $^4J_{HH}$ = 1.9 Hz , 2H, XA-*p*-CH), 6.99-28 (m, 6H ArH).

^{13}C{^{1}H} NMR (126 MHz, C_6D_6, 298 K): δ_C = 15.2, 16.2 (CH_2CH_3), 22.9, (CH(CH_3)$_2$), 25.1, 27.4 (C$H_2$$CH_3$), 24.8, 25.6, 26.4 (C(C$H_3$)$_3$), 27.6, 28.2 (C(C$H_3$)$_2$), 28.7, 29.2 (CH(C$H_3$)$_2$), 31.8 (d, $^2J_{CP}$ = 6.0 Hz, P{C(CH_3)$_3$}$_3$), 31.9 (C(CH_3)$_3$), 35.2 (d, $^1J_{CP}$ = 6.0 Hz, P{C(CH_3)$_3$}$_3$), 105.2, 110.8, 123.1, 124.0, 124.9, 128.35, 132.6, 140.9, 142.8, 144.0, 145.4, 147.8 (Ar*C*), 157.3 (d, $^3J_{CP}$ = 6.9 Hz, Al-C=*C*), 184.9 (Al-*C*) 288.6 (d, $^2J_{CP}$ = 66.6 Hz, *C*=O).

^{31}P{^{1}H} NMR (162 MHz, C_6D_6, 298 K): δ_P = 60.6.

IR *v* (cm^{-1}) 2954, 2863, 1632, 1573, 1504, 1456, 1403, 1291, 1243, 1200, 1137, 1089, 1009, 891, 774.

$C_{66}H_{99}AlCuN_2O_2P$ requires: C, 73.81%; H, 9.29%; N, 2.61%; found: C, 73.57%; H, 9.31%; N, 2.50%.

Synthesis of (NON)Al{$C_{10}H_{12}O$}CuP^tBu_3 (12-Pr,Ph)

To a suspension of **3-Cu** (50 mg, 0.051 mmol) in benzene (2 mL) was added 1-phenyl-1-pentyne (15 µL, 0.103 mmol). The solution was immediately frozen, and the headspace evacuated. The headspace was backfilled with CO (1 atm) and the solution was allowed to thaw, upon which a colour change from colourless to yellow was observed. The solution was lyophilised from benzene twice and the resulting yellow powder was dissolved in hexane. The solution was filtered and concentrated to ~2 mL. Yellow crystals formed upon standing at room temperature (40 mg, 69%).

^{1}H NMR (400 MHz, C_6D_6, 298 K): δ_H = 0.83 (d, $^3J_{HP}$ = 13.3 Hz, 27H, PC(CH_3)$_3$), 0.89 (t, $^3J_{HH}$ = 6.3 Hz, 3H, $CH_2CH_2CH_3$), 1.11 (d, $^3J_{HH}$ = 6.9 Hz, 6H, CH(CH_3)$_2$), 1.24 (d, $^3J_{HH}$ = 6.9 Hz, 6H, CH(CH_3)$_2$), 1.25 (d, $^3J_{HH}$ = 6.9 Hz, 6H, CH(CH_3)$_2$), 1.27 (s, 18H, C(CH_3)$_3$), 1.48 (d, $^3J_{HH}$ = 7.0 Hz, 6H, CH(CH_3)$_2$, 1.81 (s, 3H, C(CH_3)$_2$), 1.85 (s, 3H, C(CH_3)$_2$), 2.07 (m, 2H, $CH_2CH_2CH_3$), 2.91 (m, 2H, $CH_2CH_2CH_3$), 3.60 (sept, $^3J_{HH}$ = 6.9 Hz, 2H, CH(CH$_3$)$_2$), 4.00 (sept, $^3J_{HH}$ = 7.0 Hz, 2H, CH(CH$_3$)$_2$), 6.34 (d, $^4J_{HH}$ = 1.9 Hz, 2H, XA-*o*-CH), 6.77 (d, $^4J_{HH}$ = 1.9 Hz, 2H, XA-*p*-CH), 7.03-7.30 (m, 11H ArH).

^{13}C{^{1}H} NMR (126 MHz, C_6D_6, 298 K): δ_C = 14.3 ($CH_2CH_2CH_3$), 16.0 (*C*H(CH$_3$)$_2$), 23.1 (C(*C*H$_3$)$_2$), 25.0, 26.0, 26.4 (*C*H(CH$_3$)$_2$), 24.7 ($CH_2CH_2CH_3$), 27.9, 28.7, (CH(*C*H$_3$)$_2$), 31.8 (d, $^2J_{CP}$ = 6.0 Hz, P{C(*C*H$_3$)$_3$}$_3$), 31.9 (C(*C*H$_3$)$_3$), 32.0 (*C*(CH$_3$)$_3$), 32.8 (C(*C*H$_3$)$_2$), 35.1 (*C*(CH$_3$)$_2$), 36.4 (d, $^1J_{CP}$ = 9.0 Hz, P{*C*(CH$_3$)$_3$}$_3$), 38.89 ($CH_2CH_2CH_3$) 105.2, 110.6, 123.2, 123.9, 124.8, 125.8, 130.2, 132.7, 141.0, 143.6, 143.6, 145.2, 147.7, 147.9, 148.0 (Ar*C*), 157.1 (d, $^3J_{CP}$ = 7.0 Hz, Al-C=*C*), 186.2 (Al-*C*) 287.4 (d, $^2J_{CP}$ = 65.3 Hz, *C*=O).

^{31}P{^{1}H} NMR (162 MHz, C_6D_6, 298 K): δ_P = 60.3.

IR *v* (cm^{-1}) 2954, 2863, 1632, 1569, 1537, 1467, 1382, 1307, 1254, 1174, 1105, 1014, 891, 785, 689.

$C_{71}H_{101}AlCuN_2O_2P$ requires: C, 75.06%; H, 8.96%; N, 2.47%; found: C, 75.37%; H, 9.53%; N, 2.29%.

Formation of (*E*)-2-ethylpent-2-enal

To a solution of **12-Et** in C_6D_6 in a J. Young's NMR tube was added H_2O (excess). The reaction mixture was sonicated for 10 min, after which time a precipitate formed. Volatiles were vacuum transferred to second NMR tube and ^{1}H NMR showed only water and (*E*)-2-ethylpent-2-enal.

^{1}H NMR (400 MHz, C_6D_6, 298 K): δ_H = 0.68 (t, 1H, $^3J_{HH}$ = 6.8 Hz, CH_2CH_3), 1.79 (m, 2H, CH_2CH_3), 2.70 (q, $^3J_{HH}$ = 7.9 Hz, 2H, CH_2CH_3), 5.72 (t, $^3J_{HH}$ = 7.3 Hz, 1H, *H*C=C), 9.20 (s, 1H, O=C*H*).

ESI mass spec: 113.1 (m/z = 112.1).

5.6 Kinetic studies

Kinetic studies were carried out using ^{31}P NMR monitoring. All reactions were carried out in C_6D_6 at 318K.

Determination of order in PhCCPh: A stock solution of PhCCPh in benzene was prepared (519.2 mM). To a sample of **3-Cu** in C_6D_6 (10 mg, 20.77 mM) in a J. Young's NMR tube was added the requisite quantity of PhCCPh solution (10.38, 20.77, 31.15, 41.54 mM, respectively) at room temperature. The sample was then quickly placed in the NMR spectrometer at 318 K and ^{31}P NMR spectra were measured every 528 s. The spectra were analysed using MestreNova and MS Excel.

Determination of order in **3-Cu**: To a sample of **3-Cu** in C_6D_6 (5.5 mg, 11.42 mM; 10.0 mg, 20.77 mM, 15.0 mg, 31.16 mM, 19 mg, 39.5 mM) in a J. Young's NMR tube was added PhCCPh in benzene (41.54 mM) at room temperature. The sample was then quickly placed in the NMR spectrometer at 318 K and ^{31}P NMR spectra were measured every 528 s. The spectra were analysed using MestreNova and MS Excel.

5.7 References

1 J. March and M. B. Smith, in *March's Advanced Organic Chemistry*, John Wiley & Sons, Ltd, New Jersey, 6th edn., 2007, pp. 999–1014.
2 V. P. Ananikov and I. P. Beletskaya, *Top. Organomet. Chem.*, 2013, **43**, 1–20.
3 J. Clayden, N. Greeves and S. G. Warren, *Organic Chemistry*, Oxford University Press, Oxford, 2nd edn., 2012.
4 A. S. K. Hashmi, *Chem. Rev.*, 2007, **107**, 3180–3211.
5 M. Meldal and C. W. Tomøe, *Chem. Rev.*, 2008, **108**, 2952–3015.
6 A. Fürstner, *Angew. Chemie Int. Ed.*, 2018, **57**, 4215–4233.
7 G. Fang and X. Bi, *Chem. Soc. Rev*, 2015, **44**, 8124.
8 H. V. Rasika Dias, J. A. Flores, J. Wu and P. Kroll, *J. Am. Chem. Soc.*, 2009, **131**, 11249–11255.
9 H. Lang, A. Jakob and B. Milde, *Organometallics*, 2012, **31**, 7661–7693.
10 R. Dorel and A. M. Echavarren, *Chem. Rev.*, 2015, **115**, 9028–9072.
11 S. Bhunia, P. Ghosh and S. R. Patra, *Adv. Synth. Catal.*, 2020, **362**, 3664–3708.
12 C. J. V. Halliday and J. M. Lynam, *Dalt. Trans.*, 2016, **45**, 12611–12626.
13 P. Sivaguru, S. Cao, K. R. Babu and X. Bi, *Acc. Chem. Res.*, 2020, **53**, 662–675.
14 M. S. Ziegler, K. V Lakshmi and T. D. Tilley, *J. Am. Chem. Soc.*, 2017, **139**, 5378–5386.
15 D. S. Müller and I. Marek, *Chem. Soc. Rev*, 2016, **45**, 4552.
16 R. J. Sundberg, *Advanced Organic Chemistry. Part B. Reactions and Synthesis*, Kluwer Academic, New York, 4th edn., 2001.
17 J. C. Fettinger, P. A. Gray, C. E. Melton and P. P. Power, *Organometallics*, 2014, **33**, 6232–6240.
18 A. J. Downs, *Chemistry of aluminium, gallium, indium and thallium*, Blackie Academic and Professional, London, 1993.
19 Z. Yang, M. Zhong, X. Ma, S. De, C. Anusha, P. Parameswaran and H. W. Roesky, *Angew. Chemie*, 2015, **127**, 10363–10367.
20 A. Bismuto, S. P. Thomas and M. J. Cowley, *Angew. Chemie - Int. Ed.*, 2016, **55**, 15356–15359.
21 K. Hobson, C. J. Carmalt and C. Bakewell, *Inorg. Chem.*, 2021, **60**, 10958–10969.
22 H. Zhu, R. B. Oswald, H. Fan, H. W. Roesky, Q. Ma, Z. Yang, H. G. Schmidt, M. Noltemeyer, K. Starke and N. S. Hosmane, *J. Am. Chem. Soc.*, 2006, **128**, 5100–5108.
23 S. J. Urwin, G. S. Nichol and M. J. Cowley, *Chem. Commun.*, 2018, **54**, 378–380.
24 A. Hofmann, A. Lamprecht, O. F. González-Belman, R. D. Dewhurst, J. O. C. Jiménez-Halla, S. Kachel and H. Braunschweig, *Chem. Commun.*, 2018, **54**, 1639–1642.
25 I. Beletskaya and C. Moberg, *Chem. Rev.*, 2006, **106**, 2320–2354.
26 D. Dange, A. R. Gair, D. D. L. Jones, M. Juckel, S. Aldridge and C. Jones, *Chem. Sci.*, 2019, **10**, 3208–3216.
27 Y. Zhao, Y. Liu, Y. Lei, B. Wu and X. J. Yang, *Chem. Commun.*, 2013, **49**, 4546–4548.
28 M. Joost, P. Gualco, S. Mallet-Ladeira, A. Amgoune and D. Bourissou, *Angew. Chemie Int. Ed.*, 2013, **52**, 7160–7163.
29 M. Joost, L. Estevez, S. Mallet-Ladeira, K. Miqueu, A. Amgoune and D.

Bourissou, *J. Am. Chem. Soc.*, 2014, **136**, 10373–10382.
30 A. Suzuki, L. Wu, Z. Lin and M. Yamashita, *Angew. Chemie - Int. Ed.*, 2021, **60**, 21007–21013.
31 M. K. Karunananda and N. P. Mankad, *J. Am. Chem. Soc.*, 2015, **137**, 14598–14601.
32 B. L. Ramirez and C. C. Lu, *J. Am. Chem. Soc.*, 2020, **142**, 5396–5407.
33 S. P. Desai, J. Ye, T. Islamoglu, O. K. Farha and C. C. Lu, *Organometallics*, 2019, **38**, 3466–3473.
34 T. Hu, Y.-H. Li, X.-F. Kuang and C.-Z. Lu, *CrystEngComm*, 2017, **19**, 3445–3454.
35 Y.-L. Shen, J.-L. Jin, J.-J. Fang, Z. Liu, J.-L. Shi, Y.-P. Xie and X. Lu, *Inorg. Chem.*, 2021, **60**, 6276–6282.
36 R. J. Oeschger, R. Bissig and P. Chen, *J. Am. Chem. Soc.*, 2022, **144**, 23, 10330-10343..
37 P. J. Stevenson, *Org. Biomol. Chem.*, 2011, **9**, 2078–2084.
38 I. Ibni Hashim, T. Scattolin, N. V. Tzouras, L. Bourda, K. Van Hecke, I. Ritacco, L. Caporaso, L. Cavallo, S. P. Nolan and C. S. J. Cazin, *Dalt. Trans.*, 2022, **51**, 231–240.
39 A. Makarem, R. Berg, F. Rominger and B. F. Straub, *Angew. Chemie*, 2015, **127**, 7539–7543.
40 L. Jin, D. R. Tolentino, M. Melaimi and G. Bertrand, *Sci. Adv.*, 2015, e1500304.
41 M. K. Karunananda and N. P. Mankad, *Organometallics*, 2017, **36**, 220–227.
42 S. Bajo, C. A. Theulier and J. Campos, *ChemCatChem*, **14**, 15, e202200157..
43 S. Fujimori and S. Inoue, *J. Am. Chem. Soc.*, 2022, **144**, 2034–2050.
44 A. Haynes, P. M. Maitlis, G. E. Morris, G. J. Sunley, H. Adams, P. W. Badger, C. M. Bowers, D. B. Cook, P. I. P. Elliott, T. Ghaffar, H. Green, T. R. Griffin, M. Payne, J. M. Pearson, M. J. Taylor, P. W. Vickers and R. J. Watt, *J. Am. Chem. Soc.*, 2004, **126**, 2847–2861.
45 J. G. Cordaro and R. G. Bergman, *J. Am. Chem. Soc.*, 2004, **126**, 3432–3433.
46 T. Zhou, S. Malakar, S. L. Webb, K. Krogh-Jespersen and A. S. Goldman, *Proc. Natl. Acad. Sci. U. S. A.*, 2019, **116**, 3419–3424.
47 R. R. Reinig, E. L. Fought, A. Ellern, T. L. Windus and A. D. Sadow, *Dalt. Trans.*, 2018, **47**, 12147–12161.
48 Y. Yuan, F. Wu, J. Xu and X. Wu, *Angew. Chemie*, 2020, **132**, 17203–17209.
49 F. P. Wu, J. Holz, Y. Yuan and X. F. Wu, *CCS Chem.*, 2021, **3**, 2643–2654.
50 Q. Luo, C. Wang, W. X. Zhang and Z. Xi, *Chem. Commun.*, 2008, 1593–1595.
51 H. Q. Geng, T. Meyer, R. Franke and X. F. Wu, *Chem. Sci.*, 2021, **12**, 14937–14943.

Chapter 6 : Conclusions

This thesis details the synthesis and reactivity of complexes containing a direct, covalent bond between aluminium and a group 11 metal. Chapter 3 showed the applicability of the aluminyl anion, **K_2[(NON)Al]$_2$** as a nucleophilic partner in salt metathesis reactions with common electropositive coinage metal precursors. A diverse range of complexes featuring an Al–M bond (M = Cu, Ag, Au) could be synthesised using this approach, with the structure depending on the phosphine co-ligand. A potassium bisaluminylcopper complex, **2-Cu**, was formed by reaction of the aluminyl reagent with Ph_3PCuI, while trimetallic complexes of the form **(NON)Al(MPPh_3)$_2$I** were accessible by altering the stoichiometry. The series of bimetallic coinage metal aluminyl complexes **(NON)AlMP^{t}Bu$_3$** were also prepared, making use of the more sterically hindered phosphine P^{t}Bu$_3$. The gallyl reagent **K_2[(NON)Ga]$_2$** was used to provide a direct comparison of Al–M and Ga–M bonds bearing the same supporting ligand and to delineate the relative properties of the aluminyl- and gallyl- fragments as metalloligands. It was found that the aluminyl fragment is a stronger σ-donor than the heavier gallyl donor, a property which may be exploited in the reactivity of these systems. The work in this chapter sets a precedent for the use of nucleophilic aluminyl anions as a means to form covalent bonds between aluminium and transition metals.

Turning to reactivity, Chapter 4 described the reactivity of the bimetallic complexes of the form **(NON)AlMP^{t}Bu$_3$** towards CO_2, which was chosen as a carbon-based electrophilic probe and also as an environmentally important small molecule. Similarly to the reactivity of the previously reported gold aluminyl complex **3-Au**, it was found that CO_2 could be inserted into the Al–M bond to give species featuring μ-κ^1(C):κ^2(E,E′)

(E = O, N) bridging units, with the regiochemistry reflecting the polarity of the bond i.e. $Al^{\delta+}$–$M^{\delta-}$. While the products of carbodiimide insertion were stable towards further reaction, CO_2 insertion products could undergo subsequent reaction, depending on the identity of the group 11 metal. As such, bridging carbonate complexes could be formed. Experimental and quantum chemical investigation found this to be *via* extrusion of CO from the CO_2 insertion products to give an Al–O–M oxide, followed by incorporation of a second CO_2 molecule. Comparison to related recently reported systems featuring Al–M bonds reveals that the μ-κ^1(C):κ^2(O,O′) binding mode appears to be a common feature of such systems, and therefore bimetallic aluminyl complexes such as these should be considered useful reagents to bring about such reactivity.

Chapter 5 explored the reactivity of coinage metal aluminyl complexes towards alkynes, which are versatile and readily available organic building blocks. It was found that the Al–Cu bond of copper aluminyl complex **3-Cu** could add across the C–C triple bond of internal alkynes, producing aluminylalkenyl copper species. By employing kinetic or thermodynamic control, examples of both *cis* and *trans* dimetallated alkenes could be isolated and structurally characterised, and the mechanism of isomerisation from the *cis* isomer to the *trans* isomer was investigated through kinetic studies. Furthermore, the aluminylalkenyl copper complexes could be functionalised in such a way that exploited the differing nature of the Al–C and Cu–C bonds. The first structurally characterised copper acyl compounds were formed by selective insertion of CO into the Cu–C bond, aided by the proximal Al centre. The isolation of these acyl compounds, which have been proposed as intermediates in a number of catalytic processes, shows the power of Lewis acid cooperation in accessing new structural motifs.

The work in this thesis, along with the growing body of literature on directly bonded Al–M complexes, shows that there is still much to be understood on how the Al–M bond reacts. Variation of the aluminyl fragment, the supporting ligand bound to M, and indeed, the metal itself, were shown to have an important effect on the nucleophilicity of M, which is itself key to reactivity. The nature of the Al–M bond has led to much theoretical interest and discussion, much of it centred around the nucleophilic behaviour. Undoubtedly, continued experimental probes and quantum chemical analysis will shed light on this issue.

From the perspective of small molecule activation, it is clear that an important mode of reactivity for coinage metal aluminyl complexes is insertion into the Al–M bond, as was observed for both heteroallenes and internal alkynes. The Al–M bond was shown to be an efficient method of introducing an aluminium and copper fragment into a molecule in one step, and both Al–C and Cu–C bonds are useful functional handles. Future work could expand upon this, looking at other unsaturated small molecules such as alkenes and carbonyl compounds. There are also many E–H bonds which have potential to be activated in a bimetallic fashion, such as B–H and Si–H linkages. In this respect, there may be the possibility for catalytic hydrosilation or hydroboration reactions, both of which are valuable in organic synthesis. A key future goal involves attempting to build these bond activations into catalytic processes. In any reaction involving addition across the Al–M bond, a critical factor in making the reaction catalytic will be reformation of the Al–M bond. Again, this is a place where careful tuning of the ligand scaffold around the bond may be beneficial, perhaps through adding a tethering unit to connect the two metal fragments. Bimetallic complexes have much to contribute in terms of strong bond activation, and the work in this thesis demonstrates that aluminium is a highly valuable partner in achieving this.